UNIVERSITY OF NOTTINGHAM MALAYSIA

Development of a Medical System to Indicate Risk of Cardiovascular Disease

DENESH SOORIAMOORTHY, MEng

Thesis submitted to University of Nottingham for the degree of Doctor of Philosophy

November 2021

This thesis is dedicated to all those who suffer from cardiovascular disease and to their families who have lost their loved ones owing to this disease. This study hopes to reduce cardiovascular-related fatalities in the future.

We hereby declare that we have read this thesis and in our opinion this thesis is sufficient in terms of scope and quality for the award of the degree of Doctor of Philosophy (Electrical and Electronic Engineering)

Signature	:	----------
Name of Main Supervisor	:	Dr. Marwan Nafea
Date	:	18/11/2021

Signature	:	----------
Name of Co-Supervisor	:	Anandan Shanmugam
Date	:	18/11/2021

DECLARATION

I declare that this thesis entitled "***Development of a Medical System to Indicate Risk of Cardiovascular Disease***" is the result of my own research except as cited in the references. The thesis has not been accepted for any degree and is not concurrently submitted in candidature of any other degree.

Signature : ----------
Name : Denesh Sooriamoorthy
Date : 18/11/2021

ABSTRACT

One significant issue that is encountered by individuals who experience ill effects of cardiovascular sickness, is not having the option to distinguish their illness until the manifestations give an evident sign, generally at the critical stage, which brings about a high threat of death. Furthermore, the most common method of treating severe cases is by invasive medical treatment, which is agonizing to patients. As a means to reduce this threat of severe cases or abrupt demise among individuals today due to cardiovascular disease, this research proposes to create a medical system focusing on the upstream blood pressure waveform and artificial intelligence, which would indicate the risk of cardiovascular disorder. The work in this thesis lays the groundwork for a novel risk indication system with three key sub systems. First a data acquisition system that uses a human wrist wearable device for acquiring data non-invasively, next a signal conversion system to transform radial waveforms to aortic waveforms, and finally the risk prediction system that uses a combination of a Convolutional Neural Network (CNN) and a zero-dimensional cardiovascular model's parameters. In today's world, this combination of methods to indicate the risk of cardiovascular diseases has yet to be explored and developed, giving rise to a new pathway of risk indication. This thesis shows the details of the proposed medical system, along with testing of the hardware and the various sub systems.

For data acquisition, as currently marketed devices could not be used for this project, a wearable device with an embedded pressure sensor (Honeywell FSS005WNSB) was selected to acquire radial waveforms from the wearer's wrist. As this is yet to be developed into a fully wearable device, pairs of radial and aortic signals were obtained from two databases (PhysioNet and HaeMod) for this research. These radial signals are then converted to aortic signals with the use of the newly developed Electrical Impedance Function (EIF), which is then compared to current conversion methods such as the Generalised Transfer Function (GTF), N-Point Moving Average (NPMA), and the Adaptive Transfer Function (ATF). Waveforms produced by the EIF have an average RMSE of 9.4838 and MAPE of 0.0661, with a peak difference of 6.35mmHg and 0.0129ms computational time, demonstrating a comparable performance with the GTF and a better estimation approach when compared with NPMA and ATF.

The transformed signals were then used for risk indication, utilizing Vincent Rideout's cardiovascular model to produce data for the CNN. From the iterative investigation of the Vincent Rideout model, it is discovered that there are 16 parameters that significantly influences the model's aortic wave. Next a regression-based CNN is trained, with aortic waveforms as inputs, and their corresponding 16 parameters as outputs. When the trained CNN is tested with cardiovascular disease aortic pulse waveforms, which were converted from radial pulse waveforms utilizing both transfer functions (EIF and GTF) separately, it is observed that 2 key parameters out of the 16 could be used for indicating cardiovascular diseases. The two parameters - Pulmonary Vein 2 (RL2) and Systemic Aortic Artery 1 (RA1) – could be related biologically, as it can be postulated that they relax concurrently to permit the blood to flow smoothly in its closed-loop framework resulting in the decrease of the resistance value.

From the experiments conducted, the values of RL2 and RA1 when it acclimates to cardiovascular conditions is equal to or beneath 10.640691 $g \cdot s/cm^4$and 9.7667933 $g \cdot s/cm^4$ respectively when using EIF as the transfer function. On the other hand, by using GTF as the transfer function, the values of RL2 and RA1 when it acclimates to these cardiovascular conditions is equal to or beneath 10.530969 $g \cdot s/cm^4$ and 9.8313036 $g \cdot s/cm^4$ respectively. An 80.0% and 82.5% classification accuracy was obtained when these limits were used as identifiers on cardiovascular disease data obtained from Hospital Sultanah Bahiyah using EIF and GTF respectively as the transfer function.

Overall, this research shows that the proposed medical system can provide a minimum identification accuracy of 80% for cardiovascular disease, which can be considered a reasonably good performance, increasing the number of early detections and thus helping those at risk of cardiovascular disease on time.

ACKNOWLEDGEMENTS

This section documents the many names of all those unsung heroes who provided support, encouragement, and advice and without whom I would not have succeeded in presenting this thesis. I owe a huge debt of gratitude to everyone who contributed so much of their time, love, and energy.

First and foremost, I am grateful to God for providing me with a good mind and sound health to pursue this study. Thank you does not begin to express my gratitude for my wonderful family's unwavering support during this undertaking. My parents are the centre of my universe. I would not be where I am now if it weren't for their blessing and support. I'd want to thank Mrs. Shubathira Sooriamooorthy, my sister, who guided me to understand the cardiovascular system as per her medical background, and Mr Kathiramar, my brother-in-law, for his unwavering support and encouragement during this journey. In addition, I do want to use this occasion to express my gratitude to Mrs. Jeya Thevi and Ms. Navilashini Rajasekar for their unwavering support throughout my PhD studies.

I am greatly indebted to my supervisor, Mr. Anandan Shanmugam who guided and supported me in every stage of the research. Despite being extremely busy with his duties, his scrutiny of the analysis and his comments has helped to shape this work and my own research skills. He ensured I was going on the right track and constantly guided me throughout this project. Thank you, sir.

I would also like to thank the experts who were involved in my work and gave guidance and ideas despite their busy schedule: Dr. Marwan Nafea and Ir. Dr. Khor Jeen Ghee. The research would not have been possible without their enthusiastic participation and input. Their valuable time spent with me is greatly appreciated.

Prof. Dr. Yousif Abdalla Abakr deserves special recognition. I'll never forget the insightful discussions and suggestions. I've always looked forward to his insightful advice, and he's always been there for me when I needed help with my study.

This path would not have been any easier if my great supporter had not been present. Dr. Mohammed Ayoub Juman deserves special recognition for always motivating and supporting me in my efforts to become a better researcher. I have always sought his

advice and opinions on research issues, particularly in the areas of artificial intelligence and machine learning.

I would also like to thank Dr. Rajeev Ramnath who had been a pillar of support in my PhD studies journey. Additionally, I would like to thank Dr. Vimal Rau Aparow, Dr. Se Yong Eh Noum, Ir. Dr. Sivakumar Sivanesan and Prof. Dr. T.Nandha Kumar who had motivated me to keep pursuing my journey.

I also want to thank the lab technicians at the E&E department, who have never hesitated to answer any of my queries. Their great experience in the sector has saved me a lot of time and trouble in the development and component selection process. Their suggestions were extremely beneficial for my project.

Besides, I would like to express my heartfelt gratitude to Dr. Saravanan Krishinan and his team from Hospital Sultanah Bahiyah for providing me with a sufficient amount of data to conduct this research. I am using this opportunity to express my gratitude to everyone who supported me during my presence in Hospital Sultanah Bahiyah for data collection. Not forgetting my valuable participants who had given me crucial information, without them this project would not be feasible. I'd want to take this opportunity to thank everyone who helped me during my data collection visit to Hospital Sultanah Bahiyah.

Finally, I'd like to express my gratitude to all of my friends who have helped me open up new ideas for my project, directly or indirectly. They've been quite beneficial, especially in terms of training my mind to think out of the box whenever I'm stagnant. My friendships and their unwavering support are something I hope to take with me into the professional world.

LIST OF PUBLICATIONS

Journal papers:

1) **Denesh Sooriamoorthy**, S. Anandan Shanmugam, and M A Juman. 2021. "A novel electrical impedance function to estimate central aortic blood pressure waveforms," in *Biomedical Signal Processing and Control*, 68, p.102649. Published.

Conference papers:

1) **Denesh Sooriamoorthy,** Audrey Li-Huey Wee, Anandan Shanmugam, Khor Jeen Ghee, Pei Cheng Ooi, Marwan Nafea. "A Study on the Effect of Electrical Parameters of Zero-Dimensional Cardiovascular System on Aortic Waveform", in *2020 IEEE Student Conference on Research and Development (SCOReD),* Published.

LIST OF CONTENTS

LIST OF FIGURES

LIST OF TABLES

LIST OF ABBREVIATIONS

ADC	Analog Digital Converter
ANN	Artificial Neural Network
ATF	Adaptive Tranfer Function
CAD	Coronary Artery Disease
CASP	Central Aortic Systolic Pressure
CHD	Coronary Heart Disease
CNN	Convolutional Neural Network
CVD	Cardiovascular Disease
DOSM	Department of Data Malaysia
ECG	Electrocardiography
EIF	Electrical Impedance Function
FSI	Fluid Structure Interaction
GTF	Generalized Transfer Function
KVL	Kirchhoff's Voltage Law
LOA	Limit of Agreement
MAPE	Mean Absolute Percentage Error
NCVD-ACS	National Cardiovascular Disease – Acute Coronary Syndrome
NPMA	N-Point Moving Average
OLED	Organic Light-Emitting Diode
PA1	Aortic Pressure
PDMS	Polydimethylsiloxane
PLV	Left Ventricular Pressure
PPV	Pulmonary Artery Pressure

PRV	Right Ventricular Pressure
RMSE	Root Mean Square Error
PTT	Pulse Transit Time
PWV	Pulse Wave Velocity
WHO	World Health Organisation

LIST OF SYMBOLS

Symbol	Description	Units
P	Pressure	Millimetre of mercury (mmHg)
R	Resistance	Ohm (Ω)
L	Inductance	Henry (H)
C	Capacitance	Farad (F)
V	Voltage	Volt (V)
I	Electric Current	Amperes (A)
A_F	Gain	-
f_c	Cut off Frequency	Hertz (Hz)
R	Radius	Millimetre (mm)

CHAPTER 1 : INTRODUCTION

1.1 Introduction

Cardiovascular diseases (CVD) are the leading cause of death worldwide and are becoming one of the most life-threatening diseases in most countries. By developing a medical system which monitors and provides risk indication to the user, the risk of sudden death among heart patients today can be significantly reduced. Distinguishing early on signs of unhealthy conditions using effective approaches will certainly be a major step forward. The motivation behing this research as well as the key problems to be addressed are stated in this chapter. Furthermore, the research objectives with which these accomplishments could be attained through this research are discussed, providing the research with a direction. The scope and the significance of the research is well defined in this chapter as well. Finally, the potential impact and contributions of the research is described in detail.

1.2 Overview of research

Cardiovascular diseases (CVD) causes nearly 30% of mortality worldwide and may even lead to disability [1] . Approximately 17.7 million people died from CVD in 2017[2] . This makes CVD the largest cause of death globally and it is becoming one of the most life-threatening diseases in most countries. It is known that total world-wide mortality caused by the various forms of CVD are approximately 2.2% or 16.7 million of the total global deaths [3].

In today's era, CVD still poses a grand challenge as its occurrence on aged people are more frequent [4]. Hence, early identification and prevention are critical to decrease cardiovascular mortality by giving the required treatments early. This could be done by having a reliable monitoring framework that would continuously monitor and indicate risk for people's health condition. However, the early detection of CVD is typically conducted discontinuously by a one-off measurement of blood pressure, Doppler ultrasonography, photo-plethysmography [5], magnetic resonance imaging and electrocardiography[6]. These methods are costly, intermittent, bulky and inconvenient [7]. A wearable sensor with a compact size, high sensitivity, ultralow energy consumption, and accessible usage in various scenarios are desired to monitor various cardiovascular conditions in a comfortable, continuous, real-time manner to uncover the deterioration

of cardiovascular conditions [7], [8]. In today's technological world, the above mentioned devices do exist, to estimate the central aortic blood pressure waveform from the peripheral artery (radial artery) pulses such as SphygmoCorCVMS (AtCor Medical, Australia) [9]–[11] and BPro + A-Pulse(HealthSTATS) [9], [12], [13]. For estimating the central aortic blood pressure waveform from the user's wrist, the SphygmoCorCVMS (AtCor Medical, Australia) utilizes the Generalize Transfer Function (GTF) [9]–[11] where else the BPro + A-Pulse (HealthSTATS) utilizes the N-point moving average [9], [12], [13] . These devices estimate the central aortic blood pressure waveform to continuously update the user on their blood pressure reading (systolic and diastolic values) where these values are used to determine hypertension as a risk indicator.

1.3 Motivation

There are two main reasons to develop this system. Firstly, hospitals attain the blood pressure measurement from the arm using sphygmomanometer (Blood pressure cuff) to attain the blood pressure reading to indicate high or low blood pressure of the patient. This method doesn't analyse the blood pressure features but just indicates the systolic and diastolic pressure values. Secondly, patients showing obvious symptoms can be exposed to extra tests, different types of imaging and invasive techniques such as angiogram are done for a more conclusive diagnosis, despite the fact that it can convey critical dangers that must be deliberately gauged. This invasive method where a part of the body is catheterized, either by puncture or incision is the current method of diagnosis. This medical procedure is painful as well as time-consuming for patients who are suspected of illness in the blood circulatory system.

By developing a medical system that monitors and provides risk indication non-invasively for healthy users, one can significantly reduce the risk of sudden cardiac arrest among users by creating awareness on their health status all the time. The medical system will acquire radial waves for predicting possibilities of a patient having a cardiovascular risk. Additionally, the medical system will lay a foundation in developing a wearable device that will reduce the patient's frequent visit to the hospital as it provides regular monitoring. It would be convenient to wear, thus, can be used throughout the day.

Central aortic pressures signal has the factors of cardiac loading and perfusion which is important on cardiovascular function [14]. Information of this signal is often crucial for

precise monitoring and diagnosis of cardiovascular diseases [14]. However, central aortic pressure signal is currently obtained invasively, it would be ideal if the central aortic blood pressure waveform can be accurately estimated. In this research, the medical system is placed on the wrist of the user, hence the radial blood pressure waveform needs to be utilized to estimate the nearest representation of the aortic blood pressure waveform to be used as a risk indicator.

By collecting and analysing various radial wave signals and converting to the nearest estimation of the aortic blood pressure waveform, the patterns of healthy and unhealthy signals can be identified by feature extraction, and the algorithm formed can be integrated into the hardware.

1.4 Problem statement and project direction

Analysing the wearables described above, the main point of focus on the systolic pressure reading which is related to hypertension. Which is treated as a key indicator for cardiac risks and has generated many debates and editorial commentaries[15]–[17]. Alternatively, by analyzing the entire blood pressure pulse, rather than just the systolic and diastolic values, more information about the health condition of the user could be obtained. As current devices do not focus on this aspect, this research aims to investigate this.

In clinical diagnoses, it is known that central aortic pressure is a better physiological indicator for diagnosing diseases [18]–[20]. However, measuring central aortic pressure waveform is an invasive and expensive procedure. In hospitals, to measure the central aortic pressure non-invasively, blood pressures measured non-invasively from peripheral locations are taken and approximated. An example of this is the use of a brachial oscillometer [21]–[24] where the reading of the brachial artery is used to estimate the reading of the central aortic blood pressure. In addition, current research shows a lot of interest in investigating the relationship of central aortic pressure and peripheral pressure at the location of brachial, radial, carotid, and femoral arteries to be used as a risk factor for cardiovascular diseases [25]–[29]. Therefore, this research focuses on developing a medical system which acquires the signal from the wrist (radial artery) of a normal user to estimate the aortic blood pressure waveform, which will then be used

to indicate the risks. This would alert the user to be aware of their health conditions and identify the risks associated to CVD.

Once the central aortic blood waveform has been estimated, risk indication needs to be performed, and one of the key methods being used is artificial intelligence. In today's research world, numerous research [30]–[33] are published, relating artificial intelligence to diverse areas of importance to the cardiovascular expert. Majority of the implementation of artificial intelligence are on the blood pressure signal directly from the radial artery from the wrist [34]. This research intends to utilize the central aortic blood pressure waveform as the blood pressure signal to indicate risk, because it is the gold standard blood pressure measurement internationally [34] whereby it has a better physiological indicator for diagnosing diseases. However, there is an imbalance of data for the central aortic blood pressure waveform where hospitals would only provide diseased central aortic blood pressure waveforms. It is worth highlighting that doctors will not perform angiograms on subjects who appear healthy and the proposed medical system is intended for healthy users. This problem is addressed by introducing a zero-dimension (0D) model that would provide data of the central aortic blood pressure waveform to be utilized for the risk indicator.

The zero-dimension (0D) model of the cardiovascular system was developed to simulate the global hemodynamics of the entire circulation system as a lumped circuit model. This 0D model is able to simulate the aortic blood pressure waveform. The model represents the blood pressure and flow-rate with voltage and current, describing the effects of friction and inertia in blood flow and of vessel elasticity with resistance R, inductance L and capacitance C in the electric circuit respectively [35]. The 0D model utilizes the hydraulic-electric concept where non-linearities in cardiovascular mechanics including the convective acceleration terms in the momentum equation and/or the nonlinear relationship between pressure and volume in a real vessel can be specifically addressed in solving the governing equations [35]. Sensitivity analysis is done later in this work, to identify the R, L and C parameters which contributes to changes in the aortic blood pressure waveform of the 0D model. There are two type of sensitivity analysis which are the local sensitivity analysis (LSA) and the global sensitivity analysis (GSA). LSA is a sensitivity analysis technique that iterates one parameter value at a time around its default value by keeping the rest of the other parameters fixed at their default values [36], [37]. This procedure is repeated for all the parameters to

study the parameter's independent response to the output signal. On the other hand, the GSA is an advanced technique compared to the LSA that explores the interrelationship and the entire parameter response on the output signal [38]–[41]. When comparing the LSA and GSA, it is known that LSA is simple, easy to implement and computationally less expensive compared to the GSA. This research utilizes LSA as the sensitivity analysis technique because it is less computationally intensive and it studies the parameter's independent response to identify the significant parameter that affects the feature of the model's output signal.

These significant parameters are trained into the Artificial Intelligence (AI) whereby when a blood pressure signal is fed to the AI, the numerical change in each parameter will be output and will be used to identify the cardiac risk for the user. In this research, the artificial intelligence is built based on the feature extraction of the aortic pressure wave using the convolutional neural network. This artificial intelligence establishes the relationship between the independent response of the R, L and C parameters to the 0D model's aortic blood pressure by the sensitivity analysis conducted. The insignificant parameters are not utilized to train the artificial intelligence because there would not be a significant change in the signal's feature which may provide trivial information to the AI, consequently contributing errors.

In addition, since the 0D model has multiple degree of freedom to reconstruct the same aortic blood pressure waveform with different variables, the AI resolves this problem because it is constrained to the data it is trained with from the sensitivity analysis. Therefore, an input of a blood pressure signal will give a specific output of R, L and C parameters in respect to the sensitivity analysis conducted to the 0D cardiovascular model, where the change in the numerical values is analysed to indicate risk to the user.

1.5 Research Aims and Objectives

The aim of this work is to develop a medical system for users to detect and indicate blood circulatory system risk by analysing the blood pressure signal where the system is strapped on the user's wrist. In order to achieve the aims of the proposed research, the work here was broken down into specific objectives which are as follows:

1. Identify a sensor to acquire the radial blood pressure signal in order to develop a prototype.
2. Identify and implement a method to convert a radial blood pressure waveform to an aortic blood pressure waveform which has the closest representation of the actual aortic blood pressure waveform.
3. Utilize the converted aortic blood pressure waveform for indicating risk by the implementation of a convolutional neural network.
4. To develop an algorithm for the risk identification for healthy users from the radial blood pressure waveform data collected, based on the features of blood pressure wave variations.
5. To validate the developed algorithm against clinical patient data.

1.6 Research scope

The main scope of this study is to create a medical system capable of indicating risk of cardiovascular disease to the users, by implementing a convolutional neural network on the upstream blood pressure waveform, which is the central aortic blood pressure waveform, while the medical system would be strapped on the user's wrist. Hence, a conversion from a radial blood pressure waveform to an estimation of the aortic blood pressure needs to be done. The system is broken into 3 key subsystems – the wearable device (prototype), radial to aortic blood pressure waveform conversion, and finally risk indiciation. For each subsystem, choices are made in this research to prove that the proposed medical system with the said subsystems works with an acceptable performance, and further in-depth research can be carried out in the future for each subsystem to improve the overall performance.

As data for healthy aortic blood pressure waveform of humans is not available in today's world, because angiogram's are not conducted on healthy subjects, this research utilizes Vincent Rideout's zero-dimension complete cardiovascular loop model system's default aortic blood pressure waveform to create the data set for the convolutional neural network. The Local Sensitivity Analysis technique is conducted on the model to identify the independent response of each parameter to the model's aortic output signal whereby the parameters and the response signals are used to identify the significant parameters that were used to create the datasets. Hence, the convolutional neural

network doesn't remodel the Vincent Rideout zero-dimension model but develops a relationship between the parameters and the aortic blood pressure signals in respect to the independent response of each parameter attained by the local sensitivity analysis.

In its current form, the developed medical system is restricted to the usage of blood pressure signals obtained using an invasive method due to the wearable device being at the prototype stage and not viable for data collection in a medical setting. This research is done in collaboration with Collaborative Research in Engineering, Science and Technology (CREST) Malaysia and Chulia Facilities Management Sdn. Bhd, and the core requirement of this research was to identify a sensor to acquire the radial blood pressure signal in order to develop a prototype as well as a risk indication system, which could be embedded in it. Following the identification of the sensor in this study, Chulia Facilities Management Sdn Bhd will continue to develop the wearable device.This prototype uses Arduino as its current computing platform, though this does not restrict other available wearable devices to be utilized for the implementation of this medical system.

The datasets for validating the medical system were obtained via an invasive method from Hospital Sultanah Bahiyah, and online sources: HaeMod database and PhysioNet database. As previously mentioned, doctors will not perform angiograms on subjects who are healthy. Hence, the HaeMod database is an ideal choice for this research as it has many healthy subjects' blood pressure waveform. Physionet has both cardiovascular disease subjects and non-cardiovascular disease subject's radial waveforms, which will be used in this research to identify unhealthy blood pressure signals. Both the HaeMod and Physionet databases were verified by Dr. Saravanan Krishinan, the Head of Hospital Sultanah Bahiyah's Cardiology Department. The computer programming language used to conduct this research is MATLAB.

1.7 Research significance

The development of a medical system to indicate risk of cardiovascular disease allows the user to discern their condition before the consequences lead to an undeniable indication, which is usually at the crucial stage, resulting in a significant risk of death. Early identification and prevention are critical to decrease cardiovascular mortality. This might be accomplised by having a reliable medical system that would indicate risk for people's cardiovascular condition. In the current age, there are several wearables that

estimate the central aortic blood pressure waveform from the peripheral artery (radial artery) pulses to continuously update the user on their blood pressure reading (systolic and diastolic). This is used to determine hypertension as a risk indicator for cardiovascular disease, which is not the most ideal approach according to several other research as previously mentioned. Hence, there is a lack in today's available medical device systems to analyze the entire blood pressure pulse to provide reliable information to indicate risk of cardiovascular disease.

In addition, recent developments in biomedical engineering research, specifically in biomedical signal analysis, the entire blood pressure pulse waveform was utilized in training deep learning models. According to them, Convolutional Neural Networks (CNN) are the ideal deep learning method as they mimic the human's neuron network interpreting the entire signal with regards to the signal's features to relate to the cardiovascular disease [42]–[46]. However, these CNN models are used for pattern/feature classification and does not indicate risk or act as a predictive role for cardiovascular disease.

During the development of this medical system, novelty was introduced in the risk indication algorithm by applying CNN with a numerical regression output trained with parameters of the zero-dimensional cardiovascular model to indicate risk of cardiovascular disease. A pressure sensor acquires the radial waveform from the user's wrist and transforms it to an estimated aortic blood pressure waveform using a transfer function, which is then fed into a CNN trained with a zero-dimensional cardiovascular model's parameters to be applied for risk prediction. The hardware and software foundation for the medical system to indicate the risk of cardiovascular disease in this approach has yet to be studied and established in today's world. The overall system is built on 3 key subsystems, and this unique combination and connections between the subsystems in a novel method proposed in this research. The created system could also be continuously improved by either improving or replacing the methods in each subsystem, giving rise to more possible risk indicators and performances. Other significant novelties are present in the form of a newly developed transfer function for converting radial to aortic blood pressure waveforms (EIF), as well as the combination of CNN and 0D model for risk indication.

1.8 Research impact and contribution

Sustainable human development is strongly influenced by CVD which is one of the major reasons for mortality in the world [47]. Up to 422.7 million and 17.92 million people died of CVD all over the world in 2015 [48]. It is highly recommended in clinical practice to screen high-risk population, and early intervention of CVD would be ideal [49]. The challenges of prediction and evaluation of potential CVD remains unsolved despite a lot of effort taken by the medical community [49]. Research shows that cardiovascular coincidences occur at uneven distribution during 24 hours of the day [50] and has a high tendency to occur during the moment between wakefulness and sleep instead of later in the day [51]. However, the reason for the increase in cardiovascular occurrences in the morning is still unclear [51]–[56]. Patients normally visit the hospital for a medical check-up during the day which results in blood pressure monitoring. Isolated clinic blood pressure measurements from patients are not satisfactory to represent the daily blood pressure of the patients away from the medical environment over the last 50 years [57], [58]. Blood pressure measurements taken during daily activities by continuous ambulatory blood pressure monitoring will provide a more valid evaluation of a patient's true blood pressure reading [59]. In addition, inconsistency in heart rate over 24 hours is an important indicator of the disease progression [60], [61]. Hence, a continuous monitoring medical system would be ideal for a patient to be aware of their health condition and to be able to be on time to get the treatment from doctor before the critical stage. A medical system to monitor healthy users and indicate CVD risks is yet to be developed in the present-day context.

The main research contribution is indicating risk for healthy users using electrical parameters obtained from the combination of the zero-dimension cardiovascular circulatory system and a convolutional neural network. Hence, the numerical changes in the parameters shall be analysed to classify the risk of irregular blood circulation which may lead to a cardiovascular disease, so that the user is well aware of their health condition. These parameters can then be utilised further by the medical practitioners as a reference to correlate the patient's parameters before prescribing a treatment.

The success of proving this research methodology is very impactful to the world because it may give reasonable hope to construct a wearable device which would guarantee persistent monitoring and risk indication to the user. This would ensure the user to

be aware of their health and identify the risk of illness before the symptoms shows obvious signs, usually at the critical stage, which results in high risk of mortality.

1.9 Thesis outline

This thesis is divided into five chapters. Chapter 1 introduces the research's main aims, problem statement, the proposed solution, research aim, objectives and scope, as well as the significance and contributions of this work, Chapter 2 outlines the literature review carried out on cardiovascular disease and medical technologies, choices of the sensor, transfer function techniques in estimating aortic blood pressure waveform from the radial blood pressure waveform, risk indication for cardiovascular disease, Artifical Intelligence for detection of cardiovascular disease, cardiovascular system modelling and a summary of literature explaining the novel approach of this research. In this chapter, comparisons and choices are made for the sensors and the heart's blood flow model to be implemented for the research. Chapter 3 talks about the methodology of the research. In this chapter, system design and its methodology are explained. Besides that, the calculation related to the choice of the sensor and the implementation of the sensor hardware is presented. Electrical impedance function, Generalised transfer function, N-point moving average, Adaptive transfer function and their implementations is also shown. The model parameter values and the convolutional neural network where these parameters are fed is explained. In Chapter 4, the results obtained during the testing of the hardware are presented. Electrical impedance function study results are shown with comparisons to Generalised transfer function, N-point moving average and Adaptive transfer function. Results obtained by the parameter model and its values, which are fed into the convolutional neural network (CNN) are presented. The results of the prediction of the CNN and the results of classification of data for cardiovascular disease and non-cardiovascular disease are well explained. These results are discussed to get a better understanding of the cardiovascular risk prediction proposed in this research. Lastly, Chapter 5 concludes the thesis, by summarising the key points of the overall developed system.

CHAPTER 2 : LITERATURE REVIEW

2.1 Introduction

The persistent overall incline in deaths due to cardiovascular disease has instilled motivation for researchers to develop strategies and methods to assist medical professionals. These areas of research on the development of a medical system to indicate risk of cardiovascular disease have been growing gradually, yet are to be implemented in the medical world. This chapter provides a literature review on understanding cardiovascular disease and recent medical technologies used for risk indication for cardiovascular disease to obtain a better understanding of the recent advances in this field. Additionally, the medical technology subsection discusses the selection of sensors to obtain the radial blood pressure waveform. Since most medical technology acquires the radial blood pressure waveform from the wrist and estimates the aortic blood pressure waveform, transfer function methods to estimate the aortic blood pressure waveform have been reviewed to gain a better understanding of them. That knowledge can be then used to convert the radial pressure signal obtained from the patient's wrist to their respective aortic signal in this project. This chapter addresses risk indication for cardiovascular disease and artificial intelligence for detection of cardiovascular disease in order to comprehend and create a risk indication algorithm that incorporates artificial intelligence. Furthermore, cardiovascular models are evaluated in order to determine the heart's response and reaction to other factors without the requirement for patient testing. To summarize the interpretation of the literature to be used for this research, a review of equivalent work and a summary of the literature review were done.

2.2 Cardiovascular disease

Cardiovascular disease continues to be the dominant cause of demise worldwide, resulting in deaths that are higher than 17.3 million per year [62]. A study conducted by The Global Burden of Disease in 2010 concludes that 29.6% of all deaths globally were resulted by cardiovascular disease [63] and the percentage increased to 31% in 2013 [62]. Studies also show that cardiovascular diseases show higher mortality than all forms of cancer combined [62]. An estimated 17 million people died from cardiovascular disease in 2005, which represents 30% of all global deaths; reported by the World Health Organization (WHO). The WHO also estimates that the number could increase to 23.6 million by the year 2030 if the current trend remains [64] where it incorporates

coronary heart disease (CHD), cerebrovascular disease and arterial disease. Figure 2.1 shows the graphical representation of the major cause of deaths.

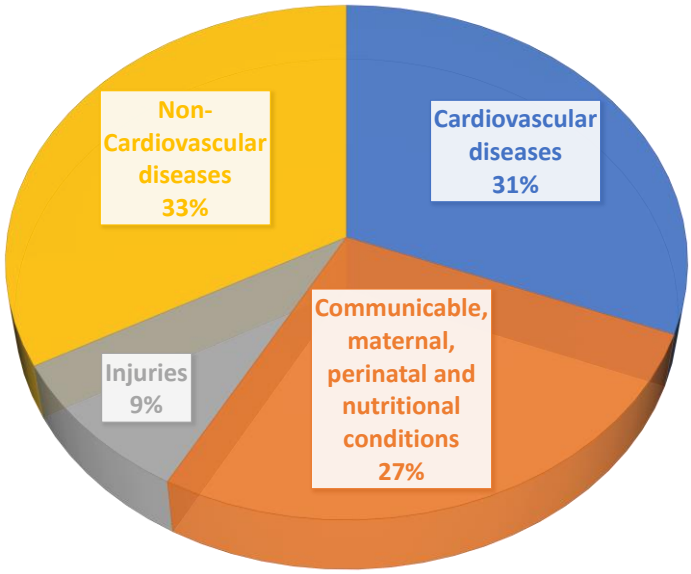

Figure 2.1.Major causes of death

In addition, Cardiovascular disease (CVD) includes several conditions that affect the heart and vasculature [65]. This may also include those influencing the blood vessels, for example, coronary artery, peripheral artery, or cerebrovascular infection. The basic reason for diminished bloodstream is the development of atherosclerotic plaque, which brings about the narrowing of veins and confines bloodstream [66]. This expansion is related to an increase in smoking and dietary changes provoking an addition in serum in cholesterol levels [67], [68]. The chronic CVD can hasten into a solitary horrible mishap whenever it is left untreated, for example, myocardial infarction or stroke, the two of which are related to high death rates [69]–[72]. Moreover, CHD and cerebrovascular disease were the first and second reasons for demise in 2016, with a rise of 39.6% and 23.8% individually since 2005 [18]. According to the National Cardiovascular Disease-Acute Coronary Syndrome (NCVD-ACS) Registry for 2011-2013, 96.8% of patients had at least one cardiovascular hazard factor, for example, hypertension [73].

Screening tests and increasingly complex examinations for the early detection of ischemic coronary illness are sketched out. They can be depended upon to distinguish the individuals who are susceptible to heart disease in future. Screening in essential primary

settings and frequent wellbeing advancement to increase community awareness and responsibility to healthy living and care should be constantly emphasized [73].

It is accepted that a greater part of the deaths due to CVD are totally preventable by fundamental alterations in lifestyle habits [74]–[77]. While this underlines the significance of improved instruction and a huge scope counteraction activities, it additionally focuses on the significance of having successful methods for distinguishing indications of ailment in the clinic, especially at an early stage [77]–[79]. Sustainable human development is strongly influenced by CVD which is one of the major reasons for mortality in the world [47]. Up to 422.7 million had CVD and 17.92 million people died of it all over the world in 2015 [48]. It is highly recommended in clinical practice to screen a high-risk population and early intervention of CVD [49]. The challenges of prediction and evaluation of potential CVD remains unsolved despite a lot of effort taken by the medical community [49]. Research shows that cardiovascular coincidences occur at uneven distribution during the 24 hours of the day [50] and has a high tendency to occur during the moment between wakefulness and sleep instead of later in the day [51]. However, the reason for the increase in cardiovascular occurrences in the morning is still unclear [51]–[56]. Patients normally visit the hospital for a medical check-up during the day which results in blood pressure monitoring. Isolated clinic blood pressure measurements from patients are not satisfactory to represent the daily blood pressure of the patients away from the medical environment over the last 50 years [57], [58]. Blood pressure measurement taken during daily activities by continuous ambulatory blood pressure monitoring will provide a more valid valuation of a patient's true blood pressure reading [59]. In addition, inconsistency in heart rate over 24 hours is an important indicator of the disease progression [60], [61]. Hence, a continuous monitoring medical system would be ideal for a patient to be aware of their health condition and to assist the doctor in prescribing treatment.

Coronary artery disease (CAD) is the common type of cardiovascular disease that involves angina pectoris and myocardial infarction commonly known as heart attack [80]. Other types of cardiovascular diseases include heart failure, stroke, rheumatic heart disease, venous thrombosis, peripheral artery disease, congenital heart disease, blood vessels disease and heart valve disease [80], [81]. One of the main underlying cause of coronary artery disease, stroke and diseases of the aorta and arteries are known as atherosclerosis which is the narrowing of the arteries wall due to the deposition of fatty

deposits, known as atheroma [80]. The deposits cause the inner surface of the arteries to become irregular and narrow, hence disrupting the blood flow. Eventually, atheroma in the arteries can break away, causing the formation of a blood clot. When the blood clot blocks the artery that transports blood to the brain, the blood supply to the part of the brain is cut thus causing stroke [59]. Similarly, when the blood clot occurs in the coronary artery, it can lead to a heart attack.

Several risk factors may contribute to an increased likelihood of developing cardiovascular diseases, such as genetics, age, gender, ethnic background, smoking habits, high blood pressure, high blood cholesterol, obesity and diabetes. Inherited DNA sequence, which is a form of a fixed risk factor increases the possibility of an offspring developing cardiovascular disease, by 3 times if the parent has a history of cardiovascular disease [82]. Besides that, mortality is also found to be higher by 2.3 to 2.7-fold for every decade of life for men and 2.9 to 3.7-fold for women in terms of gender [83]. The risk factor of gender also shows that men are more vulnerable to cardiovascular diseases than pre-menopausal women [84] due to the oestrogen hormone that is present in women which improves the endothelial cell function and functioning as a defence [85].

Lifestyle and behavioural changes such as mindful eating and implementing physical exercises into daily life are highly recommended. For instance, it is found that diets rich in saturated fat leads to 31% of coronary heart disease and 11% stroke worldwide [86]. On top of that, it is also important for a person to always be updated on their current health status through regular medical check-ups for early detection and prevention.

For early detection and prevention, blood pressure is one of the biggest indicators of cardiovascular diseases during a medical check-up. Blood pressure mirrors the contracting and relaxing of arterial walls that creates pressure waves, which is known as a pulse wave signal [87]. The pressure sensor is best in detecting arteriosclerosis, a condition of thickening and the hardening of blood vessels and deposition of plaque on the inner walls of the vessels that creates blocks and ultimately leads to cardiac arrest. Therefore, using the pressure sensor to detect and collect wrist pulse signals can assist in conducting further studies on better arteriosclerosis prediction [88], [89].

Besides arteriosclerosis, arrhythmia is another form of cardiac diseases which can be detected by using the same pulse wave signal. Arrhythmia is an abnormal electrical activity in the cardiovascular system where it’s irregularity that will appear in the signal

reflecting the increase and decrease of heart rate. In addition to that, the time variance that exists between continuous pulses exceeding the average level, incomplete waveform and merged waveform will also further help to detect arrhythmia by using pulse wave signals [90].

2.3 Medical technology

Constant and rapid technological advancement, especially in mobile and electronic healthcare has significantly expanded the capabilities of physiological monitoring such as the usage of wearable devices in recent times. A wearable device is a smart electronic device that is small enough to be worn on a human body and also able to incorporate powerful sensor technology for collecting and providing information about its surroundings. Wearable devices are currently used in healthcare services in the medical world, ranging from clinical-centric to patient-centric services, known as telemedicine. There are two types of telemedicine, namely live communication and store-and-forward. Live communication telemedicine functions by creating a real-time communication between the doctor and the patient by using a wearable device that is equipped with high bandwidth and good data speed for timely data transmission. Meanwhile, store-and-forward telemedicine functions by collecting and storing the patient's medical data on their specific medical condition to be passed to the doctor for assessment upon request [91]–[94]. It has become easier for doctors to monitor a patient's body response constantly if the patient is using a wearable device [95]–[97]. Moreover, some intermediate level of local real-time classification is proposed by researchers, for example, the classification of heart rates, by utilizing smartphones or Personal Digital Assistants (PDAs) [98]–[101]. These methods have yet to give a total CVD diagnosis solution [102]. There are also telemedical functionalities through remote real-time monitoring system where most of it uses (PDAs) to collect Electrocardiography (ECG) where those signals are sent to a monitoring centre for analysis and classification, subsequently denying the user for the continuous outcome of their health [103]–[105].

Wearable devices are also useful to patients as it gives the patient flexibility to carry out their daily routine while ensuring that their health is constantly monitored. When a patient performs various activities throughout the day, medical monitoring is widened as a bigger range of data can be obtained to provide better analysis for any conditions that may be present [106]. Patients who live further away from medical centres can benefit from using a wearable device as it allows monitoring of chronic cardiovascular

diseases such as heart attack, by using a wireless monitoring system, reducing the patient's travelling frequency to hospitals [107]. Furthermore, a wearable device can also be made an integral part of routine care for acute or chronic diseases as it will provide information to both the hospital and the patient, raising the awareness level of both parties on the patient's health condition [94]. Several wireless and sensor technologies have been developed, such as finger-ring sensors [108], smartwatches [109]and mobile applications [110], [111], to help patients understand and control their heart conditions in their daily lives. Studies show that patients who are more aware of their health condition tend to give higher importance in bettering their lifestyle and habits [112], [113].

The common way of monitoring health condition is to monitor a person's blood pressure. In today's technological era, the wearable device can monitor a person's blood pressure. This wearable device is placed at the user's wrist where the radial artery is located. There are three types of sensors that are used universally to measure signals from the radial artery which are: pressure sensors such as strain gauges, photoelectric sensors such as plethysmography and ultrasonic sensors such as Doppler. Table 2.1 shows the current available medical technologies and their type of sensors. Table 2.2 shows the accuracy, sensitivity and specificity of the three types of sensors which are pressure to measure the blood pressure waveform, photoelectric for measuring the pressure-dependent vessel diameter change and ultrasound sensor for measuring the blood flow.

Table 2.1.Summarizes currently available medical technologies for measuring central blood pressure.

Medical technology	**Type of care**	**Site of record**	**Type of sensor**	**Estimation method**	**Pressure calibration**	**Invasive validation**	**FDA aproval**
ABPM 7100Welch Allyn, Inc (acquired by Hillrom)	Ambulatory care	Brachial artery	Brachial cuff pulse volume plethysmography	Generalised Transfer Function	Brachial cuff SBP/DBP	No	No
ARCsolver + VaSeraVS-1500Austrian Institute of	Non-Ambulatory care	Brachial artery	Brachial cuff pulse volume plethysmography	Generalise Transfer Function	Brachial cuff SBP/DBP	Yes[114]	Yes

Technol-ogy, Austria							
Arterio-graph 24 h, TensioMED Ltd., Hun-gary	Ambu-latory care	Bra-chial artery	Supra-sys-tolic bra-chial cuff plethys-mography	SBP2 + re gression	Brachial cuff MAP/DBP	Yes [115], [116]	No
Arteri-ographTen-sioMed Ltd., Hun-gary	Non-Ambu-latory care	Bra-chial artery	Supra-sys-tolic bra-chial cuff plethys-mography	SBP2 + re gression	Brachial cuff MAP/DBP	Yes	No
BP + Usco m Ltd., Aus-tralia (ac-quire Pulse-cor Ltd., Cardio-scope II)	Non-Ambu-latory care	Bra-chial artery	Supra-sys-tolic bra-chial cuff plethys-mography	Physical model Brachial supra-sys-tolic wave-form	Brachial cuff SBP/DBP	Yes [117]	No
BPLab Petr Telegin, Russia	Non-Ambu-latory care	Bra-chial artery	Brachial cuff pulse volume plethys-mography	Generalise Transfer Function	Brachial cuff SBP/DBP	Yes [118]	Yes
BPro + A-Pulse, Health-STATS, Singapore (acquired by Hillrom)	Ambu-latory care	Radial artery	Applana-tion to-nometry Single, fixed (watch type	N-point moving average	Brachial cuff SBP/DBP	Yes [9], [12], [13]	Yes
cBP301Cen tron Diag-nostics, UK (acquired bySunTech Medical)	Non-Ambu-latory care	Bra-chial artery	Brachial cuff ple-thysmog-raphy	GTF	Brachial cuff SBP/DBP	Yes [119]	Yes
Complior Alam Medi-cal, France	Non-Ambu-latory care	Carotid artery	Applana-tion to-nometry, Single, fixed	Simple substitu-tion	Brachial cuff MAP/DBP	Yes [120]	No

DynaPulse Pulse Metric Inc, USA	Non-Ambulatory care	Brachial artery	Supra-systolic brachial cuff plethysmography	Physical model	Brachial cuff SBP/DBP	Yes [121]	Yes
GaonHanbyul Meditech, Korea	Non-Ambulatory care	Radial artery	Applanation tonometry Single, fixed	Generalise Transfer Function	Brachial cuff SBP/DBP	Yes [122]	Yes
HEM-9000AI Omron Healthcare, Japan	Non-Ambulatory care	Radial artery	Applanation tonometry Arrayed [123], fixed	SBP2 + regression	Brachial cuff SBP/DBP	Yes [10], [124]–[126]	No
Mobil-O-Graph NGI.EM GmbH, Germany	Ambulatory care	Brachial artery	Brachial cuff pulse volume plethysmography	Generalise Transfer Function	Brachial cuff SBP/DBP	Yes [11]	Yes
Mobil-O-GraphI.EM GmbH, GermanyBrachialartery	Non-Ambulatory care	Brachial artery	Brachial cuff pulse volume plethysmography	Generalise Transfer Function	Brachial cuff SBP/DBP	Yes [11]	Yes
NIHem Cardiovascular Engineering Inc, USA	Non-Ambulatory care	Carotid artery	Applanation tonometry, Single, manual	Simple substitution	Brachial cuff MAP/DBP	Yes [127]	No
Oscar 2 with SphygmoCor SunTech Medical, USA-Brachial	Non-Ambulatory care	Brachial artery	Subdiastolic brachial cuff plethysmography	Generalise Transfer Function	Brachial cuff SBP/DBP	Yes	Yes
Oscar 2 with SphygmoCor, SunTech Medical	Ambulatory care	Brachial artery	Subdiastolic brachial cuff plethysmography	Generalise Transfer Function	Brachial cuff SBP/DBP	Yes [128]	Yes

PulsePen DiaTecne srl., Italy	Non-Ambulatory care	Carotid artery	Applanation tonometry Single, manual	Simple substitution	Brachial cuff MAP/DBP	Yes [129]	No
Sphygmo-Cor XCELAtCor Medical, Australia	Non-Ambulatory care	Brachial artery	Subdiastolic brachial cuff plethysmography	Generalise Transfer Function	Brachial cuff SBP/DBP	Yes [130]	Yes
Sphygmo-CorCVMS, AtCor Medical, Australia	Non-Ambulatory care	Radial artery	Applanation tonometry Single, manual	Generalise Transfer Function	Brachial cuff SBP/DBP	Yes [9]–[11], [14], [131]–[135]	Yes
Vicorder Skidmore Medical Ltd., UK	Non-Ambulatory care	Brachial artery	Brachial cuff pulse volume plethysmography	Generalise Transfer Function	Brachial cuff MAP/DBP	Yes [132], [136]	Yes
WatchBP Microlife Corp, Taiwan	Non-Ambulatory care	Brachial artery	Brachial cuff pulse volume plethysmography	(SBP2, DBP, As, Ad) + regression	Brachial cuff SBP/DBP	Yes [137], [138]	Yes
WatchBP O3, Microlife AG, Widnau, Switzerland	Ambulatory care	Brachial artery	Brachial cuff pulse volume plethysmography	(SBP2, DBP, As, Ad) + regression	Brachial cuff SBP/DBP	Yes [139]	Yes

Table 2.2 Diagnosis performance of the three types of sensor[140]

	Accuracy	**Sensitivity**	**Specificity**
Pressure	86.4%	87.6%	85.2%
Photoelectric	79.3%	83.1%	75.8%
Ultrasonic	83.7%	85.4%	82.1%
Combination of three types of signals	89.7%	91.0%	88.4%

After comparing these three electronic sensors through Table 2.2, it can be concluded that a pressure sensor may best suit the need to develop the medical device for continuous monitoring. The pressure sensor has the best accuracy, sensitivity and specificity to detect the radial pulse wave compared to the photoelectric and ultrasonic sensors. Pressure sensors (Strain gauge sensor) also echoes the way a traditional diagnosis is done to a certain extent besides generating pulse wave signals with less noise as compared to the photoelectric sensor and ultrasonic sensor.

2.3.1 Pressure sensor

The pressure sensor is a type of sensor that is used to determine the transmural pressure at the radial blood vessel to obtain the wrist pulse signal. Figure 2.2 below shows the radial pulse wave signal that was formed using pressure sensors. Figure 2.3 below shows the parameters which can be obtainable through a pressure sensor reading.

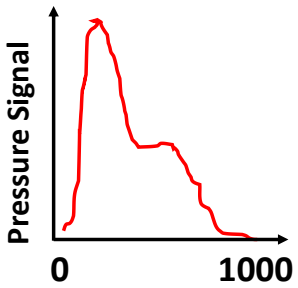

Figure 2.2. Radial pulse wave obtained from pressure sensor [140]

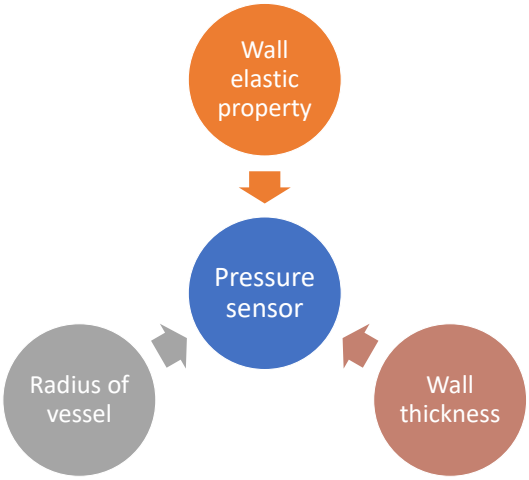

Figure 2.3. Parameters obtainable by readings from the pressure sensor [140]

There are a lot of researchers working on pressure sensors. For example, M.Sharmila et.al, [141] have done research on diagnosing diseases through radial pulse wave signal

using a piezoelectric sensor. The research objective was to obtain a radial pulse wave signal from the wrist and relate it to the Indian traditional method of diagnosis. The Indian traditional method takes the pulse from the wrist by using three fingertips. The three energies which significantly influence the pulse rhythms that can be detected using the fingertips are called Kapha, Pitta and Vata. Therefore, three pressure transducers were attached at the wrist to obtain the three pulses. The first sensor which was used was '1 PSI' pressure sensor from 'Sensym Products'. This was a failure as it was unable to capture intricacies of the pulse. Therefore, 'Millivolt Output Medium Pressure Sensor' form Mouser Electronics, Inc was used which could be seen in Figure 2.4. There is a tiny diaphragm at the centre which has '0–4 inches H2O' pressure range. The data was captured with a sampling rate of 500Hz by using 16-bit multifunction data acquisition card NI USB-6210 which inter-links to collect data from the pressure sensor. Lab view was used as the data acquisition software to control the digitization. The research had two phases [141]. Figure 2.5 shows the flow of how the research was conducted.

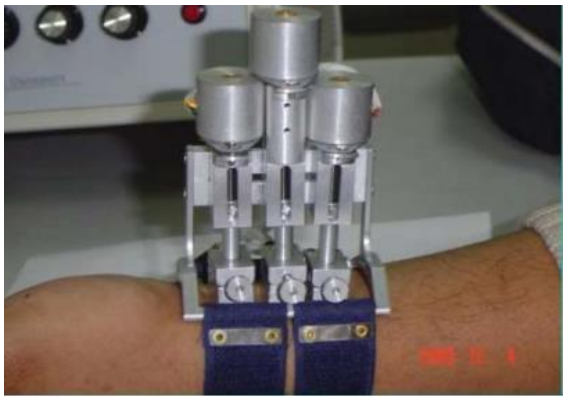

Figure 2.4. The sensor of reading the (Vata, Pitta and Kapha data) [141]

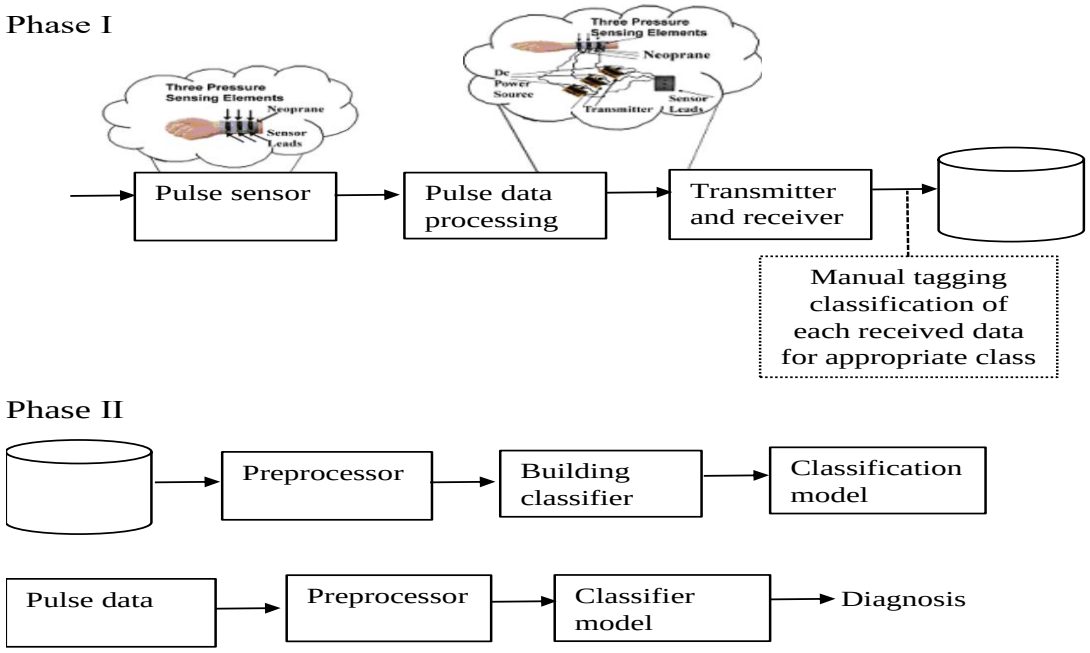

Figure 2.5. The flow of the research which has two-phase by M.Sharmila et.al [141]

Suket, et al. had used a pressure sensor to obtain a radial pulse wave signal. The work was mainly about wrist pulse acquisition and recording system. The pressure sensor which was used for this project was MPXM2053D piezo-resistive pressure sensor [142], as shown in Figure 2.6. Along the line, ARM Cortex M4 architecture was used for digitization of signals and fed into the LCD for real-time monitoring. The signals were recorded into a micro SD memory card for offline processing and analysis. The purpose of the project was to have a better understanding of the wrist pulse wave signal and to support the Ayurvedic practitioner to detect pulse wave signals [143] . Figure 2.7 shows the wrist pulse signal data which was stored in an Excel sheet.

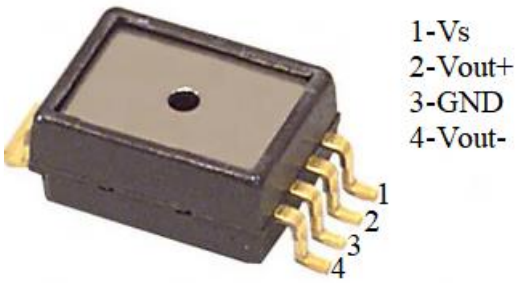

Figure 2.6. MPXM2053D piezo-resistive pressure sensor [142]

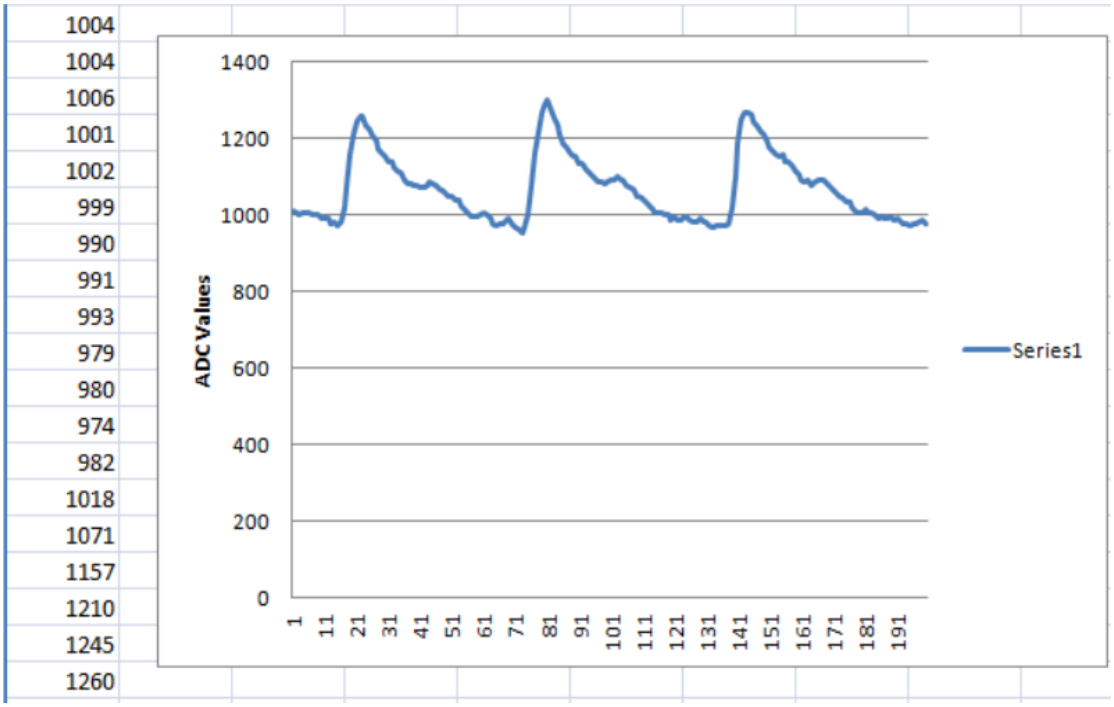

Figure 2.7. Wrist pulse signal data stored in excel sheet [143].

Research about flexible polymer transistors with high-pressure sensitivity for application in electronic skin and health monitoring was done by Gregor Schwartz, et al. The research was aimed towards developing a pressure sensor by using Polydimethylsiloxane (PDMS) material. PDMS materials are from a group of polymeric organosilicon compounds which are also known as silicones. The sensor was fabricated in the form of pyramids of 3mm height, 6mm base length and 8.85mm spacing, as shown in Figure 2.8. The sensor showed that it had a response time less than 10ms due to the effect of the micro structured PDMS dielectric upon pressure release [144]. The result of this research is shown in Figure 2.9.

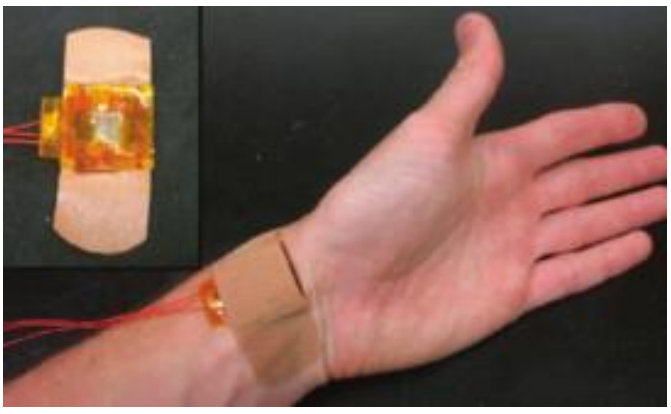

[5186940874102]: [Nature] [Nature Communication] [144], [COPYRIGHT] (2013)

Figure 2.8. Sensor measuring the radial pulse wave of the patient [144]

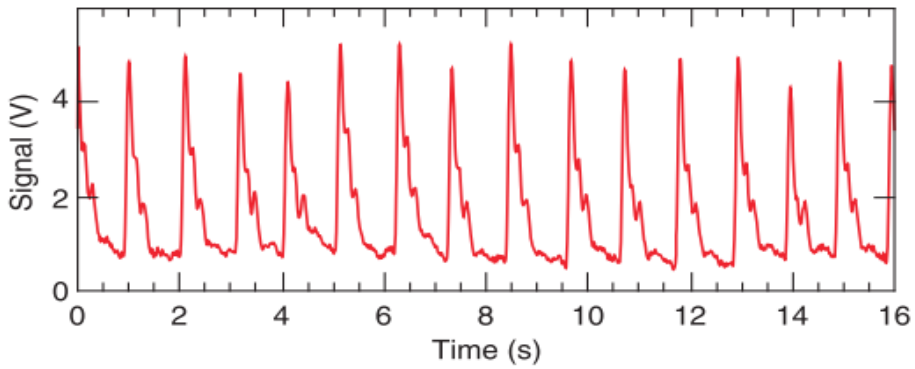

[5186940874102]: [Nature] [Nature Communication] [144], [COPYRIGHT] (2013)

Figure 2.9. A real-time signal of the radial pulse wave [144]

Choon Meng Ting and Ngak Hwee Chua invented the Bpro watch which functions as a radial pulse wave acquisition device. This device can be used in either right or left wrist to obtain the radial pulse wave signal. The watch measures in 10-second intervals to obtain a block of the radial pulse wave signal. It can be connected through Bluetooth to ease data transfer and weighs only around 60 grams. However, it has onboard memory to save only 96 blocks of radial pulse wave signals. The watch monitors systolic and diastolic blood pressure, heart rate, central aortic systolic pressure (CASP) and 24-hour blood pressure patterns. The watch currently can only diagnose hypertensive patients [145], [146]. Figure 2.10 and Figure 2.11 shows the BPro® Radial Pulse Wave Acquisition Device.

Figure 2.10. BPro® Radial Pulse Wave Acquisition Device [145].

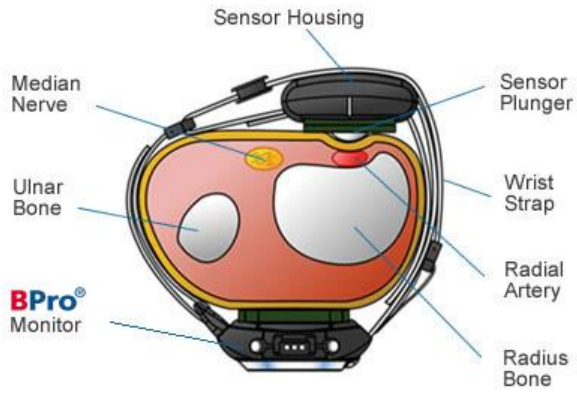

Figure 2.11. The cross-section of the wrist that the BPro® is attached [145]

2.3.2 Photoelectric sensor

The photoelectric sensor, on the other hand, is used to measure the blood volume at the radial blood vessel by transmitting light and receiving the signal by the reflected light, which is in proportion with the volume of the vessel. Figure 2.12 below shows the radial pulse wave signal that was formed using photoelectric sensors. Figure 2.13 below shows the parameters which can be obtainable through a photoelectric sensor reading.

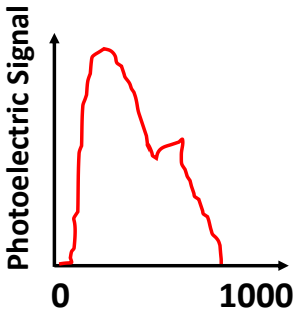

Figure 2.12. Radial pulse wave obtains from photoelectric sensor[140]

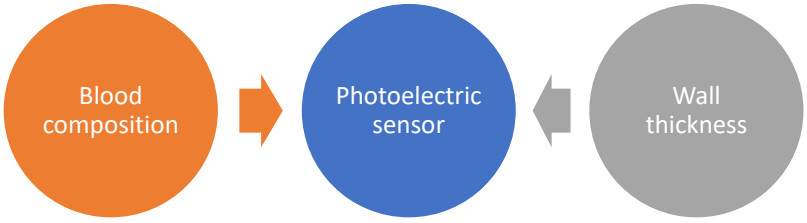

Figure 2.13. Parameters obtainable by readings from the photoelectric sensor[140]

Photoelectric sensors have various designs but all of them provide similar results where they measure the change in blood volume[147]. The change in blood volume is measured by the LEDs emitting light and using the photodiode to measure the intensity of the non-absorbed light reflected from tissue [148]. Red and green are the most common LED colours used in most studies but there are some studies showing yellow LED been used [149]. The LED light which has longer wavelengths will be able to penetrate more deeply into the tissue such as infrared light. It can penetrate deeper compared to the green light LED [150]. The infrared light which has longer wavelength do have its disadvantage where it is more prone to motion artifacts. Motion artifact is a patient-based artifact that occurs with voluntary or involuntary patient movement during data acquisition. Hence, green light LED which has shorter wavelength would be a better option in certain applications [150]. To avoid motion artifact, wearable devices nowadays are equipped with accelerometer to record the movements [149] especially during physical activity.

2.3.3 Ultrasonic sensor

The ultrasonic sensor which works similarly to the photoelectric sensor uses sound wave rather than light to measure the blood velocity in the vessel [88], [140]. Figure 2.14 below shows the radial pulse wave signal that was formed using ultrasonic sensors. Figure 2.15 below shows the parameters which can be obtainable through a ultrasonic sensor reading.

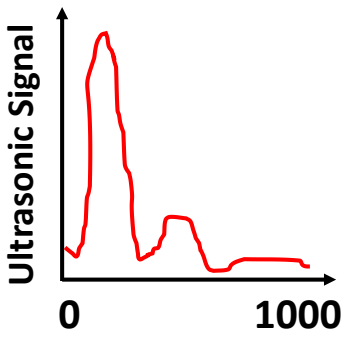

Figure 2.14. Radial pulse wave obtains from ultrasonic sensor [140]

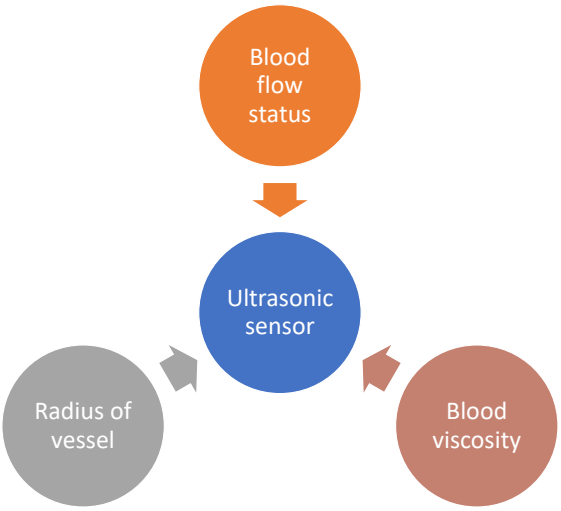

Figure 2.15. Parameters obtainable by readings from the ultrasonic sensor [140]

The ultrasonic waves can effectively penetrate human tissues up to a depth of 4cm which allows better sensing range in today's technology [151]. Moreover, the main frequency of a blood pressure waveform for an average resting heart rate of 60bpm is less than 12Hz [152], [153] which is lower than the 10 MHz frequency range of an typical ultrasonic device. An ultrasonic device can safeguard a conformal close contact with the curved skin surface when acquiring blood flow, which reduces the difficulty or instability compared to the other methods [151]. The ultrasonic sensor is similar with the cardiac ultrasound process where it uses high frequency sound wave. In doppler ultrasound, it uses an electrical signal source [154] to produce the ultrasonic wave transmitted through the human body. The doppler effect occurs when there is a change in frequency. This happens when the red blood cells move into the blood stream where the change in time from one position to another, when related to the frequency shift shows a positive or negative change depending on the direction of the blood flow. Hence, with an ultrasonic sensor, the direction of blood flow can be determined.

2.4 Estimation of central aortic blood pressure waveform from radial blood pressure waveform

In hospital practice, the blood pressure is measured using the brachial oscillometer [21]–[24] where the reading of the branchial artery is considered the same as the central aortic pressure (CAP) by clinicians[130]. Despite the fact that the branchial artery is close to the aorta artery, the branchial blood pressure waveform reading is not the same as the central aortic pressure waveform due to the wave reflection, systolic blood pressure, diastolic blood pressure, pulse pressure and mean artery pressure. It is known that

the blood pressure at the aorta and peripheral artery such as the branchial artery differs for the pulse pressure, diastolic blood pressure and mean artery pressure. Where the pulse pressure increases from the aorta to the peripheral artery while the mean artery pressure and diastolic blood pressure decreases by 1-2mmHg from the aorta to the peripheral arteries[155]–[157]. CAP waveforms have the factors of cardiac loading and perfusion which are important on cardiovascular function[14]. Information of this waveform is often crucial for precise monitoring and diagnosis of cardiovascular diseases [14]. Recent research evidence has shown that cardiovascular outcomes can be strongly related to the CAP [18], [20], [165], [57], [158]–[164]. For an instance, Agabiti-Rosei et al. has conducted a research showing that the central pressure has a closer correlation with surrogate measures of cardiovascular disease [57]. Furthermore, Conduit Artery Function Evaluation (CAFE) has studied the differential effects of interventions on central and peripheral pressure [166] and has shown that CAP provides a superior measure of hemodynamic load on the heart and central organs. CAP is commonly used to determine hypertension. Besides that, CAP has given insights into the prevention, diagnosis, and treatment of cardiovascular diseases including coronary artery disease, stroke, myocardial infarction, and heart failure[130]. Measurement of CAP is usually conducted invasively, which is not ideal for continuous monitoring or to be used as a screening tool. In today's technological world, there are commercialized wearable devices which estimates the CAP non-invasively from the peripheral artery. These wearable devices are strapped at the user's wrist to acquire the radial blood pressure waveform and estimates the CAP. Current wearable devices utilizes the radial blood pressure waveform as it would be comfortable to the user and also calibration of systolic and diastolic blood pressure using cuff-sphygmomanometric is more suitable for applying the tonometry technique at the upper limb site such as radial artery compared to another peripheral artery such as carotid artery due to the pulse pressure amplification[167]. In addition, the bony structure (radius) underlying the radial artery gives an advantage compared to other peripheral arteries where it ensures an easy and optimal applanation tonometry[167]. However, radial blood pressure waveforms must be mathematically transformed in order to attain the central aortic blood pressure waveform[167].

2.4.1 Generalized transfer function (GTF)

The common way of converting a radial pulse wave signal to the aortic wave signal is by using "generalized transfer functions" (GTF) [14], [26], [168]–[173]. GTF in time or frequency domain is used to obtain the central aortic waveform from the radial waveform by relating the aortic hemodynamic indices [14], [26], [168]. This technique assumes the relationship between the radial blood pressure waveform and the aortic blood pressure waveform is kept the same for a set of subjects with similar physiological and pathological characteristics[130]. However, errors occur, when applying a GTF generated from one specific group of patients to another group with different ages undergoing different treatment [169], [170]. The error caused by GTF is very dependent to the heart rate and blood pressure level. Hence, this should be taken into consideration when the GTF is applied to a set of subjects with different hemodynamic conditions[174]. SphygmoCorCVMS, AtCor Medical, Australia [9]–[11] was the first device accepted by US Food and Drug Administration (FDA) that utilized GTF to estimate the central aortic blood pressure waveform. This commercial device calculates the generalized transfer function by using multiple central and peripheral blood pressure waveforms which undergo a Fourier analysis. This device obtains the peripheral pressure waveform from the user which is converted to the frequency domain and multiplied with the calculated GTF, the result of this is then converted back to time domain to obtain the estimated central aortic blood pressure waveform[11], [131], [135], [168], [175], [176]. The research conducted on 30 patients by Cloud et al [177]has shown that the GTF method by SphygmoCor for estimating the central aortic blood pressure waveform underestimates the systolic pressure and overestimates the diastolic pressure of the central aortic pressure by 13.3mmHg and 11.5mmHg respectively. Since the SphygmoCor method underestimates the systolic blood pressure, it may not be suited to determine patients for hypertension because it is known that systolic blood pressure is a better predictor of hypertension risk [178]which relates to cardiac disease.

2.4.2 N-point moving average (NPMA)

A simpler method in accessing the central aortic blood pressure waveform compared to the GTF is the N-point Moving Average (NPMA). The NPMA is a first-order low-pass filter where it removes all the high frequency related pulse wave features as it travels from central aorta to the periphery[130]. The high frequency features removed by NPMA are related to wave reflections, and the NPMA provides a smooth central aortic

blood pressure waveform capable of capturing the systolic reading [130]. The N-point moving average with a denominator of one-quarter of the tonometer sampling frequency accurately defines the central aortic pressure when applied to non-invasively-acquired radial signals from the patient [12] which is utilized by BPro + A-Pulse (HealthSTATS)[9], [12], [13]. This method is also a generalised method where it will contribute error for subject variability.

2.4.3 Adaptive transfer function (ATF)

An adaptive transfer function was created by Gao, M. et al to address the limitation of GTF's population averages where the GTF is not able to adapt to the variations in the ratio of radial to aortic pulse pressure (pulse pressure (PP) amplification)[179]. There are several adaptive transfer function methods proposed to tune the GTF to obtain a more reliable central aortic pressure[180], [181]. The simple ATF for deriving the central blood pressure waveform from a radial blood pressure waveform which was developed by Gao, M. et al was able to give a greater accuracy than GTF in the low pulse pressure amplification subjects while showing a similar accuracy with high pulse pressure amplification subjects [179]. This ATF is a model based transfer function where it takes into consideration the wave travel time and wave reflection coefficient parameters of a physiologic model of arterial wave transmission and reflection[179]. From the research by Gao, M. et al, it is known that the ATF is not able to improve the estimation of the augmentation index and ejection interval of the central blood pressure waveform. This is due to the physiological model being developed by two parameters, which is too simple to adapt to the detailed features of the central blood pressure waveform[179].

2.4.4 Second systolic pressure of periphery

The attained radial or branchial blood pressure waveform can be used to estimate the systolic blood pressure reading of the central aortic blood pressure waveform by analysing the second systolic pressure of the periphery (radial or branchial)[182]. The reflected wave peak of the radial or branchial blood pressure which is the second systolic pressure waveform approximates the systolic pressure of the aortic blood pressure waveform because the pressure gradient in the blood flow from the central aortic to the peripheral are relatively small during late systole where the late systolic shoulder represents the dominant peak in most adults in their midlife [124], [182]. On the other hand, systolic blood pressure of the central aortic blood pressure waveform for older adults [131]can be calculated using a regression equation where the second systolic

pressure of the periphery will act as an independent variable[125], [183] . The technique of utilizing the second systolic pressure of periphery to directly estimate the systolic blood pressure reading of the central aortic blood pressure waveform is used by the commercial device HEM-9000AI Omron Healthcare, Japan [10], [124]–[126] . The limitation of this technique is that it will not work when the second peak of the periphery disappears which normally occurs in old patient, patients with hypertension or arterial stiffness[130]. In addition, this technique depends on the morphology of the peripheral waveform (radial or branchial blood pressure waveform) to estimate the central aortic pressure. Hence, the systolic blood pressure of the central aortic would be inaccurate for younger individuals with non-augmented peak systolic pressure[126].

2.4.5 Summary of literature review on estimation of central aortic blood pressure waveform

From the literature, it is known that majority of the wearable ambulatory devices are utilizing generalize transfer function (GTF) to estimate the central aortic blood pressure waveform such as Mobil-O-Graph NGI.EM GmbH, Germany [11], Oscar 2 with SphygmoCor, SunTech Medical[128] and ABPM 7100Welch Allyn, Inc. There are wearable ambulatory devices that are utilizing second systolic pressure of periphery with regression to estimate the systolic blood pressure reading such as Arteriograph 24 h, TensioMED Ltd., Hungary[115], [116] and WatchBP O3, Microlife AG, Widnau, Switzerland [139]. Besides that, there is the BPro + A-Pulse, HealthSTATS, Singapore [9], [12], [13] which utilizes the N-point moving average (NPMA) to estimate the central aortic blood pressure waveform. The research conducted on 30 patients by Cloud et al [177] has shown that the GTF method by SphygmoCor for estimating the central aortic blood pressure waveform underestimates the systolic pressure and it may not be suited to determine patients for hypertension because it is known that systolic blood pressure is a better predictor of hypertension risk [178]. Moreover, the ambulatory devices that utilizes second systolic pressure of the periphery to estimate the central aortic blood pressure waveform will not work when the second peak of the periphery disappears which normally occurs in old patient, patients with hypertension or arterial stiffness[130]. The NPMA technique utilised by the Bpro watch provides the central aortic systolic blood pressure reading instead of the aortic blood pressure waveform[130]. In addition, all the current commercialized ambulatory devices utilize these techniques using a software in the central processing unit (CPU) to convert the radial to aortic

blood pressure waveform, where the device is acquiring the radial blood pressure signal and transmits the data to the computer to process the conversion of radial blood pressure waveform to aortic blood pressure waveform for analysis of the signal and indication of hypertension. For example, the BPro wearable watch which is an ambulatory device acquires the radial blood pressure waveform and transfers the acquired data via Bluetooth or cable to the computer where the + A-Pulse Health STATS software with NPMA converts the acquired signal to an estimate aortic blood pressure waveform for analysis. Hence, there is a need to identify a current method or develop a novel method with low computational intensity which is able to give a close estimate of the actual aortic blood pressure waveform with a close prediction of the systolic pressure that can be embedded in the user's watch (micro-controller) to ensure continuous conversion of central aortic blood pressure waveform. Then, the estimated central aortic blood pressure waveform can be directly analyzed to indicate the risk to the user without the need of transmitting data to a computer or any cloud platforms. This will ensure the user is always aware of their health even if there isn't any WIFI, Bluetooth or wireless communication to a computer or cloud platforms for processing and analyzation.

2.5 Risk indication for cardiovascular disease

Cardiovascular disease risk indication scores were initially conducted in the Framingham study [184] which was used to predict an individual's cardiovascular risk by using variables such as age, gender, cholesterol, smoking habit, blood pressure levels, etc. This Framingham technique in indicating risk of cardiovascular diseases had certain methodological drawbacks when it was applied to different populations around the world (Seven Countries Study dataset) such as over-estimates risk in young people and overpredict absolute risk in low-risk European populations which was identified by Menotti et al [185] in the early 2000s. To address the drawbacks when applied risk indication to different population size and types, the European Society of Cardiology (ESC) established the SCORE project in the early 2000s which developed a more accurate risk prediction tool for the European populations [186]. The European Society of Cardiology (ESC) SCORE was recalibrated later by a Greek team into the HellenicSCORE which takes the consideration of the pervasiveness of cardiovascular risk factors in the Greek population [187]. This shows that a variety of cardiovascular disease risk prediction tools exist with different set of risk factors from different countries and populations, which have large variations in regards to their performance [188]. Majority

of the scores use a common set of risk factors which is known as classical and are similar to that mentioned previously such as age, gender, etc. [188], while other risk prediction tools which have incorporated more advance markers of cardiovascular disease like C-Reactive Protein (CRP) Test, Heart-type fatty acid binding protein (H-FABP) ,etc. [188]. The majority of the risk prediction tools are based on stochastic statistical models that consider individual variables based on cohort studies to calculate the overall risk for a future event [189]. Some recent studiest of risk indication of cardiovascular disease utilizing United Kingdom Prospective Diabetes Study (UKPDS) cardiovascular risk equations, Framingham Risk Score (FRS), Systematic Coronary Risk Evaluation (SCORE) , Reynolds Risk scores(RRS), Joint British Society risk calculator 3(JBS3), American College of Cardiology/American Heart Association (ACC/AHA), Pooled Cohort Risk Equation (PCE- ASCVD) and National institute for health and care excellence (NICE) risk is shown in Table *2.3* where odds ratios is OR, Area under the curve is AUC, net reclassification improvement is NRI and integrated discrimination improvement is IDI.

Table 2.3 shows some of the recent studies that compared conventional statistically driven predictive CVD risk models [190].

References	**Database**	**Data size**	**Age**	**Indication**	**Method**	**Risk Stratification**	**PE Metrix**	**Summary**
Davis et.al 2009 [191]	Australia	815	30–74	MI, CHD, Stroke	FRS-CVD, & UKPDS	28% fewer CHD events than occurred, underestimated the number of events by 38% for stroke	AUC, Brier score, Hosmer-Lemeshow test	The UKPDS stroke equation is acceptable for the Australian population (but not the UKPDS and FRS CHD equations).
Ahn et.al 2011 [192]	Korea	1275	-	Carotid atherosclerosis	FRS-CVD, UKPDS, & SCORE	-	AUC, OR	FRS, UKPDS, and SCORE had no significance on the predictability of carotid atherosclerosis.
Cook et.al 2012 [193]	United States America	1722	50–79	CVD Events	FRS & RRS	<5%, 5%–9%, 10%–19%, ≥20%	IDI, NRI	The RRS was better calibrated than the FRS.
Van Staa et.al 2014 [194]	United Kingdgom	1.8 million	35–74	CVD Events	FRS, ASSIGN, QRISK2	<10%, 10%–14% 15%–19%, ≥20%	Relative Rate	These three risk models consistently predicted low risk (but not high risk).
Selvarajah et.al 2014 [195]	Malaysia	14,863	40–65	CVD event	FRS-CVD, SCORE high-risk chart, SCORE low-risk chart, & WHO	≥20% (FRS) ≥5% (SCORE), ≥30% (WHO)	AUC	FRS and SCORE-high risk chart (but not the WHO) may be utilized to predict the risk of CVD in Malaysian chorot.
Bansal et.al 2015 [196]	North India	489	18–75	CHD	FRS-CVD, & UKPDS	≥20%	Kappa Coefficients	Despite the strong agreement, a different population was identified as being at high risk.
Garg et.al	India	1110	25–85	CVD	FRS-CHD, FRS-	<10%, 10%–19% 20%–		FRS-CVD and NICE guidelines are appropriate

2017 [197]					CVD, QRISK2, JBS-3, ASCVD, & WHO	29%, 30%–39%, ≥40%		for the indian patients.
Albarqouni et.al 2019 [198]	Australia	5453	40–74	CVD	ASCVD, 1991 FRS, 2009 FRS, 2008 office-based FRS	≥20% (FRS) ≥7.5% (ASCVD)	Brier Score, C-statistics, D-statistics	The 1991 FRS or ASCVD models should be employed to estimate CVD risk in the Australian population.

The predictive risk models perform differently in various populations, as shown by these comparison studies between the risk assessment tools (Table 2.3), and clinicans must consider the baseline risk profile, demographics, and risk variables before proposing any treatment regimens.Despite all the above-mentioned techniques for early detection of cardiovascular disease by risk indication, there is still a high percentage of cardiovascular diseases occurrence in people without the risk factors or categories in low-to-moderate risk. Besides that, approximately 20% of the high risk category of cardiovascular disease was misjudged due to the misclassification of the risk[188]. Hence, there is a need to identify new methodologies that would improve the risk prediction of cardiovascular diseases [199]–[202]. Artificial intelligence algorithms have drastically altered the landscape of healthcare applications in today's world[203]–[206]. Local and global patterns from healthcare databases are easily recorded, and complex interactions among such patterns of health risk have been analyzed to assist clinicians in making clinical decisions using artificial intelligence-based algorithms[203], [207].

2.6 Artificial intelligence for detection of cardiovascular disease

With today’s fast developing technology with advanced computing speeds and newer artificial intelligence learning techniques, artificial intelligence has been increasingly used in the application of health care [34]. Artificial intelligence has been incorporated in risk indication techniques in various scientific fields, including health monitoring due to the large amount of data, analytical processing, and algorithms for data manipulation [188]. The two sub-areas of artificial intelligence, is called Machine learning and Deep learning. Machine learning is a scientific algorithm and statical model that is used

to perform a specific task relying on the inference derived from the data. Deep learning can process a wider range of data, requires lesser manual preprocessing of data by humans and can sometimes produce more accurate results compared to machine learning when trained with sufficient amount of data. Figure *2.16* shows the summary of the core difference between machine learning and deep learning.

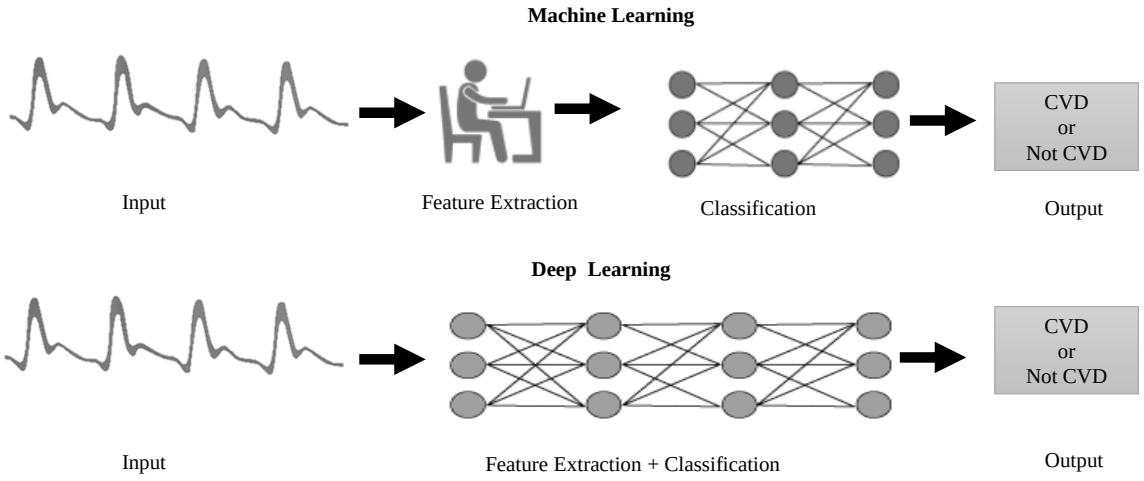

Figure 2.16 Machine learning Vs Deep learning

2.6.1 Machine learning

Since the early 2000s, machine learning has grown in the area of health science [208] where it has been applied in various healthcare and biomedicine applications [209]. This application includes cancer prediction [210], radiology imaging [211], research on ageing [212] and cardiovascular risk prediction [213]. Machine learning is a technique of learning from data which is well-known and established by statical approach where the model is built based on the data which is a subset of a larger population [188]. For machine learning, there is a need of human intervention in each stages to build the model [214] such as manual feature extraction of data and the efficiency of the machine learning is evaluated by the prediction performance. Currently for cardiovascular disease risk indication, machine learning techniques are built with complex models considering features from the accessible data of patient's bio-clinical risk factors, socio-economic, lifestyle and psychological characteristics [188]. Artificial Neural Networks (ANN) is a machine learning technique which has been used in current research in the area of healthcare. ANN is an arithmetic tool for pattern recognition that have been the subject of renewed research interest during the past 10 years. In 1960, Minsky [215]

showed that the research in neural networks which began in the 1940s had applications to solve simple problems. Neural network research is being revived currently as learning models which are commonly used in different network formats and learning rules. ANN is a computer system modelled on the human brain and nervous system for decision-making, and the artificial neuron is called a perceptron. Therefore, ANN is formed by a multi-layer perceptron, which is a combination of multiple perceptrons in more than one layer as shown in Figure 2.17.

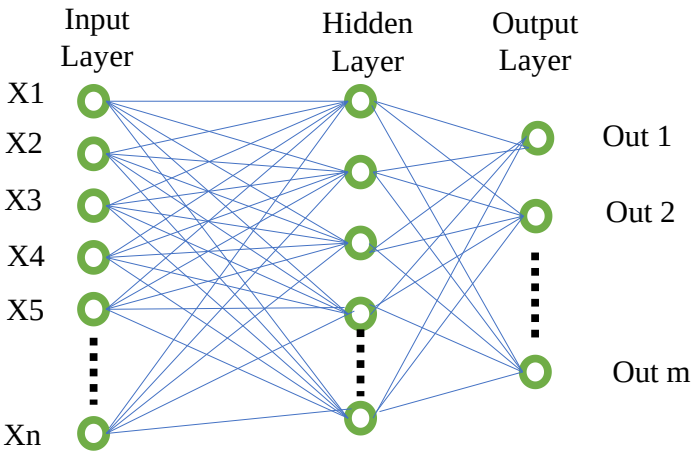

Figure 2.17 Multi-layer perceptron

Each neuron is a sum weighted input that transmits a transfer function to the next neuron level, which finally activates the output unit and produces the artificial neural network output [216] . Feeding in training data and adapting the weights according to the error from network output to intended output, is the process of training the ANNs. There are two types of methods, one of which is supervised learning and the other, unsupervised learning. Supervised learning technique is to connect inputs to learned outputs whereas unsupervised learning techniques are typically used for classifications of the database. A key algorithm for the weight update procedure is the introduction of the backpropagation algorithm by Rumelhart et al. [217], [218] in 1986, which is commonly used although there are alternative processes, such as cascade correlation and general regression [216], [219].

In the identification of cardiovascular disease, ANN is utilized in four significant cardiovascular medicinal zones, which are coronary artery disease, electrocardiography, cardiac image analysis and cardiovascular drug dosing [164]. Numerous research [30], [31], [220] have been published that relates ANNs to diverse areas of importance to

cardiovascular experts. ANNs was a contrivance by Akay [32] to diagnose coronary artery disease with a backpropagation trained algorithm with the input data of the history of the patient, physical examination data and pre-processed recordings of diastolic heart sound. From the research study of 63 abnormal and 37 normal subjects, the ANNs gave an output of 84% for positive prediction accuracy and 89% for negative accuracy. ltchhaporia D et al. [219] have done similar research for diagnosing coronary artery disease. This research obtained 80% positive prediction accuracy and 90% for negative prediction accuracy. By setting >50% obstruction of the left main coronary artery, the ANNs was trained to recognize significant coronary artery disease.

Electrocardiography (ECG) can be interpreted and analysed using computer technology [221], [222] and ANNs can be used to automate the analysis and interpretation of the ECG signals. Bortolan et al. [223] mentioned that ANNs can also be used for interpretation of ECGs to statistical analysis of conventional linear discriminant analysis and multi-group logistic discriminant analysis. Edenbrandt et al. [224] used ANNs to categorize ECG ST-T segment and compared it with clinical findings. The output of ANNs gave an 80% accuracy compared to an experienced cardiologist. Heden et al. [225] used ANNs to diagnose myocardial infarction from the analysis of the ECGs of 1,107 patients who had undergone diagnostic cardiac catheterization. This research study has compared the ANNs with the conventional automated ECG interpretation with the Glasgow program [221]. The conventional method showed a 66% sensitivity where else ANNs showed a 78% sensitivity. Therefore, there is only a minor difference between both approaches.

Radiofrequency catheter ablation is used as therapy for patients with cardiac arrhythmias. Before performing radiofrequency ablation, ANNs are used to focus on the accessory pathways. The trained ANN provides an output of each of the network which indicates the presence or absence of the accessory pathway site. After the ANN was trained manually by Dassen et al [226] to generate data from 60 cases, 25 cases were used to test the network. Predicted locations and actual locations were exact fits for 15 cases, a border zone between two locations predicted by the network for 8 cases and the prediction was incorrect for two other cases. ANNs could be useful in these types of studies even where causal relations between physiologic mechanisms and ECG findings are concluded by the investigators. ANNs will potentially reduce process time, decrease radiation exposure, prevent unsuccessful energy applications and increase

overall success rates by optimizing the ablation technique with the localization of an accessory pathway by pre-processing information. Recognition of lesions as benign or malignant images on mammography, hepatic ultrasound images and avascular necrosis of the femoral head in magnetic resonance images have been trained in ANNs [222]. ANNs can be used to automate the segmentation and recognition of structures or regions of interest in echocardiographic and scintigraphy images in cardiovascular applications.

The limitation of above-mentioned techniques of utilising ANNs for cardiovascular disease detection is that it cannot be incorporated for 24-h monitoring as the technique of acquiring the data is by Holter monitoring or one time measurement. Hence, ANNs using blood pressure data would be ideal as in today's technology era where there are ambulatory medical devices which could acquire the blood pressure readings non-invasively such as SphygmoCorCVMS, AtCor Medical, Australia [9]–[11] and BPro + A-Pulse, HealthSTATS[9], [12], [13]. Many researchers are working in the field of cardiovascular disease prediction utilizing blood pressure data with other additional information such as chronic risk factors (diabetes, obesity, smoking, etc) , psychobehavior (physical activity, sleep quality, respiration, stress, depression, etc) , genome (family history) and others [227]. An ANN based system that utilizes 24-h blood pressure monitor input to diagnose and analyse therapeutic interventions for ambulatory hypertensive patients named "Hypernet" was developed by Poll et al. [31]. The therapeutic recommendations of Hypernet were tested against those of an experienced specialist for a test set of 35 patients. The output showed that Hypernet achieved a sensitivity of 92% and a specificity of 96% when evaluated for both diagnosis and treatment ability. The Self-Applied Questionnaire (SAQ) study to predict cardiovascular disease proposed by Shen et al [228] was utilised where the study was based on the analysis of the common risk features of the disease and other data information by the SAQ. The study was based on blood pressure, smoking, blood cholesterol, sex and age to determine the risk of having cardiovascular disease. The study utilised an ANN which is a multi-layered feed forward neural network with the backpropagation method. The outcome of the ANN was a 67% accuracy for the detection. A hybrid system constructed by genetic algorithm and ANN was proposed by Amin et al.[229] to predict cardiovascular disease based on risk factor. Amin et al.[229] highlighted the two major disadvantages of the algorithm which are: it is impossible to find the initial weights which

are globally optimised and the algorithm takes a lot of time to converge. To address these disadvantages, these researchers applied genetic algorithm to optimize the weights of the ANNs which gave a better performance than the basic ANN which resulted in 96.2% accuracy for training and 89% accuracy for testing. Sonawane and Patil [230] developed an ANN trained by Vector Quantization algorithm using random order incremental training to predict cardiovascular disease. The input layer of the ANN consists of 13 neurons which are the clinical features of cardiovascular disease dataset and the output layer was a single neuron which shows the presence or absence of cardiovascular disease. The output is set to a single neuron to obtain less error and high accuracy. The performance of the ANN is improved by training the network with higher number of epochs where the obtained accuracy was 85.55%. Other than ANNs, a hybrid machine learning model based on Decision Tree, Support Vector Machine, and Naïve Bayes was proposed by Bashir et al.[231]. This research utilized different classifiers to obtain the majority voting scheme where the scheme works in two different steps. The first step is the three classifiers output results, and the second step combines the decisions of the three classifiers output to develop a new model created by the majority voting scheme. The approach attained a 74% sensitivity, 82% accuracy and 83% specificity for the prediction of cardiovascular disease. Feshki and Shijani [232] developed a model on cardiovascular disease prediction by using feature selections and classification for a specific dataset. The developed model operates by partitioning the dataset into subsets (sick and healthy people) and identifying the subset having the highest accuracy using particle swarm optimization with a feed-forward backpropagation algorithm as a classifier. From the outcome of the model, it is known that the feature selection and backpropagation feed-forward neural network with particle swarm optimization is an effective method as it was able to give 91.94% accurate results.

These studies illustrate the potential of artificial neural networks in blood pressure monitoring wearable devices as it can continuously monitor the blood pressure reading and incorporate risk factors of cardiovascular diseases such as age, gender, smoking habits, obesity, etc. However, these studies with ANNs or machine learning techniques which utilise history and physical examination data such as obesity, is just an indication of risk but can’t be relied as a predictive indicator for cardiovascular disease. For example, despite obesity being a strong independent cardiovascular disease predictor even in the absence of other risk factors, the clinical outcome is not linear for a relationship

between higher BMI with the onset of cardiovascular disease [233]. Assumption of excess body mass (obesity) as a lead to cardiovascular disease is not necessarily accurate because there are studies showing the potential of protective effects of obesity when it coexists with cardiovascular disease where this phenomenon is call obesity paradox [234]–[236]. This paradox has been investigated with heart failure and coronary heart disease [233], and recently research data has also shown that this paradox applies to hypertension[237], [238], atrial fibrillation [239], [240], pulmonary arterial hypertension [241] and congenital heart disease [242]. As for blood pressure monitoring, the reading of systolic and diastolic are normally a good indicator for hypertension. Despite hypertension being a leading risk factor for premature death worldwide [243] which typically relates to cardiovascular risk, there are many generated debates and editorial commentaries [15]–[17] in regards of hypertension being an indicator for cardiovascular disease. Therefore, there is a need of using the entire blood pressure pulse as training for machine learning, rather than just the systolic and diastolic values to give a better detection of cardiovascular disease. As by feeding in the entire blood pressure pulse waveform into an artificial intelligence, the waveform's morphology change can be used to determine cardiovascular disease. The blood pressure waveform is a fusion of the forward waveform generated by left ventricular ejection and a reverse/backward travelling reflected waveform caused by the sites of impedance mismatch, for example the arterial taper and difference in vessel stiffness, which often occur at bifurcations [244], [245] . The impedance change generates numerous reflected 'wavelets 'which are summed together to produce the effective reflected wave, which results in the increase of the systolic pressure in the central arteries and also produces the features in the blood pressure waveform such as the notch. Other than the systolic pressure being an indicator for hypertension resulting to cardiovascular events, the feature of the blood pressure waveform can be used to indicate cardiovascular events. For example, the notch which is one of the blood pressure waveform features, is the primary signaling that facilitates the endothelial-to-mesenchymal transformation during cardiac valve formation. The endothelium is conceivably one of the largest organ systems, and research on its diversity and the multiplex functions it performs continues to emerge. Significant evidence has implicated 'endothelial dysfunction' as a contributing factor to a number of cardiovascular diseases [246]. To feed in the entire blood pressure waveform into an artificial intelligence, the blood pressure waveform would need a feature extractor to extract the features of the signal. However, the extraction of features is a laborious task

[247] and would need tremendous amount of information to identify the features which are related to cardiovascular disease. Hence, by utilizing deep learning the feature extraction can be automated without the need of manual extraction as the deep learning model would identify the key features of the signal and relate to signal classification.

2.6.2 Deep learning

Deep learning originated from the study of Artificial Neural Networks (ANNs), which are computation models inspired by biological neural networks in human brains which has been extensively studied since the 1980s[248]. The idea of implementation of deep learning is inspired by biological processes, powered by high performance computing hardware which has made very deep models computationally practicable for a real-world application. For example, in the convolutional neural network, the connectivity between neurons reassembles the network of neurons in the animal/human visual cortex [249]. Deep learning models have achieved superior results compared to other high end machine learning models and even compared to human experts in many applied areas in recent years [248]. Furthermore, in recent years of research and development in deep learning, various neural network's structures have been designed for signal processing. Recurrent neural network (RNN) [250] is a deep learning model based on internal memory where it is used to process arbitrary time series input sequences such as speech recognition, handwriting recognition, etc. Long Short-Term Memory (LSTM) [251], another deep learning model can effectively prevent the occurrence of gradient vanishing from processing time series signals. The most remarkable achievements in recent years for pattern/feature classification using deep learning is done using Convolutional Neural Networks (CNN) [42]–[46]. Convolutional neural networks provide an end-to-end learning model where a trained CNN by gradient descent method can learn the characteristics of the input data and further complete the pattern classification. CNN has a very strong ability of learning the features and pattern classification because the features of the lower layers are derived from the partial information and convolutional kernel with sharing weights from the upper layer [42]. In the field of biomedical engineering, as in biomedical signal analysis the entire blood pressure pulse waveform was utilized in training deep learning models, CNN is the ideal deep learning method as it mimics the visual of the human's neuron network interpreting the entire signal with regards to the signal's features to relate to the cardiovascular disease. A

typical CNN consists of a number of convolutional layers, pooling layers and fully connected layers as its hidden layers shown in Figure 2.18.

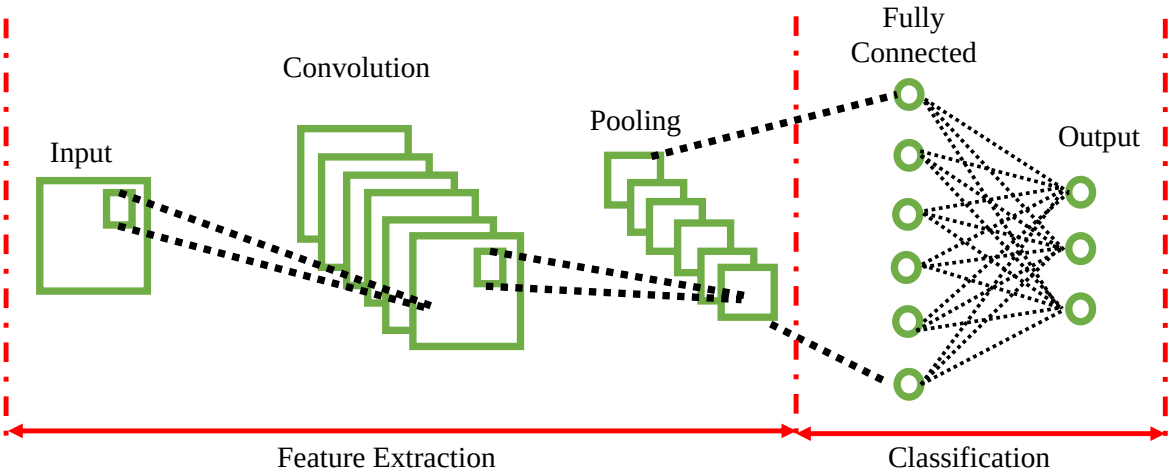

Figure 2.18 A typical Convolutional Neural Network architecture

In recent years, the CNN has been used for classification of human physiological signal patterns such as electrocardiogram (ECG), Phonocardiogram (PCG) and blood pressure waveform. Table 2.4 shows some of the recent work of using the electrocardiogram (ECG) signal for classification/detection. For Phonocardiogram (PCG), there are researchers who utilized the Aalborg University heart sounds database from PhysioNet/Computing in Cardiology Challenge 2016 to verify the developed algorithms for classification of normal and abnormal heart sound recordings using CNN shown in Table 2.5. The database consists of five databases labelled from A to E that contains 3126 phonocardiogram (PCG) recordings, with recording lasting from 5 to 120 seconds.

Table 2.4. Convolutional neural network (CNN) using Electrocardiogram (ECG)

Reference	Detection	Method	Accuracy
Zubair et.al 2016 [252]	Arrhythmia	non-linear transform for R-peak detection and a 1D CNN with a variable learning rate	92.7%
Li et.al 2017 [253]	Arrhythmia	Wavelet transform (WT) for denoising and R-peak detection and a two-layer 1D CNN	97.5%
Isin et.al 2017 [254]	Arrhythmia	Denoising filters, Pan-Tomkins, AlexNet for feature extraction and PCA for classification	92.0%

Rajpurkar et.al 2017 [255]	Arrhythmia	34-layer CNN to classify the ECG signals into 14 types of output classes.	80%
Acharya et.al 2017[256]	Arrhythmia	11-layer CNN with the output layer of four neurons, each representing the normal (Nsr), Afib, Afl, and Vfib ECG class.	92.5%
R.Acharya et.al 2017 [257]	Myocardial Infarction	CNN for the automated detection of a normal and MI ECG beats (with noise and without noise).	93.53%, 95.22%
R.Acharya et.al 2017 [258]	Coronary Artery Disease	Using different durations (two- and five-seconds durations) of ECG segments with CNN.	94.95%, 95.11%
Yao et.al 2017 [259]	Atrial Fibrillation	Multiscale CNN (AFDB, LTAFDB, private)	98.18%
Jin et.al 2017 [260]	Abnormal ECG	Identify abnormal ECG using lead-CNN and rule inference	86.22%
Wu et.al 2018[261]	Arrhythmia	active learning and a two-layer CNN fed with ECG and RR interval	Multiple [nearly 100% accuracy in normal and ventricular ectopic beat predictions]
Xia et.al 2018 [262]	Atrial Fibrillation	CNN with spectrograms from short time Fourier transform or stationary WT (AFDB)	98.29%
R.Acharya et.al 2018 [263]	Congestive Heart Failure	11-layer CNN model for CHF diagnosis	98.97%
Xiao et.al 2018[264]	ST event	Classify ST events from ECG using transfer learning on Inception v3	0.867b
Zhong et.al 2018 [265]	Fetal ECG segments	Three-layer CNN for classifying fetal ECG segments	77.85%
Yao et.al 2020[266]	Arrhythmia	Attention-based time-incremental CNN, achieving both spatial and temporal fusion of information from ECG signals	81.2%
Avanzato et.al 2020 [267]	Heart disease	Automatic ECG diagnosis using CNN to detect normal, atrial premature beat and premature ventricular	98.33%

		contraction for the classification of heart disease.	
Wang et.al 2021 [268]	Arrhythmia	Continuous Wavelet Transform (CWT) is used to decompose ECG signals to obtain different time-frequency components, and CNN is used to extract features from the 2D-scalogram composed of the above time-frequency components	98.74%

Table 2.5 Convolutional neural network (CNN) using Phonocardiogram (PCG)

Reference	**Method**	**Accuracy**
Potes et.al 2016 [269]	124 time-frequency features were extracted as the input to a variant of the AdaBoost classifier and a second classifier using CNN was trained using PCGs cardiac cycles decomposed into four frequency bands. The outputs were combined with the decision rule from both AdaBoost and CNN.	86.02%
Ryu et.al 2016 [270]	Filtered by using Windowed-sinc Hamming filter algorithm to remove signals regarded as noise. The filtered recordings are then scaled and segmented. Using the filtered and segmented recordings, a 4-layer CNN was trained to extract features and construct a classification function.	79.5%
Rubin et.al 2017 [271]	2-layer CNN and Mel-frequency cepstral coefficients for automatic classification of heart sound	83.99%
Kucharski et.al 2017 [272]	Spectrogram by extracting a set of time-frequency parameters to be fed into a 5-layer CNN with dropout	91.6%
Dominguez et.al 2018 [273]	Spectrogram by segmenting and preprocessing by using the neuromorphic auditory sensor to decompose the audio information into frequency bands to feed into the CNN which has a modified AlexNet	94.16%

On the other hand, for blood pressure waveforms, Hu et al utilized Shannon Energy Envelope, Hilbert Transform (SEEHT) and a convolutional neural network to classify the blood pressure pulse waveform into health and subhealth [274]. The outcome of the research shows a 72.31% accuracy on classification of health against subhealth and a 96.33% accuracy on arteriosclerosis against non-arteriosclerosis. This research also shows that TCM doctors are able to identify health for about 60% using pulse wave because the effective features for classification are uncertain [274]. This shows that the

CNN performs better in feature identification and classifying the blood pressure pulse signal compared to a human. Young-Jin Moon et al applied arterial blood pressure waveform data recorded from liver transplantation surgeries to the convolutional neural network to estimate stroke volume (SV) which attained a concordance rate of 74.15% during surgery [275]. Shota Shimazaki et.al investigated convolutional neural network on Photoplethysmography (PPG) signals based on the relationship between pulse waveform and blood pressure reading. The pulse wave and blood pressure data were collected from 78 subjects to conduct a precision assessment experiment where the CNN was able to attain a correlation coefficient (R) of 0.71 compared to using conventional methods (geometric features + Multiple Regression Analysis (MRA)) which attained 0.63 correlation coefficient [276]. In addition, Gaoyang Li et.al utilized a convolutional neural network model to identify one to one pulse pattern to its corresponding cardiovascular disease [42]. In the study by Gaoyang Li et. al, five cardiovascular diseases and complications were extracted from medical records for the first CNN classifier and four physiological parameters related to selected diseases were also extracted to build the second CNN classifier. The outcome of each CNN was able to attain 95% and 89% accuracy for the first and second CNN respectively [42]. From these research areas, it is known that the diversity of pulse wave morphology results in difficulty in pulse-based diagnosis especially in pulse waveform pattern classification. Nevertheless, from the above findings, it known that convolutional neural network is a promising method that can be utilized for pulse waveform pattern classification and it outperforms the conventional methods in pattern classification due to its ability to extract informative features. Furthermore, majority of convolutional neural network [42]–[46] models are used for pattern/feature classification but this doesn't indicate risk or act as a predictive role.

Hence, to attain a risk indication-based convolutional neural network for future implementation in a predictive role, the output must be based on a numerical regressive outcome where the input of the convolutional neural network would be a full physiological signal waveform and the output would be a numerical number rather than a classifier. By having the numerical output for CNN, this technique can mimic the conventional technique of risk assessment, similar to how it was conducted for indicating the risk for hypertension. For example, the numerical reading of blood pressure over a time of 24 hours is considered healthy if the blood pressure reading is in the range between

90/60mmHg and 120/80mmHg and if the blood pressure reading is in the range of 140/90mmHg or higher, it would be high blood pressure which is a risk indication for hypertension. Therefore, to develop a pulse waveform pattern regression based on CNN to attain a numerical output, there is a need of input data of blood pressure pulse waveform and its corresponding numerical output. This can be attained as in today's research world cardiovascular models are available, where the inputs of the models are numerical values, and the output is the corresponding blood pressure waveform.

2.7 Cardiovascular system model

Modelling of the cardiovascular system was first done to study the circulation of blood in the human body. By studying the blood circulation of the human body using cardiovascular models, conceptional ideas can be tested out before proceeding to clinical trials. Harvey announced the discovery of the cardiovascular system in the 17th century by denoting the heart as the pump of the cardiovascular system [277]. The model sets the blood flow in a unidirectional flow in a closed-loop circuit through systemic and pulmonary circulations [278]. Modelling starts by doing a mathematical model of the cardiovascular system. The equation for each part of the cardiovascular system is identified, and all the equations are then combined to form a full equation for the cardiovascular system. The mathematical model uses basic fluid dynamic equations especially Navier-Stokes equations. Poiseuille flow and Reynolds number play a big part in determining the mathematical model of the cardiovascular system. The lower the Reynolds number, the higher the viscosity of the blood. The equation is then placed into a computational simulation, which is known as a fluid-structure interaction (FSI) model so that the unknown parameters can be altered using an iterative method to know the effect of the parameters to the cardiovascular system. The FSI model can be converted to a 3D model, and then, to a 1D and finally to a simplified 0D model [279]–[286]. In some 3D models, a Navier-Stokes equation can be utilise to couple with a structural model for the vessel wall. On the other hand, in the 1D model, a net of systems of hyperbolic equations are used to determine mean pressure and flow rate. The 0D model uses a system of algebra-ordinary differential equations which is often non-linear to determine the mean pressure and flow rate in time [279]–[286]. By comparing all the 3D, 1D and 0D models in Table 2.6 below, it reasonably justified to use the 0D model as the model for overall cardiovascular blood circulation analysis to detect cardiovascular disease because it is comprehensively simple, requires less computational effort

and the model covers the whole cardiovascular circulation system which analyses the overall pressure, volume and flow of the blood. Figure 2.19 shows all the scales of the 3D, 2D and 1D modelling from the 0D model.

Table 2.6.Summarised comparison of various computational cardiovascular models [287]

Model	**Type of parameter model**	**Type of flow distribution**	**Types of governing equations**	**Applications of model**
0-D	Lumped	Uniform	Ordinary differential equation (ODE) for conservation of mass and momentum, and Algebraic Equilibrium Equation to convert volume to pressure	Appropriate for analysation of pressure, flow and volume of blood distribution in system. Can, at times, give boundary conditions for three-dimensional models.
1-D	Distributed	Non-Uniform	Partial differential equation (PDE) of conservation of mass and momentum, and Equilibrium Equations	Appropriate for analysation of reflection or transmission impact which permits for better boundary conditions for three-dimensional models.
2-D	Distributed	Non-Uniform	Partial differential equation (PDE) of conservation of mass and momentum, and Equilibrium Equations	Appropriate for analysation on the change of velocity in an axisymmetric tube which permits for better boundary conditions for three-dimensional models with certain limit off applicability.
3-D	Distributed	Non-Uniform	Partial differential equation (PDE) of conservation of mass and momentum, and Equilibrium Equations	Appropriate for analysation of complex flow pattern in small region of the cardiovascular circulatory system.

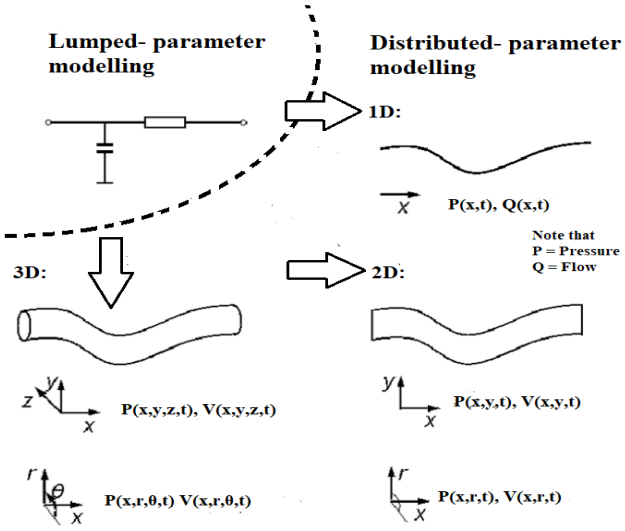

Figure 2.19 Different scales of modelling [35]

2.7.1 Zero-Dimensional model

For modelling a 0D model, the concept of hydraulic-electrical analogue is often used. The 0D model relates the blood flow circulation to electric conduction in a circuit. In 0D models, blood flow follows the law of mass conservation, Poiseuille law for steady-state momentum equilibrium and Navier-Stokes law for unsteady-state momentum balance, which in the analogy is similar to an electric circuit, which uses Ohms law for steady-state voltage-current relation, Kirchhoff law for current balance and the transmission line equation for the high frequency voltage-current relation [35]. The electrical circuit has a resistor, capacitor and inductance, which correlates with a cardiovascular system. Inductance represents inertance, which is the measure of the pressure difference in a fluid due to the change in blood flow rate over time. Capacitance represents compliance that is the measure of the change in blood volume when subjected to an applied force. Resistance represents the peripheral resistance in the vessels of the blood flow in the cardiovascular system [288].

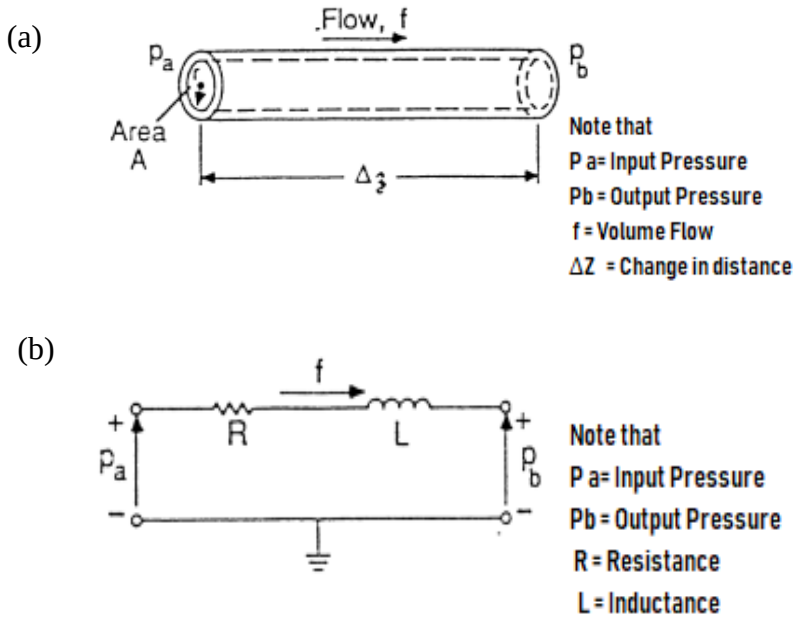

Figure 2.20 shows (a) Idealized segment of a vein or artery and (b) Equivalent lumped fluid-flow circuit, ignoring wall compliance [288].

Figure 2.20 (a) is a 3D model which is converted to its 0D model as shown in Figure 2.20 (b) . In Figure 2.20 (b) , R and L are used to model resistance and represent the wall inertia respectively. The change of pressure from p_a (input pressure) to p_b (output pressure) can be discovered in Equation 2.1.

$$(p_a - p_b)|vis = f * R \tag{2.1}$$

For this Equation 1, it is assumed that flow is uniform across the vein or artery where the volume flow rate is f. Mass of the blood flow can be determined by Equation 2.2.

$$M = \rho * A * \Delta Z \tag{2.2}$$

where ρ is blood density, A is the cross-sectional area of the vessel and ΔZ is the change of length of the vessel for Equation 2.2. Blood flow velocity (v) across the vessel radius is assumed to be uniform, whereby the total flow is given as:

$$f = v * A. \tag{2.3}$$

The second law of motion rule in Newton relates to the behaviour of objects for which all existing forces are not balanced. This second law states that the acceleration of an object is dependent upon two variables which are the net force acting upon the object and the mass of the object. In this case, Newton's second law is used to drive the force needed to balance the acceleration of blood using Equation 2.3

$$M\frac{dv}{dt} = (\rho * A * \Delta z) * \frac{d\left(\frac{f}{A}\right)}{dt} = (\rho * \Delta z) * \frac{df}{dt} \quad (2.4)$$

This acceleration force must be equal to the acceleration at the pressure difference at the end of the cross-sectional area of the vein or artery. Hence, the pressure differences between p_a and p_b is multiplied with the cross-sectional area of the vein or artery using Newton's second law of motion.

$$(p_a - p_b) * A \quad (2.5)$$

To obtain the acceleration part of the pressure drop equation of

$$(p_a - p_b)|accel = (\rho * \Delta z/A) * \frac{df}{dt}. \quad (2.6)$$

Inertance is the coefficient of the flow derivative in this equation resulting in:

$$l = \rho * \Delta z/A \quad (2.7)$$

The resistance of flow is obtained by using Poiseuille steady-state formula which is given as:

$$R = 8 * \pi * \mu * \Delta z/A \quad (2.8)$$

Therefore, the pressure drop is equated to the sum of the viscous resistance and mass of acceleration, which is:

$$p_a - p_b = f * R + l * \frac{df}{dt} \quad (2.9)$$

In fact, velocity is lower near to the wall of the vessel with an overall parabolic cross section of the flow velocities which gives a slightly better value for the inertance base on a two radial segment approximation resulting in:

$$l = 9 * \rho * \Delta z/4 * A = 9 * \rho * \Delta z/(4 * \pi * r^2) \quad (2.10)$$

So far, the elasticity of the vessel walls has been neglected. However, the compliance of a cylindrical vessel can be shown using Equation 2.11.

$$C = 3 * \pi * r^3 * \Delta z/2 * E * h \quad (2.11)$$

where the radius is r, the length is Δz, wall thickness is h, and young bulk modulus of elasticity, E. The wall material is uniform with a Poisson ratio of:

$$\sigma = 1/2 \quad (2.12)$$

When the fluid velocity is zero, pressure through the vessel is pa. Meanwhile, q is the total volume of the segment and qu is the unstressed volume when transmural pressure is zero.

$$q = qu + pa * C \tag{2.13}$$

Compliance may be determined by varying pa by Δpa in $q = qu + pa * c$ by observing diameter and the volume change rather than using Equation 2.14 as E and h are usually unavailable because it will not be practical to be obtained from a living being. Compliance is found by:

$$C = \Delta q / \Delta pa\ . \tag{2.14}$$

Compliance has a limited range of positive transmural pressure. This is to ensure that the vessel walls would not reach its limit of expansion and result in vessel rupture [127]. As can be seen below in Figure 2.21 and Figure 2.23 are two examples of 0D models of cardiovascular circulations.

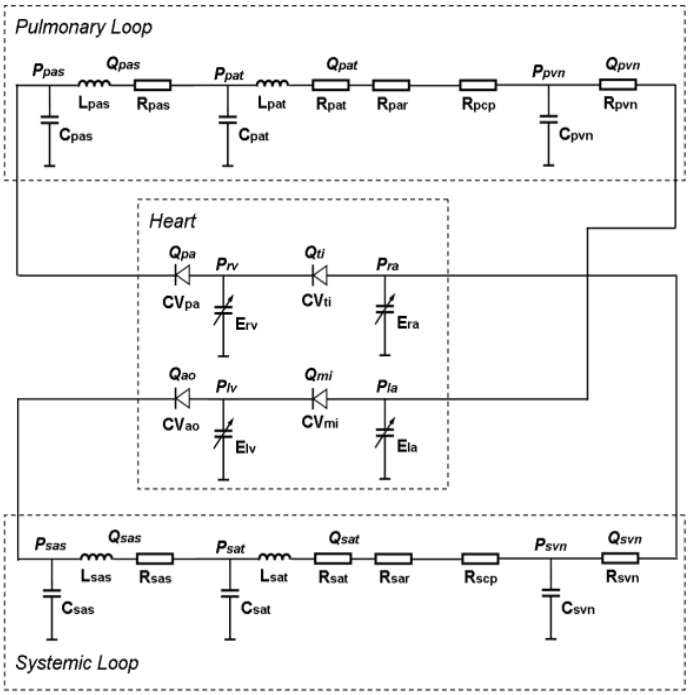

Figure 2.21 A complete 0D cardiovascular circulatory system by T. Korakianitis and Y. Shi [35].

Figure 2.21 shows a complete 0D cardiovascular circulatory system by T. Korakianitis and Y. Shi which shows the human cardiovascular system in the simplest form where the schematic of the model was extracted from Shi et al.'s model in the CellML model

repository. This 0D cardiovascular circulation model can be regarded as a limited representation of a 1D model [289]. The model is made up of 3 main parts which are the heart, systemic loop and pulmonary loop, as can be seen in Figure 2.21. The above model divides the heart model with chambers exactly like the human heart and diodes are used as valves to ensure the flow is in one direction. The systemic loop is modelled with 5 main parts which are systemic aortic sinus, systemic artery, systemic arteriole, and systemic capillary and systemic vein. Same as the systemic loop, the pulmonary loop is modelled with 5 main parts which are pulmonary aortic sinus, pulmonary artery, pulmonary arteriole, pulmonary capillary and pulmonary vein. The systemic aortic sinus, systemic artery, pulmonary aortic sinus and the pulmonary artery are modelled as RLC components. Moreover, systemic arteriole, systemic capillary, pulmonary arteriole and pulmonary capillary are modelled as resistors. Finally, the systemic vein and pulmonary vein are modelled as RC components like the Windkessel model [289].

For this model, the parameters related to electrical equivalents, such as pressure, flow, resistance, compliance, and inertance, are represented by the voltage, current, resistance, capacitance, and inductance in the circuit respectively. Table 2.7 shows the parameters represented by its electrical equivalent in the circuit.

Table 2.7 Electrical Equivalence of Parameters in Blood Flow Model by T. Korakianitis and Y. Shi [35].

Symbol	**Parameter**	**Electrical Equivalent**
P	Pressure	Voltage
Q	Flow	Current
R	Resistance	Resistance
C	Compliance	Capacitance
L	Inertance	Inductance

The same table can also be used to relate the body cardiovascular system to give the correlation between the electrical equivalents and the human body cardiovascular system. Table 2.8 below shows the parameters represented by its cardiovascular system.

Table 2.8 Cardiovascular System Described by Parameters in Blood Flow Model by T. Korakianitis and Y. Shi [35]

Symbol	**Parameter**	**Cardiovascular system**
R	Resistance	Frictional Loss
C	Compliance	Wall Elasticity
L	Inertance	Blood Inertia
E	Elastance	Wall Stiffness
CV	Flow Coefficient	Blood Flow Through Valves

There are three templates (TempR, TempRC and TempRLC) which were defined to provide zero dimensional representations of the linearized governing equations for pressure and flow in the vessel segments to establish the relationships between P, Q, R, L and C components at the input to express the output. The TempR defines the relationship between pressure and flow whereas the TempRC defines the first derivative of the input pressure in terms of flow and capacitance. Meanwhile, the TempRLC defines the first derivative of the output flow where this shows the relationship between the R, L and C components. Table 2.9 shows the equations that were obtained from the 'Mathematics' section of Shi et al.'s CellML model in the CellML model repository [290].

Table 2.9 The relationship between the model parameters and TempR, TempRC and TempRLC equations respectively [290].

Components	**Equations**
TempR	$P_{in} = P_{out} + RQ_{in}$ $Q_{out} = Q_{in}$
TempRC	$\frac{d}{dt}(P_{in}) = \frac{Q_{in} - Q_{out}}{C}$ $Q_{out} = \frac{P_{in} - P_{out}}{R}$
TempRLC	$\frac{d}{dt}(P_{in}) = \frac{Q_{in} - Q_{out}}{C}$ $\frac{d}{dt}(Q_{out}) = \frac{P_{in} - P_{out} - RQ_{out}}{L}$

This complete 0D cardiovascular circulatory system by T. Korakianitis and Y. Shi can simulate pressure, flow and volume of blood and generates results which are

satisfactory given its simplicity. However, the downside of the 0D model is its inability to simulate the nonlinear convective acceleration term compared to its 1D model. The output responses simulated by the 0D model are shown in Figure 2.22.

(a)

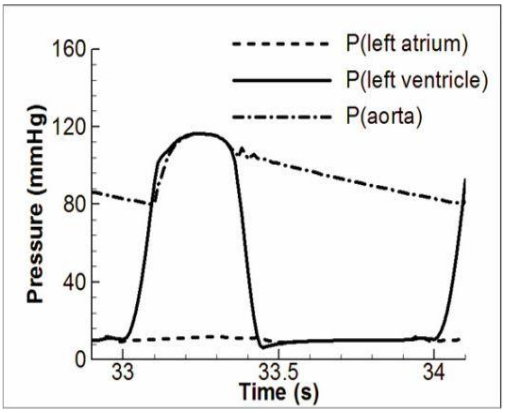

(b)

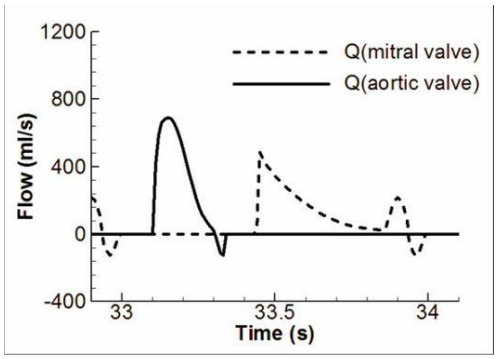

(c)

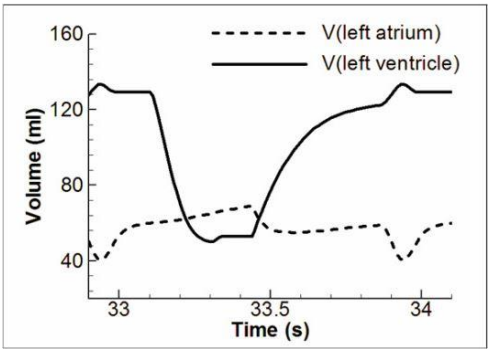

Figure 2.22 shows the (a) Pressure Output (b) Flow Output and (c) Volume Output of Model by Korakianitis and Shi [35].

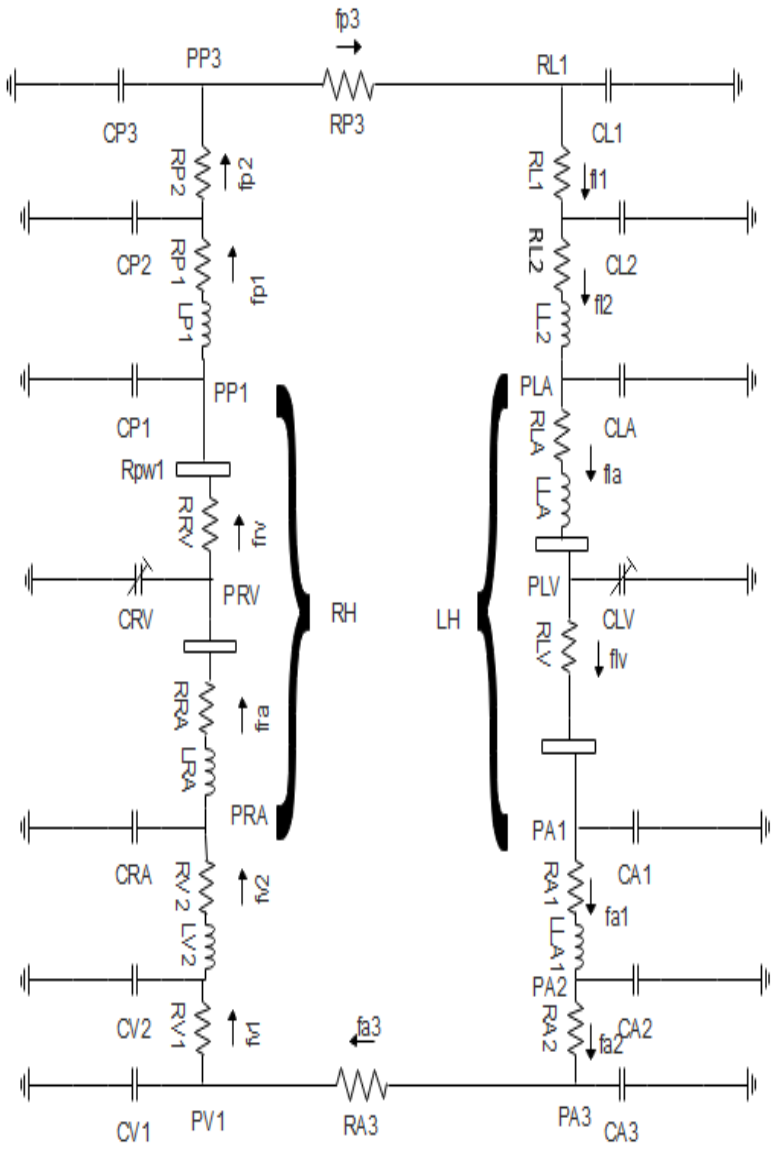

Figure 2.23 A complete 0D cardiovascular circulatory system by V. Rideout [288].

Figure 2.23 shows the cardiovascular circulatory system that was modelled by Vincent Rideout. This system uses the pressure-flow model while incorporating RLC components of an electrical circuit. The model is made up of 4 main parts which are the right heart, left heart, systemic loop and pulmonary loop which can be seen as segments in the figure. The heart is modelled with right and left heart chambers to allow blood to flow from the left heart through the systemic loop and to the right heart before travelling to the rest of the body. The heart is modelled with atrium and ventricle for both right and left using RLC components with the capacitance as the ventricle variable. The systemic loop has 3 major parts which are aorta, systemic artery, and systemic vein whereas the pulmonary loop has 2 major parts which are pulmonary artery and pulmonary vein. For the systemic loop, the aorta and the systemic vein are divided into two

parts where the first part of the aorta and the second part of the systemic vein are modelled using RLC components, and the second part of the aorta and the first part of the systemic vein are modelled using RC components. However, for pulmonary loop, the pulmonary artery is divided into three parts, the first part is modelled using an RLC component while the second and third parts are modelled using RC components and lastly, the pulmonary vein is divided into two parts where the first part is modelled using an RC component and the second part is modelled using an RLC component.

For this model, the parameters are also related to its electrical equivalents. For example, pressure, flow, resistance, compliance, inertance and volume are represented by the voltage, current, resistance, capacitance, inductance and charge in the circuit respectively. Table 2.10 summarizes this information of parameters and their electrical equivalent in the circuit.

Table 2.10 Electrical Equivalence of Parameters in Blood Flow Model by V. Rideout.

Pressure-Flow-Volume (V.Rideout model)			**Electrical Circuit Equivalent**		
Symbol	**Model Parameter**	**Units**	**Symbol**	**Electrical Parameter**	**Units**
P	Pressure	mmHg or g/cm/s^2	V	Voltage	Volt
F	Flow	ml/s	I	Current	Amper
Q	Volume	ml	Q	Charge	Coulomb or Ampere×s
R	Resistance	g/cm^4/s	R	Resistance	Ohm or Volt/Amper
C	Compliance	cm^4×s^2/g	C	Capacitance	Farad or s/Ohm
L	Inertance	g/cm^4	L	Inductance	Henry or s*Ohm

Pressure-Flow components of the model obey the same fundamental equations as the electrical circuit equivalent referring to Table 2.10, for example:

$$P = R \times F \qquad V = R \times I \qquad (2.15)$$

$$P = L\frac{dF}{dt} \qquad V = L\frac{dI}{dt} \qquad (2.16)$$

$$P = Q/C \qquad V = Q/C \tag{2.17}$$

$$F = \frac{dQ}{dt} \qquad I = \frac{dQ}{dt} \tag{2.18}$$

The compliances in this model are modelled linearly with unstressed volumes. Equation 2.19 sums of the volume of stressed and unstressed are as shown below.

$$Q_n = Q_{nu} + Q_{ns} \tag{2.19}$$

Volume at a node in this model is defined as Equation 2.20 of this model:

$$Q_n = \int_0^t (F_{in} - F_{out})\, dt + Q_n(0) \tag{2.20}$$

The pressure is calculated from the stressed volume using Equation 2.21 of this model:

$$P_n = \frac{Q_{ns}}{C_n} = \frac{Q_n - Q_{nu}}{C_n} \tag{2.21}$$

This complete 0D cardiovascular circulatory system by Vincent Rideout generates results which are satisfactory even though it does not include baroreceptor sensor connections to the central nervous system. Besides that, despite the model being uncontrolled, it is stable due to the Frank-Starling mechanism. Pressure, flow, and volume of the blood can be simulated using this model. The output responses simulated by the model are shown in Figure 2.24 below [288].

(a)

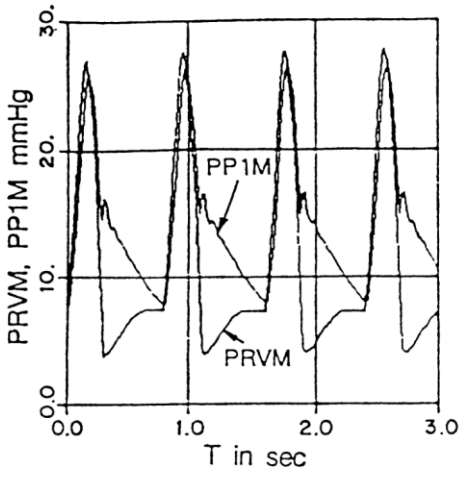

(b)

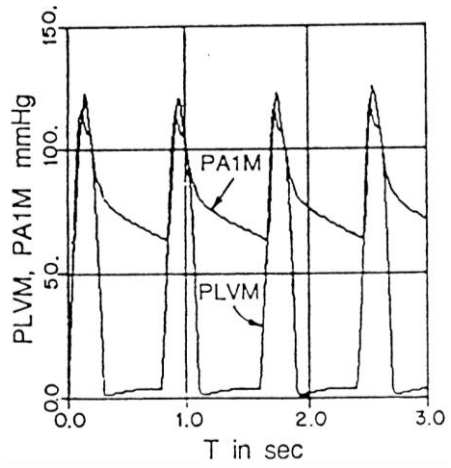

(c)

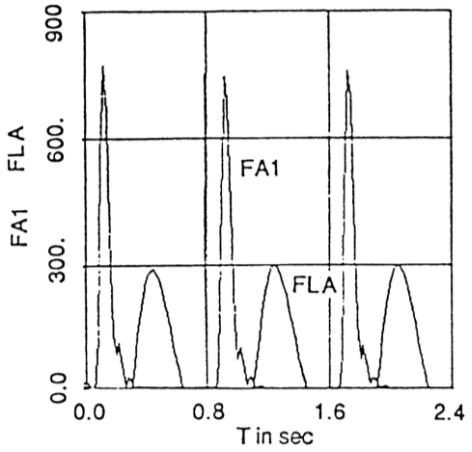

(d)

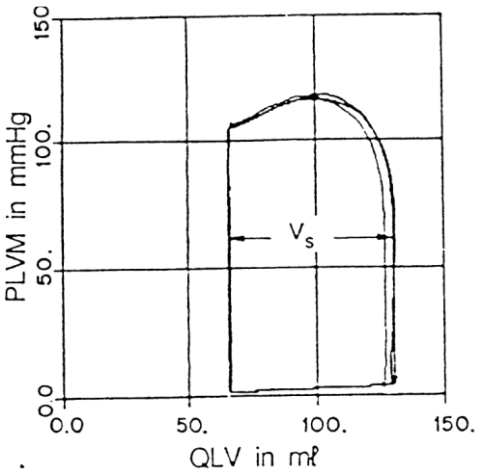

Figure 2.24. shows the (a) Right Ventricular and Pulmonary Artery Pressures (b) Left Ventricular and Aortic Pressures (c) Aortic Flow and Mitral Valve Inflow to Ventricle and (d) Pressure-Volume Plot for Left Ventricle of Vincent Rideout model [288]

The Vincent Rideout model has 36 different dynamic parameters which consist of 16 resistance parameters, 12 compliance parameters and 8 inductance parameters. All the parameters' default value is given to form a healthy patient output signal. The Vincent

Rideout model can produce four main output signals, which are right ventricular pressure (PRV), the pulmonary artery pressure (PPV), the left ventricular pressure (PLV), and the aortic pressure (PA1). The aortic pressure (PA1) can be used to study the feature of the signal which coincides with a cardiovascular disease signal as an aortic signal is common for medical experts to determine the patient's heart condition.

2.7.2 One-Dimensional model

1-Dimension (1-D) model is developed using the simplified Navier–Stokes equations which represents the pressure and flow at any point of the blood vessel of the cardiovascular system [291]–[293]. With large amount of computation, a 1D model can be used to represent the phenomenon of blood pressure wave propagation. The common applications of 1-D model are simulation of pulse wave propagation dynamics [28], [294]–[299], wave intensity analysis [300]–[302], estimation of central aortic pressure [303]–[306] and assessing the performance of algorithms and indexes [307]–[309]. The blood in the cardiovascular system is assumed to be an incompressible Newtonian fluid and the vessel is an axisymmetric cylindrical tube for a 1-D model. Hence, the 1-D model is governed by two equations which are the continuity equation and momentum equation [310] . Both these equations describe the motion of the blood flow in the vessel and contraction and expansion of the vessel's wall during blood flow. Equation 2.22 is the continuity equation and equation 2.23 is the momentum equation where F is the blood flow rate, x is the distance along the vessel, A is the cross-sectional area of the blood vessel, t is time taken for the flow, ρ is the blood density, p is the blood pressure, r is the vessel radius and μ is the viscosity.

$$\frac{\partial F}{\partial x} + \frac{\partial A}{\partial t} = 0 \tag{2.22}$$

$$\frac{\partial F}{\partial t} + \frac{4}{3}\frac{\partial \left(\frac{F^2}{A}\right)}{\partial x} = -\frac{A}{\rho}\frac{\partial p}{\partial x} - \frac{8\mu}{\rho r^2}F \tag{2.23}$$

For solving a 1-D model using the Navier–Stokes equations, there are two type of domain methods which are time domain and frequency domain. In time domain, the method can solve for linear and non-linear equations. However, frequency domain can only solve linear equations. The Navier–Stokes equations for 1-D model are generally non-linear where it is solved in time domain using numerical methods. There are many numerical methods for solving the partial differential equation of Navier–Stokes such as the method of characteristics, finite difference method, finite volume method, finite

element method and spectral method. It is very complicated to utilize the method of characteristic to solve the differential equation which has three independent variables and there may still be problems to be solved. By using the method of characteristics, the governing equations can be solved [311]–[313]. The finite difference method is used for solving complex partial differential equations. The complex partial differential equations are solved by approximating the derivatives with finite differences. In addition, the finite volume method is derived from the finite difference method where the area of calculation is focused on the series of control volumes and there is a control volume at the surrounding of each grid point. This control volume is integrated, and a set of discrete equations are formed where they need to be solved. The finite volume method needs a high computing speed and low requirements for the grid. This method is commonly used for computations of fluid and recently this method can also be used to solve differential equations [314], [315]. On the other hand, the spectral method is a method that uses an orthogonal function or intrinsic function with a class of computing techniques to solve certain differential equations where this method is able to obtain a higher precision using fewer grid points. However, the weakness of this method is that it has poor stability and high complexity in setting the boundary conditions. This method had been used by several researchers to resolve the 1-D model's pulse wave propagation equations [316], [317].

In the frequency domain method, a transmission line method is utilised to solve the Navier–Stokes equations in order to minimise the computational complexity of the non-linear model where the method requires the 1D Navier–Stokes equations to be linearized. Equation 2.27 and 2.28 are the equations of linear 1D Navier–Stokes equations in hemodynamic where $\mathrm{C} = \frac{\mathrm{dA}}{\mathrm{dp}} = \frac{3\pi r^2}{2Eh}$ is the capacitance (*E* is the Young's modulus, and *h* is the arterial wall thickness), $\mathrm{L} = \frac{\rho}{\mathrm{A}} = \frac{\rho}{\pi r^2}$ is the inductance and $\mathrm{R} = \frac{8\mu}{\pi r^4}$ is the resistance. These equations are converted to equation 2.29 and 2.30 which are electrical transmission line equations in a circuit [318] where *I* is the current, *V* is the voltage, and *G* is the conductance that describes the leakage of blood flow (usually neglected). Hence, methods of solving circuit equations can be utilized to solve 1D Navier–Stokes equations where the electrical parameters are resistive, inductive and capacitive elements. The values for these elements are obtained from the mechanical and geometric parameters of the blood vessel of the human cardiovascular system.

$$-\frac{\partial q}{\partial x} + C\frac{\partial p}{\partial t} = 0 \quad (2.24)$$

$$-\frac{\partial p}{\partial x} = L\frac{\partial q}{\partial t} + Rq \quad (2.25)$$

$$-\frac{\partial I}{\partial x} = VG + C\frac{\partial V}{\partial t} \quad (2.26)$$

$$-\frac{\partial V}{\partial x} = IR + L\frac{\partial I}{\partial t} \quad (2.27)$$

2.7.3 Multi-Dimensional model

Multi-scale models are a combination of 3-D, 2-D, 1-D and 0-D to form a complex model of the cardiovascular system.The 2-D and 3-D models are mostly based on the Navier-Stokes equations which are non-linear partial differential equations. The model behaviour may be parabolic, hyperbolic or elliptic which depends on the specific study. These models can provide detailed information of the blood flow in the vessel where the model describes the hemodynamic phenomena in a specific region of the cardiovascular system. The 2-D models are usually utilised to describe the change of blood flow velocity of the radial vessel in an axisymmetric tube [319], [320] . On the other hand, the 3-D models are generally utilised to simulate and study the interaction between blood flow and the vascular walls [321], [322]. 2-D and 3-D models need a great amount of computational resources since they provide detailed pressure and velocity distribution in a certain vessel segment of the cardiovascular system using the concept of computational fluid dynamics. Furthermore, a multi-scale model needs special attention as it is required to handle all the boundary conditions to ensure the desired output of the model is obtained mathematically. This is because one boundary condition is needed for each part of the blood vessel parameters which interlinks with the next part of the blood vessel to form a proper blood flow in the cardiovascular circulatory system. Hence, to establish a multi-scale model such as a 3-D model of the whole cardiovascular system, it would need complex geometrical and mechanical information which results in massive computational complexity. It would not be practical to be done. However, by using a multi-scale model with segments of 3-D or 2-D with another model such as 1-D or 0-D, this would be possible. For example, a 3-D model of a ventricular blood flow merged with a 0-D model for the rest of the cardiovascular circulatory system was done by Watanabe et al [323] where the 0-D model was able to provide the pressure values as the boundary conditions for the 3-D model. Similarly, Migliavacca et al.[324] merged a 3-D model of a systemic to pulmonary flow in a 0-D model of multiple branched circulation system model. The 0-D model was used to calculate the total sum

of static and kinetic pressure which was used as the boundary condition for the upstream interface of the 3-D model and for the downstream interface, the static pressure of the 0-D model was used as the boundary condition. In addition, a 0-D model of a vessel network was used by Vigono-Clementel et al. [325] as terminal loads to a complex 3-D model of arterial branching where the 0-D model was supplied with the pressure-flow rate relation to obtain the impedance values for the 3-D model's boundary condition. On the other hand, a 1-D model was merged by Formaggia et al. [326] with a 3-D model to remove the effect of the outgoing pressure waves and reduce computational complexity when analysis of blood flow was done in regards to the compliance of the vessels. A variational approach and a Lagrange multiplier approach are the two approaches proposed by Formaggia et al. [281], [327] to derive the variable distributions at the model interface. These approaches were further elaborated by Formaggia et al to be utilised for transient flow problems which was implemented by Vigono-Clementel et al.[325] for the model interfaces. Hence, to obtain a cardiovascular system model by minimizing the computational complexity using multi-scale is possible by combining two or more model such as combination of 3-D or 2-D models which are high dimensional models with lower dimensional models such as 1-D and 0-D models.

2.8 Summary

From the literature review, it is identified that there are many wearables to estimate the central aortic blood pressure waveform from the peripheral artery (radial artery) pulses to monitor the blood pressure reading. The findings from the literature review also show that a pressure sensor is the best choice to acquire the blood pressure waveform at the radial artery and it is possible to utilise the tonometry method as the pressure sensor has the best accuracy, sensitivity and specificity compared to a photoelectric or ultrasonic sensor [140]. The existing wearable devices estimate the central aortic blood pressure waveform to continuously update the user on their blood pressure reading (systolic and diastolic values) where these values are used to determine hypertension as a risk indicator. It is also known that hypertension is treated as a key indicator for cardiac risks which has generated many debates and editorial commentaries [15]–[17]. In regards of risk indication for cardiovascular disease, classical cardiovascular disease risk factors such as age, gender, smoking habits, obesity and blood pressure which can be obtained non-invasively, leads to misclassification of risk despite utilizing artificial intelligence such as ANN. Therefore, there is a need to utilize the entire blood pressure pulse with

artificial intelligence, rather than just the systolic and diastolic values, to give a better risk indication of cardiovascular disease. This is because by feeding in the entire blood pressure pulse waveform into an artificial intelligence, the waveform's morphology change (feature of the waveforms) can be used to determine cardiovascular disease.

Current research in artificial intelligence has shown remarkable achievements for pattern/feature classification using deep learning which is called Convolutional Neural Networks (CNN)[42]–[46]. CNN utilizing blood pressure waveform to classify cardiovascular disease has been established by some researchers [42], [274]–[276] and the research by Hu et al discovered that the CNN performs better in feature identification and classifying the blood pressure pulse signal compared to TCM doctors . Furthermore, majority of convolutional neural network [42]–[46] models using physiological waveform are used for pattern/feature classification although this doesn't indicate risk or act as a predictive role. Hence, to attain a risk indication-based convolutional neural network for future implementation in a predictive role, the output must be based on a numerical regressive output where the input of the convolutional neural network would be a full physiological signal waveform and the output would be a numerical number rather than a classifier. For blood pressure waveforms, this can be attained as today's research world has cardiovascular models where the inputs of the models are numerical values and the output is the corresponding blood pressure waveform. From the literature, it is known that the 0D model can provide the complete cardiovascular model for analysation of pressure, flow and volume of blood distribution in the system compared to the 1D, 2D, and 3D with the least amount of computational resources. If inputs of the 0D model (R, L and C parameters) are altered it would provide its corresponding output waveform where each parameter would relate to each output of time in the output waveform.

There are many 0D complete cardiovascular models in today's world that can be utilised to produce dataset for the convolutional neural network. The architecture of the CNN will vary depending on the dataset. For the dataset, from the literature review, V. Rideout complete cardiovascular model looks promising to be implemented for this technique, where a model is used in conjunction with a CNN. However, the research concept of this technique does not constrain the choice of the model, as long as there is a dataset of input of blood pressure waveform and numerical output where the numerical output can be utilised to indicate risk due to the variation of feature in the input

signal (blood pressure waveform). In the literature review, two 0D cardiovascular system models were reviewed which are the Vincent Rideout 0D model and the Korakianitis and Shi 0D model. The Vincent Rideout 0D complete cardiovascular model is preferred because the model represents a real human cardiovascular system with more insight whereas the model by Korakianitis and Shi is simplified. Moreover, Vincent Rideout model has more parameters than Korakianitis and Shi's model which can be helpful in studying the numerical change in the parameters to its corresponding output waveform to be utilised as a risk indicator. This is because each parameter would relate to each output of time in the signal. The computational time and complexity are also well balanced in the Vincent Rideout model. On top of that, end-diastolic pressure, initial flow, and unstressed volumes of the blood vessels are also provided by Vincent Rideout. Should these values be obtained via clinical study, it would have been time-consuming. So, this model presents an advantage in terms of time as well. Hence, the Vincent Rideout 0D model, seems more promising and adaptable to this technique while still enabling this technique to be implemented with other 0D models such as the Korakianitis and Shi 0D model.

In this project, a prototype would be developed to obtain the non-invasive radial pulse waveform by using a pressure sensor, which is then converted to an aortic pulse waveform. An investigation will be carried out to identify the best approach for converting the acquired radial waveform to the estimated aortic blood pressure waveform. Then, analysis would take place on the 0D model to identify the parameters that affects the model's aortic waveform. These identified parameters and its corresponding output waveform will be the dataset to be trained to the CNN. The trained CNN with the dataset is then utilised to provide the numerical output of the estimated aortic blood pressure waveform. This numerical output is then investigated against the 0D model's default values to identify the numerical output values of healthy and cardiovascular disease waveforms. By knowing the distinct numerical output value's range of healthy to cardiovascular disease, this CNN can be a risk indicator for cardiovascular disease.

CHAPTER 3 : METHODOLOGY

3.1 Introduction

This chapter addresses the methodology used to establish a medical system to indicate risk of cardiovascular disease. The system is split into 3 key subsystems, which are the wearable device, estimation of aortic waveform from radial, and finally the artificial intelligence for risk indication. This section describes the overall system design, the databases used, as well as the in-depth methodology of each sub-system. This chapter demonstrates the selection of sensors for non-invasive acquisition of the radial blood pressure waveform. Next, available transfer functions are investigated and the methodology for converting the radial blood pressure waveform into an estimated aortic blood pressure waveform was developed via an electrical impedance function. Finally an artificial intelligence (CNN) is used to identify and relate the features of the blood pressure waveform to the parameters of the estimated aortic waveform. These parameters are then used to indicate risk of cardiovascular disease by understanding the parameter changes with relation to healthy and unhealthy individuals' data.

3.2 Overall system design

The pressure sensor is placed on the medical system user's wrist to collect a pulse wave signal from the radial artery. The radial pulse wave signal is used to estimate the aortic wave signal by employing a transfer function, chosen and developed after reviewing the available techniques. The estimated aortic wave signal is then fed into the Convolutional Neural Network, which was trained with the 0D cardiovascular model to generate parameter values. After determining the inidicating parameter values, the change in parameter value that indicates the occurrence of cardiovascular disease will be identified. Finally, the proposed medical system would show the user's risk for cardiovascular disease. This design is summarized in a block diagram shown in Figure 3.1.

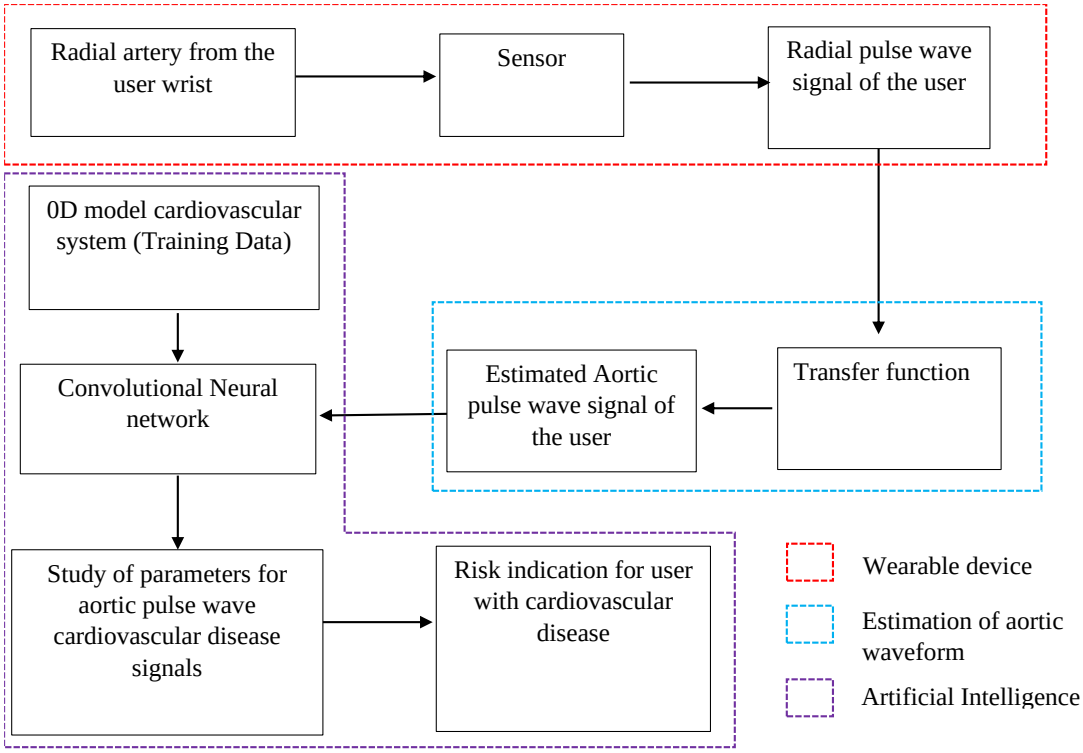

Figure 3.1 Proposed design of the medical system

For evaluating the system, as live patient data could not be collected using the prototype wearable device, and the system had to be verified before data could be requested from the hospital, two online databases were used to supplement the need for data. The two types of databases are PhysioNet MIMIC II Database [328] and HaeMod Database [329] of virtual subjects. In this project, the PhysioNet MIMIC II Database was used as the first batch of patient data while HaeMod Database of Thousands of Virtual Subjects used as the second batch of patient data. The reason for using online patient data is to ensure that the methodology works, and the hypothesis can be proven before visiting the hospital in order to verify the system with the cardiologist (Appendix 1). PhysioNet MIMIC II Database [328] contains radial blood pressure waveform of cardiovascular disease signals and other medical disease signals while HaeMod Database [195] has healthy virtual subjects of radial blood pressure waveforms and aortic blood pressure waveforms. The PhysioNet MIMIC II Database's other medical disease radial waveforms and HaeMod Database of virtual healthy subjects' radial waveforms were categorized as non-cardiovascular disease signals while the PhysioNet MIMIC II Databases' cardiovascular disease radial waveform is categorized as cardiovascular disease signals.

3.3 Non-invasive wearable device for blood pressure waveform acquisition

The findings from the literature review has shown that a pressure sensor is the best choice for the medical system to conduct continuous monitoring. The pressure sensor has the best accuracy, sensitivity and specificity to detect the radial pulse wave compared to the photoelectric and ultrasonic sensor [140]. As for the choice of pressure sensor, the piezo-resistive pressure sensors are taken in consideration because they are commonly used to measure blood pressure pulse waves of the human radial artery. This represents the most prominent method for precisely measuring radial artery blood pressure waveforms, because they can acquire both static and dynamic information of pulse waves with high sensitivity [330]. The piezoelectric sensor has a diaphragm structure, which is an ideal design for measuring fluctuating input pressure signals [331]. Piezoelectric sensors use piezoelectric-sensitive materials which contacts the human body skin directly to measure artery blood pressure waveform by generating charge and changes by itself in response to mechanical pressure applied on the material [331] and converting the sensed pressure reading into electric signals. Since this research is done in collaboration with Collaborative Research in Engineering, Science and Technology (CREST) and Chulia Facilities Management Sdn. Bhd, there is a requirement to identify a sensor which is able to acquire the radial blood pressure waveform to ensure the development of the wearable device. Figure 3.2 below shows the block diagram of the methodology on identifying the sensor and developing the prototype.

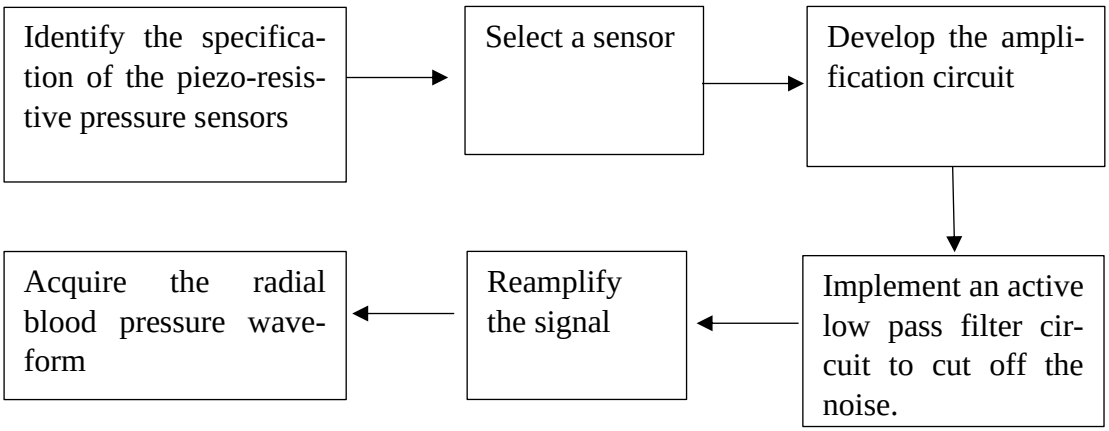

Figure 3.2 Methodology for sensor selection

Table 3.1 Specification of piezo-resistive pressure sensor to acquire radial blood pressure waveform

Parameter	**Definition**
Pressure range	0 to ≥300 mmHg
Pressure sensitivity	≤2 mV/mmHg
Response time	<0.4 ms
Precision	≤0.5%

3.4 Estimation of central aortic blood pressure waveform from radial blood pressure waveform

From the literature review, it is known that there is a need to investigate the current methods or develop a novel method which is able to give a close estimate of the actual aortic blood pressure waveform with a close prediction of the systolic pressure. In addition to this, the method should have a low computational intensity so that the overall system can be embedded in the user's wearable device, to guarantee onboard continuous monitoring even without wireless communication. This section investigates the existing methods and proposes a new mathematical technique using circuit analysis to reconstruct the central aortic blood pressure waveform from the acquired radial blood pressure waveform with low computing requirements. A circuit analysis approach was taken as the approach for the newly proposed technique, because circuits can be designed to modify, reshape or reject all unwanted frequencies of an electrical signal and accept or pass only those signals wanted by the circuit's designer. This is similar to the NPMA, which is a first-order low-pass filter which removes all the high frequency related pulse wave features as it travels from the central aorta to the periphery [130]. Furthermore, the pressure transducer acquires the radial blood pressure signal as a voltage reading which would be ideal to utilize the circuit analysis approach. Since the circuit analysis is done using electrical impedance circuit analysis, the derived mathematical function is called the electrical impedance function (EIF) and is then compared with the GTF, NPMA and ATF to evaluate its performance. The second systolic pressure technique was not compared, due to its limitation where it will not work if the second peak of the periphery disappears, which normally occurs in old or hypertension patients [130]. Figure 3.3 is the methodology on constructing the electrical impedance function to estimate central aortic blood pressure waveform.

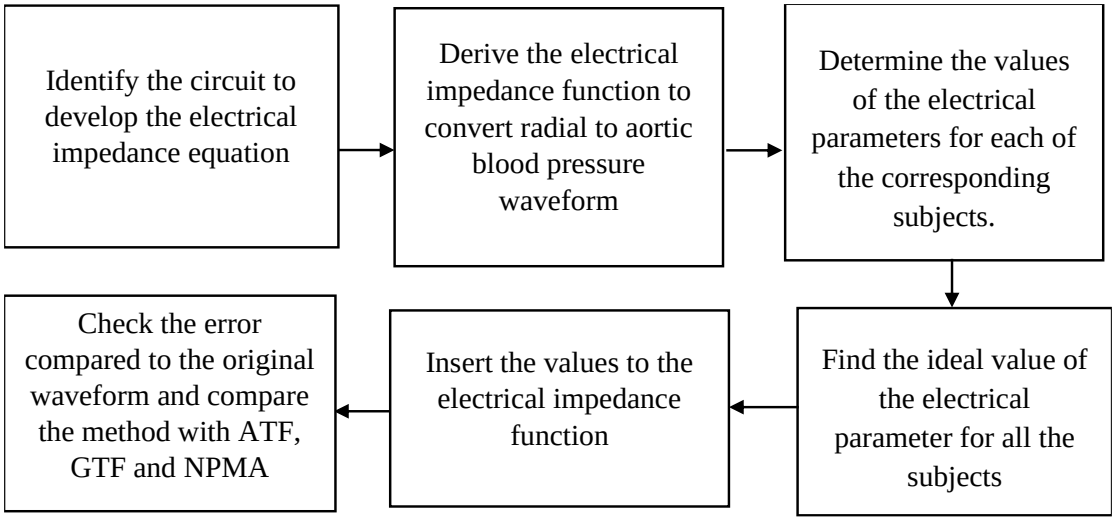

Figure 3.3 Methodology flow chart for developing a mathematical equation to estimate the central aortic blood pressure waveform

For the choice of the circuit to develop the Electrical Impedance Function (EIF), the Windkessel circuit model is taken as a reference. The Windkessel model has three types of variants: a two-element model, three-element model and four-element model [332]. The two-element model assumes a constant pressure-to-volume ratio and that the outflow from the Windkessel model is proportional to fluid pressure. For the two-element model, the volumetric inflow must equal the sum of the capacitive element's volume and the resistive element's volumetric outflow. The three-element model is an improved version of the two-element model as it considers the characteristic resistance of the aorta. However, the two-element model and three-element model does not have an inductor in their model where inductance represents the total inertia of the arterial system. This is implemented in the four-element Windkessel model and research by Roberto et.al [333] , which shows that the inductor placed in series to aorta characteristic resistance (W4S) is suitable to represent the inertial properties of blood motion compared to the inductor placed in parallel to aorta characteristic resistance (W4P). Furthermore, the research by Roberto et.al [333] showed that the W4S was able to attain a lower root mean square error compared to the W4P for experimental and model predicted pressure readings. These modelling techniques utilises the hydraulic-electric analogue where it would require more computing time due to the ODE solver. Hence, for this research an electrical impedance technique was utilised as a signal processing approach to reduce the computing time as this research requires to embed the conversion algorithm in the micro-controller. This research utilised the W4S four-element windkessel model circuit

to derive the electrical impedance function to estimate the central aortic blood pressure waveform. Figure 3.4 shows the equivalent circuit of the four-element Windkessel model where R and r are resistors, L is an inductor and C is a capacitor.

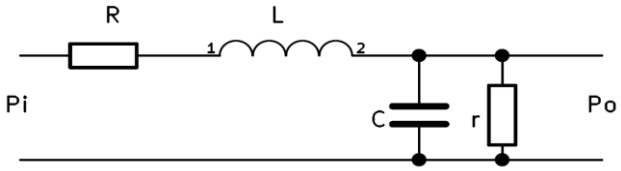

Figure 3.4 Four-element Windkessel model

The effective impedance of the four-element Windkessel model is given by the equation stated below.

$$Z_e(s) = sL + \frac{R + r + sCRr}{1 + sCr} \tag{3.1}$$

where *R* and *r* are resistors, *C* is the capacitance, and *L* is the inductance.

The input equation is given by

$$Pi = Z_e \times I \tag{3.2}$$

where Pi is input, Z_e is total impedance and I is total current.

Hence, the total current equation is given by

$$I = \frac{Pi}{Z_e} \tag{3.3}$$

and the output equation is given by

$$Po = I \times \frac{r}{1 + sCr} \tag{3.4}$$

The input and output, which are the aortic and radial waveforms respectively, were taken from the HaeMod database [329] and Hospital Sultanah Bahiyah in Malaysia. HaeMod contains 3325 virtual subject's aortic and radial waveforms. The clinical data of 40 patients for evaluating the system was obtained from Hospital Sultanah Bahiyah (HSB) under the ethical approval of the Clinical Research Centre (CRC) for this research. The cardiologist of HSB attained the consent from the patients before collecting the data for this research. The clinical data comes from a cohort of cardiac catheterization patients. Each patient's record had a radial blood pressure waveform and aortic

blood pressure waveform which was obtained by the cardiologist of the above-mentioned hospital during an angiogram procedure. The cardiologist first collects the radial blood pressure waveform at the wrist and then continues to the aortic blood pressure waveform close to the patient's heart. A continuous eight blood pressure waveforms of both aortic and radial blood pressure waveforms were recorded from each patient by the medical officer of HSB. The best out of the eight-blood pressure waveforms of both radial and aortic blood pressure waveforms which did not have distortion in the signal was selected to conduct this research. Since the cardiovascular system is a closed loop system, the continuous aortic blood pressure waveform was analysed, and it was determined that each pulse had a similarity of 98.5% on average to the other pulses obtained from the reading of a patient. This analysis was undertaken to ensure that the aortic blood pressure waveform retains its shape and features during the angiogram procedure. Table 3.2 summarizes the patient data characteristics. Appendix 2 has a breakdown of subject numbers and associated cardiovascular diseases for the hospital data. An example of the aortic and radial waveforms of HaeMod can be seen in Figure 3.5.

Table 3.2 Patient data characteristics

Patient Characteristics	**Cohort (n= 40)**
Men	23
Women	17
Age (years)	55 ± 18
Aortic systolic pressure (mmHg)	137 ± 44
Aortic diastolic pressure (mmHg)	74 ± 16
Branchial systolic pressure (mmHg)	132 ± 37
Branchial diastolic pressure (mmHg)	77 ± 21
Radial systolic pressure (mmHg)	159 ± 54
Radial diastolic pressure (mmHg)	74 ± 28
3 Vessel Defect	1

Dilated Cardiomyopathy	2
Hypertension & Diabetes Mellitus	1
Ischemic Heart Disease	10
Ischemic Heart Disease & 3 vessel defect	1
Myocardial Infarction (MI)	11
Positive Exercise Stress Test (EST)	5
Unstable Angina	8
Vascular heart disease	1

(a)

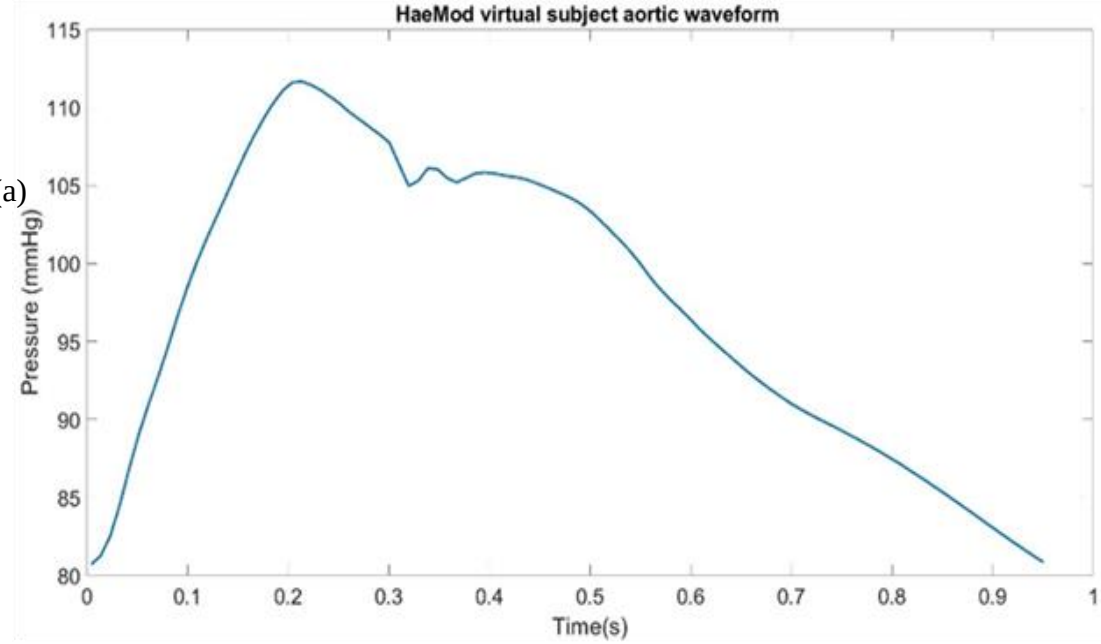

(b)

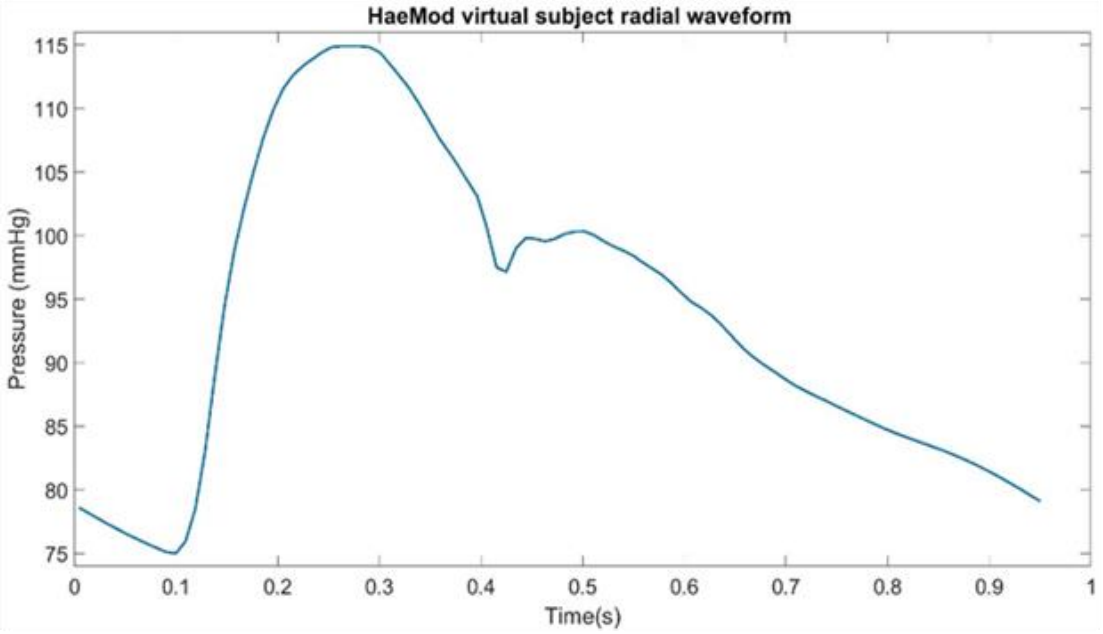

Figure 3.5 (a) HaeMod virtual subject aortic waveform & (b) HaeMod virtual subject radial waveform.

There are multiple unknown parameters to identify the optimum values for each parameter. Hence, the MATLAB optimization function 'fminsearch' was used to generate the values for the four-elements of the Windkessel model. The function uses the Nelder-Mead simplex algorithm which is a numerical method used to find the optimum of an unconstrained objective function in a multidimensional space. The boundary condition is set to start from 1 Farads for capacitor, 1 Henry for inductor and 1 Ohm for resistor. Since the databases (HaeMod and Hospital) provide the waveforms in pressure readings (mmHg), this pressure waveform is converted to voltage values following the prototype calibration where 1Volt = 3215.6178 mmHg. This was identified in the sensor selection section where the prototype can sense a maximum of 5N with 5Volts which is equivalent to 16078.089 mmHg. The equation 3.5 below shows the derivation for 1 Volt's pressure reading.

The development of the EIF is broken down into five steps:

(i) The four-element Windkessel model is coded in MATLAB using electrical impedance circuit analysis and the Symbolic Math Toolbox™ is used to obtain the resulting equation (EIF) which is used to generate the radial waveform from the aortic waveform.

(ii) This function is then mathematically rearranged so the equation (EIF) will now take the radial waveform as an input, to output the estimated aortic waveform.

(iii) A set of 20 random data each from HaeMod and Hospital is the training data that were taken to be fed to the Symbolic toolbox to obtain all the four-element's value of its corresponding subject for these datasets. These 20 randomly selected data from HaeMod and Hospital are chosen because the Hospital data has 40 data and half of it is used to identify the ideal/generalized four-element's value. Another 20 data were taken from HaeMod to maintain a balanced dataset for healthy (non-cardiovascular disease) and cardiovascular disease in identifying the ideal/generalized four-element's value and the rest of the HaeMod data is used for validation.

(iv) These 4 element values are then substituted into the equation and calculations are done for all the values to obtain the lowest Root Mean Square Error (RMSE) and mean absolute percentage error (MAPE), when comparing the calculated aortic waveforms to the actual ones from the database. The four-element values which had the lowest RMSE value and MAPE for all these datasets (20 CVD & 20 non-CVD) were considered to be the ideal/generalized four-element values. This is done because the four-elements values are interlinked to one-another. Hence, mathematically averaging all the four-elements values obtained in (iii) to identify the generalized four-element's value will contribute to error.

(v) These generalized values of the four-elements are then fed into the function to create an EIF to convert the radial to an aortic waveform.

After developing the EIF to estimate the central aortic blood pressure, it is then compared with the GTF, NPMA and ATF. The GTF is derived by extracting the radial and aortic pressure waveforms from the subject. Similar to the EIF, since Hospital data has only 40 data and half of it is 20 data, to keep the data set balanced, 20 healthy blood pressure signals were taken from HaeMod and 20 cardiovascular disease blood pressure signals was taken from Hospital data to develop the GTF. This is to test the efficiency of GTF for the balanced signals of the database. The extracted waveforms are transformed into the frequency domain. A Transfer Function (TF) was derived for each specific subject's radial and aortic blood pressure waveform for all the half data as mentioned above. All the attained TFs were averaged in order to obtain a GTF. To obtain the estimated aortic blood pressure waveform, the radial blood pressure waveform is

transformed to frequency domain and multiplied with the obtained GTF. The estimated aortic pressure waveform is then transformed back into the time domain. Equation 3.7 is the defined generalized transfer function of pressure waveforms between radial and aortic blood pressure waveform where $P_{a}(\omega)\ and\ P_{r}(\omega)$ are the pressure waveforms represented in the frequency domain of the aortic and radial blood pressure waveform respectively and (ω) is the angular frequency. If the moduli are denoted as $M_{a}(\omega)$ and $M_{r}(\omega)$ and phases denoted as $\varphi_{a}(\omega)\ and\ \varphi_{r}(\omega)$ the pressure waveforms can be written as $P_{a}(\omega) = M_{a}(\omega)e^{i\varphi}\ \ and\ P_{r}(\omega) = M_{r}(\omega)e^{i\varphi}$ for aortic and radial blood pressure waveforms respectively.

$$H_{(a-r)} = \frac{P_{a}(\omega)}{P_{r}(\omega)} \tag{3.7}$$

For the NPMA, the technique generates an array of incrementally averaged data points based on a constant denominator. The optimal NPMA denominator to derive the central aortic blood pressure waveform from the radial blood pressure waveform would be in one of a range of fractions of the sampling frequency of the signal. It is known from [12], that the N value as 4 is the best denominator for the averaging method to convert radial to aortic blood pressure waveforms for their sampling frequency of 128Hz. Similarly, this research followed the exact same method as [12] and identified the N value for the dataset which is used in this research.

For ATF, the transfer function is defined in the terms of the wave travel time (Td) and reflection coefficient parameters (Γ) of an arterial model. The parameters are estimated from the radial blood pressure waveform by investigating the visualization that central blood pressure waveforms exhibit exponential diastolic decays [123], [179] . Figure 3.6 shows the procedure of the ATF method to derive the central blood pressure waveform. Equation 3.8 is the ATF to estimate the central blood pressure waveform from the radial blood pressure waveform. For the ATF, an investigation was carried out to identity the Td in the wide range of 0 to 150 ms, with increments of 5 ms, and Γ in the physical range of 0 to 1, with increments of 0.05, following exactly the method done in this paper [179].

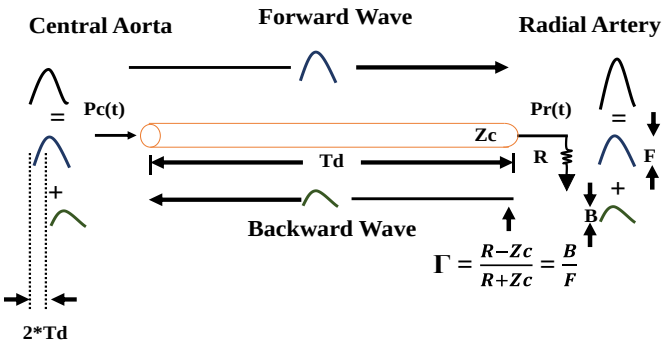

Figure 3.6 Adaptive transfer function (ATF) for deriving the central blood pressure waveform from a radial blood pressure waveform where radial blood pressure is Pr(t) , central blood pressure Pc(t), the wave travel time is Td, wave reflection coefficient is Γ [179].

$$Pc(t) = \frac{1}{1+\Gamma}\Pr(t+Td) + \frac{\Gamma}{1+\Gamma}\Pr(t-Td) \tag{3.8}$$

All the methods were developed and compared in the results and discussion section for the Root Means Square Error (RMSE), Mean Average Percentage Error (MAPE), peak difference and computational time. This is to identify a low computational intensity method which would be able to give a close estimate of the actual aortic blood pressure waveform with a close prediction of the systolic pressure. So that the system can be embedded in a wearable device to ensure continuous conversion of central aortic blood pressure waveform.

3.5 Modelling and artificial intelligence

This section shows the overall development of the risk indication system, based on the use of a convolutional neural network (CNN), as CNNs have shown remarkable contribution in recent years for pattern/feature classification based on the literature review. As opposed to the regular CNNs for classification, this CNN's output must be based on a numerical regressive output where the input of the CNN would be the blood pressure waveform and the output would be numerical rather than a classifier. Vincent Rideout's complete cardiovascular model is utilised to produce the dataset for the convolutional neural network. This model was chosen as it is a zero-dimensional model, making it less complex and easier to be implemented into this newly proposed medical system.

To have a better understanding of Vincent Rideout's complete cardiovascular loop model, an iterative study of the parameters is done. This is to study the relationship

between each parameter and its response to the aortic pressure signal. The study is focused on the second peak of the aortic pressure signal (PA1), as the second peak onwards of the model's output would have obtained a steady-state response which can be utilised to measure the effect on PA1. This is evaluated and proven in the results section (Section 4.4.1 **Modelling**). After identifying parameters of Vincent Rideout's model that affects the aortic signal, these parameters and the corresponding aortic blood pressure waveform is used to produce the dataset for the CNN where the input of the CNN would be the aortic blood pressure waveform and the output would be the identified parameters that affect the aortic blood pressure waveform. Figure *3.7* shows the overall methodology flowchart of the risk indication-based convolutional neural network (CNN), where it is split into two sections (Modelling and AI) for ease of explanation.

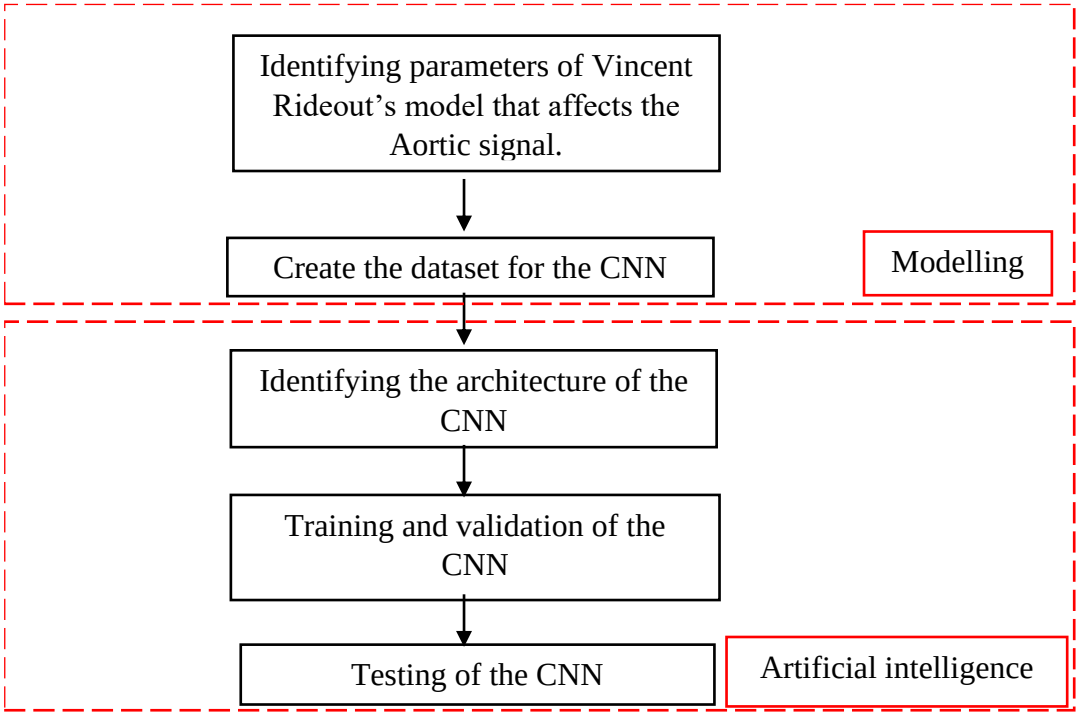

Figure 3.7 The flowchart of the overall methodology of the risk indication-based convolutional neural network (CNN)

3.5.1 Modelling

This section elaborates the method used to obtain the dataset for the CNN from Vincent Rideout's complete cardiovascular model. Firstly, Vincent Rideout's complete cardiovascular loop model was coded in MATLAB and the model was analysed to investigate the effects of the parameters. This was done to eliminate the parameters that are not significant to the aortic pressure signal by keeping them as constants. There are 36

parameters in Vincent Rideout's complete cardiovascular loop model, which are shown in Table 3.3 with their corresponding default values where the units for the resistance is $g \cdot s/cm^4$, compliance is $cm^4 \cdot s^2/g$ and inertance is g/cm^4.

Table 3.3 The 36 parameters in Vincent Rideout's complete cardiovascular loop model and their corresponding default values.

No	Parameter	Description	Default values	No	Parameter	Description	Default values
1	RP1	Pulmonary Artery 1 Resistance	10	19	LLA	Left Atrium Inertance	1
2	RP2	Pulmonary Artery 2 Resistance	40	20	LLV	Left Ventricle Inertance	1
3	RP3	Pulmonary Artery 3 Resistance	80	21	LA1	Aortic 1 Inertance	1
4	RL1	Pulmonary Vein 1 Resistance	30	22	LV2	Systemic Veins 2 Inertance	1
5	RL2	Pulmonary Vein 2 Resistance	10	23	LRA	Right Atrium Inertance	1
6	RLA	Left Atrium Resistance	5	24	LRV	Right Ventricle Inertance	1
7	RLV	Left Ventricle Resistance	5	25	CP1	Pulmonary Artery 1 Capacitance	0.00010
8	RA1	Aortic 1 Resistance	10	26	CP2	Pulmonary Artery 2 Capacitance	0.00030
9	RA2	Aortic 2 Resistance	160	27	CP3	Pulmonary Artery 3 Capacitance	0.00270
10	RA3	Systemic Artery Resistance	1000	28	CL1	Pulmonary Veins 1 Capacitance	0.00100
11	RV1	Ventricle 1 Resistance	90	29	CL2	Pulmonary Veins 2 Capacitance	0.00100

12	RV2	Ventricle 2 Resistance	10
13	RRA	Right Atrium Resistance	5
14	RRV	Right Ventricle Resistance	5
15	RPW1	Relative Pulmonary Resistance 1	10
16	RPW2	Relative Pulmonary Resistance 2	10
17	LP1	Pulmonary Aortic 1 Inertance	1
18	LL2	Pulmonary Vein 2 Inertance	1

30	CLA	Left Atrium Capacitance	0.01176
31	CA1	Aortic 1 Capacitance	0.00018
32	CA2	Aortic 2 Capacitance	0.00023
33	CA3	Aortic 3 Capacitance	0.00182
34	CV1	Systemic Veins 1 Capacitance	0.02100
35	CV2	Systemic Veins 2 Capacitance	0.04500
36	CRA	Right Atrium Capacitance	0.04500

The R, L, and C parameters that significantly contribute to changes in the aortic blood pressure waveform of Vincent Rideout's full cardiovascular loop model were found using a sensitivity analysis. This is done to identify the essential parameters that affect the aortic waveform. There are two types of sensitivity analysis, which are the local sensitivity analysis (LSA) and the global sensitivity analysis (GSA). LSA is a sensitivity analysis technique that iterates one parameter value at a time around its default value by keeping the rest of the other parameters fixed at their default values [36], [37]. This procedure is repeated for all the parameters to study the parameter's independent response to the output signal. On the other hand, the GSA is an advanced technique compared to the LSA, as it explores the interrelationship and the entire parameter response on the output signal [38]–[41]. When comparing the LSA and GSA, it is known that LSA is simple, easy to implement and computationally less expensive compared to the GSA. This research utilizes LSA as the sensitivity analysis technique because it is less computationally intensive and it studies the parameter's independent response to identify the significant parameter that affects the features of the model's output signal. In addition to this, as this work focuses on the use of these parameters as CNN outputs, it is preferable to be able to tune the outputs to each parameter's changes when trained

with the CNN, to ensure a better relationship with each parameter and their corresponding influence on the signal shape and feature can be obtained. Hence the choice of LSA over GSA is deemed to be the correct one for this work overall.

Furthermore, as previously mentioned, this study focuses on the second peak of the aortic pressure signal (PA1), as the from second peak onwards of the model's output (second output waveform) a close to steady-state response would be achieved, which can be utilised to measure the effect on PA1. At the second peak, one full blood flow circulation is completed whereas the first peak only quantifies the first pump of blood flow out of the heart (initial conditions of the model before reaching a steady-state response). A range from the parameter's nominal or default value was selected to examine the effect of an independent response of the R, L and C parameters in model inputs. For the value selection, two conditions had to be followed: the R, L and C values should not be zero; and all the parameter values should be positive. This resulted in the choice of a range of $\pm 75\%$ from the default values stated in Table 3.3, with a resolution of 25% in between the range, which gave an evaluation of 7 values for each parameter, and 252 evaluations overall. The model's runtime was kept constant while each parameter was changed from its default value, as indicated above, with the variation ranging from 0.25 to 1.75 times the default value, known as the minimum and maximum values respectively. This method is done by iterating one model input parameter value around its default value, while keeping all other parameters fixed at their default values to see the effect of the model's output [36], [37]. Then, the iterated input variable is returned to its default value and the procedure repeated for all parameters one by one, to capture the effect of each individual input parameter variation on the output. The results were analysed, and the parameters that affect the aortic pressure signal were computed. Figure 3.8 shows the methodology flowchart that is used for identifying the V.Rideout model's parameters that affect the aortic blood pressure waveform.

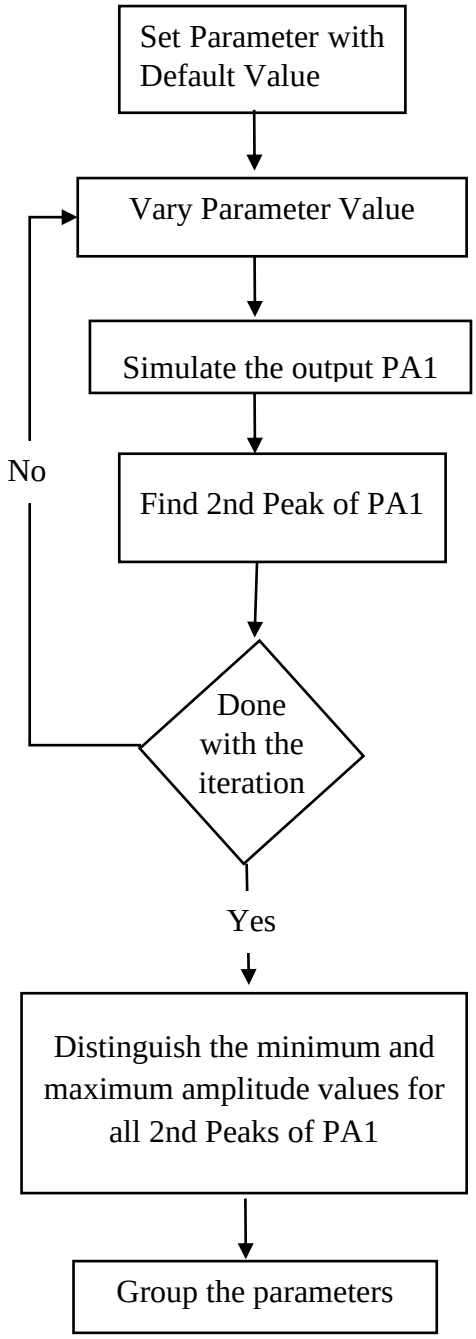

Figure 3.8 The methodology flowchart for identifying the V.Rideout model's parameters that affect the aortic blood pressure waveform

This analysis in Figure 3.8 is used to identify the independent response of the parameters that affect the aortic blood pressure waveform. This is done by differentiating the minimum and maximum amplitude values of the PA1 signal's second peak, where 7 output PA1 signals were obtained for the assessment of each parameter. If the difference between the minimum and maximum amplitude values of the second peak is greater than 2.5 mmHg, then the parameter is shortlisted as a parameter that contributes

in affecting the aortic blood pressure waveform. Any differences in the minimum and maximum amplitude values of the second peak that are lower than 2.5mmHg is not considered as parameters that affect the aortic blood pressure waveform. A change of pressure lesser than 2.5mmHg is considered as not significant. This pressure change can be related to physical activities done by humans. When a physical activity is conducted, there is a change in the blood pressure due to the intensity of the heart to pump blood to muscles during a vigorous activity. Hence, this pressure may be considered insignificant because it does not indicate any heart related disease as it is a part of normal human physiology [334].

3.5.2 Artificial intelligence

This section is divided into two subsections that provides details on the technique used to develop the risk indication-based CNN. The first subsection elaborates on the data generation process using Vincent Rideout's complete cardiovascular model, and the second subsection elaborates on the methodology of CNN development for the identification of parameter values for cardiovascular disease (CVD) and non-cardiovascular disease (non-CVD).

3.5.2.1 Data Generation

After shortlisting the parameters that affect the aortic pressure signal (PA1), these parameters were used to create the training data and validation data for the neural network. The data creation process is done by utilising two ranges of parameter values, where the first range is the maximum range of the parameter values and the second range is the initial range of the parameter.The data creation process starts by identifying the maximum range of values of each parameter, while keeping the rest of the parameters in the initial range, where the identified maximum range and the initial range of the parameters will be utilised to create the dataset.

To determine the maximum range, a standard deviation of $\pm 10\%$ times of the default value given by Vincent Rideout that affects PA1 is used as the initial range for the parameters. This is done while changing each parameter's standard deviation in an increment of ($\pm 10\%$) of the corresponding parameters default value, to obtain the maximum standard deviation of that parameters before the Vincent Rideout's complete cardiovascular loop model starts simulating a non-physiological aortic pressure signal. These default values given by Vincent Rideout produces a healthy aortic pressure signal

(PA1). By knowing the maximum standard deviation of each parameter that affects the PA1 signal, training data was formed by keeping all the parameters that affect the PA1 as randomised data within the ($\pm$ 10%) initial range of its parameter's default value, while changing each of those parameters one at a time to a randomised value within the maximum range.

The parameters that affect the PA1 were kept in an initial randomised range of ($\pm$ 10%) of the parameter's default value, to avoid the neural network from having a bias of one dominant parameter output compared to all the parameters that affect the PA1. This process of data creation is repeated to form the validation data, which is 20% of the total training data made. The sample size of the data would be dependent on the number of identified parameters, which affects the aortic blood pressure waveform.

3.5.2.2 Convolutional Neural Network

This subsection elaborates the methodology for the development of the risk indication-based CNN by using the dataset produced from Vincent Rideout's complete cardiovascular model. In addition to this, the identification of the parameter values for cardiovascular disease (CVD) and non-cardiovascular disease (non-CVD), which includes healthy cardiovascular signals is covered here. The training data (parameters) is fed into the neural network as the output and its corresponding PA1 signals of those parameters are placed as the input. Convolutional neural networks (CNN) were used as the neural network to replicate the idea of a doctor investigating a patient's signal and extracting its features to predict or identify the patient's health condition. CNNs have shown greater achievement in recent years for pattern / feature identification [42]–[46] which is suitable to be applied in this work, since the aortic pressure signal can be fed into the CNN, so that its features can be identified and related to the model's parameter values. The CNN structure which was selected is one with two-convolution layers. This is because by viewing the waveform, it can be observed that the crucial features of the waveform are minuscule and would be difficult to be captured by a single convolution layer structure. Furthermore, a majority of current research works utilising CNN for physiological signals have utilised more than a single convolution layer structure [42], [255], [256], [259], [263], [274] which has shown better accuracy. Hence, a two-convolution layer structure would increase the detection of these features due to the higher number of processes performed on it. This research investigates the feasibility of this method of detection, which utilizes a CNN structure of 2 convolution layers, with other

supplementary layers in between that are required for the CNN, which are two max-pooling and a fully connected layer, as shown in Figure 3.9.

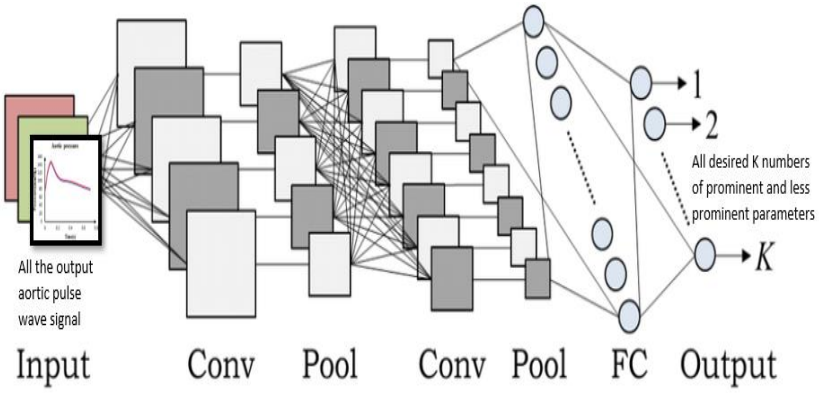

Figure 3.9 The CNN structure used in this work, with 2 convolution layers, 2 pooling layers, and 1 fully connected layer along with the input and output layers

An investigation must be conducted to identify the ideal CNN architecture, in which each layer of the CNN structure has its own hyperparameters that must be adjusted in order to determine the best combination. To find the optimal CNN architecture, a grid search of hyperparameters must be performed to find the best combination of hyperparameters. The CNN structure has 2 convolution layers and 2 maximum pooling layers where the convolution layer consists of hyperparameters, which are filter size, number of filters and stride while the maximum pooling layers has filter size and stride. In addition, the CNN has a learning rate which needs to be investigated, where the learning rate is a hyperparameter that controls how much to change the model in response to the estimated error each time the model weights are updated. These hyperparameter values need to be identified to attain the CNN's best architectures with the lowest validation RMSE. After the CNN is trained with the best architecture, it is validated with the validation data. If the validation achieves the lowest root mean square error (RMSE), the CNN is accepted. This is to ensure that the CNN will give reliable parameter results when an aortic pressure signal is fed into it. The overall methodology for identifying the CNN is shown in Figure 3.10 .

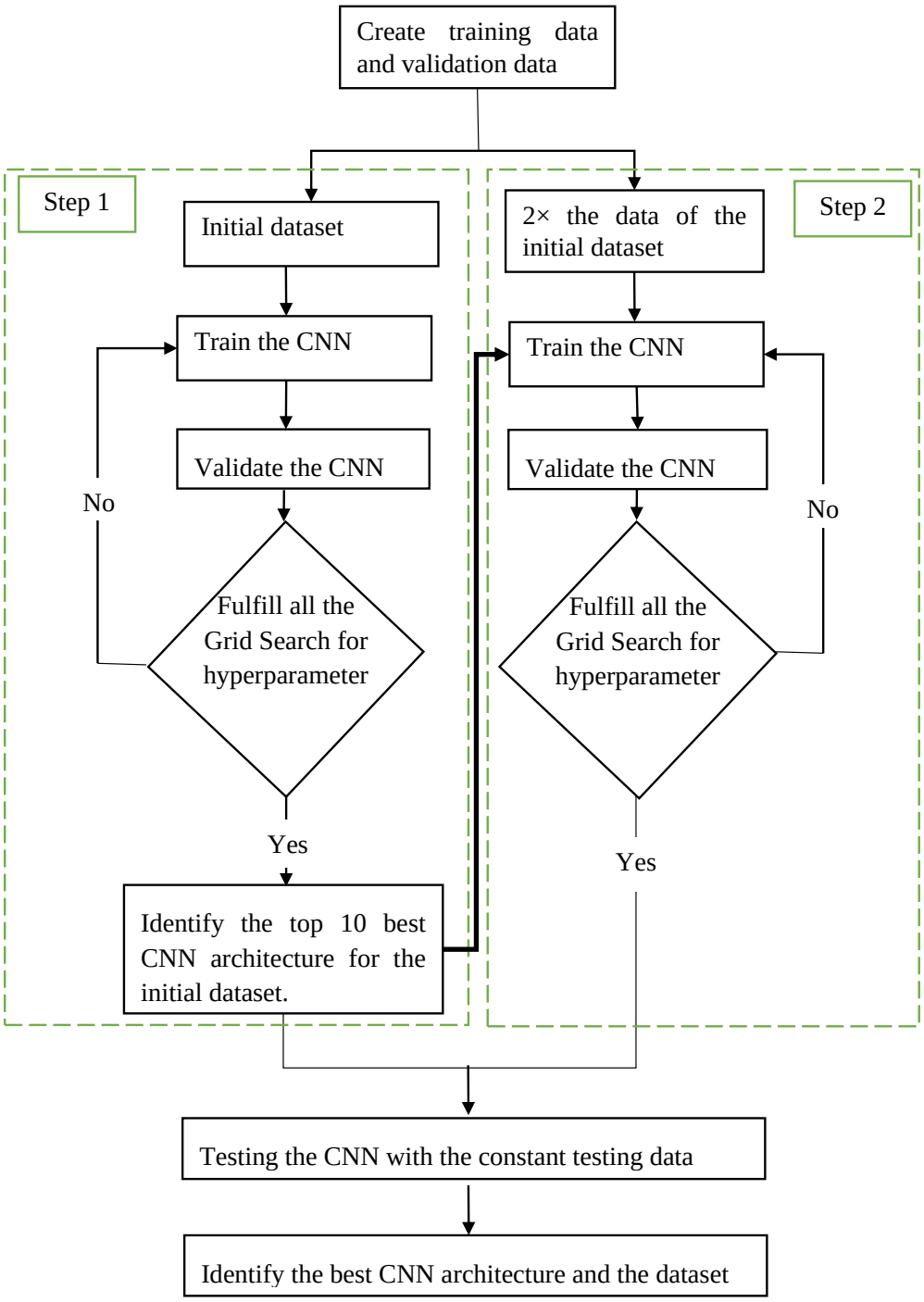

Figure 3.10 The methodology flow chart in identifying the CNN using the dataset produced from V. Rideout cardiovascular model.

As seen from Figure 3.10, there are two datasets being investigated, which are the initial dataset and twice the sample size of the initial dataset. The initially available training data would be dependent on the number of identified parameters that affects the aortic blood pressure waveform. Hence, a $sample\ size\ = k \times 100$ is chosen, where k is the total number of parameters that affect the aortic blood pressure waveform. As CNNs

usually take thousands of data, 100 samples for each parameter that affects the aortic blood pressure waveform were selected to attain a sufficient number of samples per parameter. Two datasets were made available to investigate the requirement of data for fine tuning the CNN where another dataset was made available which is double the size of the initial dataset, $sample\ size\ = k \times (100 \times\ 2)$. The initial dataset is utilised to identify the CNN's top 10 architectures with the lowest validation RMSE (Step 1 in Figure 3.10), where these top 10 architectures are used to retrain and validate with the dataset which is double the sample size of the initial dataset (Step 2 in Figure 3.10). The top 10 lowest validation RMSE CNN of both datasets are tested with a constant testing dataset to obtain the lowest RMSE, where the constant testing data is 20% of the total initial training data. This is done to investigate if the initial dataset is sufficient for the finetuning of the CNN, or if there is a necessity to increase the sample size of the dataset to improve the accuracy of the CNN, and to avoid overfitting in the neural network due to a large sample size of dataset.

Finally, the selected choice of the best CNN from the analysis is then utilized to obtain the parameters for the signals obtained from the online database, PhysioNet [328]. These parameter values are used as the base indicator parameters for cardiovascular disease and non-cardiovascular disease. After identifying the indicator parameters for CVD and Non- CVD, they are used to verify the classification of parameters for the healthy signals from HaeMod [329] and the cardiovascular disease signals obtained from the hospital. Figure 3.11 summarizes the flow chart of identifying the parameters of CVD and non-CVD and the verification of the classification by the CNN. The reason for using online patient data is to ensure that the methodology works, and the hypothesis can be proven before visiting the hospital in order to verify the system with the cardiologist (Appendix 1).

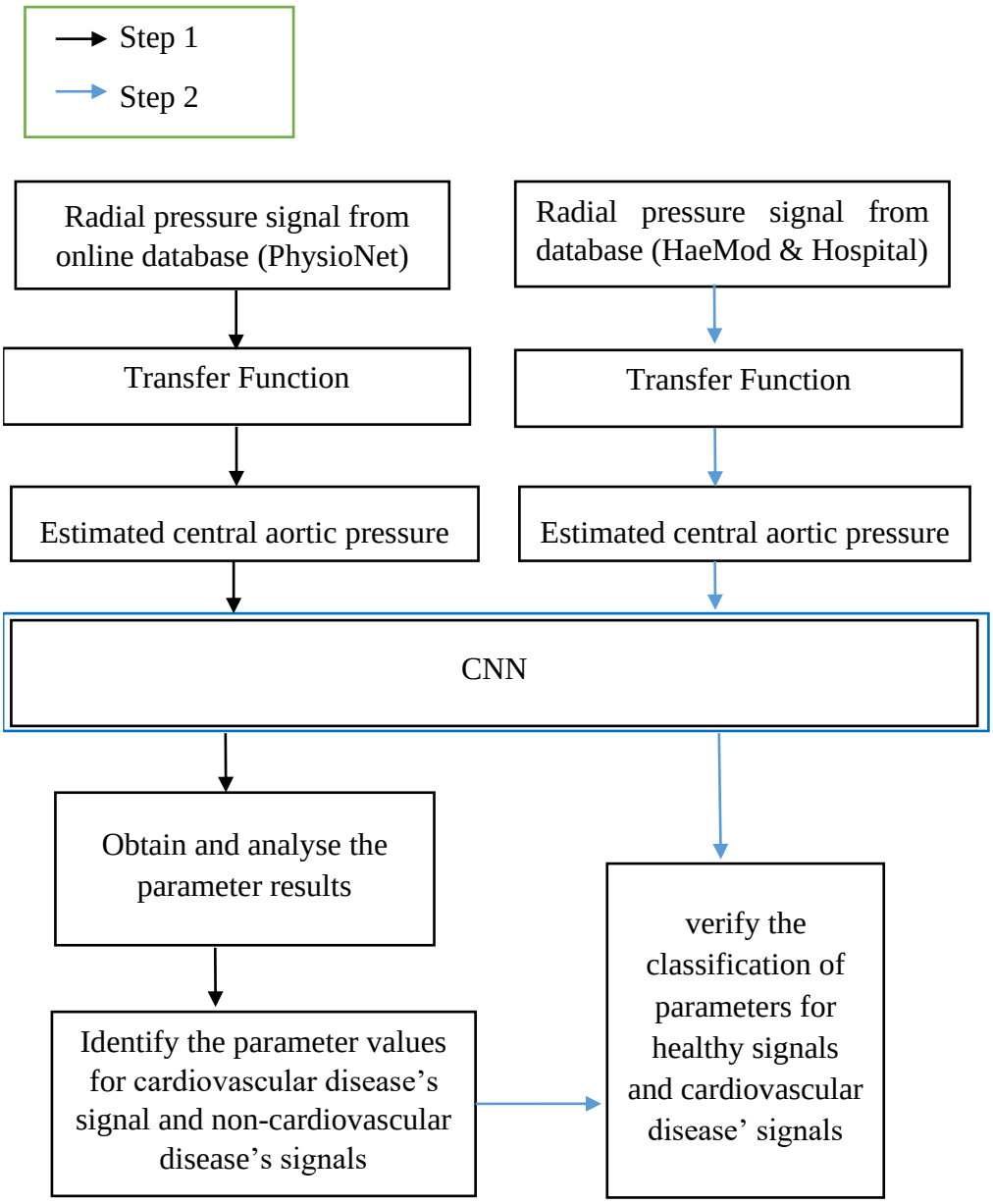

Figure 3.11 The flowchart of identifying the parameters of CVD and non-CVD and the verification of the classification by the CNN

CHAPTER 4 : RESULTS AND DISCUSSION

4.1 Introduction

This chapter presents the findings and discussion of the medical system to indicate risk of cardiovascular disease. As previously mentioned, the system is divided into three main subsystems that cover key sections of this research. First, the results of the sensor used in the prototype are shown and discussed. Next, the developed Electrical Impedance Function was used to convert the radial blood pressure waveform to an estimated aortic blood pressure waveform, and the results obtained were analysed. In order to demonstrate comparable estimation capabilities, the EIF was also compared with the Generalised Transfer Function, N-Point Moving Average and Adaptive Transfer Function. In addition, a study was shown in this chapter on the parameter which affects the zero-dimension cardiovascular model's aortic blood pressure. Afterwhich the best CNN architecture to interlink the parameter of the zero-dimension cardiovascular model with the estimated aortic blood pressure waveform has been utilised to identify baseline parameters for risk indication of cardiovascular disease. Finally the chapter reveals the overall outcome of the medical system methodology which was assessed using the hospital data obtained.

4.2 Non-invasive wearable device for blood pressure waveform acquisition

This section is broken into three subsection. The first subsection elaborates the choice of the sensor and its findings. The second subsection elaborated on the development of the hardware for the non-invasive prototype device to acquire the radial blood pressure waveform from the user's wrist. Finally, the third subsection elaborates the limitation of the hardware of the non-invasive prototype device for blood pressure waveform acquisition.

4.2.1 Sensor selection

For this research, the pressure sensor (Honeywell FSS005WNSB) shown in Figure 4.1 was selected to be used as the sensor to acquire the radial blood pressure waveform.

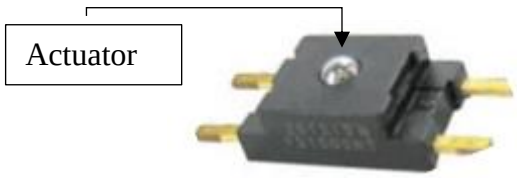

Figure 4.1. Honeywell FSS005WNSB

The sensing force of Honeywell FSS005WNSB is from 0 to 5N. The maximum sensing ability of this sensor is calculated by using the pressure Equation 4.1, while Equation 4.2 shows the calculation of the sensing area where *r* is the radius of the actuator and *h* is the height of the actuator.

$$Pressure = \frac{Force}{Area} = Stress \tag{4.1}$$

$$Sensor\ sensing\ Area\ =\ 2\pi rh \tag{4.2}$$

$$Sensor\ sensing\ Area = 2\ \times \pi \times 0.99mm \times 0.375mm = 2.3326 \times 10^{-6}\ m^2$$

$$Pressure = \frac{5}{2.3326 \times 10^{-6}} = 2143530.824\ Nm^{-2}$$

$$Maximum\ sensing\ capability = 2143530.824\ Nm^{-2}$$

Converting Millimetres of mercury (mmHg) to Newtons per metre squared(Nm^{-2})

$$1\ \text{mmHg}\ =\ 133.32\ Nm^{-2}$$

Hence,

$$\text{the maximum sensing capability}\ =\ \frac{2143530.824}{133.32} = 16078.089\ mmHg$$

The specification on the choice of sensor has been compared with HK-2000B (Hefei Huake Electronic Technology Research Institute, Hefei, China) [335]and MPX2053 [141] which were previously used in other research to acquire the radial blood pressure waveform pulse. Table 4.1 shows the specification comparison of the sensors.

Table 4.1 Comparisons of sensor specification

Parameter	**HK-2000B**	**MPX2053**	**FSS005WNSB**
Pressure range	300 mmHg	362mmHg	16078mmHg
Pressure sensitivity	2 mV/mmHg	1 mV/mmHg	0.18mV/mmHg
Response time	0.4ms	1ms	0.1ms
Repeatability error	0.5%	-	0.2%
Operating Voltage	5V	10V	5V
Operating Current	1.5mA	6mA	1.2mA
Price	RM 382.27	RM 50	RM 281.57

From Table 4.1, it can be seen that the Honeywell FSS005WNSB sensor gives the largest sensing range which is up to 16078mmHg, the best pressure sensitivity, the fastest response time and the lowest repeatability error (best precision). Moreover, the Honeywell FSS005WNSB sensor requires the least power compared to the HK-2000B and MPX2053 where it has the lowest current requirement. The large sensing range of FSS005WNSB sensor is crucial for the tonometry method because there will be an opposing force exerted to the sensor where the sensor is pressed directly against the skin to measure the pressure pulse waveform. Figure 4.2 shows the tonometry method conducted using Honeywell FSS005WNSB sensor.

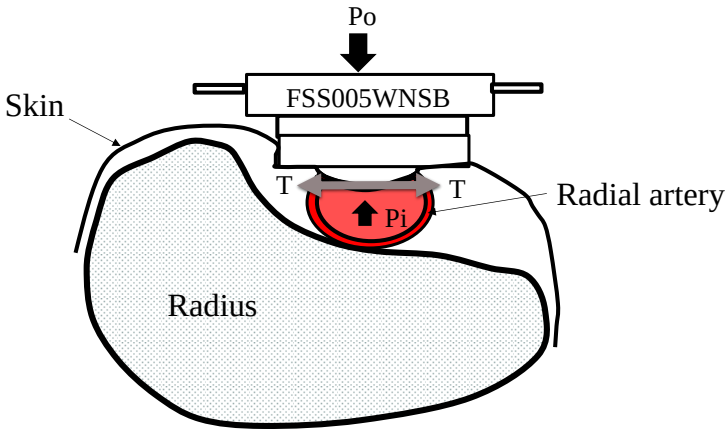

Figure 4.2 Diagram of the tonometry method

When the Honeywell FSS005WNSB sensor is pressed against the skin above the radial artery as shown in Figure 4.2, the dynamic equilibrium on the pressed surface can be expressed by Equation 4.3 considering the thickness of the blood vessel wall based on Laplace's law [336] where *T* is the circumferential tension on the blood vessel wall, P_i is the blood pressure, P_o is the external pressure and the curvature radii on the sensor pressing surface on the inner and outer walls of blood vessel are r_i and $r_o$respectively.

$$T = P_i r_i - P_o r_o \tag{4.3}$$

The Equation 4.3 can be rewritten in the form of representing the blood pressure (P_i) as shown in Equation 4.4.

$$P_i = \frac{r_o}{r_i} P_o + \frac{T}{r_i} \tag{4.4}$$

As can be seen in Figure 4.2, if the blood vessel is squashed on the FSS005WNSB sensing surface and hold, $r_o \approx r_i$ and $r_i \approx \infty$. Hence, Equation 4.4 can be approximated to Equation 4.5.

$$P_i \approx P_o \tag{4.5}$$

In other words, when an appropriate pressing force is exerted by the sensor to the blood vessel, the force detected by the FSS005WNSB sensors becomes equivalent to the force exerted by the blood flow. Therefore, if the FSS005WNSB sensor is retained with the optimum pressing force, it is possible to measure the blood pressure continuously without interrupting the blood flow. This would measure the pressure pulse waveform which is equivalent to the blood pressure waveform measured by inserting a catheter in to the blood vessel. The best way to detect the pressure waveform is to locate it directly above the blood vessel so that the condition of Equation 4.5 can be attained. Hence, it is necessary that the sensor's diameter be close to the diameter of the radial artery. In this case, the sensor has a diameter of 1.98mm and it is known from literature that the radial artery has a diameter of 2.2 +/- 0.4 mm [337], [338]. The diameter of the sensor is sufficient because the sensor will not be pressed till the center of the radial blood vessel to avoid interruption to the blood flow. Therefore, the sensor should have at least ¾ of the diameter of the radial artery (1.65mm) as its sensing diameter where in this case, the sensor has a diameter of 1.98mm.

4.2.2 Development of the hardware for blood pressure waveform acquisition device

The chosen sensor acquires the signal in milli voltage where there is a need to amplify the signal before feeding it to the microcontroller. The amplification of the output signal is done by 1000 gain using AD524c. Then, an active low pass filter was placed with a gain of 5 where R1 = $16k\Omega$, R2 = $1k\Omega$, R3 = $4k\Omega$ and C3 = $1\mu F$. An average healthy person at rest would have about 60 beats per minute and when in motion up to 100 beats per minutes. As the normal heart beat ranges from 1Hz to 1.7Hz (60bpm to 100bpm), the cut-off frequency is set to 10Hz. This is because the 10^{th} harmonic produces the central aortic blood pressure waveform [153], and this research is focusing on the upstream blood pressure waveform which is the central aortic blood pressure waveform, excluding the high frequency that is present in the radial blood pressure waveform. The Figure 4.3 shows the RC circuit diagram for the cut off frequency where the input signal is from the ADC524c and the output signal is fed to TL071CP. Equation 4.6 shows the derivation on obtaining the resistor (R1) and capacitor (C5) values for the cut off frequency of 10Hz. After low passing the signal, the signal is reamplified with TL071CP where the gain is set to 5. Figure 4.4 shows the circuit diagram of the reamplification with TL071CP where the input is obtained for the RC circuit in Figure 4.3 and the output is fed to the 16-bit Analog-Digital Converter (ADC). Equation 4.8 shows the derivation on obtaining both the resistors, R2 and R3 for reamplification.

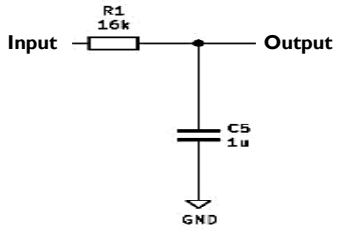

Figure 4.3 RC circuit.

$$f_c = 10\ Hz$$

$$f_c = \frac{1}{2\pi R_1 C_5} \tag{4.6}$$

Let R1 = $16k\Omega$

$$C_5 = \frac{1}{2\pi R_1 f_c} \tag{4.7}$$

$$C_5 = \frac{1}{2\pi \times 16k\Omega \times 10}$$

$$C_5 = 1.005309649\mu F \approx 1\mu F$$

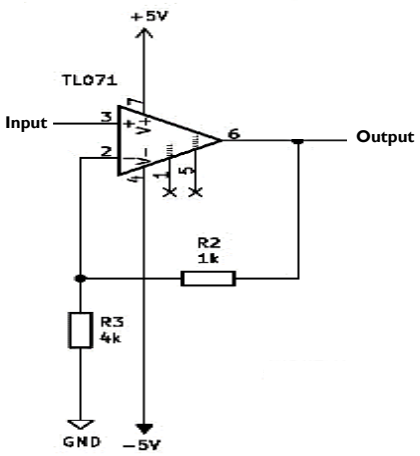

Figure 4.4 TL071CP amplifier circuit diagram

$$A_F = 1 + \frac{R_3}{R_2} = 5 \tag{4.8}$$

Let R2 = $1k\Omega$

$$R_3 = (5-1)R_2$$

$$R_3 = 4R_2$$

$$R_3 = 4k\Omega$$

For the power supply, two lithium-ion polymer batteries of 7.4V sources the 2 units of 7805 voltage regulators, which is used to power the sensor, microcontroller and both the amplifiers. The power supply circuit is built with two capacitors, which are C1 & C3 = $100nF$ and C2 & C4 = $220nF$ for each voltage regulator respectively. Figure.4.5 shows the hardware and the circuit to acquire the radial pulse waveform. The hardware consists of a pressure sensor Honeywell FSS005WNSB, two amplifiers which are AD524C and TL071CP, 1 microcontroller which is NodeMCU Lua V3 ESP8266 WIFI with CH340C, 1 SD card module and 1 organic light-emitting diode (OLED) which is SSD1306. Figure 4.6 shows the printed circuit board (PCB) developed in KiCad EDA where the AD524C, NodeMCU Lua V3 ESP8266 WIFI with CH340C, SD card module, the OLED and batteries will be plugged into it to form the prototype.

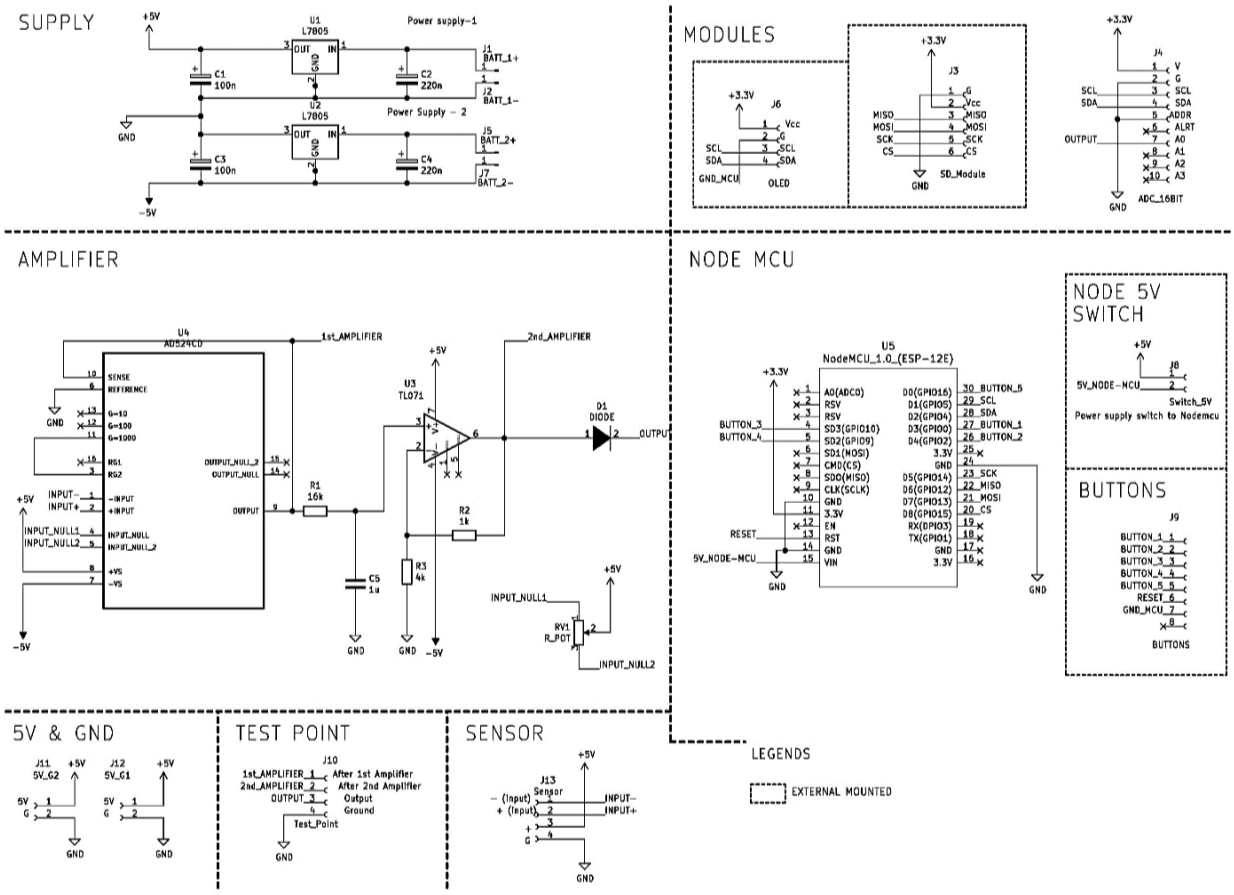

Figure.4.5 Hardware to obtain the radial signal from the patient

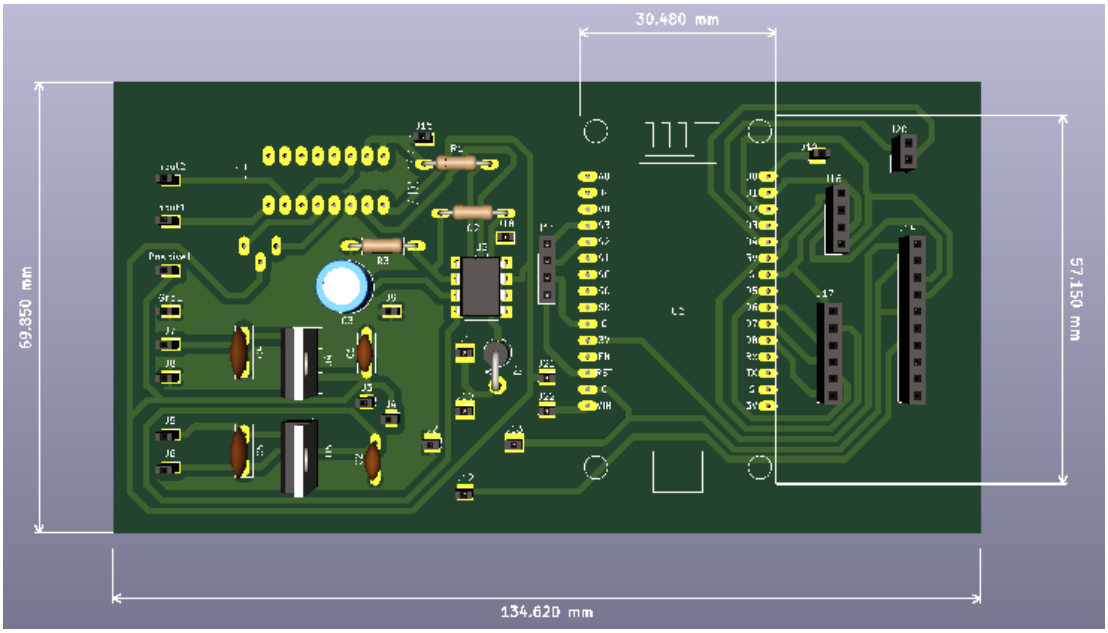

Figure 4.6 Printed Circuit Board (PCB) developed in KiCad EDA

The radial pressure waveform data acquisition device is shown in Figure 4.7. Figure 4.8 shows the radial signal obtained from the hardware, projected on to the oscilloscope after the first amplification of ADC 524 while Figure 4.9 shows the radial signal after

it is lowpassed and reamplified by TL071CP before transmission to the microcontroller. Figure 4.10 shows the radial signal obtained from the hardware with the microcontroller.

(a)

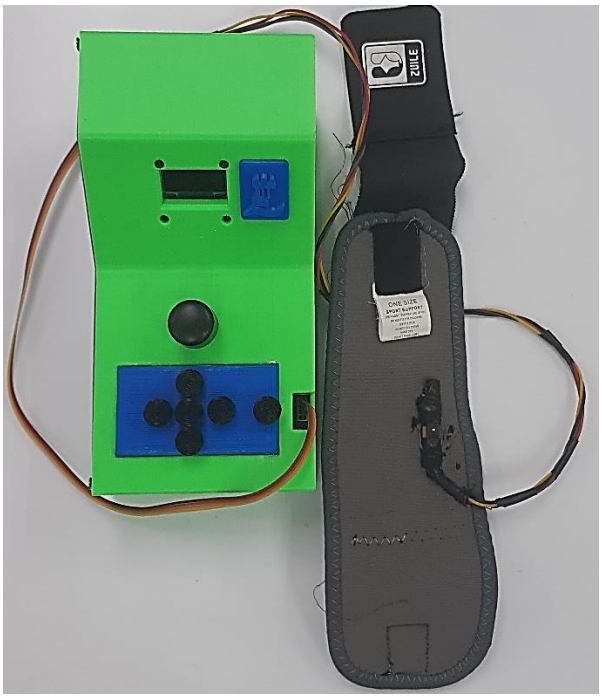

(b)

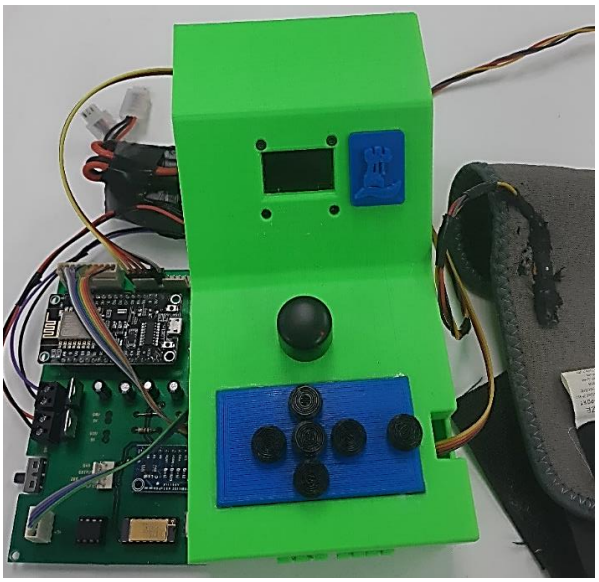

Figure 4.7 (a) Prototype of the overall device and (b) the circuit board displayed outside of the 3D printed enclosure of the prototype

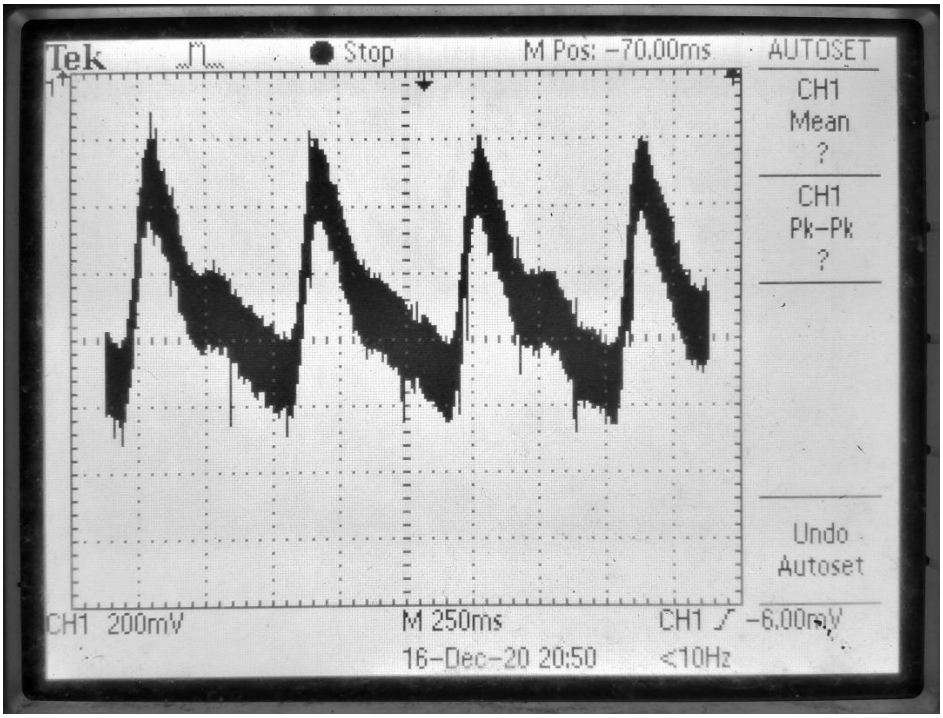

Figure 4.8. The radial signal obtained from the hardware on to the oscilloscope after the first amplification

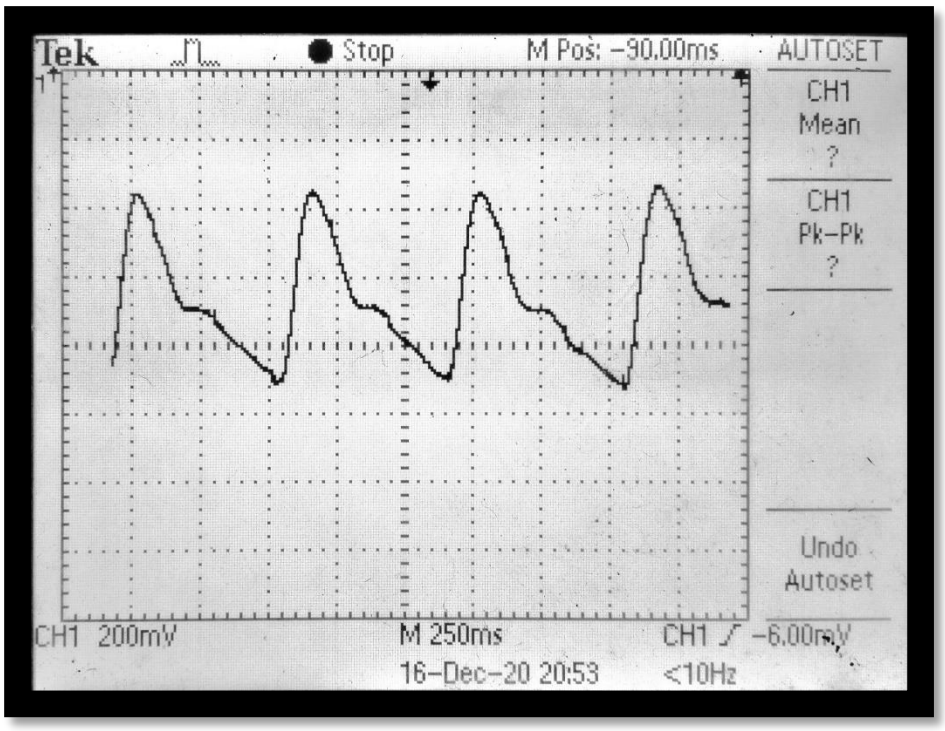

Figure 4.9.The radial signal after lowpass and reamplified by TL071CP before acquiring by the microcontroller

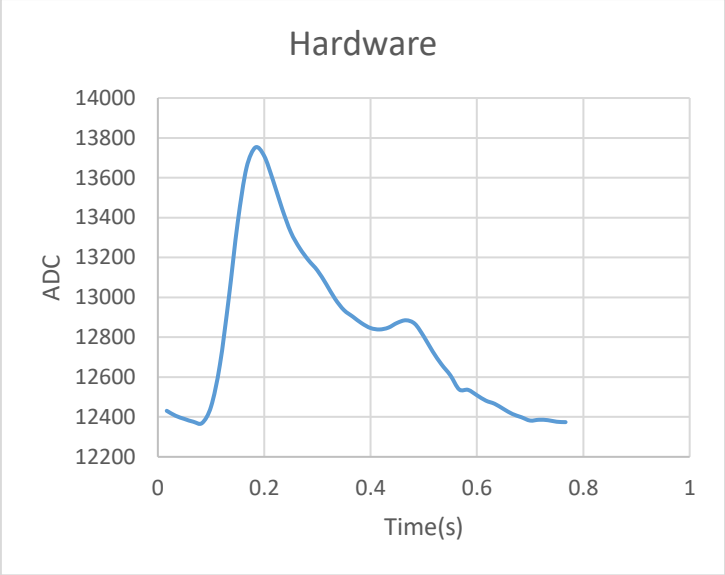

Figure 4.10 ADC values of the Radial pulse waveform from the microcontroller

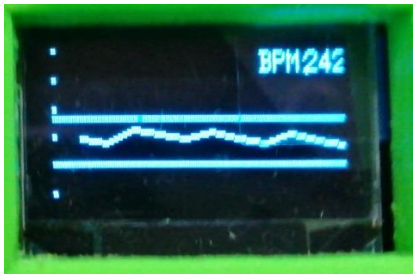

Figure 4.11 Radial signal captured by the hardware which is displayed by the OLED

When comparing the Figure 4.8 and Figure 4.9, it can be seen that the lowpass filter was able to eliminate the noise in Figure 4.8 to produce the signal in Figure 4.9. Moreover, the resolution of the signal obtained from the hardware to the oscilloscope in Figure 4.9 shows that it is much more detailed compared to the resolution of the signal obtained from the hardware to the microcontroller in Figure 4.10. This is because the oscilloscope has a sample rate of up to 1GigaSamples/Second compared to the microcontroller attached with a 16-bit Analog-Digital Converter (ADC) which has only a sample rate of 860 Samples/Second. Moreover, Figure 4.11 shows the OLED display of the signal captured by the microcontroller which has a resolution of 128 x 64 dot matrix panel of organic / polymer light-emitting diode which is too small-scale to display all the features of the signal obtained by the microcontroller. The purpose of the OLED is to display the signal process by the microcontroller. Hence, its resolution is good enough to visualise the signal acquired by the prototype.

4.2.3 Limitations of hardware

It is known that the arterial tonometry is used to measure the blood pressure waveform within the blood vessel, which needs a controlled force to maintain the radial artery in an applanated state over time [339], [340]. However, applanation has been proven to be difficult because it must be frequently calibrated in practice to ensure the blood pressure measurement to be accurate. Moreover using oscillometric blood pressure measurement for calibration of the arterial tonometry method contributes significantly to error [341]. Therefore, for this prototype, obtaining the user's invasive radial blood pressure waveform is required for this prototype in order to calibrate the ADC values to blood pressure values and to examine the accuracy or correlation between non-invasive and invasive blood pressure waveforms. This can be done in the hospital by strapping the prototype on the patient before an angiogram procedure where the doctor would puncher through the radial blood vessel. In addition to this, the signal attained from the prototype can be examined for its accuracy with the invasive signal acquired in the hospital. However, the current state of the hardware doesn't fulfill the criteria of Clinical Research Centre (CRC) in Malaysia where the prototype needs to be miniaturised to be a wearable device, so that it would be compact and handy to collect data in the hospital. To ensure miniature prototypes are produced, there would be a need of industrial soldering and changing the current components to Surface-mount technology (SMT) components. For this ongoing development, the industrial collaborator Chulia Facilities Management Sdn. Bhd will further develop the prototype into the wearable device.

4.3 Estimation of central aortic blood pressure waveform from radial blood pressure waveform

This section present the findings on the existing and developed transfer function for estimating the central aortic blood pressure wave from the radial blood pressure waveform. This section is divided into three subsections: development of the Electrical Impedance Function, identification of all transfer function method parameters, and comparison of the electrical impedance function to the Generalised Transfer Function, N-Point Moving Average, and Adaptive Transfer Function.

4.3.1 Development of the electrical impedance function

The four-element Windkessel circuit was coded using its equivalent circuit, by using the concept of Kirchhoff's voltage law (KVL) which implements complex frequency ('s'), and the function is transformed to time domain using inverse Laplace transform as the acquired signal by the prototype is in time domain. By converting to time domain, this would reduce computational time as the signal doesn't need to convert to frequency domain. Equation 4.9 shows the output equation to generate the radial from the aortic waveform.

$$Po = Pi \times r \times \exp\left(\frac{R \times t \times \left(\frac{1}{2}\right)}{L}\right) \times \exp\left(\frac{t \times \left(-\frac{1}{2}\right)}{C \times r}\right) \times \sinh\left(\frac{t \times \sqrt{(L^2 + C^2 \times R^2 \times r^2 - C \times L \times r^2 \times 4 + C \times L \times R \times r \times 2)}}{C \times L \times r \times 2}\right) \times \frac{1}{\sqrt{(L^2 + C^2 \times R^2 \times r^2 - C \times L \times r^2 \times 4 + C \times L \times R \times r \times 2)}} \times 2 \quad (4.9)$$

where *Po* is the output of the radial waveform, *Pi* is the input of the actual aortic waveform and *t* is the time (seconds).

Equation 4.9 is then mathematically rearranged to obtain the EIF to estimate the central aortic blood pressure, which is shown in Equation 4.10.

$$"Po" = "Pi" / (r \times \exp\left(\frac{R \times t \times \left(\frac{1}{2}\right)}{L}\right) \times \exp\left(\frac{t \times \left(-\frac{1}{2}\right)}{C \times r}\right) \times \sinh\left(\frac{t \times \sqrt{(L^2 + C^2 \times R^2 \times r^2 - C \times L \times r^2 \times 4 + C \times L \times R \times r \times 2)}}{C \times L \times r \times 2}\right) \times \frac{1}{\sqrt{(L^2 + C^2 \times R^2 \times r^2 - C \times L \times r^2 \times 4 + C \times L \times R \times r \times 2)}} \times 2) \quad (4.10)$$

where "*Po*" is the output of the aortic waveform, and "*Pi*" is the input of the actual radial waveform and *t* is the time (seconds).

4.3.2 Paramater identification for the estimation methods

Once equation 4.10 was obtained, the estimated aortic waveform of the randomly selected 20 data each of HaeMod and Hospital were fed in, and when compared with the actual aortic waveform, the four-element parameters with the lowest RMSE and MAPE were taken as the generalized values. Table 4.2 shows the top five lowest average RMSE and MAPE generalized four-element values for the random 40 data, where the first row is the four-element parameter with the lowest RMSE which was taken as the generalized values.

Table 4.2 The top five lowest average RMSE and MAPE generalized four-element values for the random 40 data from HaeMod and Hospital

No	**R (Resistor) Ohm, Ω**	**L (Inductor) Henry, H**	**C (Capacitor) Farads, F**	**r (Resistor) Ohm, Ω**	**RMSE (mmHg)**	**MAPE (mmHg)**
1	4.583	5.934	0.000421	6.268	12.55	0.1000
2	4.843	6.142	0.000394	6.422	12.60	0.0988
3	15.679	20.879	0.000121	22.086	12.73	0.1054
4	1.877	2.611	0.000828	2.885	12.75	0.1092
5	6.351	8.393	0.000608	9.243	12.82	0.1021

Subsituting the lowest RMSE values into Equation 4.10 a simplified version (rounded to 3 s.f) of the EIF used in this research is shown in Equation 4.11.

$$"Po" = "Pi" /(2.12 \times \exp(0.386t) \times \exp(-189t) \times \sinh(189t)) \quad (4.11)$$

where "*Po*" is the output of the aortic waveform, and "*Pi*" is the input of the actual radial waveform and *t* is the time (time).

After attaining the four-element parameter's generalised value, it is fed into the electrical impedance function and this function is then compared with the GTF, NPMA and ATF. All the compared methods utilised the same dataset of random 20 data each from HaeMod and Hospital to attain their generalised function which was then validated with the overall database. For the NPMA, an investigation is carried out to identify the ideal N value, by investigating the impact of changing the N value from 2 to 10. Table 4.3 below shows the N values which were investigated for the average RMSE, MAPE and peak difference compared to the database central aortic blood pressure waveform.

Table 4.3 Average RMSE, MAPE and Peak difference for the N value of NPMA

N value	**RMSE (mmHg)**	**MAPE (mmHg)**	**Peak difference (mmHg)**
2	22.93	0.1751	20.59
3	17.60	0.1157	13.03
4	14.04	0.0880	11.38

5	11.83	0.0813	10.93
6	10.71	0.0798	10.65
7	9.89	0.0794	10.26
8	9.73	0.0796	10.14
9	9.64	0.0803	9.97
10	9.73	0.0808	10.04

From Table 4.3 above, it is identified that N = 9 is the ideal value for this dataset as it was able to attain the lowest RMSE and Peak difference. For the ATF, an investigation was carried out to identify the *Td* in the wide range of 0 to 150 ms, with increments of 5 ms, and *Γ* in the physical range of 0 to 1, with increments of 0.05. The Td and Γ are 25 ms and 0.65 respectively for the random 20 data from HaeMod and Hospital respectively which had the lowest average RMSE of 8.498 mmHg.

4.3.3 Comparison of electrical impedance function with other methods

The above-mentioned methods were then used to estimate the aortic blood pressure for all 3365 data from HaeMod (3325data) and Hospital (40 data), and the subject that had the lowest RMSE and MAPE for the 4 methods was chosen for comparison, as shown in Figure 4.12. After analyzing all the 3365 subjects, Table 4.4 shows the Average RMSE, MAPE, Peak difference and computational time for 3325 virtual subjects using all 4 methods. The results were obtained from a computer with Intel Core i7- 4510U CPU(2.0GHz) with 12GB RAM.

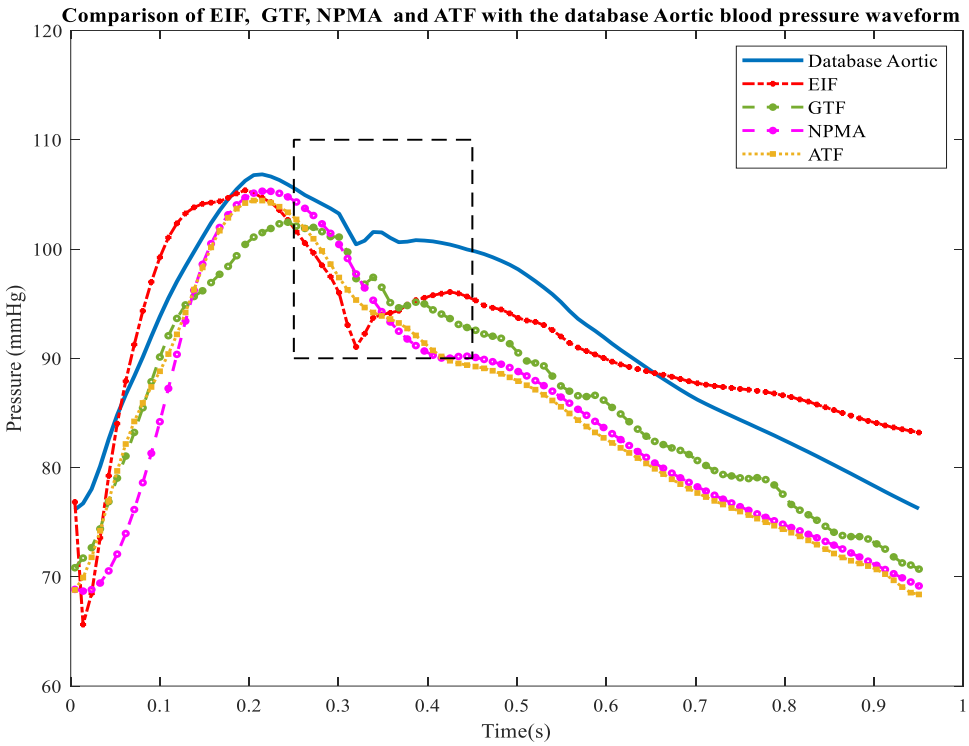

Figure 4.12 The estimated central aortic blood pressure of all the 4 methods against the corresponding database's central aortic blood pressure waveform; highlighted is the feature of the database aortic waveform captured by the EIF method.

Table 4.4 Averages of RMSE, MAPE, Peak difference and computational time for 3365 datasets using all 4 methods

Method	**RMSE (mmHg)**	**MAPE (mmHg)**	**Peak Difference (mmHg)**	**Computational time (ms)**
EIF	9.4838	0.0661	6.35	0.0129
GTF	6.2698	0.0477	7.46	0.0142
NPMA	9.3596	0.0762	5.99	0.6481
ATF	8.4952	0.0713	5.75	119.79

Table 4.4 shows that estimating the aortic blood pressure by using the EIF had a lower average MAPE when compared to NPMA and ATF. When compared with GTF, the EIF has shown the lowest peak difference. The GTF was able to give the lowest average

RMSE and MAPE compared to all the methods. Overall, the EIF had the best computational time by far, having a big margin between the NPMA and ATF and a close difference between the GTF. A visual display of 3 simulated signals by all the methods compared to their respective aortic blood pressure waveform of the dataset is shown in Figure 4.13. All the methods are further investigated using the Bland Altman plot shown in Figure 4.14 for the diastolic, systolic and pulse pressure reading for all the 3365 data where the Bland Altman plot gives a graphical representation of how accurate the data is within the tolerance of the Limit of Agreement (LOA) which is tabulated in Table 4.5. It is known that the notch is one of the primary signaling that facilitates the endothelial-to-mesenchymal transformation and significant evidence has implicated 'endothelial dysfunction' as a contributing factor to cardiovascular diseases [246]. Hence, as seen in Figure 4.12 the highlighted area of the signal which displays the notch is further investigated to study the correlation between the estimated central aortic blood pressure waveform signals of all methods against the aortic blood pressure for all 3365 from HaeMod (3325data) and Hospital (40 data) as shown in Table 4.6.

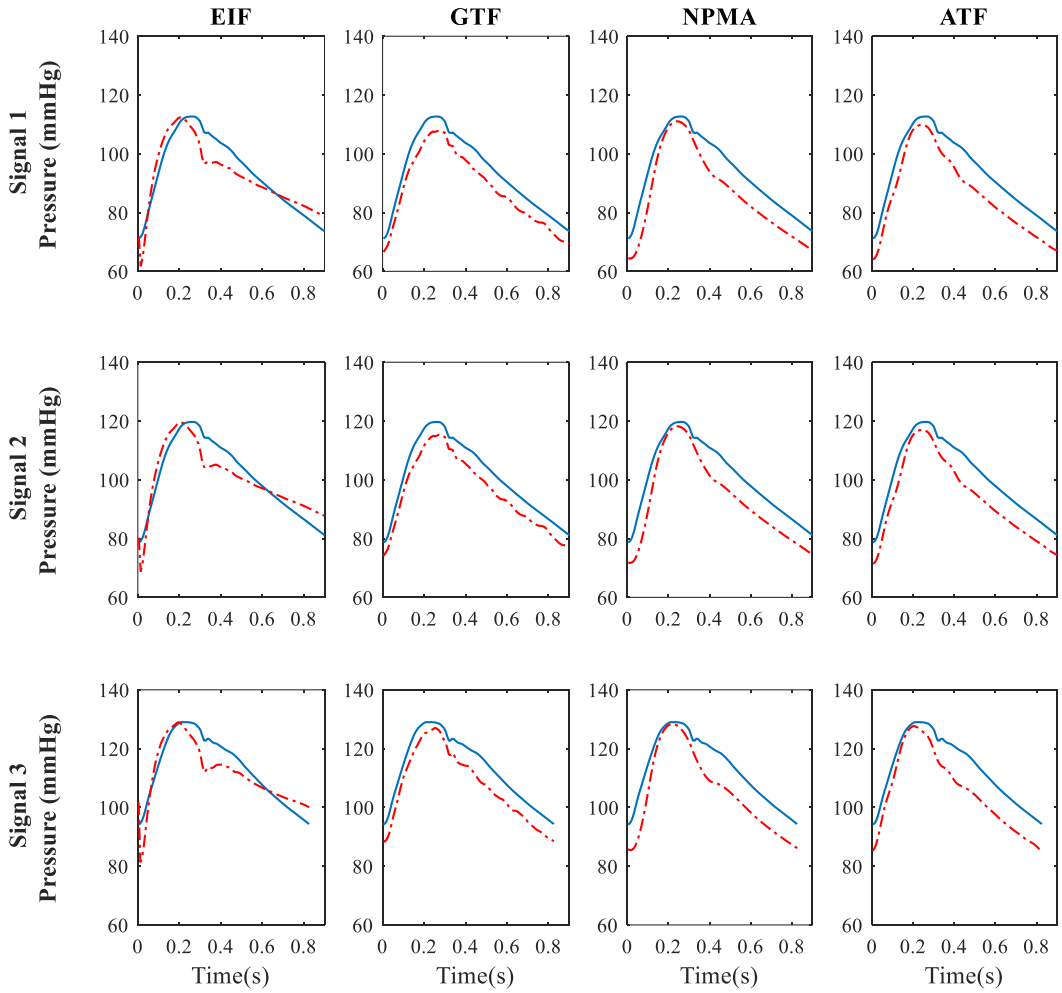

Figure 4.13 Comparison of the conversion performance for 3 signals of all the methods to the dataset's aortic blood pressure waveform (Blue (solid) line: original signal, Red (dashed) line: estimated).

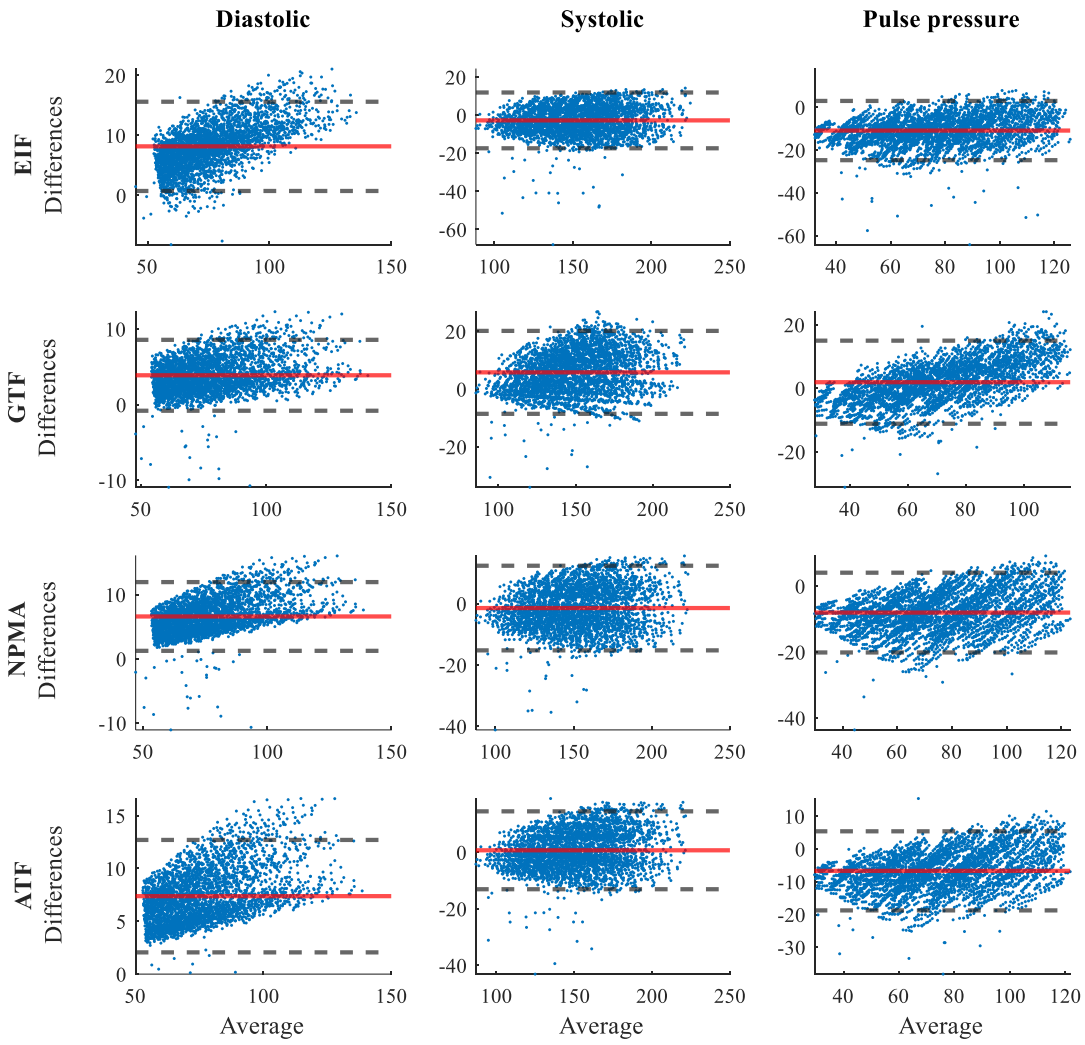

Figure 4.14 Bland Altman Plot for all the methods' estimated blood pressure waveforms against the 3365 dataset of aortic blood pressure waveform. (Dashed lines are the Lower and Upper Limit of Agreement (LOA), Solid (Red) line is the Mean difference)

Table 4.5 Number of points that were exceeding the Limit of Agreement (LOA) for the Bland Altman Plot

Method	**EIF**	**GTF**	**NPMA**	**ATF**
Diastolic	196	150	159	157
Systolic	57	102	103	119
Pulse Pressure	146	168	157	170

Table 4.6 Average correlation percentage of all the method against the 3365 datasets.

Method	**Correlation (%)**
EIF	99.92± 0.05
GTF	99.97± 0.03
NPMA	99.90± 0.08
ATF	99.96± 0.04

From the above results in Table 4.4, the GTF has shown the best results in estimating the central aortic blood pressure waveform as it was able to give the lowest RMSE, MAPE and a reasonable computing time. However, GTF has a greater peak difference compared to EIF, NPMA and ATF. Table 4.4 also shows that EIF was able to give the lowest MAPE compared to the NPMA and ATF and a reasonable peak difference of 0.36 mmHg and 0.6mmHg respectively. As for the RMSE, when the EIF was compared with the NPMA and ATF, it was able to give a close difference of 0.1242 and 0.9886 respectively. From the Bland Altman plot in Figure 4.14, it can be seen that the EIF shows a better estimation for systolic pressure and pulse pressure as it was able to keep 98.31% and 95.66% respectively of the data of the 3365 datasets in the limit of agreement (LOA) compared to GTF, NPMA and ATF where GTF attained 96.97% and 95.01% respectively, NPMA attained 96.93% and 95.33% and ATF attained 96.46% and 94.95% respectively. The Bland Altman plot in Figure 4.14 also shows that the EIF was able to keep 94.18% data of the 3365 data's diastolic pressure in the limit of agreement (LOA) which is a reasonably close difference of 1.36% to the GTF method which is the best estimator for the diastolic pressure, as it was able to keep 95.54% data of 3365 dataset in the limit of agreement (LOA). Generally, in studies where readings of systolic and diastolic blood pressure have been compared, systolic blood pressure has been a better predictor of hypertension risk [178]. Epidemiological and treatment studies suggest that systolic blood pressure should be the primary target of antihypertensive therapy [178]. Hence, EIF has shown that the method is capable to be a good predictor for hypertension risk compared to GTF, NPMA and ATF. Furthermore, this is line with this research, as it needs a low computing method to estimate the aortic blood pressure waveform to be embedded in the microcontroller to ensure that the risk is always

indicated to the user even if there is no wireless communication, EIF and GTF are the optimum choices. It is known from literature [169], [170] that GTF contributes error if the GTF is applied to patients which are not in the specific group of patients which was used to generate the GTF. Hence, the EIF and GTF methods are further investigated to see its reliability when it is constructed with one dataset of patient's specification and compared with the dataset of patients which are not in the dataset of patient's specification. This analysis is crucial as the medical system would be utilised by various users, and if the user characteristics is not considered in the method to estimate central aortic blood pressure waveform, the method will contribute to significant error. Since hospital data has 40 data, it will be utilised as the validation of the methods and 40 data randomly selected from HaeMod will be used to reconstruct the methods. Table 4.7 shows the average RMSE and MAPE for the 40-hospital data when the EIF and GTF were constructed from the 40 data randomly selected from HaeMod. A visual display of 3 simulated signals by EIF and GTF constructed by the above-mention data comparing to the respective hospital aortic blood pressure waveform is shown in Figure 4.15 and these methods were further investigated using the Bland Altman plot shown in Figure 4.16 for the diastolic, systolic and pulse pressure reading.

Table 4.7 Averages of RMSE and MAPE for 40 hospital datasets

Method	**RMSE (mmHg)**	**MAPE (mmHg)**
EIF	13.5234	0.1131
GTF	11.9634	0.1141

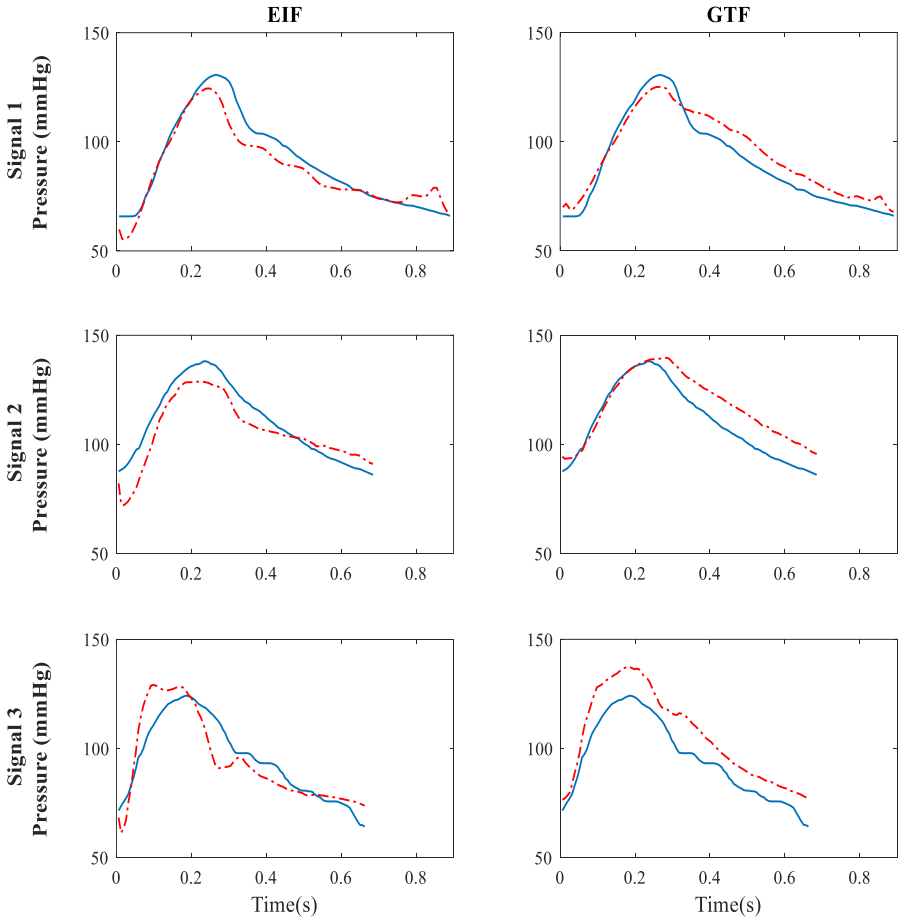

Figure 4.15 Comparison of conversion performance for 3 signals of EIF and GTF to the hospital's aortic blood pressure waveform (Blue (solid) line: original signal, Red (dashed) line: estimated).

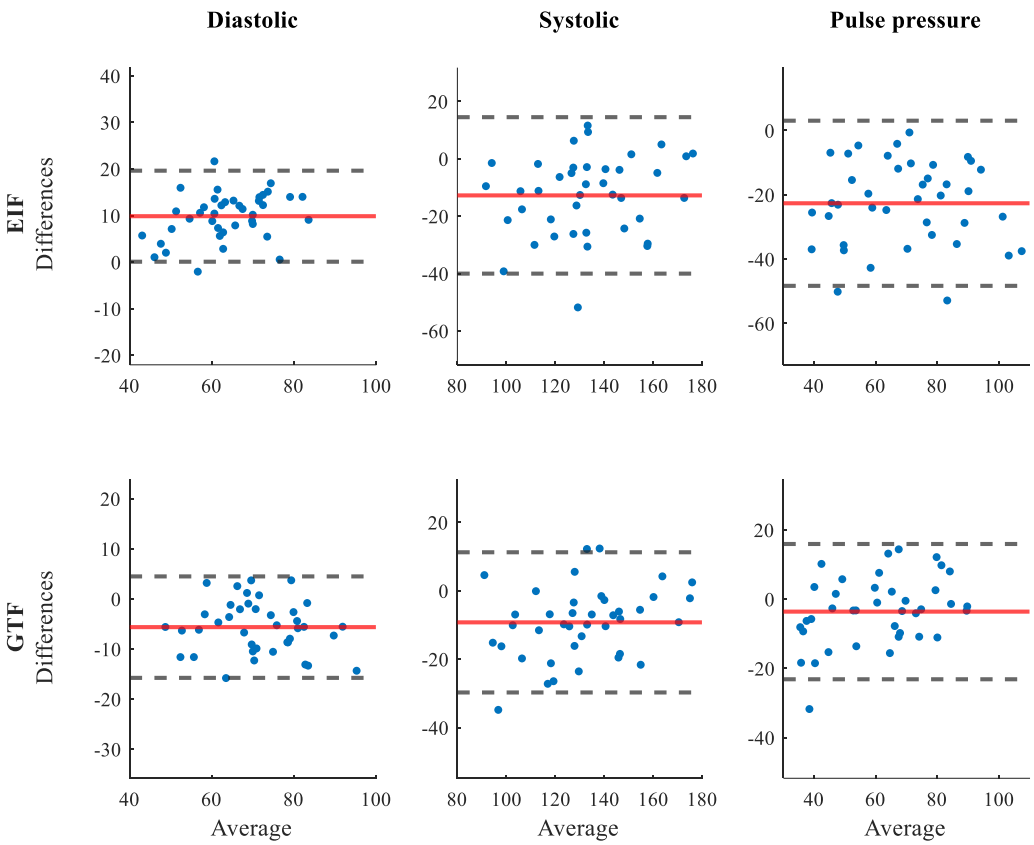

Figure 4.16 Bland Altman Plot for the EIF and GTF estimated blood pressure waveform against the 40-hospital dataset of aortic blood pressure waveform. (Dashed lines are the Lower and Upper Limit of Agreement (LOA), Solid (Red) line is the Mean difference)

From Table 4.7, EIF was able to give a lower MAPE and a RMSE with a reasonable difference of 1.56mmHg compared to the GTF method. When further investigated using the Bland Altman plot in Figure 4.16, the EIF was able to keep majority of the systolic data in the limit of agreement (LOA) except for underestimating 1 data which falls below the lower LOA, while the GTF overestimates 2 and underestimates 1 data's systolic pressure, showing that 3 data's systolic pressure were not able to be kept in the LOA. This shows the EIF is a better estimator of the systolic pressure despite its parameters being attained from the random 40 HaeMod data compared to the GTF. However, the GTF gives a better average correlation of 99.86± 0.15 compared to the EIF which was able to attain an average correlation of 99.62± 0.25. The limitation of the hospital data is that the radial blood pressure waveform and aortic blood pressure waveform obtained from the hospital patients were not taken simultaneously due to procedural limitations of obtaining an invasive reading, which results in the feature of the

aortic and radial waveform not being in-sync, as compared to the signals obtained from HaeMod. However, the EIF and GTF managed to retain the shape of the estimated aortic blood pressure waveform to the waveform of the patient's blood pressure which can be seen in Figure 4.15.

From the overall results obtained, the EIF has shown to be a comparable method to the GTF and it was a better estimator of the systolic pressure. The EIF has better computational performance when compared against NPMA and ATF, and it was comparable to the GTF method. It has proven its estimation capability for systolic blood pressure which is utilized to indicate risk of hypertension in medical practice, as it was able to attain the least number of data exceeding the Limit of Agreement for the Bland Altman plot when compared to the GTF, NPMA and ATF. In addition, the EIF requires lower computing time which would be very useful for today's ambulatory wearable devices that would require to embed the conversion algorithm in the micro-controller to continuously indicate cardiac risk to users without the need of wireless communication for CPU or cloud computing. Thus, it is evident that the EIF can be used to estimate the central aortic blood pressure waveform as a simple, accurate and low computing method when compared to GTF, NPMA and ATF methods.

4.4 Modelling and artificial intelligence

This section is divided into two subsections: modelling, and artificial intelligence. The modeling section elaborates the findings and discussion of the parameter selection for the CNN training, and the artificial intelligence section elaborates the results and discussion of the CNN development for the risk indication system.

4.4.1 Modelling

As stated in the methodology section above for modelling (Section 3.5.1 **Modelling**), the first step is to simulate a healthy aortic signal from the complete cardiovascular loop model using MATLAB, as shown in Figure 4.17. The simulated aortic signal is healthy, and it has a blood pressure reading close to 120/65mmHg, which is within the normal range[342].

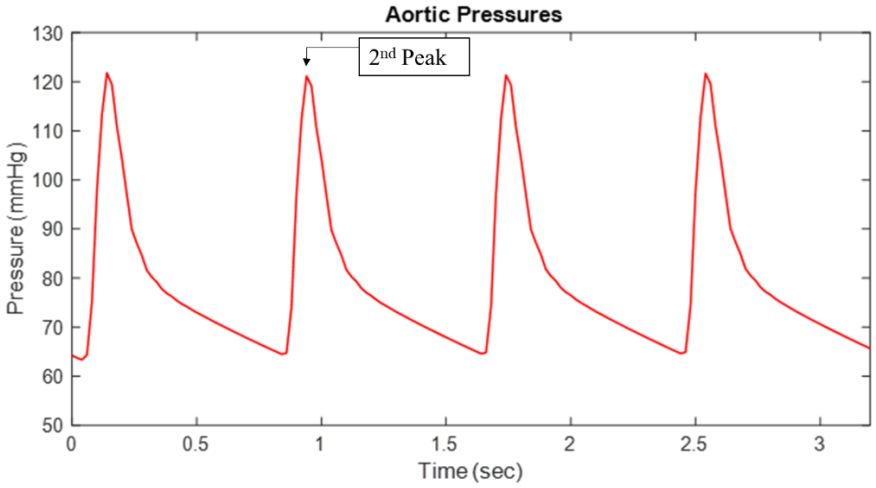

Figure 4.17 MATLAB simulation of PA1 signal in a healthy human

This study focused on the second peak of the aortic pressure signal (PA1) as the second peak onwards of the model's output would have reached a steady-state response which can be utilised to measure the effect on PA1. At the second peak, one full blood flow circulation is completed whereas the first peak only quantifies the first pump of blood flow out of the heart (initial conditions of the model before reaching a steady-state response). As such, the RMSE of the first pulse waveform against the next two corresponding pulses (second and the third pulse waveforms), is 0.05±0.01. On the other hand, the RMSE of the second pulse waveform against the next two corresponding pulses (third and fourth pulse waveforms) is 0.02±0.01. This shows the second peak can be considered as a steady-state response with slight discrepancies, as the RMSE is closer to 0 as compared to the first pulse waveform. The sensitivity analysis is first performed in accordance with the methodology section (Section 3.5.1 **Modelling**) to determine the independent response of all 36 parameters that influence the aortic blood pressure waveform, and these 36 parameters were assessed to extract the parameters that will affect the aortic pressure signal (PA1) significantly. *Table* 4.8 shows the 36 parameters and their minimum and maximum amplitude values of the 2nd peak of the PA1 signal.

Table 4.8.Minimum and maximum amplitude values of the 2nd peak of the PA1 signal.

No	Parameter	Minimum (mmHg)	Maximum (mmHg)	No	Parameter	Minimum (mmHg)	Maximum (mmHg)
1	RP1	120.1	122.4	19	LLA	116.1	126.2
2	RP2	117.7	126.7	20	LLV	114.2	127.5
3	RP3	115.4	130.5	21	LA1	119.4	124.3
4	RL1	118.1	125	22	LV2	121.2	121.2
5	RL2	119.7	122.8	23	LRA	121.2	121.2
6	RLA	116.9	129	24	LRV	120	122.3
7	RLV	120	122.3	25	CP1	121	121.3
8	RA1	119.8	122.4	26	CP2	121.2	121.2
9	RA2	105.1	127.8	27	CP3	117.8	124.4
10	RA3	96.22	126.3	28	CL1	120.3	121.9
11	RV1	120.6	121.3	29	CL2	121.2	121.2
12	RV2	121.2	121.2	30	CLA	118.3	122.1
13	RRA	121.2	121.2	31	CA1	116.6	128.1
14	RRV	120.6	121.7	32	CA2	112.4	127.7
15	RPW1	121.2	121.2	33	CA3	118.4	121.2
16	RPW2	120.8	121.4	34	CV1	121.2	121.2
17	LP1	120.9	121.2	35	CV2	121.2	121.2
18	LL2	121.2	121.2	36	CRA	121.2	121.2

Table 4.8 shows the minimum and maximum amplitude values of the aortic signal for 36 different parameters, where this analysis is used to categorize the 36 parameters into the key parameters that are affecting the aortic blood pressure waveform and the

insignificant parameters. This is done by distinguishing the minimum and maximum amplitude values of the 2nd peak of the PA1 signal for each parameter. If the difference between the minimum and maximum amplitude values of the second peak is greater than 2.5 mmHg, then the parameter is shortlisted as the parameter that may affect the aortic blood pressure waveform. If the difference between the minimum and the maximum amplitude values of the second peak are lower than 2.5 mmHg; it is not considered as a parameter that affect the aortic blood pressure waveform, otherwise stated as insignificant parameters. Figure 4.18 shows the plot of the pressure difference between the minimum and maximum values for each parameter. It can be seen that 16 parameters have a difference higher than 2.5mmHg, which makes them the most significant potential parameters relating to the changes in the signal. The 16 parameters are: RP2, RP3, RL1, RL2, RLA, RA1, RA2, RA3, LLA, LA1, LLV, CP3, CLA, CA1, CA2, and CA3. A detailed explanation of the parameters and the resultant signal when changing them from their default values can be seen in Appendix 3.

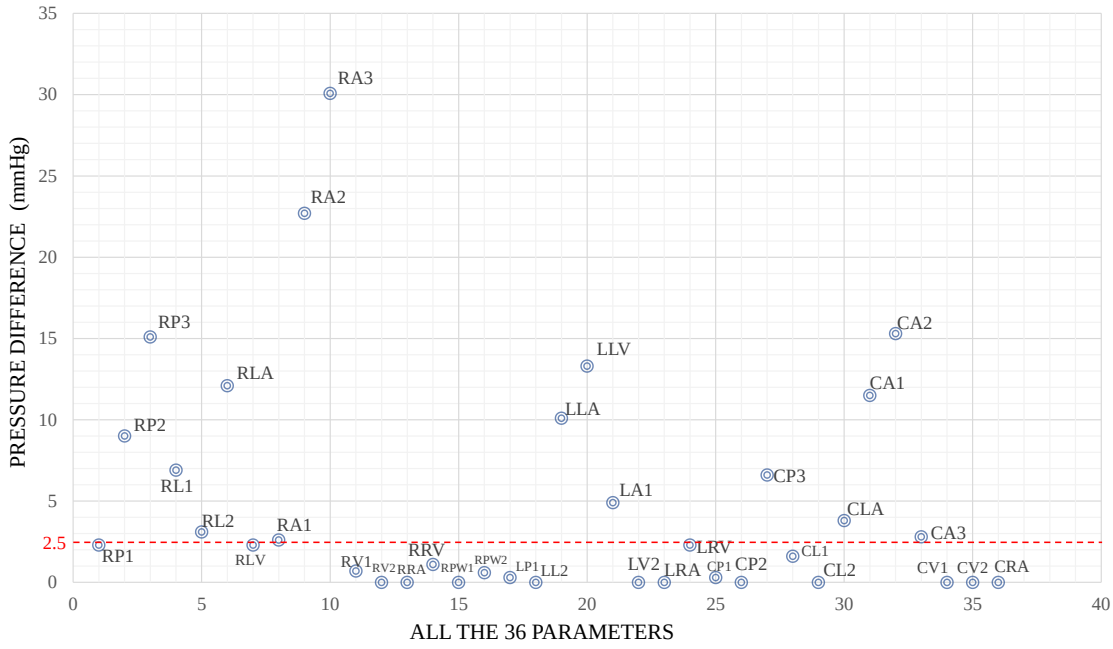

Figure 4.18. Difference between maximum and minimum values of the aortic pressure

As an example, in Figure 4.19 shows the effect of changing RA3 on PA1, where RA3 is categorized as a parameter that affects PA1 is shown and Figure 4.20 shows the effect of changing CP2 on PA1 where CP2 is categorized as a parameter that does not affects PA1, otherwise known as an insignificant parameter. For both cases, the other

parameters were kept constant. When comparing Figure 4.19 and Figure 4.20, it can be seen that the response of RA3 has multiple changes, while CP2 remains constant regardless of the changes that occur in the parameter values.

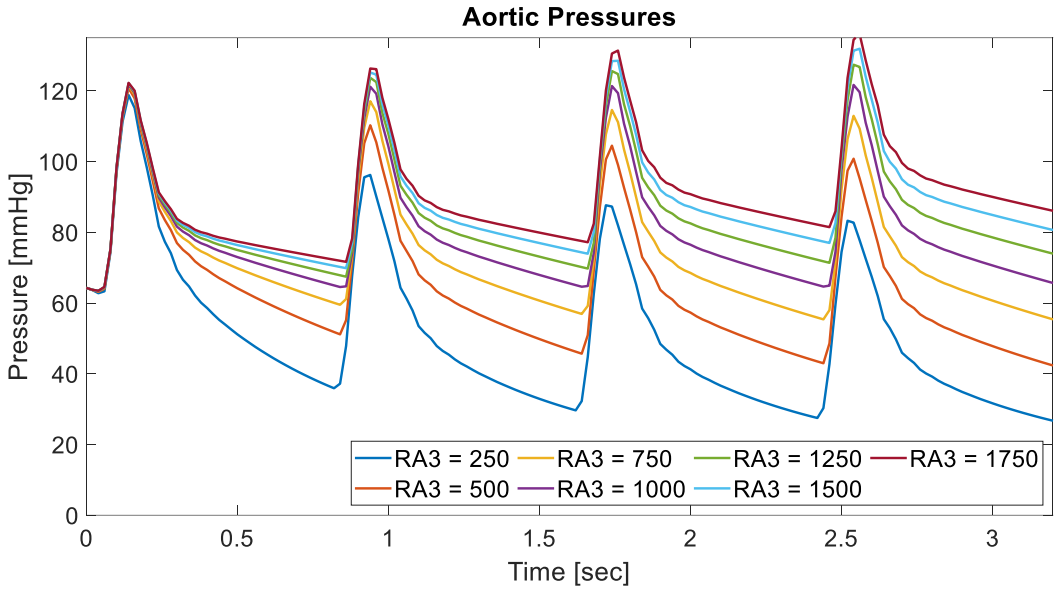

Figure 4.19 Effect of changing RA3 on PA1

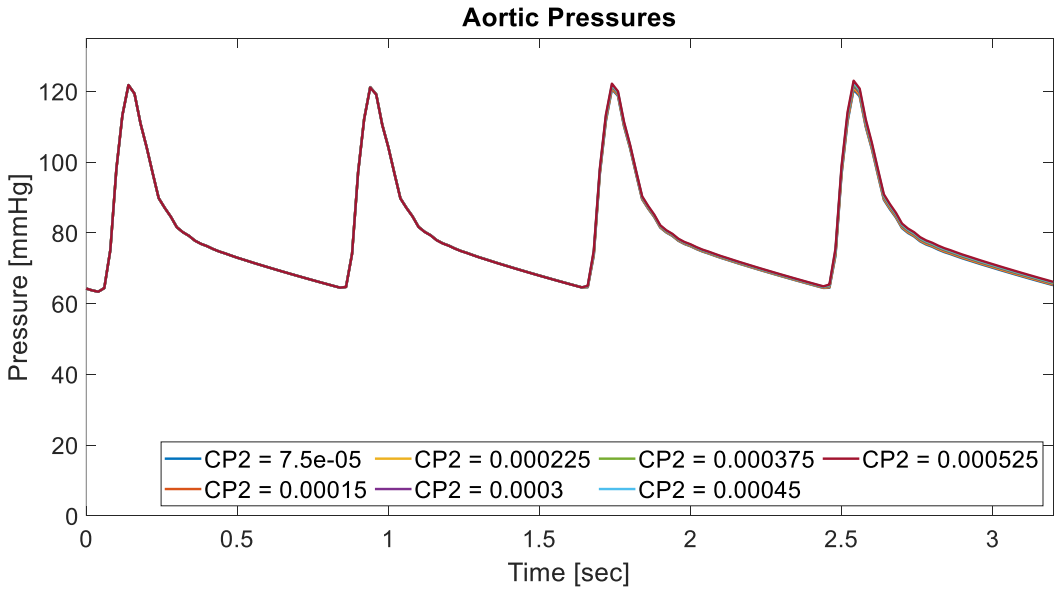

Figure 4.20 Effect of changing CP2 on PA1

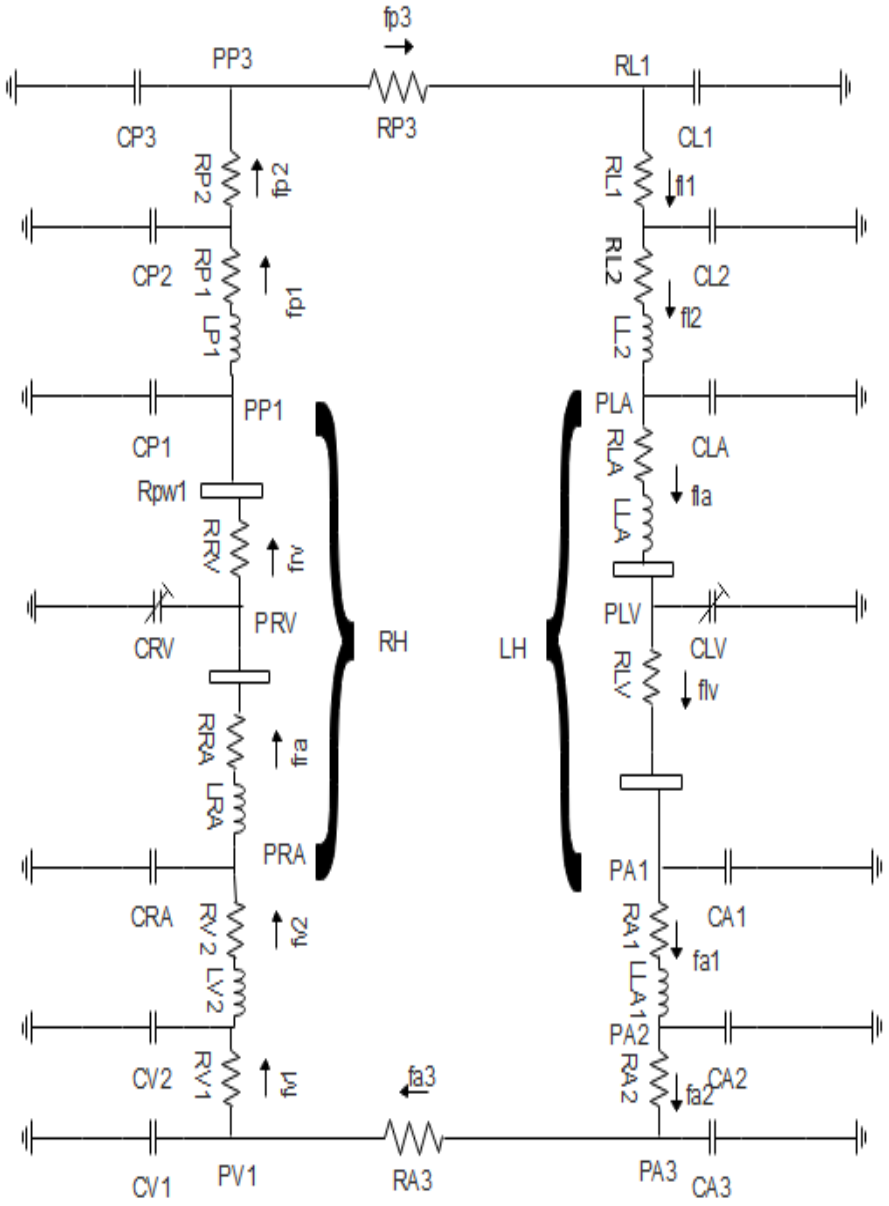

Figure 4.21 Rideout's complete cardiovascular loop model [288]

To further relate the chosen significant parameters to the impact on PA1, a deeper look is taken at Rideout's model. Human blood circulation starts when the heart relaxes between two heartbeats. At this point, the atriums which are located at the upper two chambers of the heart will contract and this is made up of CRA, CLA, RRA, RLA, LRA, LLA in the model shown in Figure 4.21. Blood then flows into the ventricles made up of CRV, CLV, RRV, RLV, LRV, LLV of the model shown in Figure 4.21, which are located at the lower two chambers of the human heart. The ventricles then contract and pumps blood into the large arteries during the ejection period.

In the systemic circulation, the left ventricle pumps oxygen-rich blood into the aorta to reach all parts of the body. The blood travels from the aorta, which is PA1 in the model to larger and smaller arteries into the capillary network.

The pulmonary circulation begins when the right ventricle pumps deoxygenated blood into the pulmonary artery, which is PPV in the model then branches off into smaller arteries and capillaries in the lungs.

The analysis in Figure 4.18 and *Table* 4.8 shows that there are 9 parameters out of the 16 parameters that affect the PA1 which has more than 8mmHg difference between the minimum and maximum amplitude values of the PA1 signal and these parameters are located near to the aorta in the model. On the other hand, the remaining 7 parameters out of the 16 parameters' minimum and the maximum amplitude values of the 2nd peak, which are greater than 2.5mmHg and below 8mmHg, are either located further from the aorta or generally do not have a major effect on blood flow. The 20 insignificant parameters do not have any significant effect on PA1 since its difference of the minimum and the maximum amplitude values of the peak are less than 2.5mmHg, which is considered to be not significant and a majority of them are located away from the aorta, which can be seen in Figure 4.21.

Since blood circulation is a closed-loop system, any obvious change in the system will affect the heart more, resulting in a significant change in parameters near the heart compared to parameters away from it. Likewise, the Vincent Rideout model follows the blood flow system of the heart which caused the parameters near the heart to have a higher effect on the aortic pressure (PA1) compared to parameters away from it. Furthermore, PA1 increases considerably for all resistor parameters that impact PA1 and are placed near the aorta in the model; RP2, RP3, RLA, RA1, RA2 and RA3 and vice versa. These resistances have a significant impact on the blood flow to the body resulting in a big change in the PA1. This is because the higher the resistance at the pathway of the flow, the higher the pressure at PA1. Therefore, as the pressure drop is equivalent to the voltage drop when resistance increases, this obeys Kirchhoff's voltage law, as the 0D model relates to an electrical circuit.

Furthermore, PA1 increases significantly when all the inertance parameters that affect the PA1, which are located near to the aorta in the model, LLA and LLV, increases and vice versa. LLV is a measurement of the required pressure gradient to cause a unit

change in blood flow rate at the left ventricle while LLA is a measurement of the required pressure gradient to cause a unit change in blood flow rate at the left atrium. LLV and LLA are represented by the inductance and PA1 are represented by the voltage at a point after LLV and LLA. This shows that, when LLV or LLA increases, the back electromotive force (EMF) across it also increases resulting in PA1 to increase as well.

PA1 is affected by CA1 and CA2 because CA1 and CA2 are the elasticity of the wall at the first and second part of the aorta where the blood from the heart flows to the rest of the body. Therefore, when CA1 or CA2 increases, the pressure of the blood flow decreases due to the widening of the vessel. In the 0D model, CA1 and CA2 are represented by capacitance while PA1 is represented by the voltage at a point before CA1 or CA2. Therefore, as CA1 or CA2 increases, the systolic part of the response decreases due to charging of capacitance while the diastolic part increases due to discharging of capacitance.

From Figure 4.18, RP2, RP3, RL1, RL2, RLA, RA1, RA2, RA3, LLA, LLV, LA1, CP3, CLA, CA1, CA2 and CA3 are grouped as the 16 parameters that affect the PA1 signal. These parameters are then used further to create the training and validation data for the Convolutional Neural Network.

4.4.2 Artificial intelligence

This section is broken down into three subsection which are data generation, convolutional neural network (CNN) and indicator parameters of CVD and Non-CVD including healthy. The data generation subsection shows the data creation process and outcome while the convolutional neural network subsection shows the choice of CNN architecture, and the parameters results of the methodology incorporating both transfer fuctions which are EIF and GTF. Finally, the indicator parameter subsection shows the choice of the indicator parameters for both the transfer functions.

4.4.2.1 Data Generation

To create the training and validation data, the maximum standard deviation of a parameter value needs to be identified. Hence, a standard deviation of $\pm$ 10% times of the default value given by Vincent Rideout that affects PA1 is used as the initial range for the parameters, while changing each parameter's standard deviation in an increment of ($\pm$ 10%) of the corresponding parameters default value to obtain the maximum standard deviation of that parameters. Table 4.9 shows the default value and the maximum

standard deviation value of each parameter one at a time while the rest are kept within a standard deviation of $\pm$ 10% of their corresponding default value.

Table 4.9 The default and the maximum standard deviation value of each parameter.

Parameter	**Default value**	**Maximum standard deviation value**
RP2	40	20
RP3	80	32
RL1	30	12
RL2	10	10
RLA	5	5
RA1	10	5
RA2	160	32
RA3	1000	200
LLA	1	0.4
LLV	1	0.4
LA1	1	0.3
CP3	0.0027	0.00081
CLA	0.01176	0.004704
CA1	0.00018	0.000036
CA2	0.00023	0.000046
CA3	0.0018	0.00036

4.4.2.2 Convolutional neural network

The training data and validation data are then fed into the convolution neural network as the output and its corresponding PA1 signals of those parameters are placed as the input to be trained and validated. For the choice of architecture, 118098 different

architectures were trained to obtain the top 10 CNNs with the lowest validation RMSE for a data size of 1920 samples (20% is used for validation). The top 10 architechtures were chosen as there is no guarantee that the CNN with the lowest validation of RMSE will perform the best on testing data, hence 10 are chosen and the best was chosen at a later stage. Table 4.10 shows the grid search hyperparameter ranges that were attained from the 118098 different CNN architectures.

Table 4.10 shows the grid search hyperparameter ranges

Layer type	**Hyperparameters**	**Range**	**Step size**
1st Convolution layer	Filter size	15 to 25	5
	Number of filters	10 to 30	10
	stride	1 to 3	1
1st Maximum pooling layer	Filter size	1 to 3	1
	Stride	5 to 15	5
2nd Convolution layer	Filter size	3 to 9	3
	Number of filters	200 to 400	100
	Stride	1 to 3	1
2nd Maximum pooling layer	Filter size	1 to 3	1
	Stride	2 to 6	2
Overall	Learning rate	0.001 to 0.003	0.002

The top 10 CNN architecture is then retrained with a data set that is twice the size of the initial data. This is to verify if there would be a need for more data to be fed into the CNN to obtain a better prediction of the 16 parameters and to avoid saturation of data in the CNN. The top 10 CNNS with lowest RMSE for both versions of the CNNs are tested with the use of the same testing data to obtain the lowest testing RMSE CNN architecture. Table 4.11 shows the best 10 CNN architectures with their Validation

RMSE values. Table 4.12 shows the best 10 CNN architectures testing RMSE values for initial data and data twice the size of the initial data.

Table 4.11 Best 10 CNN architectures with Validation RMSE of initial data and data which is twice the size of the initial data

No	Convolution layer			Max pooling		Convolution layer			Max pooling		Learning rate	RMSE for initial data	RMSE for data twice the size of the initial data
	Filter size	No. of filters	Stride	Filter size	Stride	Filter size	No. of filters	Stride	Filter size	Stride			
1	15	10	2	1	15	3	400	2	1	6	0.003	0.3927	0.3308
2	15	10	3	1	15	3	300	2	1	4	0.003	0.3967	0.3293
3	15	10	3	1	15	3	400	3	1	2	0.001	0.3990	0.3400
4	15	10	3	1	15	3	400	3	1	4	0.003	0.4064	0.3286
5	25	10	3	1	15	9	400	2	1	6	0.001	0.4167	0.3615
6	25	10	3	1	15	3	300	3	1	6	0.001	0.4184	0.3293
7	20	10	3	1	10	3	300	3	1	6	0.003	0.4221	0.3309
8	20	10	3	2	15	3	400	3	1	6	0.001	0.4232	0.3306
9	15	10	3	2	15	3	200	3	1	6	0.003	0.4235	0.3284
10	15	10	2	1	10	3	400	2	1	6	0.001	0.4274	0.3538

Selected

Table 4.12 Best 10 CNN architecture testing RMSE values for initial data and data that is twice the size of the initial data

No	RMSE for initial data	RMSE for data twice the size of the initial data

1	10.388	9.675
2	9.853	9.522
3	9.583	9.591
4	9.594	9.622
5	12.291	11.627
6	10.677	9.507
7	11.110	9.582
8	15.817	10.006
9	17.514	9.487
10	10.587	9.829

Selected

From Table 4.11 and Table 4.12, CNN with architecture 9 was selected as the best choice of CNN to predict the 16 parameters. CNN architecture 9 was selected because it has the lowest validation RMSE. Although the trend in the RMSE shows that this CNN could be further optimized by investigating it with an even larger data size for training, the investigation process would take more computational time to develop the CNN which is not possible with the time constraints of this research. However, as this CNN had the lowest RMSEs and these values are acceptable for performing the required detections, it was chosen to be used for the rest of this work.

The CNN architecture 9 trained with the data twice the size is then utilized to obtain the parameter values of the cardiovascular disease signal and the non-cardiovascular disease signal for the online database PhysioNet [328], which contained radial blood pressure waveforms. The PhysioNet [328] radial blood pressure waveforms were transformed to aortic blood pressure waveforms using transfer functions; Electrical Impedance Function (EIF) and Generalised Transfer Function (GTF) before being fed into the CNN. These parameters' values were analysed to obtain the baseline parameter values to differentiate between cardiovascular disease and non-cardiovascular disease, which includes healthy signals. The baseline parameter values obtained from PhysioNet [328] data is then used to verify the classification of parameters for the healthy signals from

HaeMod [329] and the cardiovascular disease' signal obtained from the hospital (Appendix 2).

(i) Results for CNN using EIF as the transfer function to estimate the aortic waveform

Table 4.13 shows the 16 parameters values of the cardiovascular disease signals while Table 4.14 shows the 16 parameters values of some of the non-cardiovascular disease signals, for the data obtained from the online database, PhysioNet [328]. The complete table of the parameter values of the non-cardiovascular disease signals for the data obtained from the online database, PhysioNet [328] is shown in Appendix 4.

Table 4.13 The parameters values of the cardiovascular disease' signal for the data obtained from the online database, PhysioNet [328] (Using EIF as the transfer function)

Parameters	**Patient with angina -subject 240**	**Patient with angina -subject 284**	**Patient with MI/cardiogenic shock -subject 237**	**Patient with MI/cardiogenic shock -subject 248**
RP2	39.921528	39.597858	39.702312	39.67569
RP3	82.805679	81.922409	81.398293	83.753044
RL1	29.193281	29.111124	29.259352	28.539837
RL2	10.348585	10.421631	10.554657	10.369467
RLA	5.2339392	5.2276015	5.2430434	5.3171124
RA1	9.669692	9.5897036	9.6836967	9.3078136
RA2	162.979	161.27461	161.77939	162.88301
RA3	991.039	993.10828	997.87134	985.96411
LLA	0.99918717	1.0070424	0.99170023	1.0056787
LLV	0.96733814	0.96744424	0.9652229	0.95281929
LA1	1.0035754	1.0066992	1.011359	1.0128677
CP3	0.002615935	0.00264803	0.002592987	0.002610098
CLA	0.01153529	0.011476284	0.01134548	0.01144887
CA1	0.000180867	0.000181172	0.000180671	0.000182461
CA2	0.00022572	0.000224255	0.000224976	0.000220873
CA3	0.001871489	0.001895231	0.001903462	0.001935462

Table 4.14 The parameters values of the non-cardiovascular disease' signal for the data obtained from the online database, PhysioNet [328] (Using EIF as the transfer function)

Parameters	**No Clinical class-subject 037**	**Bleed- Subject039**	**Respiratory failure-Subject055**	**Brain injury-Subject449**	**Sepsis-Subject438**
RP2	39.23801	39.618458	39.517422	39.949261	40.007732
RP3	80.074959	81.849365	79.926659	82.93	83.22155
RL1	28.938517	29.250366	29.728354	29.327848	29.303034
RL2	10.98221	10.436772	10.442408	10.225227	10.407898
RLA	5.2627368	5.2122388	5.1205125	5.2059598	5.2632961
RA1	9.6456795	9.7677408	9.8907404	9.7514456	9.767061
RA2	161.39848	161.18443	159.62439	162.36986	163.10709
RA3	998.10468	992.06769	1001.031	989.80725	988.79169
LLA	0.97762614	1.0057852	1.0112896	1.0091474	0.98952574
LLV	0.95166695	0.9693464	0.98382866	0.97404778	0.96573919
LA1	1.0309312	1.0054561	0.99837852	0.99653339	1.0061437
CP3	0.002556005	0.002653254	0.002694746	0.002657074	0.002592569
CLA	0.01107895	0.011499938	0.011528086	0.011652189	0.011500692
CA1	0.000181434	0.000180926	0.000179776	0.00018065	0.000180655
CA2	0.000221951	0.000225127	0.00022816	0.000226793	0.00022569
CA3	0.001973349	0.00188379	0.001846782	0.00184561	0.001874694

Table 4.15 shows the values of the parameters of some of the healthy signals for the data obtained from the online database, HaeMod [329] while Table 4.16 shows the values of the parameters of some of the cardiovascular disease signals for the data obtained from the hospital. The continuation of the results of parameter values of the healthy signal for the data obtained from the online database, HaeMod [329] until subject 40 is in Appendix 5(if necessary, the results of the remainder of the 3325 signals will be provided). The list of patients from the hospital with their corresponding

cardiovascular disease and the complete results of parameters values of the cardiovascular disease signals for the data obtained from the hospital is in Appendix 6.

Table 4.15 The parameters values of the healthy signal for the data obtained from the online database, HaeMod [329] (Using EIF as the transfer function)

Parameters	Subject 1	Subject 2	Subject 3	Subject 4	Subject 5
RP2	39.363396	39.454655	38.828232	39.150955	38.963463
RP3	79.68325	80.748711	76.25531	78.760406	77.664665
RL1	29.419716	29.537537	28.887789	29.303574	29.03619
RL2	10.586229	10.695358	10.772797	10.780199	10.882107
RLA	5.1359968	5.2041492	5.0384417	5.138916	5.1250744
RA1	9.8594103	9.8616428	9.782794	9.8556538	9.7955608
RA2	160.21736	159.6792	160.8645	159.94731	160.39261
RA3	1037.8148	1012.5735	1104.2269	1047.605	1070.3629
LLA	0.96337026	0.9679085	0.92263293	0.94860929	0.93214291
LLV	1.016646	0.99671686	1.0551758	1.0195162	1.0282322
LA1	1.0075091	1.012231	1.0192057	1.016116	1.0233076
CP3	0.002596709	0.002608718	0.002485219	0.002561808	0.002506604
CLA	0.011348858	0.011325932	0.011040625	0.011188992	0.011042911
CA1	0.000189	0.000189	0.000184	0.000188	0.000188
CA2	0.000236	0.000237	0.000235	0.000235	0.00023
CA3	0.001936	0.001905	0.001861	0.001895	0.00175

Table 4.16 The parameters values of the cardiovascular disease' signal for the data obtained from the hospital (Using EIF as the transfer function)

Parameters	Subject 1	Subject 2	Subject 3	Subject 4	Subject 5

RP2	39.785065	40.307888	40.885029	39.217758	39.722198
RP3	83.867638	84.293564	83.204002	79.830353	84.99749
RL1	28.310261	28.860296	28.168083	29.058203	28.149103
RL2	10.566881	10.640691	9.9095135	10.300001	10.54658
RLA	5.3266177	5.3173108	5.4921885	5.1036787	5.3104224
RA1	9.3937855	9.7667933	9.2371397	9.5508881	9.307847
RA2	165.15138	167.1254	174.10156	159.77499	166.95908
RA3	1002.1	998.43964	1038.4802	1018.0665	989.87372
LLA	0.97002822	0.94503933	0.94788522	1.0128267	0.97050256
LLV	0.96185231	0.96500391	0.92404985	0.99447042	0.95068413
LA1	1.0225915	1.0207258	1.0196979	0.99986732	1.022458
CP3	0.002514981	0.002453004	0.00212411	0.002686109	0.002504415
CLA	0.011344761	0.011350284	0.010799509	0.011503946	0.011368714
CA1	0.000181961	0.000180534	0.000180794	0.000180747	0.000182949
CA2	0.000218869	0.000223349	0.000227229	0.000222646	0.000218259
CA3	0.001917958	0.001876021	0.001877336	0.001854069	0.001925695

(ii) Results for CNN using GTF as the transfer function to estimate the aortic waveform

Table 4.17 shows the 16 parameters values of the cardiovascular disease signals while Table 4.18 shows the 16 parameters values of some of the non-cardiovascular disease signals, for the data obtained from the online database, PhysioNet [328]. The complete table of the parameters values of the non-cardiovascular disease' signal for the data obtained from the online database, PhysioNet [328] is in Appendix 7.

Table 4.17 The parameters values of the cardiovascular disease' signal for the data obtained from the online database, PhysioNet [328] (Using GTF as the transfer function)

Parameters	**Patient with angina -subject 240**	**Patient with angina -subject 284**	**Patient with MI/cardiogenic shock -subject 237**	**Patient with MI/cardiogenic shock -subject 248**
RP2	39.75359	39.484039	39.57814	39.688686
RP3	81.605675	80.394775	80.656425	82.179977
RL1	29.48073	29.428125	29.512667	29.253183
RL2	10.30215	10.469533	10.463786	10.26719
RLA	5.178339	5.1620483	5.1674013	5.2037396
RA1	9.763979	9.7570581	9.7415239	9.6252308
RA2	161.14561	160.26077	160.47523	161.06248
RA3	993.88867	1000.5076	998.40875	990.21497
LLA	1.011261	1.0088592	1.0060869	1.0164105
LLV	0.97682303	0.97681522	0.97556126	0.97218823
LA1	0.99642134	1.0032064	1.0031608	0.99833977
CP3	0.002673849	0.002671023	0.002660859	0.002680585
CLA	0.011596347	0.011472742	0.011477972	0.011602929
CA1	0.000180402	0.000180355	0.000180276	0.00018105
CA2	0.000227316	0.000226282	0.000226733	0.000225663
CA3	0.001849402	0.001871477	0.001870879	0.001868958

Table 4.18 The parameters values of the non-cardiovascular disease' signal for the data obtained from the online database, PhysioNet [328] (Using GTF as the transfer function)

Parameters	**No Clinical class-subject 037**	**Bleed-Subject039**	**Respiratory failure-Subject055**	**Brain injury-Subject449**	**Sepsis-Subject438**
RP2	39.768658	39.574848	39.495876	39.798492	39.849735
RP3	81.376137	80.708054	79.441338	81.754906	82.155609
RL1	29.675625	29.527449	29.815395	29.549376	29.542809
RL2	10.257393	10.416709	10.481297	10.237569	10.264812
RLA	5.1482286	5.1569929	5.1089425	5.1592989	5.1813192
RA1	9.8412342	9.7976999	9.9491205	9.7911081	9.7787857
RA2	160.60188	160.35089	159.49049	161.10236	161.32257
RA3	995.69684	998.81708	1003.4719	996.12524	992.16217
LLA	1.014523	1.0096961	1.0090551	1.0138409	1.0097182
LLV	0.98363459	0.97917503	0.98568058	0.98264277	0.97773916
LA1	0.99228376	1.0002393	0.9981938	0.99322808	0.99567628
CP3	0.002696325	0.002678379	0.002693097	0.002687736	0.002670346
CLA	0.011653398	0.01152595	0.011507052	0.011656588	0.011635758
CA1	0.000179949	0.000180185	0.000179513	0.000180114	0.000180305
CA2	0.000228428	0.000227023	0.000228736	0.000227817	0.00022744
CA3	0.001827581	0.001857216	0.001841724	0.001829117	0.001842299

Table 4.19 shows the values of the parameters of some of the healthy signals for the data obtained from the online database, HaeMod [329] while Table 4.20 shows the values of the parameters of some of the cardiovascular disease signals for the data obtained from the hospital. The continuation of the results of parameter values of the healthy signal for the data obtained from the online database, HaeMod [329] until subject 40 is in Appendix 8 (if necessary, the results of the remainder of the 3325 signals will be provided). The list of patients from the hospital with their corresponding cardiovascular disease and the complete results of parameters values of the cardiovascular disease' signal for the data obtained from the hospital is in Appendix 9.

Table 4.19 The parameters values of the healthy signal for the data obtained from the online database, HaeMod [329] (Using GTF as the transfer function)

Parameters	**Subject 1**	**Subject 2**	**Subject 3**	**Subject 4**	**Subject 5**
RP2	39.544495	39.588852	39.185055	39.371231	39.191513
RP3	80.464302	80.814926	78.544724	79.702797	78.896065
RL1	29.703077	29.648308	29.594379	29.64576	29.535976
RL2	10.553349	10.600152	10.878093	10.744882	10.898881
RLA	5.1562991	5.1745157	5.1583982	5.1639347	5.1706934
RA1	9.8934526	9.8696489	9.909936	9.8995094	9.8782415
RA2	159.77139	160.0009	159.20558	159.41393	159.19806
RA3	995.28436	991.78143	1004.9548	996.81049	1000.7808
LLA	1.0021328	0.99799275	0.98952913	0.99466252	0.98914075
LLV	0.97756845	0.97417867	0.97260004	0.97283846	0.96872723
LA1	1.004657	1.0074211	1.0175396	1.0127939	1.0198289
CP3	0.002670485	0.002659091	0.002632026	0.002649922	0.002628945
CLA	0.011474404	0.011445356	0.01121603	0.011340081	0.011212691
CA1	0.000180014	0.000180228	0.000179992	0.00018015	0.000180288
CA2	0.000227305	0.000226777	0.000225888	0.000226359	0.000225298
CA3	0.001868907	0.001880838	0.00190984	0.001898163	0.001924638

Table 4.20 The parameters values of the cardiovascular disease' signal for the data obtained from the hospital (Using GTF as the transfer function)

Parameters	**Subject 1**	**Subject 2**	**Subject 3**	**Subject 4**	**Subject 5**
RP2	39.484886	39.832764	40.788189	39.32645	39.419521
RP3	81.879539	82.596535	82.984451	79.382362	81.899635
RL1	28.929182	29.116272	28.466957	29.59531	28.735197
RL2	10.524129	10.450407	9.9516649	10.478569	10.530969
RLA	5.259716	5.2610612	5.2787962	5.1082602	5.2362547
RA1	9.5676813	9.6738129	9.290019	9.8313036	9.5152712
RA2	161.18271	162.81952	171.39651	159.14218	162.36365
RA3	992.66693	997.72192	1013.0205	1003.4451	998.27124
LLA	1.0041887	0.98832566	0.98213947	1.010844	1.0001889
LLV	0.96420538	0.97011888	0.9394691	0.98534471	0.96492863
LA1	1.0121307	1.0093026	1.0009513	1.0012674	1.0131466
CP3	0.002639923	0.002591488	0.002377217	0.002695261	0.00261981
CLA	0.011431459	0.011460503	0.011240672	0.011470653	0.011422209
CA1	0.000181356	0.000180655	0.000182175	0.000180157	0.000181713
CA2	0.000223256	0.000224313	0.000225798	0.000226798	0.000222198
CA3	0.001909683	0.001878122	0.001908644	0.001859069	0.001900423

4.4.2.3 Indicator parameters for CVD

After obtaining the parameter results of the CNN for all the datasets using both the transfer functions (EIF and GTF), a hit analysis is done to identify the indicator parameters for CVD against non-CVD and healthy. To conduct the hit analysis, the first step is to identify the ranges for each of the 16 parameters for CVD. The range for CVD was found by considering the values for all 4 PhysioNet [328] CVD and 5 out of the 40 data from the hospital. The minimum and maximum values of these parameter values were chosen as the range in which CVD could occur, as shown in Table 4.21. For example, for the classification of CVD, for a given signal, the parameter value should be above or below the minimum and maximum value respectively of the given range in Table 4.21. Only 5 hospital data were used because there is limited data available, hence only 5 from this pool was used to determine the ranges, while the remaining 35 were kept for testing at a later stage. The CNN outputs as a result of EIF and GTF were examined separately, to evaluate how well this method worked on both methods, to show the validity of this system if either method is used.

Table 4.21 shows the minimum and maximum values of all 16 parameter values of the range for CVD

Parameter	EIF		GTF	
	Minimum	**Maximum**	**Minimum**	**Maximum**
RP2	39.21776	40.88503	39.32645	40.788189
RP3	79.83035	84.99749	79.38236	82.984451
RL1	28.1491	29.25935	28.46696	29.59531
RL2	9.909514	10.64069	9.951665	10.530969
RLA	5.103679	5.492189	5.10826	5.2787962
RA1	9.23714	9.766793	9.290019	9.8313036
RA2	159.775	174.1016	159.1422	171.39651
RA3	985.9641	1038.48	990.215	1013.0205
LLA	0.945039	1.012827	0.982139	1.0164105

LLV	0.92405	0.99447	0.939469	0.98534471
LA1	0.999867	1.022592	0.996421	1.0131466
CP3	0.002124	0.002686	0.002377	0.00269526
CLA	0.0108	0.011535	0.011241	0.01160293
CA1	0.000181	0.000183	0.00018	0.00018218
CA2	0.000218	0.000227	0.000222	0.00022732
CA3	0.001854	0.001935	0.001849	0.00190968

Then, 19 data each from HaeMod [329] healthy and PhysioNet [18] non-CVD signals were chosen because PhysioNet [18] only had 19 non-CVD data and to guarantee an equivalent number of data between healthy and non-CVD. Next, the hit analysis was performed to analyze each CNN parameters results that are within or outside of a specific range of the CVD occurrences. The 19 HaeMod [329] healthy and PhysioNet [18] non-CVD were used, and their distribution within the aforementioned ranges in Table 4.21 were checked using hit analysis as shown in Figure 4.22 and Figure 4.23 for the parameter values from CNN using EIF as the transfer function and CNN using GTF as the transfer function respectively.

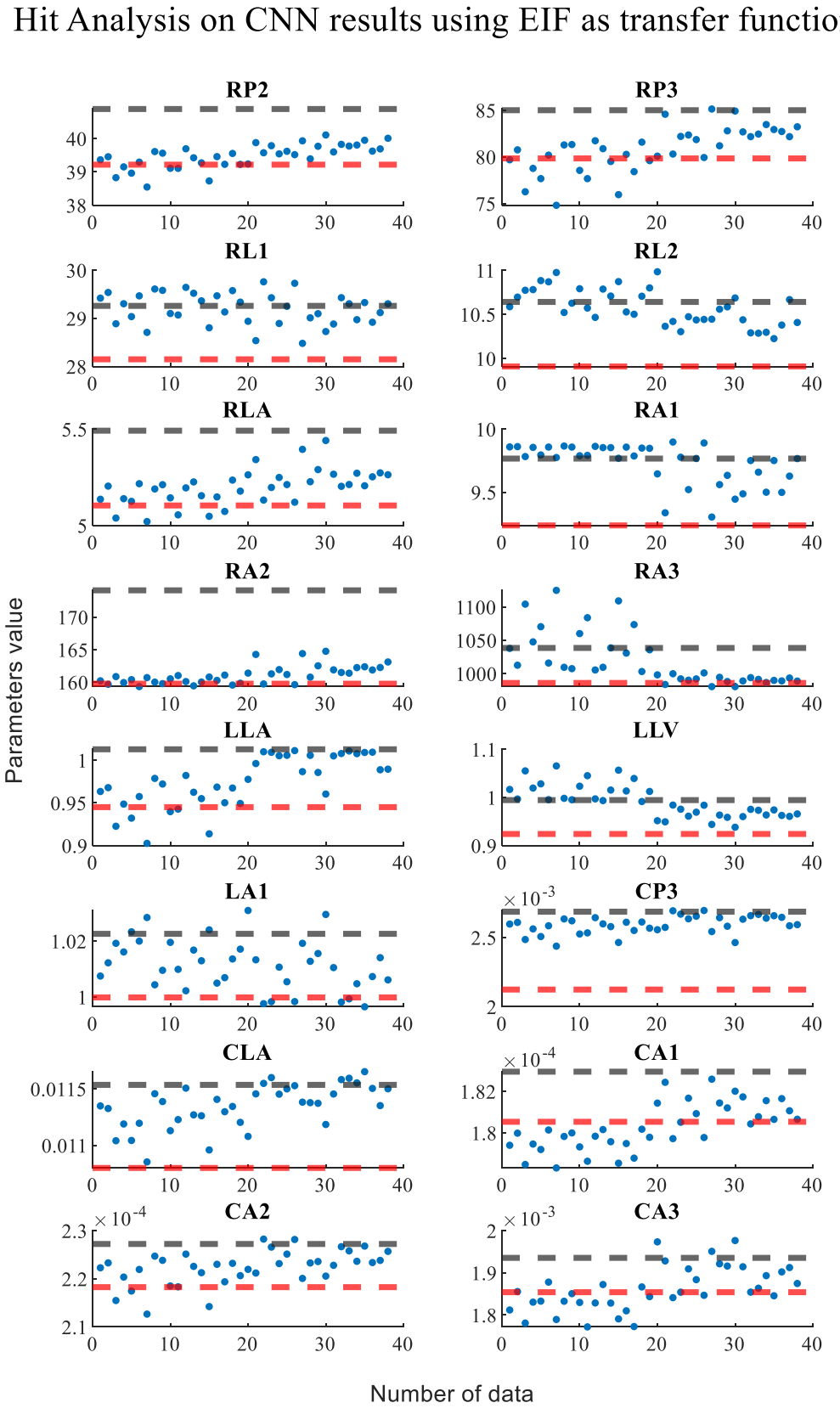

Figure 4.22 Hit analysis on the results of CNN using EIF as the transfer function (Dashed Grey line is the Maximum and Dashed Red line is the Minimum values for CVD occurrence)

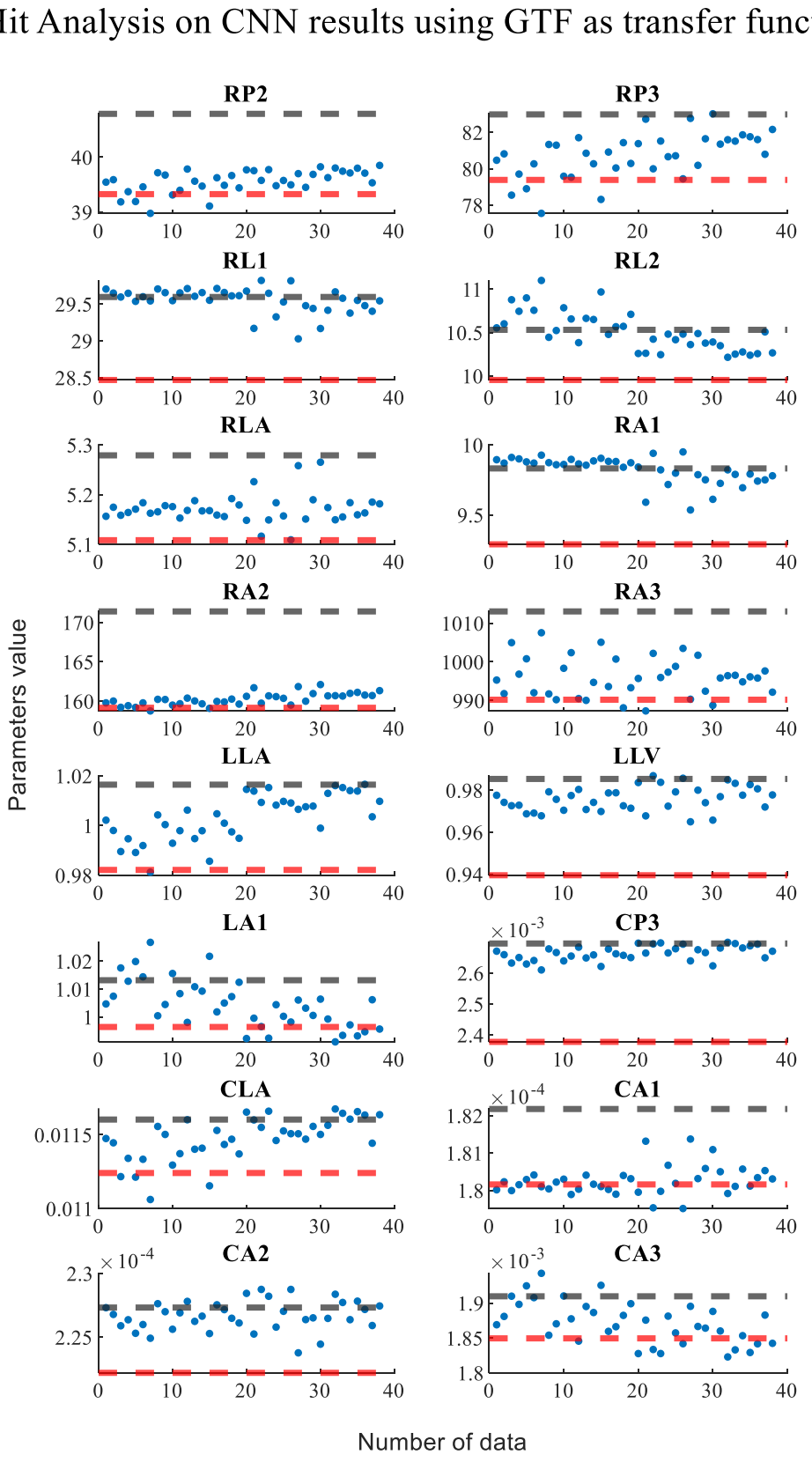

Figure 4.23 Hit analysis on the results of CNN using GTF as the transfer function (Dashed Grey line is the Maximum and Dashed Red line is the Minimum values for CVD occurrence)

From the hit analysis in Figure 4.22 and Figure 4.23, the parameter values for the 19 data from HaeMod [329] healthy and PhysioNet [18] non-CVD were analyzed to identify the number of data that fell into 3 categories, which are: above the maximum (category 1), between the minimum and maximum (category 2), and below the minimum (category 3) ranges for the CVD occurrence. Since the parameter value should be above or below the minimum and maximum value respectively for the CVD occurrence. Hence, the above or below category was determined by choosing the least number of non-CVD and healthy hits. The categories were observed and assigned for the CVD occurrence as follows:

1) Above the minimum range values:
   (Category 2 + Category 3) > Category 1
2) Below the maximum range values:
   (Category 1 + Category 2) > Category 3
3) Unusable:
   No hits or equal hits are found in Category 1 and Category 3

When there are no hits, or equal hits are found in category 1 and category 3, it means that relation of the values to the ranges for the CVD occurrences can not be determined. Table 4.22 shows the number of data hits from Figure 4.22 and Figure 4.23 for all the 3 categories and the CVD occurrence range.

Table 4.22 All the categories with the number of data hits for results of CNN using both transfer function and the CVD occurrence range.

	EIF				**GTF**			
Parameter	**above max**	**between min and max**	**below min**	**CVD occurrence range**	**above max**	**between min and max**	**below min**	**CVD occurrence range**
RP2	0	31	7	>= 39.217758	0	33	5	>= 39.32645
RP3	1	26	11	>= 79.830353	1	33	4	>= 79.382362
RL1	19	19	0	<= 29.259352	19	19	0	<= 29.59531
RL2	15	23	0	<= 10.640691	15	23	0	<= 10.530969
RLA	0	33	5	>= 5.1036787	0	38	0	Unusable
RA1	24	14	0	<= 9.7667933	22	16	0	<= 9.8313036
RA2	0	32	6	>= 159.77499	0	36	2	>= 159.14218
RA3	9	26	3	<= 1038.4802	0	34	4	>= 990.21497
LLA	0	32	6	>= 0.94503933	1	36	1	Unusable
LLV	17	21	0	<= 0.99447042	2	36	0	<= 0.98534471
LA1	5	27	6	>= 0.99986732	6	25	7	>= 0.99642134
CP3	2	36	0	<= 0.002686109	3	35	0	<= 0.002695261
CLA	6	32	0	<= 0.01153529	8	26	4	<= 0.011602929

CA1	0	15	23	>= 0.000180534	0	12	26	>= 0.000180157
CA2	2	31	5	>= 0.000218259	11	27	0	<= 0.000227316
CA3	3	17	18	>= 0.001854069	5	23	10	>= 0.001849402

From Table 4.22 it can be seen that for CNN using GTF as a transfer function, the parameters RLA and LLA have shown no hits and equal hits respectively for categories 1 and 3. These CVD occurrence range were then applied to the parameters of the 9 CVD (4 PhysioNet [328] CVD, 5 Hospital data), 19 HaeMod [329] healthy and 19 PhysioNet [328] non-CVD and the classification accuracy of CVD, healthy, and non-CVD was tallied and is shown in Table 4.23. To obtain better classification accuracy, more non- CVD was required as the range is biased against CVD.

Table 4.23 The classification accuracy of CVD and others (healthy and non-CVD) and the mean accuracy

	EIF				**GTF**			
		Accuracy			**Accuracy**			
Param-eter	**CVD**	**Others**		**Mean**	**CVD**	**Others**		**Mean**
		Hae-Mod	**Non-CVD**			**Hae-Mod**	**Non-CVD**	
RP2	100.00	36.84	0.00	45.61	100.00	26.32	0.00	42.11
RP3	100.00	57.89	0.00	52.63	100.00	21.05	0.00	40.35
RL1	100.00	63.16	36.84	66.67	100.00	73.68	26.32	66.67
RL2	100.00	63.16	15.79	59.65	100.00	78.95	0.00	59.65
RLA	100.00	26.32	0.00	42.11	-	-	-	-

RA1	100.00	100.00	26.32	75.44	100.00	100.00	15.79	71.93
RA2	100.00	21.05	10.53	43.86	100.00	10.53	0.00	36.84
RA3	100.00	47.37	0.00	49.12	100.00	10.53	10.53	40.35
LLA	100.00	31.58	0.00	43.86	-	-	-	-
LLV	100.00	89.47	0.00	63.16	100.00	0.00	10.53	36.84
LA1	100.00	0.00	31.58	43.86	100.00	0.00	36.84	45.61
CP3	100.00	0.00	10.53	36.84	100.00	0.00	15.79	38.60
CLA	100.00	0.00	31.58	43.86	100.00	0.00	42.11	47.37
CA1	100.00	100.00	21.05	73.68	100.00	52.63	36.84	63.16
CA2	100.00	21.05	0.00	40.35	100.00	15.79	42.11	52.63
CA3	100.00	78.95	15.79	64.91	100.00	5.26	47.37	50.88

Highest mean accuarcy

Furthermore, it was observed from Table 4.23, that although the CVD classification accuracy was high, the non-CVD and healthy accuracy values were low in general. This could be attributed to the lesser data used in finding the classification ranges of the parameters, but also the fact that a single parameter might not be the best classifier. As using a single parameter for classification did not give a good overall performance, it is postulated that using a combination of more than one parameter could give a better overall result. Although every combination could be evaluated, in the essence of saving time and making the process efficient, only a few parameters were chosen to be combined and further analyzed. The parameters were first ranked according to their mean accuracy values, and the top 5 parameters that were common for the EIF and GTF are shown in Table 4.24, as it is important for the overall system accuracy to be high.

Table 4.24 Top 5 list of parameters that were in common for the EIF and GTF with their highest mean accuracy

Rank	EIF		GTF	
	Parameters	**Mean accuracy**	**Parameters**	**Mean accuracy**
1	RA1	75.44	RA1	71.93
2	CA1	73.68	RL1	66.67
3	RL1	66.67	CA1	63.16
4	CA3	64.91	RL2	59.65
5	RL2	59.65	CA3	50.88

These 5 common parameters for both methods were listed in the top 6 highest mean accuracy values for both methods in Table 4.22, where LLV and CA2 were not considered as they were not in common for EIF and GTF, despite LLV and CA2 being in the top 5 highest mean accuracy values for EIF and GTF respectively. They were discarded and only the common top 5 were chosen as ideally the same parameter selection should work on both EIF and GTF, as their output signals should have similar features. Hence common parameters would have better justification in their selection.

Next, combinations of the conditions for the top 5 parameters in Table 4.24 were used to check their combined evaluation performance, by using the same CVD, healthy and non-CVD data. If the corresponding parameters for a signal satisfied each of the parameter conditions, it was deemed as CVD. To simplify the experiment, a combination of two parameters at a time was chosen, and the results are shown in Table 4.25.

Table 4.25 The parameter combination and the mean accuracy of classification for CVD and others (healthy and non-CVD).

EIF					GTF				
Parameter combination	Accuracy				Parameter combination	Accuracy			
	CVD	Others		Mean		CVD	Others		Mean
		Hae-Mod	Non-CVD				Hae-Mod	Non-CVD	
RA1 + CA1	100.00	100.00	31.58	65.79	**RA1 + RL1**	100.00	100.00	26.32	63.16
RA1 + RL1	100.00	100.00	42.11	71.05	**RA1 + CA1**	100.00	100.00	36.84	68.42
RA1 + CA3	100.00	100.00	31.58	65.79	**RA1 + RL2**	100.00	100.00	15.79	57.89
RA1 + RL2	100.00	100.00	42.11	71.05	**RA1 + CA3**	100.00	100.00	47.37	73.68
CA1 + RL1	100.00	100.00	36.84	68.42	**RL1 + CA1**	100.00	89.47	36.84	63.16
CA1 + CA3	100.00	100.00	26.32	63.16	**RL1 + RL2**	100.00	100.00	26.32	63.16
CA1 + RL2	100.00	100.00	36.84	68.42	**RL1 + CA3**	100.00	73.68	47.37	60.53
RL1 + CA3	100.00	100.00	36.84	68.42	**CA1 + RL2**	100.00	94.74	36.84	65.79
RL1 + RL2	100.00	89.47	52.63	71.05	**CA1 + CA3**	100.00	52.63	47.37	50.00
CA3 + RL2	100.00	100.00	31.58	65.79	**RL2 + CA3**	100.00	84.21	47.37	65.79

From Table 4.25, it can be observed that the mean accuracy has been increased as compared to when these parameters were previously used individually. Although the accuracy values have increased, a clear winning combination cannot be determined for both EIF and GTF as multiple combinations have attained similar accuracy values (100% for CVD and healthy). This is because of the small size of the data pool which was used in the experiment above. Therefore, all the parameter combinations from Table 4.25 were tested on the full hospital set of data (40) and the HaeMod [329] data (3325) shown in Table 4.26 where the rows for EIF and GTF are arranged separately according to the highest to lowest mean accuracy. Table 4.25 shows that non-CVD performance is poor, which is due to the fact that non-CVD may have overlapped with CVD in the way the physiological feature of the signal is, as discussed in detail later below.

Table 4.26 Accuracy for all the parameter combination for Hospital and HaeMod [329] data

EIF			
Parameter combination	**Accuracy**		
	Hospital	**HaeMod**	**Mean**
CA1 + RL2	57.50	93.95	75.73
CA3 + RL2	60.00	90.38	75.19
RA1 + RL2	80.00	68.45	74.23
RL1 + RL2	75.00	71.16	73.08
CA1 + RL1	57.50	82.98	70.24
RA1 + CA1	57.50	77.08	67.29
RL1 + CA3	57.50	72.45	64.98
RA1+CA3	57.50	65.44	61.47
CA1 + CA3	47.50	72.00	59.75
RA1 + RL1	75.00	35.82	55.41

GTF			
Parameter combination	**Accuracy**		
	Hospital	**HaeMod**	**Mean**
RL1 + RL2	82.50	63.97	73.23
RA1 + RL2	82.50	60.36	71.43
CA1 + RL2	82.50	59.04	70.77
RL2 + CA3	70.00	56.60	63.30
RA1 + RL1	90.00	18.50	54.25
RA1 + CA1	90.00	15.28	52.64
RL1 + CA1	90.00	13.89	51.95
RA1 + CA3	77.50	14.89	46.19
RL1 + CA3	77.50	12.60	45.05
CA1 + CA3	77.50	7.37	42.43

Selected

Comparing the top 3 parameter combinations of each function from Table 4.26, it can be seen that the top 3 highest mean accuracy values of EIF can not be taken because the hospital accuracy is very low for the top 2 as compared to healthy. As it would be preferred to have a false positive detection for CVD detection rather than a false positive detection for non-CVD/healthy, a high accuracy in CVD is necessary, even if non-CVD/healthy performance is lower. By giving a priority to a high CVD accuracy, as well as a relatively good performance in HaeMod, the highlighted combinations were considered to be the best from the results obtained in Table 4.26.

From the highlighted combinations, it can be seen that RL2 is prominent in almost all the selected combinations. RL2 is Pulmonary Vein 2 Resistance and it is situated before the heart's input point from the pulmonary loop. The other parameters from the highlighted combinations are RA1, CA1 and RL1. RA1 and CA1 are the Aortic 1 Resistance and Compliance respectively and these parameters are situated at the heart's exit point at the aortic. On the other hand, RL1is the Pulmonary Vein 1 Resistance and it is situated after the lungs and before RL2. The highlighted combinations of parameters are basically made up of parameters which are situated before the input or after the output of the heart. PhysioNet's CVD signals are from patients who have been diagnosed with Angina and MI/cardiogenic shock and the majority of hospital signals (72.5% of 40 hospital data) are from patients who have been diagnosed for MI/cardiogenic shock (27.5%), ischemic heart disease (25%) and Angina (20%). Angina is a condition identified by chest pain, that is caused by reduced blood flow to the heart muscles and ischemic heart disease is a heart problem caused by narrowed heart arteries when arteries are narrowed, less blood and oxygen reach the heart muscle. On the other hand, MI/cardiogenic shock is a condition in which the heart suddenly cannot pump enough blood to meet the body's needs. When confronted with these conditions, the parameters situated before and after the heart must respond in order to ensure that blood circulation continues to flow to satisfy the demands of the heart and the body. If it is a resistance parameter, it should be reduced, and if it is a compliance parameter, it should be increased, in order to assure better blood flow in the blood circulatory system.

When considering the data presented in Table 4.26, the best combination in common with EIF and GTF would be RA1+RL2, as the use of this for either system would give a minimum accuracy of 80% CVD and 60% for healthy signals, which can be considered as reasonably good performance. However, further work is needed to find the

optimum combination of the parameters, by considering a bigger dataset for the ranges, for testing, as well as using combinations of all 16 parameters and using more than 2 per combination by incorporating Fuzzy or optimization methods for the combinations. A bigger set of data is needed as it can be seen in the small data size results in Table 4.25 and bigger size results in Table 4.26, that some combinations did not perform well. This might be because the range is made up of smaller data sets. However, as the scope of this project is to investigate if the proposed medical system can perform at an acceptable level, the current results are deemed sufficient to prove that the system is capable of accurately classifying CVD and healthy signals.

Over all, this method has shown that the combination of parameters was able to show an obvious change in values to differentiate CVD signal and non-CVD including healthy signal despite using two different transfer functions which are EIF and GTF to estimate the respective aortic waveform. Since RA1+RL2 is selected as the best combination, when faced with conditions such as MI/cardiogenic shock, ischemic heart disease and angina, it is postulated from the results obtains from the CNN that the Pulmonary Vein 2 (RL2) and Aortic 1 (RA1) naturally relaxes concurrently to allow the blood flow more fluently in its closed-loop system resulting in the reduction of the resistance value. Using the EIF to estimate the aortic waveform for the CNN, the values of RL2 and RA1 when it adjusts to these cardiovascular conditions, suggest values equal and below 10.640691 $\mathrm{g \cdot s/cm^4}$ and 9.7667933 $\mathrm{g \cdot s/cm^4}$ respectively. On the other hand, using the GTF to estimate the aortic waveform for the CNN, the values of RL2 and RA1 when it adjusts to these cardiovascular conditions suggests values equal and below 10.530969 $\mathrm{g \cdot s/cm^4}$ and 9.8313036 $\mathrm{g \cdot s/cm^4}$ respectively. For both methods, the opposite of the mentioned criteria can be used to classify those with non-cardiovascular conditions including healthy individuals.

Furthermore, Table 4.25 shows that the results obtained for non-CVD data, are not optimal yet reasonable for the listed parameter combinations as PhysioNet's non-CVD signals are made up of diseases such as severe respiratory failure and sepsis which are highly related to or may eventually cause cardio problems [343], [344]. For example, for patients with severe respiratory disease such as respiratory failure, the chances of those patients' RL2 and RA1 values concurrently to be lesser than the above-mentioned indication values are high, indicating those patients may be prone to cardiovascular disease. This is because the function of the lung and heart are interrelated to maintain

the blood circulation in the human body. For example, as the heart gets weaker, the patient will have shortness of breath due to the inefficiency of the heart to attain oxygenated blood from the lungs. Some of the parameter's values of the non-cardiovascular disease signals for the data obtained from the online database, PhysioNet [328] (in Appendix 4 for using EIF as the transfer function and Appendix 7 for using GTF as the transfer function), which are tagged for respiratory failure, have RL2 and RA1 values concurrently lesser than the above-mentioned indication values, indicating those patients may be prone to cardiovascular disease.

The indication / baseline parameter values of the RL2 and RA1 are always subjective to the error contributed by the transfer function and the CNN prediction. Nevertheless, a constant error in the system allows the methodology to differentiate cardiovascular disease signals and non-cardiovascular disease signals. The combination of RA1+RL2 in Table 4.26 shows that using GTF to estimate the aortic waveform for the CNN was able to give a better classification for CVD of 82.5% compared to the EIF, which was able to give a correct classification of 80.0%, this is because the GTF was able to give a lower RMSE of 6.2698 and a better correlation percentage of 99.97± 0.03 compared to the EIF which has a RMSE of 9.4838 and correlation percentage of 99.92± 0.05 for the estimation of aortic blood pressure waveform. On the other hand, using EIF to estimate the aortic waveform for the CNN was able to give a better classification for healthy of 68.45% compared to the GTF which was able to give a correct classification of 60.36%. These maybe associated with the ability of EIF in the estimation of systolic pressure as it was able to keep 98.31% of the data of the 3365 datasets (total of hospital and HaeMod data) in the limit of agreement (LOA) compared to GTF which attained 96.97%. In the Bland Altman plot, GTF overestimates systolic pressure by 59 data, but EIF only overestimates 14 data. This may cause the healthy signal to have higher systolic pressure using GTF as the transfer function and captured as CVD classification where it is known that systolic blood pressure has been an indicator of hypertension [178] and that hypertension is associated with the majority of cardiovascular disease.

4.5 Summary

The prototype created for this project acquires the radial blood waveform using a non-invasive method. However, applanation has been proven to be difficult because it must be frequently calibrated in practice to ensure the blood pressure measurement to be accurate and using oscillometric blood pressure measurement for calibration of the arterial tonometry method can contribute to error [341]. Therefore, for this prototype, there is a need in obtaining an invasive radial blood pressure waveform of the user to calibrate the ADC values to the blood pressure values. This can be done in the hospital by strapping the prototype on the patient before an angiogram procedure where the doctor would puncture through the radial blood vessel. In addition, the signal obtained from the prototype can be examined for its accuracy with the invasive signal acquired in the hospital. However, the current state of the hardware does not fulfill the criteria of the Clinical Research Centre (CRC) in Malaysia where the prototype needs to be miniaturized to be a wearable device so that it would be compact and handy to collect data in the hospital. To ensure the miniature prototype could be produced, there is a need for industrial soldering and changing the current components to Surface-mount technology (SMT) components. For this ongoing development, the industrial collaborator Chulia Facilities Management Sdn. Bhd will further develop the prototype into a wearable device.

There is a lot of motivation in measuring central blood pressure non-invasively in the medical world [57] and researchers are driven by the evidence that central aortic blood pressure waveform provides a better assessment of cardiovascular risk [162], [345]–[348]. The EIF can be used to estimate the central aortic blood pressure waveform as a simple, accurate and low computing method when compared to GTF, NPMA and ATF methods. Furthermore, the EIF had a lower average MAPE (0.0661) when compared to NPMA (0.0762) and ATF (0.0713). When compared with GTF, the EIF has shown the lowest peak difference of 6.35 mmHg. The GTF was able to give the lowest average RMSE (6.2698) and MAPE (0.0477) compared to all the methods. Overall, the EIF had the best computational time to convert the signal, taking 0.0129ms only, having a big margin between the NPMA (0.6481ms) and ATF (119.79ms) and a close difference between the GTF (0.0142ms). Furthermore, EIF shows a better estimation for systolic pressure and pulse pressure as it was able to keep 98.31% and 95.66% respectively of

the data of the 3365 datasets in the limit of agreement (LOA) compared to GTF, NPMA and ATF where GTF attained 96.97% and 95.01% respectively, NPMA attained 96.93% and 95.33% and ATF attained 96.46% and 94.95% respectively. Since this research needs a low computing method to estimate the aortic blood pressure waveform as it requires to embed the method and the risk indication algorithm in the microcontroller to ensure that the risk is always indicated to the user even if wireless communication is not available, EIF and GTF are the optimum choices.

There are 16 parameters that were identified that significantly influence the features of the Vincent Rideout 0D cardiovascular model's aortic wave. When the trained CNN is trained with cardiovascular disease aortic pulse waveforms which were converted from radial pulse waveforms using transfer functions which are EIF and GTF, it was identified that there were 2 common combination of parameters, which are RA1 + RL2 and RL1 + RL2 for both methods, which could be used to classify the signals. The best combination in common between EIF and GTF would be RA1+RL2, as the use of this for either system would give a minimum accuracy of 80% CVD and 60% for healthy, which can be considered as good performance. However, further investigation is required to find the optimum parameter combination, by considering a larger data set for the ranges, for testing, as well as using combinations of all 16 parameters and more than two per combination by incorporating other optimization methods such as Fuzzy logic for the parameter combinations. As RA1+RL2 were selected as the best combinations from the outcome of the data presented, it is postulated from the CNN results that the Pulmonary Vein 2 (RL2) and Aortic Artery 1 (RA1) relax simultaneously to permit the blood flow smoothly in its closed-loop system resulting in the decrease of resistance. The values of RL2 and RA1 when it acclimates to these cardiovascular conditions might be equal to or beneath 10.640691 $g \cdot s/cm^4$ and 9.7667933 $g \cdot s/cm^4$ respectively when using EIF as the transfer function. On the other hand, by using GTF as the transfer function, the values of RL2 and RA1 when it acclimates to these cardiovascular conditions might be equal to or beneath 10.530969 $g \cdot s/cm^4$ and 9.8313036 $g \cdot s/cm^4$ respectively. An 80.0% and 82.5% of accurate classification was obtained when the approach was verified with cardiovascular disease data obtained from Hospital Sultanah Bahiyah using EIF and GTF respectively as the transfer function. In addition, 68.45 % and 60.36% of accurate classifications were obtained when the approach was verified with healthy data obtained HaeMod database [329] using EIF and GTF respectively, as

the transfer function. Overall, this research method of utilizing CNN trained with significant parameters of 0D model has shown that the combination of parameters was able to show obvious changes in values to differentiate CVD signal and non-CVD including healthy signal despite using two different transfer functions which are EIF and GTF to estimate the respective aortic waveform. From the results attained in this research, it proves that the methodology used in this project to create a framework for the classification of CVD and healthy signals with the use of radial waveforms is valid, and has a sufficient level of accuracy and performance for it to be implemented in its current state. Though further improvements can be made in each individual section by the use of further research, to improve the system performance as a whole.

To summarize the complete integration of the system developed, shown in Figure 4.24, the system acquires a radial blood pressure waveform from the Honeywell FSS005WNSB sensor, which is then estimated to the aortic blood pressure waveform using either the GTF or the EIF, which is then fed to the CNN. If the EIF is used as the transfer function for the system, and the CNN output for RL2 and RA1 is equal to or beneath 10.640691 $g \cdot s/cm^4$and 9.7667933 $g \cdot s/cm^4$ respectively, the user is at risk of cardiovascular disease. Similarly, if the GTF is used as the transfer function for the system, and the output for RL2 and RA1 is equal to or beneath 10.530969 $g \cdot s/cm^4$ and 9.8313036 $g \cdot s/cm^4$ respectively, the user is at risk of cardiovascular disease.

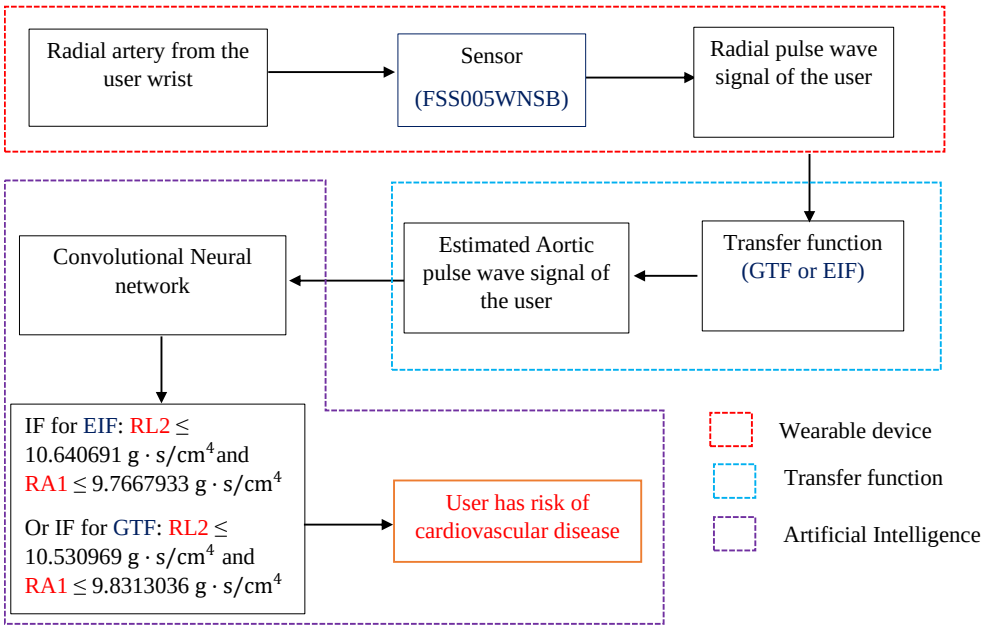

Figure 4.24 Complete integration of the system developed

CHAPTER 5 : CONCLUSION AND FUTURE WORK

The core aim of this study was to propose a solution to reduce the number of cardiovascular disease cases, as it is the leading source of death around the world. The most significant issue encountered by individuals who experience the ill effects of cardiovascular disease, is not having the option to distinguish their disease until the effects give an undeniable indication, generally at the critical stage, which results in a high risk of demise. Furthermore, the most common method of treatment, which is intrusive in nature, is agonizing to patients. Therefore, the proposed solution is to develop a medical system which would screen, and give an early identification of cardiovascular disease, to reduce the danger of abrupt demise among individuals today. The medical system consists of a pressure sensor that acquires the radial waveform from the user's wrist and converts it to an estimated aortic blood pressure waveform using a transfer function, which is then fed into a Convolutional Neural Network (CNN) that was trained with a zero-dimensional cardiovascular model's parameters to be used for risk prediction. In today's world, the hardware and software framework for the medical system to indicate risk of cardiovascular disease in this manner is yet to be explored and established. In order to achieve this functionalble medical system, certain objectives had to be met successfully which were described :

Objective 1: ***Identify a sensor to acquire the radial blood pressure signal in order to develop a prototype***

The medical system hardware comprises of a pressure sensor Honeywell FSS005WNSB, two amplifiers which are AD524C and TL071CP, 1 microcontroller which is NodeMCU Lua V3 ESP8266 WIFI with CH340C, 1 SD card module and 1 organic light-emitting diode (OLED) which is SSD1306. The Pressure sensor (Honeywell FSS005WNSB) has a diameter of 0.99 mm and can sense a force of 5N. It also has the option to detect a pressure range of 0 to 16078mmHg at the wrist. The chosen sensor could capture the radial blood pressure waveform of the user non-intrusively, which fulfils all the criteria for this objective.

Objective 2: ***Identify and implement a method to convert radial blood pressure waveform to aortic blood pressure waveform which has the closes representation of the actual aortic blood pressure waveform.***

An investigation of the current methods, which include the Generalised Transfer Function (GTF), N-Point Moving Average (NPMA), and Adaptive Transfer Function (ATF), was done to identify a method capable of providing a close estimate of the actual aortic blood pressure waveform. The method should give a close prediction of the systolic pressure while having a low computing time, to be embedded in the medical system. This it requirement is to ensure that the risk is always indicated to the user even if there is no wireless communication, to ensure continuous monitoring is possible. According to the findings, GTF is the most suitable technique among the existing methods since it has the shortest computing time (0.0142ms), the lowest mean RMSE (6.2698), the lowest mean MAPE (0.0477), and the best correlation, though on the other hand, it overestimated systolic pressure. An Electrical Impedance Function was developed to estimate the aortic blood pressure waveform using a new approach, where it was able to give a better estimation of systolic pressure and pulse pressure, as it was able to keep 98.31% and 95.66% of those values respectively in the limit of agreement (LOA), for the data of the 3365 data. As compared to GTF, NPMA and ATF where GTF attained 96.97% and 95.01% respectively, NPMA attained 96.93% and 95.33% and ATF attained 96.46% and 94.95% respectively. Since this research project requires a method with low computing requirements to estimate the aortic blood pressure waveform, EIF and GTF are the best options because they attained a run time of 0.0129ms and 0.0142ms per signal respectively. Overall, EIF proved to be a comparable method to GTF, and a better estimator of systolic pressure. Both methods of transfer functions to estimate the aortic waveform was used in this work to evaluate the remainder of the subsystems.

Objective 3: ***Utilize the converted aortic blood pressure waveform for indicating risk by the implementation of a Convolutional Neural Network.***

In this research, the EIF and GTF were utilized as transfer functions to convert the radial blood pressure waveform to an estimated aortic blood pressure waveform for determining the risk of cardiovascular disease through the implementation of Convolutional Neural Networks (CNN). A two-convolution layer structure was used for the CNN implementation, and the 118098 different CNN architectures were investigated. CNN architecture number 9 was chosen since it has the lowest RMSE of 0.3284. The CNN was trained on 3200 data and validated on 640 data. These data were generated from the zero-dimensional V.Rideout cardiovascular model. From the investigation of the

V.Rideout cardiovascular model, it was identified that 16 potential parameters significantly affects the aortic blood pressure waveform. RP2, RP3, RL1, RL2, RLA, RA1, RA2, RA3, LLA, LA1, LLV, CP3, CLA, CA1, CA2, and CA3 are the 16 parameters that were identified and then used to create the data for the CNN training. The CNN trained with the zero-dimenisonal cardiovascular model is then investigated for the parameters that can indicate the risk of cardiovascular disease. This investigation was carried out by utlising the dataset from PhysioNet [328] which has 4 cardiovascular disease (CVD) signal and 19 non-cardiovascular disease signal (Non-CVD), 19 data from HaeMod [329] database which are healthy signals and 5 data from hospital which only contains CVD signals. These data were converted to the estimated aortic blood pressure waveform using both transfer function methods (EIF and GTF) and fed into the CNN to attain the parameters. The parameters of the cardiovascular disease signal of both of the transfer functions were used to identify the minimum and maximum range of the CVD occurance. A hit analysis was then done by mapping the Non-CVD and healthy parameter values in the CVD occurance range to identify the baseline parameter value for the indication of risk of cardiovascular disease. From the investigation, it was known that one parameter was insufficient to indicate risk of CVD with a high accuracy. Hence, an investigation of a combination of two parameter was able to discriminate CVD and Non-CVD including healthy for CNN. Overall, the best combination of parameters in common between EIF and GTF would be RA1+RL2, as the use of this for either system would give a minimum accuracy of 80% for CVD and 60% for healthy, which can be considered as good performance.

Objective 4: ***To develop an algorithm for the risk identification for healthy user from the radial blood pressure wavefrom collected data based on the features of blood pressure wave variations.***

HaeMod [329] database was used as the healthy radial blood pressure waveform with the approval of the cardiologist in Hospital Sultanah Bahiyah. These HaeMod [329] signals were estimated to its aortic blood pressure waveform using both transfer function (EIF and GTF). The estimated aortic blood pressure of the HaeMod [329] is then fed into the CNN to attain the parameter values. As RA1+RL2 was selected as the best combination for indication risk of CVD, the HaeMod dataset was able to attain a 68.45 % and 60.36% correct classification for using EIF and GTF respectively as the transfer function.

Objective 5: ***To validate the developed algorithm against ranges of clinical patient data***

The clinical patient data was attained from Hospital Sultanah Bahiyah. The hospital data contained 40 patient blood pressure waveforms where from 27.5% are MI/cardiogenic shock, 25% are ischemic heart disease, 20% are Angina and the balance are other various cardiovascular diseases. These Hospital radial blood pressure wavefoms were estimated to its aortic blood pressure waveform using both transfer functions (EIF and GTF) and fed into the CNN to attain the parameter values. As RA1+RL2 was selected as the best combination for indication risk of CVD, the Hospital dataset was able to attain a 80.0 % and 82.5% correct classification for using EIF and GTF respectively as the transfer function.

Overall it can be safely stated that objectives set for this research were successfully met and completed. The developed medical system can also be considered as a novel framework with 3 subsystems, where each subsystem can be further developed in the future to optimize the system for specific diseases or increasing the system performance. Other significant novelties are present in the form of a newly developed transfer function for converting radial to aortic blood pressure waveforms (EIF), as well as the combination of CNN and 0D model for risk indication.

If this work is to be continued in the future, a list of possible future directions have been listed below :

1) Miniaturization of the protoype to be a commercial standard wearable device, by embedding the overall system, so that it would be compact and handy to collect data in hospitals.
2) Investigation of the research methodology with a larger set of data from hospitals.
3) Futher investigation on incoprating other available zero-dimensional cardiovascular model's parameters to be utilized as the dataset for the CNN training.
4) Futher investigation on optimizing the CNN in term of the structure and architecture.
5) Optimising the medical system by incorporating Fuzzy or other available optimization methods for the parameter combinations to indicate risk of cardiovascular disease in general or specific cardiovascular diseases.

6) Incorporating an IOT cloud system to the medical system to ensure the parameters are stored for daily or weekly comparison, to investigate the changes in the parameters and its relationship with risk of cardiovascular disease.

In summary, while there are many avenues of possible future additions / improvements to the system, the work described in this thesis proves that the proposed medical system has an acceptable level of performance to be able to discriminate between CVD and healthy individuals.

REFERENCES

[1] S. Kohno, A. L. Keenan, J. M. Ntambi, and M. Miyazaki, "Lipidomic insight into cardiovascular diseases," *Biochem. Biophys. Res. Commun.*, vol. 504, no. 3, pp. 590–595, Oct. 2018, doi: 10.1016/j.bbrc.2018.04.106.

[2] I. Dadgar and T. Norström, "Is there a link between cardiovascular mortality and economic fluctuations?," *Scand. J. Public Health*, p. 140349481989069, Jan. 2020, doi: 10.1177/1403494819890699.

[3] D. Ramachandran, V. Ponnusamy Thangapandian, and H. Rajaguru, "Computerized approach for cardiovascular risk level detection using photoplethysmography signals," *Measurement*, vol. 150, p. 107048, Jan. 2020, doi: 10.1016/j.measurement.2019.107048.

[4] N. K. Wenger, "Cardiovascular Disease in the Elderly," *Cardiology*, vol. 74, no. 4, pp. 310–315, 1987, doi: 10.1159/000174216.

[5] J. Allen, "Photoplethysmography and its application in clinical physiological measurement," *Physiol. Meas.*, vol. 28, no. 3, pp. R1–R39, Mar. 2007, doi: 10.1088/0967-3334/28/3/R01.

[6] S. Xu *et al.*, "Soft Microfluidic Assemblies of Sensors, Circuits, and Radios for the Skin," *Science (80-.).*, vol. 344, no. 6179, pp. 70–74, Apr. 2014, doi: 10.1126/science.1250169.

[7] S. Chen *et al.*, "Hierarchical elastomer tuned self-powered pressure sensor for wearable multifunctional cardiovascular electronics," *Nano Energy*, vol. 70, p. 104460, Apr. 2020, doi: 10.1016/j.nanoen.2020.104460.

[8] S. P. Karunathilake and G. U. Ganegoda, "Secondary Prevention of Cardiovascular Diseases and Application of Technology for Early Diagnosis," *Biomed Res. Int.*, vol. 2018, pp. 1–9, 2018, doi: 10.1155/2018/5767864.

[9] C. Ott, S. Haetinger, M. P. Schneider, M. Pauschinger, and R. E. Schmieder, "Comparison of two noninvasive devices for measurement of central systolic blood pressure with invasive measurement during cardiac catheterization," *J.*

Clin. Hypertens., vol. 14, no. 9, pp. 575–579, 2012, doi: 10.1111/j.1751-7176.2012.00682.x.

[10] F.-H. Ding, Y. Li, R.-Y. Zhang, Q. Zhang, and J.-G. Wang, "Comparison of the SphygmoCor and Omron devices in the estimation of pressure amplification against the invasive catheter measurement," *J. Hypertens.*, vol. 31, no. 1, 2013, [Online]. Available: https://journals.lww.com/jhypertension/Fulltext/2013/01000/Comparison_of_the_SphygmoCor_and_Omron_devices_in.15.aspx.

[11] T. Weber *et al.*, "Validation of a brachial cuff-based method for estimating central systolic blood pressure," *Hypertension*, vol. 58, no. 5, pp. 825–832, 2011, doi: 10.1161/HYPERTENSIONAHA.111.176313.

[12] B. Williams, P. S. Lacy, P. Yan, C.-N. Hwee, C. Liang, and C.-M. Ting, "Development and Validation of a Novel Method to Derive Central Aortic Systolic Pressure From the Radial Pressure Waveform Using an N-Point Moving Average Method," *J. Am. Coll. Cardiol.*, vol. 57, no. 8, pp. 951–961, Feb. 2011, doi: 10.1016/j.jacc.2010.09.054.

[13] B. Williams, P. S. Lacy, F. Baschiera, P. Brunel, and R. Düsing, "Novel description of the 24-hour circadian rhythms of brachial versus central aortic blood pressure and the impact of blood pressure treatment in a randomized controlled clinical trial: the ambulatory central aortic pressure (AMCAP) study," *Hypertension*, vol. 61, no. 6, pp. 1168–1176, 2013, doi: 10.1161/HYPERTENSIONAHA.111.00763.

[14] C.-H. Chen *et al.*, "Estimation of Central Aortic Pressure Waveform by Mathematical Transformation of Radial Tonometry Pressure," *Circulation*, vol. 95, no. 7, pp. 1827–1836, Apr. 1997, doi: 10.1161/01.CIR.95.7.1827.

[15] M. F. O'Rourke, "Hypertension is a myth; high(er) arterial pressure is the problem.," *Aust. N. Z. J. Med.*, vol. 14, no. 1, pp. 69–70, Feb. 1984, doi: 10.1111/j.1445-5994.1984.tb03594.x.

[16] A. E. Doyle, "Hypertension: the realities.," *Aust. N. Z. J. Med.*, vol. 13, no. 2,

pp. 185–186, Apr. 1983, doi: 10.1111/j.1445-5994.1983.tb02684.x.

[17] A. Avolio, “Central aortic blood pressure and cardiovascular risk: A paradigm shift?,” *Hypertension*, vol. 51, no. 6, pp. 1470–1471, 2008, doi: 10.1161/HYPERTENSIONAHA.107.108910.

[18] M. E. Safar *et al.*, “Central pulse pressure and mortality in end-stage renal disease.,” *Hypertens. (Dallas, Tex. 1979)*, vol. 39, no. 3, pp. 735–738, Mar. 2002, doi: 10.1161/hy0202.098325.

[19] T. K. Waddell, A. M. Dart, T. L. Medley, J. D. Cameron, and B. A. Kingwell, “Carotid pressure is a better predictor of coronary artery disease severity than brachial pressure.,” *Hypertens. (Dallas, Tex. 1979)*, vol. 38, no. 4, pp. 927–931, Oct. 2001, doi: 10.1161/hy1001.096107.

[20] M. J. Roman *et al.*, “Central pressure more strongly relates to vascular disease and outcome than does brachial pressure: the Strong Heart Study.,” *Hypertens. (Dallas, Tex. 1979)*, vol. 50, no. 1, pp. 197–203, Jul. 2007, doi: 10.1161/HYPERTENSIONAHA.107.089078.

[21] W. J. Verberk, H. Cheng, L.-C. Huang, C.-M. Lin, Y.-P. Teng, and C.-H. Chen, “Practical Suitability of a Stand-Alone Oscillometric Central Blood Pressure Monitor: A Review of the Microlife WatchBP Office Central,” *Pulse*, vol. 3, no. 3–4, pp. 205–216, 2016, doi: 10.1159/000443771.

[22] J. E. Lewis, P. Williams, and J. H. Davies, “Non-invasive assessment of peripheral arterial disease: Automated ankle brachial index measurement and pulse volume analysis compared to duplex scan.,” *SAGE open Med.*, vol. 4, p. 2050312116659088, 2016, doi: 10.1177/2050312116659088.

[23] Y. Watanabe *et al.*, “Ankle-Brachial Index, Toe-Brachial Index, and Pulse Volume Recording in Healthy Young Adults,” *Ann. Vasc. Dis.*, vol. 8, no. 3, pp. 227–235, 2015, doi: 10.3400/avd.oa.15-00056.

[24] R. E. D. Climie, M. G. Schultz, S. B. Nikolic, K. D. K. Ahuja, J. W. Fell, and J. E. Sharman, “Validity and reliability of central blood pressure estimated by upper arm oscillometric cuff pressure.,” *Am. J. Hypertens.*, vol. 25, no. 4, pp.

414–420, Apr. 2012, doi: 10.1038/ajh.2011.238.

[25] G. P. Gravlee, A. B. Wong, T. G. Adkins, L. D. Case, and A. L. Pauca, “A comparison of radial, brachial, and aortic pressures after cardiopulmonary bypass.,” *J. Cardiothorac. Anesth.*, vol. 3, no. 1, pp. 20–26, Feb. 1989, doi: 10.1016/0888-6296(89)90006-9.

[26] M. KARAMANOGLU, M. F. O’ROURKE, A. P. AVOLIO, and R. P. KELLY, “An analysis of the relationship between central aortic and peripheral upper limb pressure waves in man,” *Eur. Heart J.*, vol. 14, no. 2, pp. 160–167, Feb. 1993, doi: 10.1093/eurheartj/14.2.160.

[27] R. P. KELLY *et al.*, “Nitroglycerin has more favourable effects on left ventricular afterload than apparent from measurement of pressure in a peripheral artery,” *Eur. Heart J.*, vol. 11, no. 2, pp. 138–144, Feb. 1990, doi: 10.1093/oxfordjournals.eurheartj.a059669.

[28] N. Stergiopulos, D. F. Young, and T. R. Rogge, “Computer simulation of arterial flow with applications to arterial and aortic stenoses,” *J. Biomech.*, vol. 25, no. 12, pp. 1477–1488, 1992, doi: 10.1016/0021-9290(92)90060-E.

[29] M. Karamanoglu, D. E. Gallagher, A. P. Avolio, and M. F. O’Rourke, “Pressure wave propagation in a multibranched model of the human upper limb.,” *Am. J. Physiol.*, vol. 269, no. 4 Pt 2, pp. H1363-9, Oct. 1995, doi: 10.1152/ajpheart.1995.269.4.H1363.

[30] H. Ebell, “Artificial N eural N etw orks for Predicting Failure to Survive Follow in g In-FIospital Cardiopulm onary Resuscitation,” vol. 3, no. 3, pp. 297–303, 1993.

[31] R. Poli, S. Cagnoni, R. Livi, G. Coppini, and G. Valli, “A neural network expert system for diagnosing and treating hypertension,” *Computer (Long. Beach. Calif).*, vol. 24, no. 3, pp. 64–71, Mar. 1991, doi: 10.1109/2.73514.

[32] M. Akay, “Noninvasive diagnosis of coronary artery disease using a neural network algorithm,” *Biol. Cybern.*, vol. 67, no. 4, pp. 361–367, Aug. 1992, doi: 10.1007/BF02414891.

[33] J. K. Kim and S. Kang, "Neural Network-Based Coronary Heart Disease Risk Prediction Using Feature Correlation Analysis," *J. Healthc. Eng.*, vol. 2017, 2017, doi: 10.1155/2017/2780501.

[34] C. El-Hajj and P. A. Kyriacou, "A review of machine learning techniques in photoplethysmography for the non-invasive cuff-less measurement of blood pressure," *Biomed. Signal Process. Control*, vol. 58, p. 101870, 2020, doi: 10.1016/j.bspc.2020.101870.

[35] Y. Shi, P. Lawford, and R. Hose, "Review of zero-D and 1-D models of blood flow in the cardiovascular system.," *Biomed. Eng. Online*, vol. 10, no. 1, p. 33, 2011, doi: 10.1186/1475-925X-10-33.

[36] D. M. Hamby, "A review of techniques for parameter sensitivity analysis of environmental models," *Environ. Monit. Assess.*, vol. 32, no. 2, pp. 135–154, 1994, doi: 10.1007/BF00547132.

[37] Z. Zi, "Sensitivity analysis approaches applied to systems biology models.," *IET Syst. Biol.*, vol. 5, no. 6, p. 336, Nov. 2011, doi: 10.1049/iet-syb.2011.0015.

[38] A. Saltelli *et al.*, *Global Sensitivity Analysis. The Primer*. 2008.

[39] A. Saltelli, S. Tarantola, and K. P. S. Chan, "A quantitative model-independent method for global sensitivity analysis of model output," *Technometrics*, vol. 41, no. 1, pp. 39–56, 1999, doi: 10.1080/00401706.1999.10485594.

[40] M. D. Morris, "Factorial Sampling Plans for Preliminary Computational Experiments," *Technometrics*, vol. 33, no. 2, pp. 161–174, May 1991, doi: 10.1080/00401706.1991.10484804.

[41] T. Homma and A. Saltelli, "Importance measures in global sensitivity analysis of nonlinear models," *Reliab. Eng. Syst. Saf.*, vol. 52, no. 1, pp. 1–17, 1996, doi: 10.1016/0951-8320(96)00002-6.

[42] G. Li, K. Watanabe, H. Anzai, X. Song, A. Qiao, and M. Ohta, "Pulse-Wave-Pattern Classification with a Convolutional Neural Network," *Sci. Rep.*, vol. 9, no. 1, pp. 1–11, 2019, doi: 10.1038/s41598-019-51334-2.

[43] G. B. Huang, H. Lee, and E. Learned-Miller, "Learning hierarchical representations for face verification with convolutional deep belief networks," *Proc. IEEE Comput. Soc. Conf. Comput. Vis. Pattern Recognit.*, pp. 2518–2525, 2012, doi: 10.1109/CVPR.2012.6247968.

[44] A. Krizhevsky, I. Sutskever, and G. E. Hinton, "ImageNet Classification with Deep Convolutional Neural Networks," in *Proceedings of the 25th International Conference on Neural Information Processing Systems - Volume 1*, 2012, pp. 1097–1105.

[45] K. Simonyan and A. Zisserman, "Very deep convolutional networks for large-scale image recognition," *3rd Int. Conf. Learn. Represent. ICLR 2015 - Conf. Track Proc.*, pp. 1–14, 2015.

[46] J. Zhang, P. Liu, F. Zhang, and Q. Song, "CloudNet: Ground-Based Cloud Classification With Deep Convolutional Neural Network," *Geophys. Res. Lett.*, vol. 45, no. 16, pp. 8665–8672, 2018, doi: 10.1029/2018GL077787.

[47] H. Clark, "NCDs: a challenge to sustainable human development," *Lancet*, vol. 381, no. 9866, pp. 510–511, Feb. 2013, doi: 10.1016/S0140-6736(13)60058-6.

[48] G. A. Roth *et al.*, "Global, Regional, and National Burden of Cardiovascular Diseases for 10 Causes, 1990 to 2015," *J. Am. Coll. Cardiol.*, vol. 70, no. 1, pp. 1–25, Jul. 2017, doi: 10.1016/j.jacc.2017.04.052.

[49] X. Yan, L. Zhang, J. Li, D. Du, and F. Hou, "Entropy-Based Measures of Hypnopompic Heart Rate Variability Contribute to the Automatic Prediction of Cardiovascular Events," *Entropy*, vol. 22, no. 2, p. 241, Feb. 2020, doi: 10.3390/e22020241.

[50] R. Manfredini *et al.*, "Twenty-Four-Hour Patterns in Occurrence and Pathophysiology of Acute Cardiovascular Events and Ischemic Heart Disease," *Chronobiol. Int.*, vol. 30, no. 1–2, pp. 6–16, Mar. 2013, doi: 10.3109/07420528.2012.715843.

[51] E. A. GOFF, C. L. NICHOLAS, A. K. SIMONDS, J. TRINDER, and M. J. MORRELL, "Differential effects of waking from non-rapid eye movement

versus rapid eye movement sleep on cardiovascular activity," *J. Sleep Res.*, vol. 19, no. 1p2, pp. 201–206, Mar. 2010, doi: 10.1111/j.1365-2869.2009.00783.x.

[52] Q. Wang, Y. Cui, P. Yogendranath, and N. Wang, "Blood pressure and heart rate variability are linked with hyperphosphatemia in chronic kidney disease patients," *Chronobiol. Int.*, vol. 35, no. 10, pp. 1329–1334, Oct. 2018, doi: 10.1080/07420528.2018.1486850.

[53] N. Takeda and K. Maemura, "Circadian clock and the onset of cardiovascular events," *Hypertens. Res.*, vol. 39, no. 6, pp. 383–390, Jun. 2016, doi: 10.1038/hr.2016.9.

[54] A. Amici *et al.*, "Exaggerated morning blood pressure surge and cardiovascular events. A 5-year longitudinal study in normotensive and well-controlled hypertensive elderly," *Arch. Gerontol. Geriatr.*, vol. 49, no. 2, pp. e105–e109, Sep. 2009, doi: 10.1016/j.archger.2008.10.003.

[55] R. Furlan *et al.*, "Continuous 24-hour assessment of the neural regulation of systemic arterial pressure and RR variabilities in ambulant subjects.," *Circulation*, vol. 81, no. 2, pp. 537–547, Feb. 1990, doi: 10.1161/01.CIR.81.2.537.

[56] P. Van de Borne, H. Nguyen, P. Biston, P. Linkowski, and J. P. Degaute, "Effects of wake and sleep stages on the 24-h autonomic control of blood pressure and heart rate in recumbent men," *Am. J. Physiol. Circ. Physiol.*, vol. 266, no. 2, pp. H548–H554, Feb. 1994, doi: 10.1152/ajpheart.1994.266.2.H548.

[57] E. Agabiti-Rosei *et al.*, "Central blood pressure measurements and antihypertensive therapy: A consensus document," *Hypertension*, vol. 50, no. 1, pp. 154–160, 2007, doi: 10.1161/HYPERTENSIONAHA.107.090068.

[58] G. MANCIA, "EFFECTS OF BLOOD-PRESSURE MEASUREMENT BY THE DOCTOR ON PATIENT'S BLOOD PRESSURE AND HEART RATE," *Lancet*, vol. 322, no. 8352, pp. 695–698, Sep. 1983, doi: 10.1016/S0140-6736(83)92244-4.

[59] P. PICKERING, "Blood pressure measurement and detection of hypertension,"

Lancet, vol. 344, no. 8914, pp. 31–35, Jul. 1994, doi: 10.1016/S0140-6736(94)91053-7.

[60] M. L. Aisen, H. I. Krebs, N. Hogan, F. McDowell, and B. T. Volpe, "The Effect of Robot-Assisted Therapy and Rehabilitative Training on Motor Recovery Following Stroke," *Arch. Neurol.*, vol. 54, no. 4, pp. 443–446, Apr. 1997, doi: 10.1001/archneur.1997.00550160075019.

[61] E. A. Crisostomo, P. W. Duncan, M. Propst, D. V. Dawson, and J. N. Davis, "Evidence that amphetamine with physical therapy promotes recovery of motor function in stroke patients," *Ann. Neurol.*, vol. 23, no. 1, pp. 94–97, Jan. 1988, doi: 10.1002/ana.410230117.

[62] D. Mozaffarian *et al.*, "Executive Summary: Heart Disease and Stroke Statistics—2015 Update," *Circulation*, vol. 131, no. 4, pp. 434–441, Jan. 2015, doi: 10.1161/CIR.0000000000000157.

[63] M. Nichols, N. Townsend, P. Scarborough, and M. Rayner, "Cardiovascular disease in Europe 2014: Epidemiological update," *Eur. Heart J.*, vol. 35, no. 42, pp. 2950–2959, 2014, doi: 10.1093/eurheartj/ehu299.

[64] O. Faust, U. R. Acharya, F. Molinari, S. Chattopadhyay, and T. Tamura, "Linear and non-linear analysis of cardiac health in diabetic subjects," *Biomed. Signal Process. Control*, vol. 7, no. 3, pp. 295–302, May 2012, doi: 10.1016/j.bspc.2011.06.002.

[65] G. A. Mensah and D. W. Brown, "An Overview Of Cardiovascular Disease Burden In The United States," *Health Aff.*, vol. 26, no. 1, pp. 38–48, Jan. 2007, doi: 10.1377/hlthaff.26.1.38.

[66] R. Ross, "The Pathogenesis of Atherosclerosis — An Update," *N. Engl. J. Med.*, vol. 314, no. 8, pp. 488–500, Feb. 1986, doi: 10.1056/NEJM198602203140806.

[67] D. G. Hackam and S. S. Anand, "Emerging Risk Factors for Atherosclerotic Vascular Disease," *JAMA*, vol. 290, no. 7, p. 932, Aug. 2003, doi: 10.1001/jama.290.7.932.

[68] R. A. Vogel, "Coronary risk factors, endothelial function, and atherosclerosis: A review," *Clin. Cardiol.*, vol. 20, no. 5, pp. 426–432, May 1997, doi: 10.1002/clc.4960200505.

[69] D. H. O'Leary, J. F. Polak, R. A. Kronmal, T. A. Manolio, G. L. Burke, and S. K. Wolfson, "Carotid-Artery Intima and Media Thickness as a Risk Factor for Myocardial Infarction and Stroke in Older Adults," *N. Engl. J. Med.*, vol. 340, no. 1, pp. 14–22, Jan. 1999, doi: 10.1056/NEJM199901073400103.

[70] P. Amarenco *et al.*, "Atherosclerotic Disease of the Aortic Arch and the Risk of Ischemic Stroke," *N. Engl. J. Med.*, vol. 331, no. 22, pp. 1474–1479, Dec. 1994, doi: 10.1056/NEJM199412013312202.

[71] G. De Luca, H. Suryapranata, J. P. Ottervanger, and E. M. Antman, "Time Delay to Treatment and Mortality in Primary Angioplasty for Acute Myocardial Infarction," *Circulation*, vol. 109, no. 10, pp. 1223–1225, Mar. 2004, doi: 10.1161/01.CIR.0000121424.76486.20.

[72] F. L. Silver, J. W. Norris, A. J. Lewis, and V. C. Hachinski, "Early mortality following stroke: a prospective review.," *Stroke*, vol. 15, no. 3, pp. 492–496, May 1984, doi: 10.1161/01.STR.15.3.492.

[73] R. H. Al-Ashwal and E. Supriyanto, "Clinical Pathway in Cardiovascular Disease Management," 2020, pp. 143–153.

[74] J. Stewart, G. Manmathan, and P. Wilkinson, "Primary prevention of cardiovascular disease: A review of contemporary guidance and literature," *JRSM Cardiovasc. Dis.*, vol. 6, p. 204800401668721, Jan. 2017, doi: 10.1177/2048004016687211.

[75] T. A. Pearson *et al.*, "AHA Guidelines for Primary Prevention of Cardiovascular Disease and Stroke: 2002 Update," *Circulation*, vol. 106, no. 3, pp. 388–391, Jul. 2002, doi: 10.1161/01.CIR.0000020190.45892.75.

[76] E. Archer and S. N. Blair, "Physical Activity and the Prevention of Cardiovascular Disease: From Evolution to Epidemiology," *Prog. Cardiovasc. Dis.*, vol. 53, no. 6, pp. 387–396, May 2011, doi: 10.1016/j.pcad.2011.02.006.

[77] J. H. Park, D. Dehaini, J. Zhou, M. Holay, R. H. Fang, and L. Zhang, "Biomimetic nanoparticle technology for cardiovascular disease detection and treatment," *Nanoscale Horizons*, vol. 5, no. 1, pp. 25–42, 2020, doi: 10.1039/C9NH00291J.

[78] J. Sanz and Z. A. Fayad, "Imaging of atherosclerotic cardiovascular disease," *Nature*, vol. 451, no. 7181, pp. 953–957, Feb. 2008, doi: 10.1038/nature06803.

[79] D. S. Celermajer, C. K. Chow, E. Marijon, N. M. Anstey, and K. S. Woo, "Cardiovascular Disease in the Developing World," *J. Am. Coll. Cardiol.*, vol. 60, no. 14, pp. 1207–1216, Oct. 2012, doi: 10.1016/j.jacc.2012.03.074.

[80] H. Thomas *et al.*, "Global Atlas of Cardiovascular Disease 2000-2016: The Path to Prevention and Control," *Glob. Heart*, vol. 13, no. 3, pp. 143–163, 2018, doi: 10.1016/j.gheart.2018.09.511.

[81] S. E. V. et al Naghavi, Mohsen, Haidong Wang, Rafael Lozano, Adrian Davis, Xiaofeng Liang, Maigeng Zhou, "Global, regional, and national age–sex specific all-cause and cause-specific mortality for 240 causes of death, 1990–2013: a systematic analysis for the Global Burden of Disease Study 2013," *Lancet*, vol. 385, no. 9963, pp. 117–171, Jan. 2015, doi: 10.1016/S0140-6736(14)61682-2.

[82] D. M. Lloyd-Jones *et al.*, "Parental Cardiovascular Disease as a Risk Factor for Cardiovascular Disease in Middle-aged Adults," *JAMA*, vol. 291, no. 18, p. 2204, May 2004, doi: 10.1001/jama.291.18.2204.

[83] J. A. Finegold, P. Asaria, and D. P. Francis, "Mortality from ischaemic heart disease by country, region, and age: Statistics from World Health Organisation and United Nations," *Int. J. Cardiol.*, vol. 168, no. 2, pp. 934–945, Sep. 2013, doi: 10.1016/j.ijcard.2012.10.046.

[84] A. H. E. M. Maas and Y. E. A. Appelman, "Gender differences in coronary heart disease," *Netherlands Hear. J.*, vol. 18, no. 12, pp. 598–603, Nov. 2010, doi: 10.1007/s12471-010-0841-y.

[85] P. Jousilahti, E. Vartiainen, J. Tuomilehto, and P. Puska, "Sex, Age, Cardiovascular Risk Factors, and Coronary Heart Disease," *Circulation*, vol. 99,

no. 9, pp. 1165–1172, Mar. 1999, doi: 10.1161/01.CIR.99.9.1165.

[86] T. A. Gaziano, A. Bitton, S. Anand, S. Abrahams-Gessel, and A. Murphy, "Growing Epidemic of Coronary Heart Disease in Low- and Middle-Income Countries," *Curr. Probl. Cardiol.*, vol. 35, no. 2, pp. 72–115, Feb. 2010, doi: 10.1016/j.cpcardiol.2009.10.002.

[87] M. E. Safar, B. I. Levy, and H. Struijker-Boudier, "Current perspectives on arterial stiffness and pulse pressure in hypertension and cardiovascular diseases," *Circulation*, vol. 107, no. 22, pp. 2864–2869, 2003, doi: 10.1161/01.CIR.0000069826.36125.B4.

[88] J. E. H. Arthur C. Guyton, *Textbook of medical physiology*. .

[89] T. Pereira, C. Correia, and J. Cardoso, "Novel methods for pulse wave velocity measurement," *J. Med. Biol. Eng.*, vol. 35, no. 5, pp. 555–565, 2015, doi: 10.1007/s40846-015-0086-8.

[90] V. Krasteva, I. Jekova, R. Leber, R. Schmid, and R. Abächerli, "Real-time arrhythmia detection with supplementary ECG quality and pulse wave monitoring for the reduction of false alarms in ICUs," *Physiol. Meas.*, vol. 37, no. 8, pp. 1273–1297, Aug. 2016, doi: 10.1088/0967-3334/37/8/1273.

[91] Wang Ping, Wang Jin-gang, Shi Xiao-bo, and He Wei, "The Research of Telemedicine System Based on Embedded Computer," in *2005 IEEE Engineering in Medicine and Biology 27th Annual Conference*, 2005, pp. 114–117, doi: 10.1109/IEMBS.2005.1616355.

[92] H. S. Ng, M. L. Sim, C. M. Tan, and C. C. Wong, "Wireless technologies for telemedicine," *BT Technol. J.*, vol. 24, no. 2, pp. 130–137, Apr. 2006, doi: 10.1007/s10550-006-0050-9.

[93] A. M. Johansson, I. Lindberg, and S. Söderberg, "Patients' Experiences with Specialist Care via Video Consultation in Primary Healthcare in Rural Areas," *Int. J. Telemed. Appl.*, vol. 2014, pp. 1–7, 2014, doi: 10.1155/2014/143824.

[94] K. P. and T. N.K., "A real-time health monitoring system for remote cardiac

patients using smartphone and wearable sensors," *Int. J. Telemed. Appl.*, vol. 2015, p. no pagination, 2015, doi: 10.1155/2015/373474.

[95] L. Ricciardi, F. Mostashari, J. Murphy, J. G. Daniel, and E. P. Siminerio, "A National Action Plan To Support Consumer Engagement Via E-Health," *Health Aff.*, vol. 32, no. 2, pp. 376–384, Feb. 2013, doi: 10.1377/hlthaff.2012.1216.

[96] R. Say, M. Murtagh, and R. Thomson, "Patients' preference for involvement in medical decision making: A narrative review," *Patient Educ. Couns.*, vol. 60, no. 2, pp. 102–114, Feb. 2006, doi: 10.1016/j.pec.2005.02.003.

[97] X. Chen, C. T. Ho, E. T. Lim, and T. Z. Kyaw, "Cellular phone based online ECG processing for ambulatory and continuous detection," in *2007 Computers in Cardiology*, Sep. 2007, pp. 653–656, doi: 10.1109/CIC.2007.4745570.

[98] K. W. Goh, J. Lavanya, E. K. Tan, C. B. Soh, and Y. Kim, "A PDA-Based ECG Beat Detector for Home Cardiac Care," in *2005 IEEE Engineering in Medicine and Biology 27th Annual Conference*, 2005, pp. 375–378, doi: 10.1109/IEMBS.2005.1616423.

[99] J. Rodriguez, A. Goni, and A. Illarramendi, "Real-Time Classification of ECGs on a PDA," *IEEE Trans. Inf. Technol. Biomed.*, vol. 9, no. 1, pp. 23–34, Mar. 2005, doi: 10.1109/TITB.2004.838369.

[100] Zhanpeng Jin, Yuwen Sun, and A. C. Cheng, "Predicting cardiovascular disease from real-time electrocardiographic monitoring: An adaptive machine learning approach on a cell phone," in *2009 Annual International Conference of the IEEE Engineering in Medicine and Biology Society*, Sep. 2009, pp. 6889–6892, doi: 10.1109/IEMBS.2009.5333610.

[101] J. J. Oresko *et al.*, "A wearable smartphone-based platform for real-time cardiovascular disease detection via electrocardiogram processing," *IEEE Trans. Inf. Technol. Biomed.*, vol. 14, no. 3, pp. 734–740, 2010, doi: 10.1109/TITB.2010.2047865.

[102] J. M. Cano-Garcia, E. Gonzalez-Parada, V. Alarcon-Collantes, and E. Casilari-Perez., "A PDA-based portable wireless ECG monitor for medical personal area

networks," in *MELECON 2006 - 2006 IEEE Mediterranean Electrotechnical Conference*, pp. 713–716, doi: 10.1109/MELCON.2006.1653199.

[103] W.-Y. Chung, C.-L. Yau, K.-S. Shin, and R. Myllyla, "A Cell Phone Based Health Monitoring System with Self Analysis Processor using Wireless Sensor Network Technology," in *2007 29th Annual International Conference of the IEEE Engineering in Medicine and Biology Society*, Aug. 2007, pp. 3705–3708, doi: 10.1109/IEMBS.2007.4353136.

[104] T.-S. Lee, J.-H. Hong, and M.-C. Cho, "Biomedical Digital Assistant for Ubiquitous Healthcare," in *2007 29th Annual International Conference of the IEEE Engineering in Medicine and Biology Society*, Aug. 2007, pp. 1790–1793, doi: 10.1109/IEMBS.2007.4352659.

[105] G. Appelboom *et al.*, "Smart wearable body sensors for patient self-assessment and monitoring.," *Arch. public Heal.*, vol. 72, no. 1, p. 28, 2014, doi: 10.1186/2049-3258-72-28.

[106] P. Bonato, "Advances in wearable technology and applications in physical medicine and rehabilitation," *J. Neuroeng. Rehabil.*, vol. 2, p. 2, 2005, doi: 10.1186/1743-0003-2-2.

[107] S. Meystre, "The Current State of Telemonitoring: A Comment on the Literature," *Telemed. e-Health*, vol. 11, no. 1, pp. 63–69, Feb. 2005, doi: 10.1089/tmj.2005.11.63.

[108] K. Hung, Y. T. Zhang, and B. Tai, "Wearable medical devices for tele-home healthcare," in *The 26th Annual International Conference of the IEEE Engineering in Medicine and Biology Society*, vol. 4, pp. 5384–5387, doi: 10.1109/IEMBS.2004.1404503.

[109] D. Phan, L. Y. Siong, P. N. Pathirana, and A. Seneviratne, "Smartwatch: Performance evaluation for long-term heart rate monitoring," in *2015 International Symposium on Bioelectronics and Bioinformatics (ISBB)*, Oct. 2015, pp. 144–147, doi: 10.1109/ISBB.2015.7344944.

[110] F. Jing *et al.*, "The Influence on Medical Activities by Mobile Medical

Application," in *2018 4th Annual International Conference on Network and Information Systems for Computers (ICNISC)*, Apr. 2018, pp. 104–106, doi: 10.1109/ICNISC.2018.00028.

[111] P. Athilingam, M. A. Labrador, E. F. J. Remo, L. Mack, A. B. San Juan, and A. F. Elliott, "Features and usability assessment of a patient-centered mobile application (HeartMapp) for self-management of heart failure," *Appl. Nurs. Res.*, vol. 32, pp. 156–163, Nov. 2016, doi: 10.1016/j.apnr.2016.07.001.

[112] B. H. Dobkin and A. Dorsch, "The Promise of mHealth," *Neurorehabil. Neural Repair*, vol. 25, no. 9, pp. 788–798, Nov. 2011, doi: 10.1177/1545968311425908.

[113] A. Darwish and A. E. Hassanien, "Wearable and Implantable Wireless Sensor Network Solutions for Healthcare Monitoring," *Sensors*, vol. 11, no. 6, pp. 5561–5595, May 2011, doi: 10.3390/s110605561.

[114] S. Wassertheurer *et al.*, "A new oscillometric method for pulse wave analysis: Comparison with a common tonometric method," *J. Hum. Hypertens.*, vol. 24, no. 8, pp. 498–504, 2010, doi: 10.1038/jhh.2010.27.

[115] I. G. Horváth *et al.*, "Invasive validation of a new oscillometric device (Arteriograph) for measuring augmentation index, central blood pressure and aortic pulse wave velocity," *J. Hypertens.*, vol. 28, no. 10, 2010, [Online]. Available: https://journals.lww.com/jhypertension/Fulltext/2010/10000/Invasive_validation_of_a_new_oscillometric_device.15.aspx.

[116] N. B. Rossen *et al.*, "Invasive validation of arteriograph estimates of central blood pressure in patients with type 2 diabetes," *Am. J. Hypertens.*, vol. 27, no. 5, pp. 674–679, 2014, doi: 10.1093/ajh/hpt162.

[117] A. Lowe, W. Harrison, E. El-Aklouk, P. Ruygrok, and A. M. Al-Jumaily, "Non-invasive model-based estimation of aortic pulse pressure using suprasystolic brachial pressure waveforms," *J. Biomech.*, vol. 42, no. 13, pp. 2111–2115, 2009, doi: 10.1016/j.jbiomech.2009.05.029.

[118] S. A. Koudryavtcev and V. M. Lazarev, “Validation of the BPLab® 24-hour blood pressure monitoring system according to the European standard BS EN 1060-4:2004 and British Hypertension Society protocol,” *Med. Devices Evid. Res.*, vol. 4, no. 1, pp. 193–196, 2011, doi: 10.2147/MDER.S25800.

[119] S. E. Brett, A. Guilcher, B. Clapp, and P. Chowienczyk, “Estimating central systolic blood pressure during oscillometric determination of blood pressure: proof of concept and validation by comparison with intra-aortic pressure recording and arterial tonometry,” *Blood Press. Monit.*, vol. 17, no. 3, 2012, [Online]. Available: https://journals.lww.com/bpmonitoring/Fulltext/2012/06000/Estimating_central_systolic_blood_pressure_during.8.aspx.

[120] T. Pereira *et al.*, “Invasive validation of the Complior Analyse in the assessment of central artery pressure curves: a methodological study,” *Blood Press. Monit.*, vol. 19, no. 5, 2014, [Online]. Available: https://journals.lww.com/bpmonitoring/Fulltext/2014/10000/Invasive_validation_of_the_Complior_Analyse_in_the.6.aspx.

[121] Shiu-Shin Chio, “Pulse Dynamics. Non-invasive Blood Pressure and Hemodynamic Monitoring,” vol. 2013, no. March, pp. 0–146, 2002.

[122] P. Salvi, “Is validation of non-invasive hemodynamic measurement devices actually required?,” *Hypertens. Res.*, vol. 37, no. 1, pp. 7–9, 2014, doi: 10.1038/hr.2013.115.

[123] G. Swamy, D. Xu, N. B. Olivier, and R. Mukkamala, “An adaptive transfer function for deriving the aortic pressure waveform from a peripheral artery pressure waveform,” *Am. J. Physiol. - Hear. Circ. Physiol.*, vol. 297, no. 5, pp. 1956–1963, 2009, doi: 10.1152/ajpheart.00155.2009.

[124] K. Takazawa, H. Kobayashi, N. Shindo, N. Tanaka, and A. Yamashina, “Relationship between radial and central aeterial pulse wave and evaluation of central aortic pressure using the radial arterial pulse wave,” *Hypertens. Res.*, vol. 30, no. 3, pp. 219–228, 2007, doi: 10.1291/hypres.30.219.

[125] K. Takazawa *et al.*, "Estimation of central aortic systolic pressure using late systolic inflection of radial artery pulse and its application to vasodilator therapy," *J. Hypertens.*, vol. 30, no. 5, 2012, [Online]. Available: https://journals.lww.com/jhypertension/Fulltext/2012/05000/Estimation_of_central_aortic_systolic_pressure.14.aspx.

[126] S. S. Hickson *et al.*, "The accuracy of central SBP determined from the second systolic peak of the peripheral pressure waveform," *J. Hypertens.*, vol. 27, no. 9, 2009, [Online]. Available: https://journals.lww.com/jhypertension/Fulltext/2009/09000/The_accuracy_of_central_SBP_determined_from_the.10.aspx.

[127] R. Kelly and D. Fitchett, "Noninvasive determination of aortic input impedance and external left ventricular power output: A validation and repeatability study of a new technique," *J. Am. Coll. Cardiol.*, vol. 20, no. 4, pp. 952 LP – 963, Oct. 1992, doi: 10.1016/0735-1097(92)90198-V.

[128] M. J. Burns, J. D. Seed, A. V. Incognito, C. J. Doherty, K. Notay, and P. J. Millar, "Comparison of laboratory and ambulatory measures of central blood pressure and pulse wave reflection: hitting the target or missing the mark?," *J. Am. Soc. Hypertens.*, vol. 12, no. 4, pp. 275–284, Apr. 2018, doi: 10.1016/j.jash.2018.01.014.

[129] P. Salvi, G. Lio, C. Labat, E. Ricci, B. Pannier, and A. Benetos, "Validation of a new non-invasive portable tonometer for determining arterial pressure wave and pulse wave velocity: the PulsePen device," *J. Hypertens.*, vol. 22, no. 12, 2004, [Online]. Available: https://journals.lww.com/jhypertension/Fulltext/2004/12000/Validation_of_a_new_non_invasive_portable.10.aspx.

[130] Y. Yao, L. Wang, L. Hao, L. Xu, S. Zhou, and W. Liu, "The Noninvasive Measurement of Central Aortic Blood Pressure Waveform," in *Blood Pressure - From Bench to Bed*, InTech, 2018.

[131] A. L. Pauca, M. F. O'Rourke, and N. D. Kon, "Prospective evaluation of a method for estimating ascending aortic pressure from the radial artery pressure

waveform," *Hypertension*, vol. 38, no. 4, pp. 932–937, 2001, doi: 10.1161/hy1001.096106.

[132] G. Pucci *et al.*, "Evaluation of the Vicorder, a novel cuff-based device for the noninvasive estimation of central blood pressure," *J. Hypertens.*, vol. 31, no. 1, pp. 77–85, Jan. 2013, doi: 10.1097/HJH.0b013e32835a8eb1.

[133] H. Smulyan, D. S. Siddiqui, R. J. Carlson, G. M. London, and M. E. Safar, "Clinical utility of aortic pulses and pressures calculated from applanated radial-artery pulses," *Hypertension*, vol. 42, no. 2, pp. 150–155, 2003, doi: 10.1161/01.HYP.0000084051.34269.A9.

[134] E. Laugesen *et al.*, "Assessment of central blood pressure in patients with type 2 diabetes: A comparison between sphygmocor and invasively measured values," *Am. J. Hypertens.*, vol. 27, no. 2, pp. 169–176, 2014, doi: 10.1093/ajh/hpt195.

[135] J. E. Sharman *et al.*, "Validation of a generalized transfer function to noninvasively derive central blood pressure during exercise," *Hypertension*, vol. 47, no. 6, pp. 1203–1208, 2006, doi: 10.1161/01.HYP.0000223013.60612.72.

[136] G. Pucci *et al.*, "VALIDATION OF VICORDER & SPHYGMOCOR WITH INVASIVE BLOOD PRESSURE: PP.10.395," *J. Hypertens.*, vol. 28, 2010, [Online]. Available: https://journals.lww.com/jhypertension/Fulltext/2010/06001/VALIDATION_OF_VICORDER___SPHYGMOCOR_WITH_INVASIVE.485.aspx.

[137] H. M. Cheng, S. H. Sung, Y. T. Shih, S. Y. Chuang, W. C. Yu, and C. H. Chen, "Measurement accuracy of a stand-alone oscillometric central blood pressure monitor: A validation report for microlife WatchBP office central," *Am. J. Hypertens.*, vol. 26, no. 1, pp. 42–50, 2013, doi: 10.1093/ajh/hps021.

[138] Y. T. Shih, H. M. Cheng, S. H. Sung, W. C. Hu, and C. H. Chen, "Quantification of the calibration error in the transfer function-derived central aortic blood pressures," *Am. J. Hypertens.*, vol. 24, no. 12, pp. 1312–1317, 2011, doi: 10.1038/ajh.2011.146.

[139] H. Nakano *et al.*, "Self-monitoring of ambulatory blood pressure by the

Microlife WatchBP O3--an application test.," *Clin. Exp. Hypertens.*, vol. 33, no. 1, pp. 34–40, 2011, doi: 10.3109/10641963.2010.503300.

[140] W. Zuo, P. Wang, and D. Zhang, "Comparison of three different types of wrist pulse signals by their physical meanings and diagnosis performance," *IEEE J. Biomed. Heal. Informatics*, vol. 20, no. 1, pp. 119–127, 2016, doi: 10.1109/JBHI.2014.2369821.

[141] M. Sharmila Begum, R. Duraiarasan, and P. J. Dhivaakar, "Diagnosing diseases through pulse using pressure sensor," *Proc. - 2012 Int. Conf. Data Sci. Eng. ICDSE 2012*, no. July 2012, pp. 140–143, 2012, doi: 10.1109/ICDSE.2012.6281895.

[142] M. Gst, "On- Chip Temperature Compensated & Calibrated Silicon Pressure Sensors," 2004.

[143] S. Thakkar, "Wrist Pulse Acquisition and Recording System," *Commun. Appl. Electron.*, vol. 1, no. 6, pp. 20–24, 2015.

[144] G. Schwartz *et al.*, "Flexible polymer transistors with high pressure sensitivity for application in electronic skin and health monitoring," *Nat. Commun.*, vol. 4, no. 1, p. 1859, Oct. 2013, doi: 10.1038/ncomms2832.

[145] "BPro 24 hour Smart Watch ABPM Blood Pressure Monitor, MedTach Canada," *MedTach*, 2019. https://www.medtach.com/bpro.html (accessed Dec. 29, 2019).

[146] C. M. Ting and N. H. Chua, "Method and device for monitoring blood pressure," 2002.

[147] H. Demirezen and C. E. Erdem, "An overview of non-contact photoplethysmography," pp. 1–4, 2017, doi: 10.1109/siu.2017.7960176.

[148] C. Fischer, B. Domer, T. Wibmer, and T. Penzel, "An Algorithm for Real-Time Pulse Waveform Segmentation and Artifact Detection in Photoplethysmograms," *IEEE J. Biomed. Heal. Informatics*, vol. 21, no. 2, pp. 372–381, 2017, doi: 10.1109/JBHI.2016.2518202.

[149] P. H. Lai and I. Kim, "Lightweight wrist photoplethysmography for heavy

exercise: Motion robust heart rate monitoring algorithm," *Healthc. Technol. Lett.*, vol. 2, no. 1, pp. 6–11, 2015, doi: 10.1049/htl.2014.0097.

[150] J. Spigulis, L. Gailite, A. Lihachev, and R. Erts, "Simultaneous recording of skin blood pulsations at different vascular depths by multiwavelength photoplethysmography," *Appl. Opt.*, vol. 46, no. 10, p. 1754, Apr. 2007, doi: 10.1364/AO.46.001754.

[151] C. Wang *et al.*, "Monitoring of the central blood pressure waveform via a conformal ultrasonic device," *Nat. Biomed. Eng.*, vol. 2, no. 9, pp. 687–695, 2018, doi: 10.1038/s41551-018-0287-x.

[152] D. W. Holdsworth, C. J. D. Norley, R. Frayne, D. A. Steinman, and B. K. Rutt, "Characterization of common carotid artery blood-flow waveforms in normal human subjects," *Physiol. Meas.*, vol. 20, no. 3, pp. 219–240, Aug. 1999, doi: 10.1088/0967-3334/20/3/301.

[153] I. Moxham, "Physics of Invasive Blood Pressure Monitoring," *South. African J. Anaesth. Analg.*, vol. 9, no. 1, pp. 33–38, 2003, doi: 10.1080/22201173.2003.10872990.

[154] L. Jonveaux, "Arduino-Like Development Kit for Single-Element Ultrasound Imaging," *J. Open Hardw.*, vol. 1, no. 1, 2017, doi: 10.5334/joh.2.

[155] C. U. Choi *et al.*, "Differing effects of aging on central and peripheral blood pressures and pulse wave velocity: a direct intraarterial study.," *J. Hypertens.*, vol. 28, no. 6, pp. 1252–1260, Jun. 2010, doi: 10.1097/HJH.0b013e328337dad6.

[156] E. J. KROEKER and E. H. WOOD, "Comparison of simultaneously recorded central and peripheral arterial pressure pulses during rest, exercise and tilted position in man," *Circ. Res.*, vol. 3, no. 6, pp. 623–632, 1955, doi: 10.1161/01.RES.3.6.623.

[157] A. L. Pauca, S. L. Wallenhaupt, N. D. Kon, and W. Y. Tucker, "Does radial artery pressure accurately reflect aortic pressure?," *Chest*, vol. 102, no. 4, pp. 1193–1198, Oct. 1992, doi: 10.1378/chest.102.4.1193.

[158] A. P. Avolio *et al.*, "Role of pulse pressure amplification in arterial hypertension: experts' opinion and review of the data.," *Hypertens. (Dallas, Tex. 1979)*, vol. 54, no. 2, pp. 375–383, Aug. 2009, doi: 10.1161/HYPERTENSIONAHA.109.134379.

[159] S. Theilade, T. W. Hansen, and P. Rossing, "Central hemodynamics are associated with cardiovascular disease and albuminuria in type 1 diabetes," *Am. J. Hypertens.*, vol. 27, no. 9, pp. 1152–1159, 2014, doi: 10.1093/ajh/hpu030.

[160] R. Pini *et al.*, "Central But Not Brachial Blood Pressure Predicts Cardiovascular Events in an Unselected Geriatric Population. The ICARe Dicomano Study," *J. Am. Coll. Cardiol.*, vol. 51, no. 25, pp. 2432–2439, 2008, doi: 10.1016/j.jacc.2008.03.031.

[161] K. Wang, H. Cheng, S. Chuang, and H. A. Spurgeon, "Central or Peripheral Systolic or Pulse Pressure : Which Best Relates To Target-Organs and Future," *J Hypertens*, vol. 27, no. 201, pp. 461–467, 2011.

[162] P. Jankowski *et al.*, "Pulsatile but Not Steady Component of Blood Pressure Predicts Cardiovascular Events in Coronary Patients," *Hypertension*, vol. 51, no. 4, pp. 848–855, Apr. 2008, doi: 10.1161/HYPERTENSIONAHA.107.101725.

[163] A. Benetos *et al.*, "Mortality and cardiovascular events are best predicted by low central/peripheral pulse pressure amplification but not by high blood pressure levels in elderly nursing home subjects: The PARTAGE (Predictive Values of Blood Pressure and Arterial Stiffness i," *J. Am. Coll. Cardiol.*, vol. 60, no. 16, pp. 1503–1511, 2012, doi: 10.1016/j.jacc.2012.04.055.

[164] A. Kollias, S. Lagou, M. E. Zeniodi, N. Boubouchairopoulou, and G. S. Stergiou, "Association of Central Versus Brachial Blood Pressure With Target-Organ Damage: Systematic Review and Meta-Analysis," *Hypertension*, vol. 67, no. 1, pp. 183–190, 2016, doi: 10.1161/HYPERTENSIONAHA.115.06066.

[165] C. Vlachopoulos, K. Aznaouridis, M. F. O'Rourke, M. E. Safar, K. Baou, and C. Stefanadis, "Prediction of cardiovascular events and all-cause mortality with central haemodynamics: a systematic review and meta-analysis," *Eur. Heart J.*,

vol. 31, no. 15, pp. 1865–1871, Aug. 2010, doi: 10.1093/eurheartj/ehq024.

[166] B. Williams *et al.*, "Differential impact of blood pressure-lowering drugs on central aortic pressure and clinical outcomes: Principal results of the Conduit Artery Function Evaluation (CAFE) study," *Circulation*, vol. 113, no. 9, pp. 1213–1225, 2006, doi: 10.1161/CIRCULATIONAHA.105.595496.

[167] T. Papaioannou, A. Protogerou, K. Stamatelopoulos, M. Vavuranakis, and C. Stefanadis, "Non-Invasive Methods and Techniques for Central Blood Pressure Estimation: Procedures, Validation, Reproducibility and Limitations," *Curr. Pharm. Des.*, vol. 15, no. 3, pp. 245–253, 2009, doi: 10.2174/138161209787354203.

[168] B. Fetics, E. Nevo, Chen-Huan Chen, and D. A. Kass, "Parametric model derivation of transfer function for noninvasive estimation of aortic pressure by radial tonometry," *IEEE Trans. Biomed. Eng.*, vol. 46, no. 6, pp. 698–706, Jun. 1999, doi: 10.1109/10.764946.

[169] S. A. Hope, I. T. Meredith, D. Tay, and J. D. Cameron, ???"Generalizability??? of a radial-aortic transfer function for the derivation of central aortic waveform parameters," *J. Hypertens.*, vol. 25, no. 9, pp. 1812–1820, Sep. 2007, doi: 10.1097/HJH.0b013e328277595d.

[170] S. A. Hope, I. T. Meredith, and J. D. Cameron, "Arterial transfer functions and the reconstruction of central aortic waveforms: myths, controversies and misconceptions," *J. Hypertens.*, vol. 26, no. 1, pp. 4–7, Jan. 2008, doi: 10.1097/HJH.0b013e3282f0c9f5.

[171] M. F. O'Rourke, "Mechanical principles. Arterial stiffness and wave reflection," *Pathol. Biol. (Paris).*, vol. 47, no. 6, p. 623—633, Jun. 1999, [Online]. Available: http://europepmc.org/abstract/MED/10472073.

[172] K. C. Peebles, I. Tan, M. T. D. Cook, D. A. Theobald, A. P. Avolio, and M. Butlin, "Interarm Differences in Brachial Blood Pressure and their Effect on the Derivation on Central Aortic Blood Pressure," *Artery Res.*, 2020, doi: 10.2991/artres.k.200201.002.

[173] A. T. Butt, Y. A. Abakr, and K. B. Mustapha, "Blood Flow Modeling to Improve Cardiovascular Diagnostics: Application of A GTF to Predict Central Aortic Pressure using a 1-D Model," *Int. J. Eng. Technol.*, vol. 7, no. 4.26, p. 146, Nov. 2018, doi: 10.14419/ijet.v7i4.26.22156.

[174] T. G. Papaioannou *et al.*, "Transmission of calibration errors (input) by generalized transfer functions to the aortic pressures (output) at different hemodynamic states," *Int. J. Cardiol.*, vol. 110, no. 1, pp. 46–52, Jun. 2006, doi: 10.1016/j.ijcard.2005.07.014.

[175] S. So¨derstro¨m, G. Nyberg, M. F. O'Rourke, J. Sellgren, and J. Pontén, "Can a clinically useful aortic pressure wave be derived from a radial pressure wave? † †Declaration of interest. Professor M. F. O'Rourke is a Director of PWV Medical, Sydney. PWV Medical provided funds and facilities for analysis of the data, and markets," *Br. J. Anaesth.*, vol. 88, no. 4, pp. 481–488, Apr. 2002, doi: 10.1093/bja/88.4.481.

[176] D. Gallagher, A. Adji, and M. F. O'Rourke, "Validation of the transfer function technique for generating central from peripheral upper limb pressure waveform," *Am. J. Hypertens.*, vol. 17, no. 11, pp. 1059–1067, 2004, doi: 10.1016/j.amjhyper.2004.05.027.

[177] G. C. Cloud, C. Rajkumar, J. Kooner, J. Cooke, and C. J. Bulpitt, "Estimation of central aortic pressure by SphygmoCor requires intra-arterial peripheral pressures.," *Clin. Sci. (Lond).*, vol. 105, no. 2, pp. 219–225, Aug. 2003, doi: 10.1042/CS20030012.

[178] T. E. Strandberg and K. Pitkala, "What is the most important component of blood pressure: systolic, diastolic or pulse pressure?," *Curr. Opin. Nephrol. Hypertens.*, vol. 12, no. 3, pp. 293–297, May 2003, doi: 10.1097/00041552-200305000-00011.

[179] M. Gao, W. C. Rose, B. Fetics, D. A. Kass, C. H. Chen, and R. Mukkamala, "A Simple Adaptive Transfer Function for Deriving the Central Blood Pressure Waveform from a Radial Blood Pressure Waveform," *Sci. Rep.*, vol. 6, no. August, pp. 1–9, 2016, doi: 10.1038/srep33230.

[180] Y. Yao *et al.*, "Validation of an Adaptive Transfer Function Method to Estimate the Aortic Pressure Waveform," *IEEE J. Biomed. Heal. Informatics*, vol. 21, no. 6, pp. 1599–1606, 2017, doi: 10.1109/JBHI.2016.2636223.

[181] G. Swamy, D. Xu, N. B. Olivier, and R. Mukkamala, "An adaptive transfer function for deriving the aortic pressure waveform from a peripheral artery pressure waveform," *Am. J. Physiol. - Hear. Circ. Physiol.*, vol. 297, no. 5, pp. 1956–1963, 2009, doi: 10.1152/ajpheart.00155.2009.

[182] A. L. Pauca, N. D. Kon, and M. F. O'Rourke, "The second peak of the radial artery pressure wave represents aortic systolic pressure in hypertensive and elderly patients," *Br. J. Anaesth.*, vol. 92, no. 5, pp. 651–657, May 2004, doi: 10.1093/bja/aeh121.

[183] A. Guilcher, S. Brett, S. Munir, B. Clapp, and P. J. Chowienczyk, "Estimating central SBP from the peripheral pulse: influence of waveform analysis and calibration error," *J. Hypertens.*, vol. 29, no. 7, pp. 1357–1366, Jul. 2011, doi: 10.1097/HJH.0b013e3283479070.

[184] W. B. Kannel, D. McGee, and T. Gordon, "A general cardiovascular risk profile: The Framingham study," *Am. J. Cardiol.*, vol. 38, no. 1, pp. 46–51, Jul. 1976, doi: 10.1016/0002-9149(76)90061-8.

[185] A. Menotti, P. E. Puddu, and M. Lanti, "Comparison of the Framingham risk function-based coronary chart with risk function from an Italian population study," *Eur. Heart J.*, vol. 21, no. 5, pp. 365–370, 2000, doi: 10.1053/euhj.1999.1864.

[186] R. M. Conroy *et al.*, "Estimation of ten-year risk of fatal cardiovascular disease in Europe: The SCORE project," *Eur. Heart J.*, vol. 24, no. 11, pp. 987–1003, 2003, doi: 10.1016/S0195-668X(03)00114-3.

[187] D. B. Panagiotakos, A. P. Fitzgerald, C. Pitsavos, A. Pipilis, I. Graham, and C. Stefanadis, "Statistical modelling of 10-year fatal cardiovascular disease risk in Greece: The HellenicSCORE (a calibration of the ESC SCORE project)," *Hell. J. Cardiol.*, vol. 48, no. 2, pp. 55–63, 2007.

[188] A. C. Dimopoulos *et al.*, "Machine learning methodologies versus cardiovascular risk scores, in predicting disease risk," *BMC Med. Res. Methodol.*, vol. 18, no. 1, pp. 1–11, 2018, doi: 10.1186/s12874-018-0644-1.

[189] D. Panagiotakos, "Health Measurement Scales: Methodological Issues," *Open Cardiovasc. Med. J.*, vol. 3, no. 1, pp. 160–165, 2009, doi: 10.2174/1874192400903010160.

[190] A. D. Jamthikar *et al.*, "Artificial intelligence framework for predictive cardiovascular and stroke risk assessment models : A narrative review of integrated approaches using carotid ultrasound," *Comput. Biol. Med.*, vol. 126, no. September, p. 104043, 2020, doi: 10.1016/j.compbiomed.2020.104043.

[191] W. A. Davis, S. Colagiuri, and T. M. E. Davis, "Comparison of the Framingham and United Kingdom Prospective Diabetes Study cardiovascular risk equations in Australian patients with type 2 diabetes from the Fremantle Diabetes Study," *Med. J. Aust.*, vol. 191, no. 1, pp. 47–48, Jul. 2009, doi: 10.5694/j.1326-5377.2009.tb02684.x.

[192] H. R. Ahn *et al.*, "Comparison of the framingham risk score, UKPDS risk engine, and SCORE for predicting carotid atherosclerosis and peripheral arterial disease in Korean type 2 diabetic patients," *Korean J. Fam. Med.*, vol. 32, no. 3, pp. 189–196, 2011, doi: 10.4082/kjfm.2011.32.3.189.

[193] N. R. Cook *et al.*, "Comparison of the framingham and reynolds risk scores for global cardiovascular risk prediction in the multiethnic women's health initiative," *Circulation*, vol. 125, no. 14, pp. 1748–1756, 2012, doi: 10.1161/CIRCULATIONAHA.111.075929.

[194] T. P. Van Staa, M. Gulliford, E. S. W. Ng, B. Goldacre, and L. Smeeth, "Prediction of cardiovascular risk using framingham, ASSIGN and QRISK2: How well do they predict individual rather than population risk?," *PLoS One*, vol. 9, no. 10, 2014, doi: 10.1371/journal.pone.0106455.

[195] S. Selvarajah *et al.*, "Comparison of the Framingham Risk Score, SCORE and WHO/ISH cardiovascular risk prediction models in an Asian population," *Int. J.*

Cardiol., vol. 176, no. 1, pp. 211–218, 2014, doi: 10.1016/j.ijcard.2014.07.066.

[196] D. Bansal, R. S. R. Nayakallu, K. Gudala, R. Vyamasuni, and A. Bhansali, "Agreement between framingham risk score and united kingdom prospective diabetes study risk engine in identifying high coronary heart disease risk in North Indian population," *Diabetes Metab. J.*, vol. 39, no. 4, pp. 321–327, 2015, doi: 10.4093/dmj.2015.39.4.321.

[197] N. Garg *et al.*, "Comparison of different cardiovascular risk score calculators for cardiovascular risk prediction and guideline recommended statin uses," *Indian Heart J.*, vol. 69, no. 4, pp. 458–463, 2017, doi: 10.1016/j.ihj.2017.01.015.

[198] L. Albarqouni, J. A. Doust, D. Magliano, and J. E. Shaw, "External validation and comparison of four cardiovascular risk prediction models with data from the Australian Diabetes, Obesity and Lifestyle study," pp. 161–167, doi: 10.5694/mja2.12061.

[199] M. T. Cooney, H. C. Cooney, A. Dudina, and I. M. Graham, "Total cardiovascular disease risk assessment," *Curr. Opin. Cardiol.*, vol. 26, no. 5, pp. 429–437, Sep. 2011, doi: 10.1097/HCO.0b013e3283499f06.

[200] I. M. Graham, M.-T. Cooney, A. Dudina, and S. Squarta, "What is my risk of developing cardiovascular disease?," *Eur. J. Cardiovasc. Prev. Rehabil.*, vol. 16, no. 2_suppl, pp. S2–S7, Aug. 2009, doi: 10.1097/01.hjr.0000359226.50399.59.

[201] R. B. D'Agostino, S. Grundy, L. M. Sullivan, and P. Wilson, "Validation of the Framingham Coronary Heart Disease Prediction Scores," *Jama*, vol. 286, no. 2, p. 180, 2001, doi: 10.1001/jama.286.2.180.

[202] E. N. Georgousopoulou, C. Pitsavos, C. M. Yannakoulia, and D. B. Panagiotakos, "Comparisons between Survival Models in Predicting Cardiovascular Disease Events: Application in the ATTICA Study (2002-2012)," *J. Stat. Appl. Probab. An Int. J.*, vol. 4, no. 2, p. 203, 2015, [Online]. Available: http://dx.doi.org/10.12785/jsap/040202.

[203] K.-H. Yu, A. L. Beam, and I. S. Kohane, "Artificial intelligence in healthcare," *Nat. Biomed. Eng.*, vol. 2, no. 10, pp. 719–731, Oct. 2018, doi: 10.1038/s41551-

018-0305-z.

[204] M. Biswas *et al.*, “Symtosis: A liver ultrasound tissue characterization and risk stratification in optimized deep learning paradigm,” *Comput. Methods Programs Biomed.*, vol. 155, pp. 165–177, Mar. 2018, doi: 10.1016/j.cmpb.2017.12.016.

[205] L. Saba *et al.*, “Ultrasound-based carotid stenosis measurement and risk stratification in diabetic cohort : a deep learning paradigm,” vol. 9, no. 1, pp. 439–461, 2019, doi: 10.21037/cdt.2019.09.01.

[206] M. Biswas *et al.*, “Deep learning fully convolution network for lumen characterization in diabetic patients using carotid ultrasound: a tool for stroke risk,” *Med. Biol. Eng. Comput.*, vol. 57, no. 2, pp. 543–564, Feb. 2019, doi: 10.1007/s11517-018-1897-x.

[207] A. Jamthikar *et al.*, “A Special Report on Changing Trends in Preventive Stroke/Cardiovascular Risk Assessment Via B-Mode Ultrasonography,” *Curr. Atheroscler. Rep.*, vol. 21, no. 7, p. 25, Jul. 2019, doi: 10.1007/s11883-019-0788-4.

[208] I. Kononenko, “Machine learning for medical diagnosis: History, state of the art and perspective,” *Artif. Intell. Med.*, vol. 23, no. 1, pp. 89–109, 2001, doi: 10.1016/S0933-3657(01)00077-X.

[209] I. Yoo *et al.*, “Data mining in healthcare and biomedicine: A survey of the literature,” *J. Med. Syst.*, vol. 36, no. 4, pp. 2431–2448, 2012, doi: 10.1007/s10916-011-9710-5.

[210] K. Kourou, T. P. Exarchos, K. P. Exarchos, M. V. Karamouzis, and D. I. Fotiadis, “Machine learning applications in cancer prognosis and prediction,” *Comput. Struct. Biotechnol. J.*, vol. 13, pp. 8–17, 2015, doi: 10.1016/j.csbj.2014.11.005.

[211] S. Wang and R. M. Summers, “Machine learning and radiology,” *Med. Image Anal.*, vol. 16, no. 5, pp. 933–951, 2012, doi: 10.1016/j.media.2012.02.005.

[212] F. Fabris, J. P. de Magalhães, and A. A. Freitas, “A review of supervised machine

learning applied to ageing research," *Biogerontology*, vol. 18, no. 2, pp. 171–188, 2017, doi: 10.1007/s10522-017-9683-y.

[213] S. F. Weng, J. Reps, J. Kai, J. M. Garibaldi, and N. Qureshi, "Can Machine-learning improve cardiovascular risk prediction using routine clinical data?," *PLoS One*, vol. 12, no. 4, pp. 1–14, 2017, doi: 10.1371/journal.pone.0174944.

[214] H. Liu, "Book review: Machine Learning, Neural and Statistical Classification Edited by D. Michie, D.J. Spiegelhalter and C.C. Taylor (Ellis Horwood Limited, 1994)," *ACM SIGART Bull.*, vol. 7, no. 1, pp. 16–17, Jan. 1996, doi: 10.1145/230062.1066049.

[215] A. S. Miller, B. H. Blott, and T. K. Hames, "Review of neural network applications in medical imaging and signal processing," *Med. Biol. Eng. Comput.*, vol. 30, no. 5, pp. 449–464, Sep. 1992, doi: 10.1007/BF02457822.

[216] C. M. Shufflebarger, "What is neutral network?," *Ann. Emerg. Med.*, vol. 21, no. 12, pp. 1461–1462, Dec. 1992, doi: 10.1016/S0196-0644(05)80060-5.

[217] D. E. Rumelhart, G. E. Hinton, and R. J. Williams, "Learning Internal Representations by Error Propagation," in *Parallel Distributed Processing: Explorations in the Microstructure of Cognition, Vol. 1: Foundations*, Cambridge, MA, USA: MIT Press, 1986, pp. 318–362.

[218] D. E. Rumelhart, G. E. Hinton, and R. J. Williams, "Learning representations by back-propagating errors," *Nature*, vol. 323, no. 6088, pp. 533–536, Oct. 1986, doi: 10.1038/323533a0.

[219] D. Itchhaporia, P. B. Snow, R. J. Almassy, and W. J. Oetgen, "Artificial neural networks: Current status in cardiovascular medicine," *J. Am. Coll. Cardiol.*, vol. 28, no. 2, pp. 515–521, 1996, doi: 10.1016/S0735-1097(96)00174-X.

[220] J. A. Scott and E. L. Palmer, "Neural network analysis of ventilation-perfusion lung scans.," *Radiology*, vol. 186, no. 3, pp. 661–664, Mar. 1993, doi: 10.1148/radiology.186.3.8430170.

[221] P. W. Macfarlane, B. Devine, S. Latif, S. McLaughlin, D. B. Shoat, and M. P.

Watts, “Methodology of ECG interpretation in the Glasgow program.,” *Methods Inf. Med.*, vol. 29, no. 4, pp. 354–361, Sep. 1990.

[222] P. W. Macfarlane, “A Brief History of Computer-Assisted Electrocardiography,” *Methods Inf. Med.*, vol. 29, no. 04, pp. 272–281, Feb. 1990, doi: 10.1055/s-0038-1634791.

[223] G. Bortolan, R. Degani, and J. L. Willems, “Design Of Neural Networks For Classification Of Electrocardiographic Signals,” in *[1990] Proceedings of the Twelfth Annual International Conference of the IEEE Engineering in Medicine and Biology Society*, pp. 1467–1468, doi: 10.1109/IEMBS.1990.691842.

[224] L. EDENBRANDT, B. DEVINE, and P. W. MACFARLANE, “Classification of electrocardiographic ST-T segments -- human expert vs artificial neural network,” *Eur. Heart J.*, vol. 14, no. 4, pp. 464–468, Apr. 1993, doi: 10.1093/eurheartj/14.4.464.

[225] B. Hedén, L. Edenbrandt, W. K. Haisty, and O. Pahlm, “Artificial neural networks for the electrocardiographic diagnosis of healed myocardial infarction,” *Am. J. Cardiol.*, vol. 74, no. 1, pp. 5–8, Jul. 1994, doi: 10.1016/0002-9149(94)90482-0.

[226] W. R. M. DASSEN *et al.*, “An Artificial Neural Network to Localize Atrioventricular Accessory Pathways in Patients Suffering from the Wolff-Parkinson-White Syndrome,” *Pacing Clin. Electrophysiol.*, vol. 13, no. 12, pp. 1792–1796, Dec. 1990, doi: 10.1111/j.1540-8159.1990.tb06892.x.

[227] K. Kario *et al.*, “Development of a New ICT-Based Multisensor Blood Pressure Monitoring System for Use in Hemodynamic Biomarker-Initiated Anticipation Medicine for Cardiovascular Disease: The National IMPACT Program Project,” *Prog. Cardiovasc. Dis.*, vol. 60, no. 3, pp. 435–449, 2017, doi: 10.1016/j.pcad.2017.10.002.

[228] Z. Shen, R. W. Jones, and T. Alberti, “Detecting the risk factors of coronary heart disease by use of neural networks,” *Proc. Annu. Conf. Eng. Med. Biol.*, vol. 15, no. pt 1, pp. 277–278, 1993, doi: 10.1109/iembs.1993.978541.

[229] S. U. Amin, K. Agarwal, and R. Beg, "Genetic neural network based data mining in prediction of heart disease using risk factors," *2013 IEEE Conf. Inf. Commun. Technol. ICT 2013*, no. February, pp. 1227–1231, 2013, doi: 10.1109/CICT.2013.6558288.

[230] J. S. Sonawane and D. R. Patil, "Prediction of heart disease using learning vector quantization algorithm," *Proc. 2014 Conf. IT Business, Ind. Gov. An Int. Conf. by CSI Big Data, CSIBIG 2014*, pp. 0–4, 2014, doi: 10.1109/CSIBIG.2014.7056973.

[231] S. Bashir, U. Qamar, and M. Y. Javed, "An ensemble based decision support framework for intelligent heart disease diagnosis," *Int. Conf. Inf. Soc. i-Society 2014*, no. January 2015, pp. 259–264, 2015, doi: 10.1109/i-Society.2014.7009056.

[232] M. G. Feshki and O. S. Shijani, "Improving the heart disease diagnosis by evolutionary algorithm of PSO and Feed Forward Neural Network," *2016 Artif. Intell. Robot. IRANOPEN 2016*, pp. 48–53, 2016, doi: 10.1109/RIOS.2016.7529489.

[233] S. Carbone, J. M. Canada, H. E. Billingsley, M. S. Siddiqui, A. Elagizi, and C. J. Lavie, "Obesity paradox in cardiovascular disease: Where do we stand?," *Vasc. Health Risk Manag.*, vol. 15, pp. 89–100, 2019, doi: 10.2147/VHRM.S168946.

[234] S. Carbone, C. J. Lavie, and R. Arena, "Obesity and Heart Failure: Focus on the Obesity Paradox," *Mayo Clin. Proc.*, vol. 92, no. 2, pp. 266–279, 2017, doi: 10.1016/j.mayocp.2016.11.001.

[235] A. Elagizi *et al.*, "An Overview and Update on Obesity and the Obesity Paradox in Cardiovascular Diseases," *Prog. Cardiovasc. Dis.*, vol. 61, no. 2, pp. 142–150, 2018, doi: 10.1016/j.pcad.2018.07.003.

[236] C. J. Lavie *et al.*, "Obesity and Prevalence of Cardiovascular Diseases and Prognosis-The Obesity Paradox Updated," *Prog. Cardiovasc. Dis.*, vol. 58, no. 5, pp. 537–547, 2016, doi: 10.1016/j.pcad.2016.01.008.

[237] R. Stamler, C. E. Ford, and J. Stamler, “Why do lean hypertensives have higher mortality rates than other hypertensives? Findings of the hypertension detection and follow-up program,” *Hypertension*, vol. 17, no. 4, pp. 553–564, 1991, doi: 10.1161/01.HYP.17.4.553.

[238] A. Jayedi and S. Shab-Bidar, “Nonlinear dose–response association between body mass index and risk of all-cause and cardiovascular mortality in patients with hypertension: A meta-analysis,” *Obes. Res. Clin. Pract.*, vol. 12, no. 1, pp. 16–28, 2018, doi: 10.1016/j.orcp.2018.01.002.

[239] A. O. Badheka *et al.*, “Influence of Obesity on Outcomes in Atrial Fibrillation: Yet Another Obesity Paradox,” *Am. J. Med.*, vol. 123, no. 7, pp. 646–651, Jul. 2010, doi: 10.1016/j.amjmed.2009.11.026.

[240] R. K. Sandhu *et al.*, “The ‘obesity paradox’ in atrial fibrillation: Observations from the ARISTOTLE (Apixaban for Reduction in Stroke and Other Thromboembolic Events in Atrial Fibrillation) trial,” *Eur. Heart J.*, vol. 37, no. 38, pp. 2869–2878, 2016, doi: 10.1093/eurheartj/ehw124.

[241] M. Agarwal, S. Agrawal, L. Garg, and C. J. Lavie, “Relation Between Obesity and Survival in Patients Hospitalized for Pulmonary Arterial Hypertension (from a Nationwide Inpatient Sample Database 2003 to 2011),” *Am. J. Cardiol.*, vol. 120, no. 3, pp. 489–493, Aug. 2017, doi: 10.1016/j.amjcard.2017.04.051.

[242] M. Brida *et al.*, “Body mass index in adult congenital heart disease,” *Heart*, vol. 103, no. 16, pp. 1250–1257, Aug. 2017, doi: 10.1136/heartjnl-2016-310571.

[243] M. H. Olsen *et al.*, “A call to action and a lifecourse strategy to address the global burden of raised blood pressure on current and future generations: the Lancet Commission on hypertension,” *Lancet*, vol. 388, no. 10060, pp. 2665–2712, Nov. 2016, doi: 10.1016/S0140-6736(16)31134-5.

[244] W. W. Nichols, M. F. O’Rourke, and D. A. McDonald, *McDonald’s blood flow in arteries : theoretical, experimental, and clinical principles*. London; New York: Hodder Arnold ; Distributed in the U.S.A. by Oxford University Press, 2005.

[245] N. WESTERHOF, P. SIPKEMA, G. C. V. D. BOS, and G. ELZINGA, "Forward and backward waves in the arterial system," *Cardiovasc. Res.*, vol. 6, no. 6, pp. 648–656, Nov. 1972, doi: 10.1093/cvr/6.6.648.

[246] J. C. Kovacic, N. Mercader, M. Torres, M. Boehm, and V. Fuster, "Epithelial-to-Mesenchymal and Endothelial-to-Mesenchymal Transition," *Circulation*, vol. 125, no. 14, pp. 1795–1808, Apr. 2012, doi: 10.1161/CIRCULATIONAHA.111.040352.

[247] H. Eom *et al.*, "End-to-end deep learning architecture for continuous blood pressure estimation using attention mechanism," *Sensors (Switzerland)*, vol. 20, no. 8, pp. 1–20, 2020, doi: 10.3390/s20082338.

[248] Q. Chen *et al.*, "A Survey on an Emerging Area: Deep Learning for Smart City Data," *IEEE Trans. Emerg. Top. Comput. Intell.*, vol. 3, no. 5, pp. 392–410, 2019, doi: 10.1109/TETCI.2019.2907718.

[249] Y. Lecun, Y. Bengio, and G. Hinton, "Deep learning," *Nature*, vol. 521, no. 7553, pp. 436–444, 2015, doi: 10.1038/nature14539.

[250] A. Graves, A. Mohamed, and G. Hinton, "SPEECH RECOGNITION WITH DEEP RECURRENT NEURAL NETWORKS Alex Graves, Abdel-rahman Mohamed and Geoffrey Hinton Department of Computer Science, University of Toronto," no. 3.

[251] K. Greff, R. K. Srivastava, J. Koutnik, B. R. Steunebrink, and J. Schmidhuber, "LSTM: A Search Space Odyssey," *IEEE Trans. Neural Networks Learn. Syst.*, vol. 28, no. 10, pp. 2222–2232, 2017, doi: 10.1109/TNNLS.2016.2582924.

[252] M. Zubair and J. Kim, "An Automated ECG Beat Classification System Using Convolutional Neural Networks," 2016.

[253] D. Li, J. Zhang, Q. Zhang, and X. Wei, "Classification of ECG Signals Based on 1D Convolution Neural Network," pp. 2–7, 2017.

[254] A. Isin and S. Ozdalili, "ScienceDirect ScienceDirect Cardiac arrhythmia detection using deep learning," *Procedia Comput. Sci.*, vol. 120, pp. 268–275,

2018, doi: 10.1016/j.procs.2017.11.238.

[255] P. Rajpurkar, A. Y. Hannun, M. Haghpanahi, C. Bourn, and A. Y. Ng, "Cardiologist-level arrhythmia detection with convolutional neural networks," *arXiv*, 2017.

[256] U. R. Acharya, H. Fujita, O. S. Lih, Y. Hagiwara, J. H. Tan, and M. Adam, "Automated Detection of Arrhythmias Using Different Intervals of Tachycardia ECG Segments with Convolutional Neural Network," *Inf. Sci.*, vol. 405, no. C, pp. 81–90, Sep. 2017, doi: 10.1016/j.ins.2017.04.012.

[257] U. R. Acharya, H. Fujita, S. Lih, Y. Hagiwara, J. Hong, and M. Adam, "Application of deep convolutional neural network for automated detection of myocardial infarction using ECG signals," *Inf. Sci. (Ny).*, vol. 415–416, pp. 190–198, 2017, doi: 10.1016/j.ins.2017.06.027.

[258] U. R. Acharya, H. Fujita, O. Shu, M. Adam, J. Hong, and C. Kuang, "Knowle dge-Base d Systems Automated detection of coronary artery disease using different durations of ECG segments with convolutional neural network," *Knowledge-Based Syst.*, vol. 132, pp. 62–71, 2017, doi: 10.1016/j.knosys.2017.06.003.

[259] Z. Yao, Z. Zhu, and Y. Chen, "Atrial Fibrillation Detection by Multi-scale Convolutional Neural Networks," 2017.

[260] L. Jin and J. Dong, "Classification of normal and abnormal ECG records using lead convolutional neural network and rule inference," vol. 60, no. July, pp. 6–8, 2017, doi: 10.1007/s11432-016-9047-6.

[261] M. Wu, E. J. Chang, and T. Chu, "Personalizing a Generic ECG Heartbeat Classification for Arrhythmia Detection : A Deep Learning Approach," 2018, doi: 10.1109/MIPR.2018.00024.

[262] Y. Xia, N. Wulan, K. Wang, and H. Zhang, "Detecting atrial fi brillation by deep convolutional neural networks," *Comput. Biol. Med.*, vol. 93, no. July 2017, pp. 84–92, 2018, doi: 10.1016/j.compbiomed.2017.12.007.

[263] U. R. Acharya *et al.*, “Deep convolutional neural network for the automated diagnosis of congestive heart failure using ECG signals,” pp. 16–27, 2019.

[264] R. Xiao *et al.*, “Monitoring signi fi cant ST changes through deep learning,” *J. Electrocardiol.*, vol. 51, no. 6, pp. S78–S82, 2018, doi: 10.1016/j.jelectrocard.2018.07.026.

[265] W. Zhong, L. Liao, X. Guo, and G. Wang, “A deep learning approach for fetal QRS complex detection.,” *Physiol. Meas.*, vol. 39, no. 4, p. 45004, Apr. 2018, doi: 10.1088/1361-6579/aab297.

[266] Q. Yao, R. Wang, X. Fan, J. Liu, and Y. Li, “Multi-class Arrhythmia detection from 12-lead varied-length ECG using Attention-based Time-Incremental Convolutional Neural Network,” vol. 53, no. June 2019, pp. 174–182, 2020, doi: 10.1016/j.inffus.2019.06.024.

[267] R. Avanzato and F. Beritelli, “Automatic ECG Diagnosis Using Convolutional Neural Network,” 2020, doi: https://www.mdpi.com/2079-9292/9/6/951.

[268] T. Wang, C. Lu, Y. Sun, M. Yang, C. Liu, and C. Ou, “Automatic ECG Classification Using Continuous Wavelet Transform and Convolutional Neural Network,” pp. 1–13, 2021.

[269] C. Potes, S. Parvaneh, A. Rahman, and B. Conroy, “Ensemble of feature-based and deep learning-based classifiers for detection of abnormal heart sounds,” *Comput. Cardiol. (2010).*, vol. 43, pp. 621–624, 2016, doi: 10.22489/cinc.2016.182-399.

[270] H. Ryu, J. Park, and H. Shin, “Classification of heart sound recordings using convolution neural network,” *Comput. Cardiol. (2010).*, vol. 43, pp. 1153–1156, 2016, doi: 10.22489/cinc.2016.329-134.

[271] J. Rubin, R. Abreu, A. Ganguli, S. Nelaturi, I. Matei, and K. Sricharan, “Classifying heart sound recordings using deep convolutional neural networks and mel-frequency cepstral coefficients,” *Comput. Cardiol. (2010).*, vol. 43, pp. 813–816, 2016, doi: 10.22489/cinc.2016.236-175.

[272] D. Kucharski, D. Grochala, M. Kajor, and E. Kańtoch, “A Deep Learning Approach for Valve Defect Recognition in Heart Acoustic Signal,” 2018, pp. 3–14.

[273] J. P. Dominguez-Morales, A. F. Jimenez-Fernandez, M. J. Dominguez-Morales, and G. Jimenez-Moreno, “Deep Neural Networks for the Recognition and Classification of Heart Murmurs Using Neuromorphic Auditory Sensors,” *IEEE Trans. Biomed. Circuits Syst.*, vol. 12, no. 1, pp. 24–34, 2018, doi: 10.1109/TBCAS.2017.2751545.

[274] X. Hu, H. Zhu, J. Xu, D. Xu, and J. Dong, “Wrist pulse signals analysis based on Deep Convolutional Neural Networks,” *2014 IEEE Conf. Comput. Intell. Bioinforma. Comput. Biol. CIBCB 2014*, 2014, doi: 10.1109/CIBCB.2014.6845525.

[275] Y.-J. Moon *et al.*, “Deep Learning-Based Stroke Volume Estimation Outperforms Conventional Arterial Contour Method in Patients with Hemodynamic Instability,” *J. Clin. Med.*, vol. 8, no. 9, p. 1419, 2019, doi: 10.3390/jcm8091419.

[276] S. Shimazaki, H. Kawanaka, H. Ishikawa, K. Inoue, and K. Oguri, “Cuffless Blood Pressure Estimation from only the Waveform of Photoplethysmography using CNN,” *Proc. Annu. Int. Conf. IEEE Eng. Med. Biol. Soc. EMBS*, pp. 5042–5045, 2019, doi: 10.1109/EMBC.2019.8856706.

[277] E. M. M. Besterman, “William Harvey and his discovery of the circulation of the blood,” *West Indian Med. J.*, vol. 53, no. 6, pp. 425–426, 2004, doi: 10.1002/clc.4960080411.

[278] J. T. Ottesen, “Valveless pumping in a fluid-filled closed elastic tube-system: one-dimensional theory with experimental validation,” *J. Math. Biol.*, vol. 46, no. 4, pp. 309–332, Apr. 2003, doi: 10.1007/s00285-002-0179-1.

[279] and L. F. A. Quarteroni, “Mathematical modelling and numerical simulation of the cardiovascular system,” MOX, Mathematics Department Politecnico di Milano, Italy and Institute of Mathematics EPFL, Lausanne, Switzerland, 2002.

[280] M. A. Fernández, "Coupling schemes for incompressible fluid-structure interaction: implicit, semi-implicit and explicit," *SeMA J.*, vol. 55, no. 1, pp. 59–108, Sep. 2011, doi: 10.1007/BF03322593.

[281] L. Formaggia and A. Veneziani, "Reduced and multiscale models for the human cardiovascular system," *Lect. notes VKI Lect. Ser.*, no. May, p. 120, 2003, doi: 10.13140/RG.2.1.3668.8088.

[282] J. R. Cebral, M. A. Castro, J. E. Burgess, R. S. Pergolizzi, M. J. Sheridan, and C. M. Putman, "Characterization of Cerebral Aneurysms for Assessing Risk of Rupture By Using Patient-Specific Computational Hemodynamics Models," *Am. J. Neuroradiol.*, vol. 26, no. 10, pp. 2550 LP – 2559, Nov. 2005, [Online]. Available: http://www.ajnr.org/content/26/10/2550.abstract.

[283] C. A. Taylor and D. A. Steinman, "Image-Based Modeling of Blood Flow and Vessel Wall Dynamics: Applications, Methods and Future Directions," *Ann. Biomed. Eng.*, vol. 38, no. 3, pp. 1188–1203, Mar. 2010, doi: 10.1007/s10439-010-9901-0.

[284] L. Formaggia, A. Moura, and F. Nobile, "On the stability of the coupling of 3D and 1D fluid-structure interaction models for blood flow simulations," *ESAIM Math. Model. Numer. Anal.*, vol. 41, no. 4, pp. 743–769, Jul. 2007, doi: 10.1051/m2an:2007039.

[285] J. Janela, A. Moura, and A. Sequeira, "Absorbing boundary conditions for a 3D non-Newtonian fluid–structure interaction model for blood flow in arteries," *Int. J. Eng. Sci.*, vol. 48, no. 11, pp. 1332–1349, Nov. 2010, doi: 10.1016/j.ijengsci.2010.08.004.

[286] "Sensitivity of hemodynamics in a patient specific cerebral aneurysm to vascular geometry and blood rheology," *Math. Biosci. Eng.*, vol. 8, no. 2, pp. 409–423, 2011, doi: 10.3934/mbe.2011.8.409.

[287] A. T. Butt, Y. A. Abakr, and K. B. Mustapha, "Blood flow modelling to improve cardiovascular diagnostics: A preliminary review of 1-D modelling," *Int. J. Eng. Technol.*, vol. 7, no. 4, pp. 25–34, 2018, doi: 10.14419/ijet.v7i4.3.19547.

[288] V. C. Rideout, *Mahematical and computer modeling of physiological systems*. 1991.

[289] V. Milišić and A. Quarteroni, "Analysis of lumped parameter models for blood flow simulations and their relation with 1D models," *ESAIM Math. Model. Numer. Anal.*, vol. 38, no. 4, pp. 613–632, Jul. 2004, doi: 10.1051/m2an:2004036.

[290] T. Korakiantitis and Y. Shi., "Model Repository. CellML.," 2006. http://models.cellml.org/exposure/c49d416ae3a5132882e6ea7479ba50f5/ModelMain.cellml/cellml_math (accessed Apr. 29, 2021).

[291] N. Westerhof, F. Bosman, C. J. De Vries, and A. Noordergraaf, "Analog studies of the human systemic arterial tree," *J. Biomech.*, vol. 2, no. 2, pp. 121–143, 1969, doi: 10.1016/0021-9290(69)90024-4.

[292] T. J. R. Hughes and J. Lubliner, "On the one-dimensional theory of blood flow in the larger vessels," *Math. Biosci.*, vol. 18, no. 1–2, pp. 161–170, 1973, doi: 10.1016/0025-5564(73)90027-8.

[293] M. S. Olufsen, C. S. Peskin, W. Y. Kim, E. M. Pedersen, A. Nadim, and J. Larsen, "Numerical simulation and experimental validation of blood flow in arteries with structured-tree outflow conditions," *Ann. Biomed. Eng.*, vol. 28, no. 11, pp. 1281–1299, 2000, doi: 10.1114/1.1326031.

[294] A. S. Olufsen, "Modeling the arterial system with reference to an anesthesia simulator," Roskilde Universitet, 1998.

[295] J. Lee and N. P. Smith, "Lumped parameter outflow models for 1-D blood flow simulations," *Ann. Biomed. Eng.*, vol. 40, no. 11, pp. 2399–2413, 2012, doi: 10.1007/s10439-012-0583-7.

[296] W. E. Bodley, "The non-linearities of arterial blood flow," *Phys. Med. Biol.*, vol. 16, no. 4, pp. 663–672, 1971, doi: 10.1088/0031-9155/16/4/010.

[297] V. L. STREETER, W. F. KEITZER, and D. F. BOHR, "Pulsatile Pressure and Flow Through Distensible Vessels.," *Circ. Res.*, vol. 13, pp. 3–20, 1963, doi:

10.1161/01.RES.13.1.3.

[298] P. Reymond, F. Merenda, F. Perren, D. Rüfenacht, and N. Stergiopulos, "Validation of a one-dimensional model of the systemic arterial tree," *Am. J. Physiol. - Hear. Circ. Physiol.*, vol. 297, no. 1, pp. 208–222, 2009, doi: 10.1152/ajpheart.00037.2009.

[299] Q. Pan *et al.*, "A one-dimensional mathematical model for studying the pulsatile flow in microvascular networks," *J. Biomech. Eng.*, vol. 136, no. 1, 2014, doi: 10.1115/1.4025879.

[300] Y. Sun *et al.*, "Wave-intensity analysis: a new approach to coronary hemodynamics," vol. 1, pp. 1636–1644, 2020.

[301] E. H. Hollander, G. M. Dobson, J.-J. Wang, K. H. Parker, and J. V. Tyberg, "Direct and series transmission of left atrial pressure perturbations to the pulmonary artery: a study using wave-intensity analysis," *Am. J. Physiol. Circ. Physiol.*, vol. 286, no. 1, pp. H267–H275, Jan. 2004, doi: 10.1152/ajpheart.00505.2002.

[302] A. Zambanini, S. L. Cunningham, K. H. Parker, A. W. Khir, S. A. M. G. Thom, and A. D. Hughes, "Wave-energy patterns in carotid, brachial, and radial arteries: A noninvasive approach using wave-intensity analysis," *Am. J. Physiol. - Hear. Circ. Physiol.*, vol. 289, no. 1 58-1, pp. 270–276, 2005, doi: 10.1152/ajpheart.00636.2003.

[303] M. Harana, "MRI-Based Calculation of the Aortic Blood Pressure Waveform by 0-Dimensional Flow Modelling : Development and Testing Using In Silico and In Vivo data."

[304] S. Jiang, Z. Q. Zhang, F. Wang, and J. K. Wu, "A personalized-model-based central aortic pressure estimation method," *J. Biomech.*, vol. 49, no. 16, pp. 4098–4106, 2016, doi: 10.1016/j.jbiomech.2016.11.007.

[305] M. Khalifé, A. Decoene, F. Caetano, L. de Rochefort, E. Durand, and D. Rodríguez, "Estimating absolute aortic pressure using MRI and a one-dimensional model," *J. Biomech.*, vol. 47, no. 13, pp. 3390–3399, 2014, doi:

10.1016/j.jbiomech.2014.07.018.

[306] G. Bárdossy and G. Halász, "A 'backward' calculation method for the estimation of central aortic pressure wave in a 1D arterial model network," *Comput. Fluids*, vol. 73, pp. 134–144, Mar. 2013, doi: 10.1016/j.compfluid.2012.12.014.

[307] P. Charlton, M. Aresu, J. Spear, P. Chowienczyk, and J. Alastruey, "Indices To Assess Aortic Stiffness From the Finger Photoplethysmogram: in Silico and in Vivo Testing," *Artery Res.*, vol. 24, no. C, p. 128, 2018, doi: 10.1016/j.artres.2018.10.217.

[308] M. Willemet, P. Chowienczyk, and J. Alastruey, "A database of virtual healthy subjects to assess the accuracy of foot-to-foot pulse wave velocities for estimation of aortic stiffness," pp. 663–675, 2015, doi: 10.1152/ajpheart.00175.2015.

[309] S. Vennin *et al.*, "Noninvasive calculation of the aortic blood pressure waveform from the flow velocity waveform: A proof of concept," *Am. J. Physiol. - Hear. Circ. Physiol.*, vol. 309, no. 5, pp. H969–H976, 2015, doi: 10.1152/ajpheart.00152.2015.

[310] M. Saito, Y. Ikenaga, M. Matsukawa, Y. Watanabe, T. Asada, and P. Y. Lagrée, "One-dimensional model for propagation of a pressure wave in a model of the human arterial network: Comparison of theoretical and experimental results," *J. Biomech. Eng.*, vol. 133, no. 12, pp. 1–9, 2011, doi: 10.1115/1.4005472.

[311] K. H. Parker and C. J. H. Jones, "Forward and Backward Running Waves in the Arteries: Analysis Using the Method of Characteristics," *J. Biomech. Eng.*, vol. 112, no. 3, p. 322, 1990, doi: 10.1115/1.2891191.

[312] J. J. Wang, A. B. O'Brien, N. G. Shrive, K. H. Parker, and J. V. Tyberg, "Time-domain representation of ventricular-arterial coupling as a windkessel and wave system," *Am. J. Physiol. - Hear. Circ. Physiol.*, vol. 284, no. 4 53-4, pp. 1358–1368, 2003, doi: 10.1152/ajpheart.00175.2002.

[313] J. J. Wang and K. H. Parker, "Wave propagation in a model of the arterial circulation," *J. Biomech.*, vol. 37, no. 4, pp. 457–470, 2004, doi:

10.1016/j.jbiomech.2003.09.007.

[314] B. S. Brook, S. A. E. G. Falle, and T. J. Pedley, “Numerical solutions for unsteady gravity-driven flows in collapsible tubes: Evolution and roll-wave instability of a steady state,” *J. Fluid Mech.*, vol. 396, no. May 2014, pp. 223–256, 1999, doi: 10.1017/S0022112099006084.

[315] B. S. Brook and T. J. Pedley, “A model for time-dependent flow in (giraffe jugular) veins: Uniform tube properties,” *J. Biomech.*, vol. 35, no. 1, pp. 95–107, 2002, doi: 10.1016/S0021-9290(01)00159-2.

[316] S. J. Sherwin, V. Franke, J. Peiró, and K. Parker, “One-dimensional modelling of a vascular network in space-time variables,” *J. Eng. Math.*, vol. 47, no. 3/4, pp. 217–250, Dec. 2003, doi: 10.1023/B:ENGI.0000007979.32871.e2.

[317] D. Bessems, C. G. Giannopapa, M. C. M. Rutten, and F. N. van de Vosse, “Experimental validation of a time-domain-based wave propagation model of blood flow in viscoelastic vessels,” *J. Biomech.*, vol. 41, no. 2, pp. 284–291, 2008, doi: 10.1016/j.jbiomech.2007.09.014.

[318] L. R. John, “Forward electrical transmission line model of the human arterial system,” *Med. Biol. Eng. Comput.*, vol. 42, no. 3, pp. 312–321, May 2004, doi: 10.1007/BF02344705.

[319] A. R. Ghigo, J. M. Fullana, and P. Y. Lagrée, “A 2D nonlinear multiring model for blood flow in large elastic arteries,” *J. Comput. Phys.*, vol. 350, pp. 136–165, 2017, doi: 10.1016/j.jcp.2017.08.039.

[320] S. Boujena, O. Kafi, and N. El Khatib, “A 2D mathematical model of blood flow and its interactions in an atherosclerotic artery,” *Math. Model. Nat. Phenom.*, vol. 9, no. 6, pp. 46–68, 2014, doi: 10.1051/mmnp/20149605.

[321] A. Lopez-Perez, R. Sebastian, and J. M. Ferrero, “Three-dimensional cardiac computational modelling: METHODS, features and applications,” *Biomed. Eng. Online*, vol. 14, no. 1, pp. 1–31, 2015, doi: 10.1186/s12938-015-0033-5.

[322] X. Xie, M. Zheng, D. Wen, Y. Li, and S. Xie, “A new CFD based non-invasive

method for functional diagnosis of coronary stenosis," *Biomed. Eng. Online*, vol. 17, no. 1, pp. 1–13, 2018, doi: 10.1186/s12938-018-0468-6.

[323] H. Watanabe, S. Sugiura, H. Kafuku, and T. Hisada, "Multiphysics simulation of left ventricular filling dynamics using fluid-structure interaction finite element method," *Biophys. J.*, vol. 87, no. 3, pp. 2074–2085, 2004, doi: 10.1529/biophysj.103.035840.

[324] F. Migliavacca *et al.*, "Multiscale modelling in biofluidynamics: Application to reconstructive paediatric cardiac surgery," *J. Biomech.*, vol. 39, no. 6, pp. 1010–1020, 2006, doi: 10.1016/j.jbiomech.2005.02.021.

[325] I. E. Vignon-Clementel, C. Alberto Figueroa, K. E. Jansen, and C. A. Taylor, "Outflow boundary conditions for three-dimensional finite element modeling of blood flow and pressure in arteries," *Comput. Methods Appl. Mech. Eng.*, vol. 195, no. 29–32, pp. 3776–3796, 2006, doi: 10.1016/j.cma.2005.04.014.

[326] L. Formaggia, J. F. Gerbeau, F. Nobile, and A. Quarteroni, "On the coupling of 3D and 1D Navier-Stokes equations for flow problems in compliant vessels," *Comput. Methods Appl. Mech. Eng.*, vol. 191, no. 6–7, pp. 561–582, 2001, doi: 10.1016/S0045-7825(01)00302-4.

[327] L. Formaggia, A. Quarteroni, and A. Veneziani, "Multiscale models of the vascular system," in *Cardiovascular Mathematics*, Milano: Springer Milan, 2009, pp. 395–446.

[328] A. L. Goldberger *et al.*, "PhysioBank, PhysioToolkit, and PhysioNet," *Circulation*, vol. 101, no. 23, Jun. 2000, doi: 10.1161/01.CIR.101.23.e215.

[329] M. Willemet, P. Chowienczyk, and J. Alastruey, "A database of virtual healthy subjects to assess the accuracy of foot-to-foot pulse wave velocities for estimation of aortic stiffness," *Am. J. Physiol. Circ. Physiol.*, vol. 309, no. 4, pp. H663–H675, Aug. 2015, doi: 10.1152/ajpheart.00175.2015.

[330] M. H. Jun, Y. M. Kim, J. H. Bae, C. J. Jung, J. H. Cho, and Y. J. Jeon, "Development of a tonometric sensor with a decoupled circular array for precisely measuring radial artery pulse," *Sensors (Switzerland)*, vol. 16, no. 6,

2016, doi: 10.3390/s16060768.

[331] R. Liang and Q. M. Wang, “Pulse pressure sensor based on flexible PZT thick-film composite device,” *IEEE Int. Ultrason. Symp. IUS*, pp. 1559–1562, 2014, doi: 10.1109/ULTSYM.2014.0386.

[332] N. Westerhof, J. W. Lankhaar, and B. E. Westerhof, “The arterial windkessel,” *Med. Biol. Eng. Comput.*, vol. 47, no. 2, pp. 131–141, 2009, doi: 10.1007/s11517-008-0359-2.

[333] R. Burattini and S. Bini, “Physiological interpretation of inductance and low-resistance terms in four-element windkessel models: Assessment by generalized sensitivity function analysis,” *Med. Eng. Phys.*, vol. 33, no. 6, pp. 739–754, 2011, doi: 10.1016/j.medengphy.2011.01.012.

[334] P. O. Lim, P. Shiels, J. Anderson, and T. M. MacDonald, “Dundee step test: A simple method of measuring the blood pressure response to exercise,” *J. Hum. Hypertens.*, vol. 13, no. 8, pp. 521–526, 1999, doi: 10.1038/sj.jhh.1000869.

[335] Z. D. Liu, J. K. Liu, B. Wen, Q. Y. He, Y. Li, and F. Miao, “Cuffless blood pressure estimation using pressure pulse wave signals,” *Sensors (Switzerland)*, vol. 18, no. 12, 2018, doi: 10.3390/s18124227.

[336] K. Yuki and H. Tsuyoshi, “Sensor Technology to Realize Continuous Blood Pressure Monitoring Development and Practical Application of High-precision Multi-element MEMS Pressure Sensor,” *Omron Tech.*, vol. 50, pp. 1–10, 2019.

[337] T. Ashraf, Z. Panhwar, S. Habib, M. A. Memon, F. Shamsi, and J. Arif, “Size of radial and ulnar artery in local population,” *J. Pak. Med. Assoc.*, vol. 60, no. 10, pp. 817–819, 2010.

[338] S. Beniwal, K. Bhargava, and S. K. Kausik, “Size of distal radial and distal ulnar arteries in adults of southern Rajasthan and their implications for percutaneous coronary interventions,” *Indian Heart J.*, vol. 66, no. 5, pp. 506–509, 2014, doi: 10.1016/j.ihj.2014.08.010.

[339] L. Peter, N. Noury, and M. Cerny, “A review of methods for non-invasive and

continuous blood pressure monitoring: Pulse transit time method is promising?," *Irbm*, vol. 35, no. 5, pp. 271–282, 2014, doi: 10.1016/j.irbm.2014.07.002.

[340] G. M. Drzewiecki, J. Melbin, and A. Noordergraaf, "Arterial tonometry: Review and analysis," *J. Biomech.*, vol. 16, no. 2, pp. 141–152, 1983, doi: 10.1016/0021-9290(83)90037-4.

[341] S. Hansen and M. Staber, "Oscillometric blood pressure measurement used for calibration of the arterial tonometry method contributes significantly to error.," *Eur. J. Anaesthesiol.*, vol. 23, no. 9, pp. 781–787, Sep. 2006, doi: 10.1017/S0265021506000688.

[342] B. Bhushan, N. Rakesh, Y. Farhaoui, P. N. Astya, and B. Unhelkar, *Blockchain Technology in Healthcare Applications*. Boca Raton: CRC Press, 2022.

[343] N. N. Radovanović, S. U. Pavlović, G. Milašinović, B. Kirćanski, and M. M. Platiša, "Bidirectional cardio-respiratory interactions in heart failure," *Front. Physiol.*, vol. 9, no. MAR, pp. 1–9, 2018, doi: 10.3389/fphys.2018.00165.

[344] D. Leoni and J. Rello, "Cardiac arrest among patients with infections: causes, clinical practice and research implications," *Clin. Microbiol. Infect.*, vol. 23, no. 10, pp. 730–735, 2017, doi: 10.1016/j.cmi.2016.11.018.

[345] B. Williams and P. S. Lacy, "Central aortic pressure and clinical outcomes," *J. Hypertens.*, vol. 27, no. 6, pp. 1123–1125, Jun. 2009, doi: 10.1097/HJH.0b013e32832b6566.

[346] M. J. Roman *et al.*, "Central Pressure More Strongly Relates to Vascular Disease and Outcome Than Does Brachial Pressure," *Hypertension*, vol. 50, no. 1, pp. 197–203, Jul. 2007, doi: 10.1161/HYPERTENSIONAHA.107.089078.

[347] R. Pini *et al.*, "Central But Not Brachial Blood Pressure Predicts Cardiovascular Events in an Unselected Geriatric Population," *J. Am. Coll. Cardiol.*, vol. 51, no. 25, pp. 2432–2439, Jun. 2008, doi: 10.1016/j.jacc.2008.03.031.

[348] M. J. Roman, P. M. Okin, J. R. Kizer, E. T. Lee, B. V Howard, and R. B. Devereux, "Relations of central and brachial blood pressure to left ventricular

hypertrophy and geometry: the Strong Heart Study," *J. Hypertens.*, vol. 28, no. 2, pp. 384–388, Feb. 2010, doi: 10.1097/HJH.0b013e328333d228.

APPENDICES

Appendix 1

Date: 9th December 2019

To: **Collaborative Research in Engineering, Science & Technology (CREST) Center**
Block C, Ground Floor, Sains@USM,
No. 10 Persiaran Bukit Jambul,
11900 Bayan Lepas, Penang

Dear Sir,

Confirmation on data used for analysis from online databases for the CREST Project **"Development of a Medical Device for the Monitoring and Prediction of Cardiovascular Disease"**

This letter is submitted in support of the collaboration between **University of Nottingham Malaysia** and **Chulia Facilities Management (M) Sdn. Bhd.** to confirm the usage and validity of data from online databases.

I hereby confirm that the data used from the HeaMod and PhysioNet databases are relevant to the undertaken project and has validity for the above mentioned purpose. I have read the report given by University of Nottingham Malaysia and have been updated on the project progress. Based on the significance of the group's findings, hospital data collection is currently undergoing at the Hospital Sultanah Bahiyah Alor Setar under my supervision.
A summary of the details of the correlation and the relevance of using the online database are given below for your purview.

Yours Sincerely,

Dr. Saravanan Krishnan
Head,
Department of Cardiology
Hospital Sultanah Bahiyah
Alor Setar

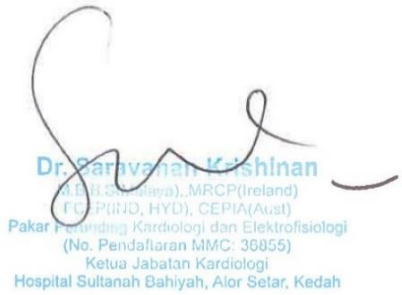

Figure A1.1 Confirmation letter from the Cardiologist on the usage of HaeMod and PhysioNet databases.

Appendix 2

Table A2.1 List of cardiovascular disease subjects from Hospital Sultanah Bahiyah

No	List of subjects	Diseases
1	Subject 1	Ischemic Heart Disease
2	Subject 2	Unstable Angina
3	Subject 3	Myocardial Infarction (MI)
4	Subject 4	Myocardial Infarction (MI)
5	Subject 5	Vascular heart disease
6	Subject 6	Positive Exercise Stress Test (EST)
7	Subject 7	Unstable Angina
8	Subject 8	Myocardial Infarction (MI)
9	Subject 9	Ischemic Heart Disease
10	Subject 10	Myocardial Infarction (MI)
11	Subject 11	Myocardial Infarction (MI)
12	Subject 12	Unstable Angina
13	Subject 13	Unstable Angina
14	Subject 14	Positive Exercise Stress Test (EST)
15	Subject 15	Myocardial Infarction (MI)
16	Subject 16	Dilated Cardiomyopathy
17	Subject 17	Ischemic Heart Disease & 3 vessel defect
18	Subject 18	Ischemic Heart Disease
19	Subject 19	Unstable Angina
20	Subject 20	Ischemic Heart Disease
21	Subject 21	Myocardial Infarction (MI)
22	Subject 22	Positive Exercise Stress Test (EST)
23	Subject 23	Ischemic Heart Disease
24	Subject 24	Positive Exercise Stress Test (EST)
25	Subject 25	Ischemic Heart Disease
26	Subject 26	Unstable Angina
27	Subject 27	Ischemic Heart Disease

28	Subject 28	Ischemic Heart Disease
29	Subject 29	3 Vessel Defect
30	Subject 30	Unstable Angina
31	Subject 31	Myocardial Infarction (MI)
32	Subject 32	Unstable Angina
33	Subject 33	Unstable Angina
34	Subject 34	Myocardial Infarction (MI)
35	Subject 35	Ischemic Heart Disease
36	Subject 36	Myocardial Infarction (MI)
37	Subject 37	Ischemic Heart Disease
38	Subject 38	Positive Exercise Stress Test (EST)
39	Subject 39	Hypertension & Diabetes Mellitus
40	Subject 40	Myocardial Infarction (MI)

Appendix 3

The 16 parameters that affect the aortic blood pressure waveform (PA1) are discussed in detail below:

1. Pulmonary Artery 2 Resistance (RP2)

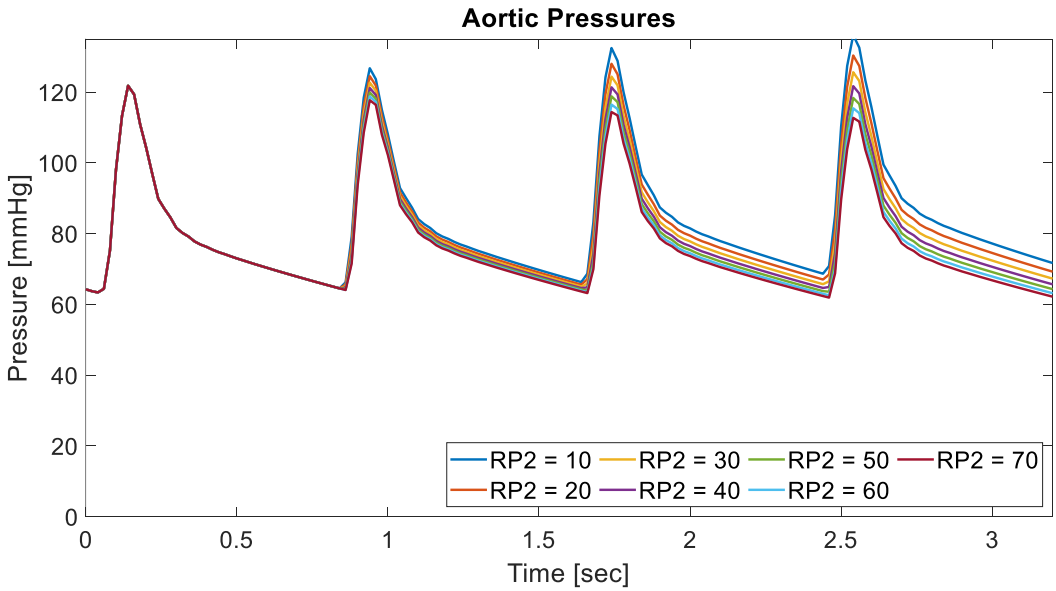

Figure A3.1 Effect of RP2 on PA1

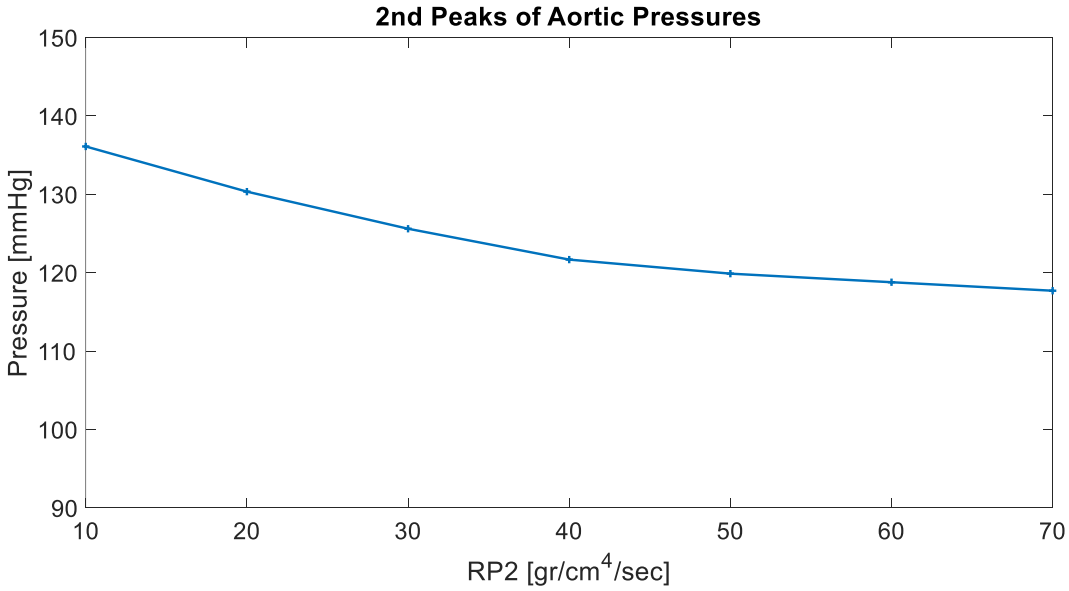

Figure A3.2 Second Peak of PA1 against RP2.

Figure A3.1 and Figure A3.2 show that RP2 increases when PA1 decreases significantly. RP2 has no effect on the changes in the shape of the response PA1.RP2 has an effect on the PA1 because RP2 is the resistance at the second part of the pulmonary artery where blood flows from the pulmonary artery into the heart through the pulmonary vein. When RP2 increases, the pressure drops across it increases resulting PA1 decreases due to the blood flows from RP2 to PA1. Since this a 0D model which related

to the electrical circuit, as RP2 increases, PA1 decreases where PA1 is represented by the voltage across at a point after RP2.

2. Pulmonary Artery 3 Resistance (RP3)

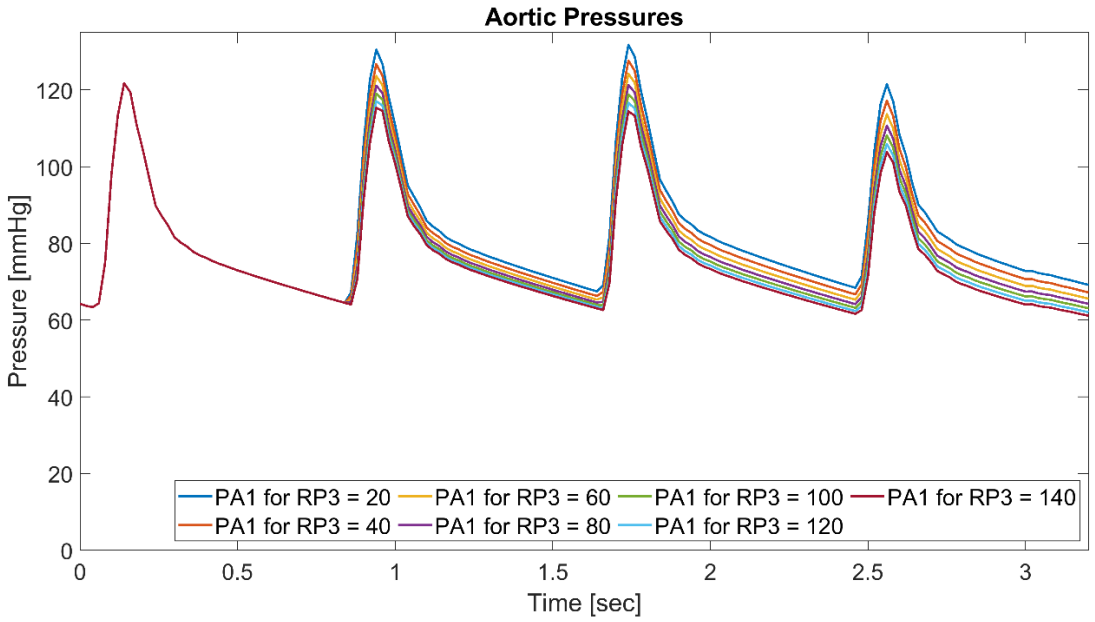

Figure A3.3 Effect of RP3 on PA1.

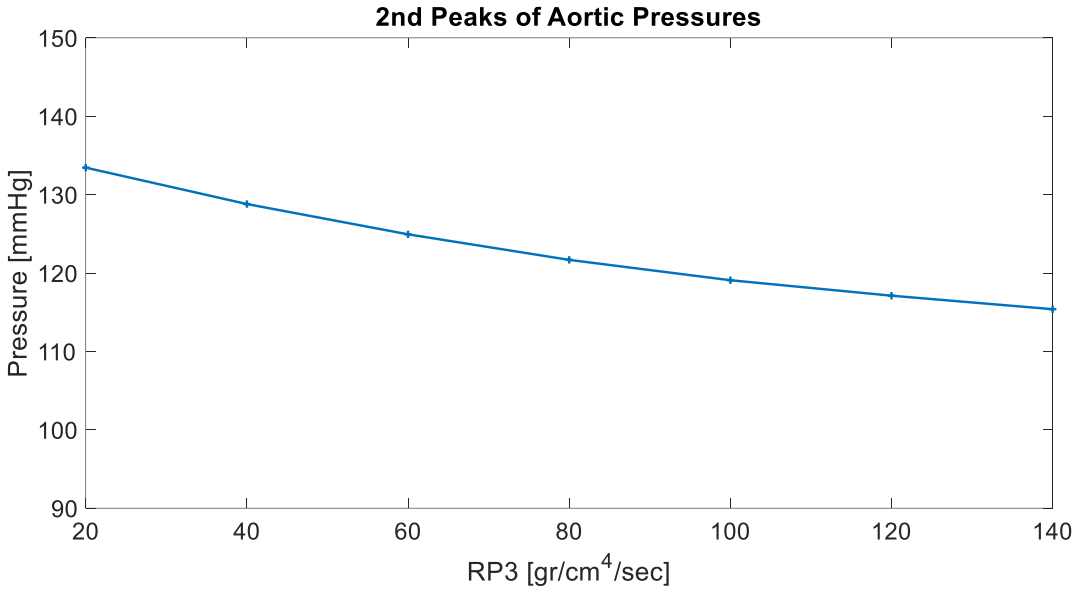

Figure A3.4 Second Peak of PA1 against RP3.

PA1 decreases significantly as RP3 increases and vice versa is shown in both Figures A3.3 and A3.4. The shape of the signal is not affected by the change in RP3. RP3 is the resistance at the third part of the pulmonary artery which the resistance at the blood back to the heart through the pulmonary vein. RP3 plays a big effect on PA1 on blood flow because for the heart to pump through the aorta it would need sufficient volume and pressure of the blood in the heart receiving it from the pulmonary vein. Since this a 0D model which is related to the electrical circuit, when RP3 increases, the voltage

drops across it also increases resulting to PA1 to decrease because PA1 is represented by the voltage at a point after RP3.

3. Pulmonary Vein 1 Resistance (RL1)

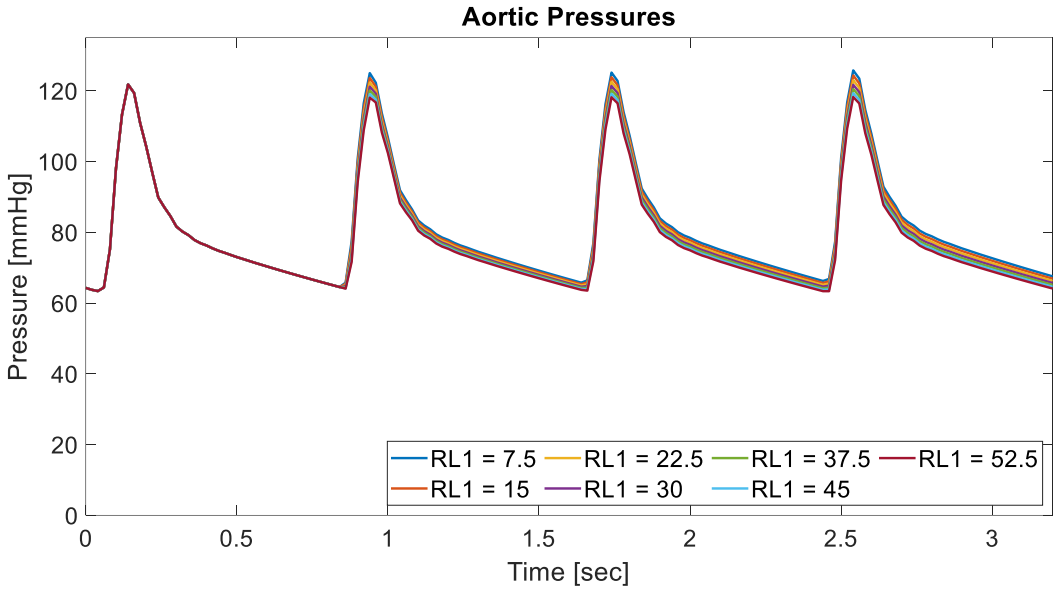

Figure A3.5 Effect of RL1 on PA1.

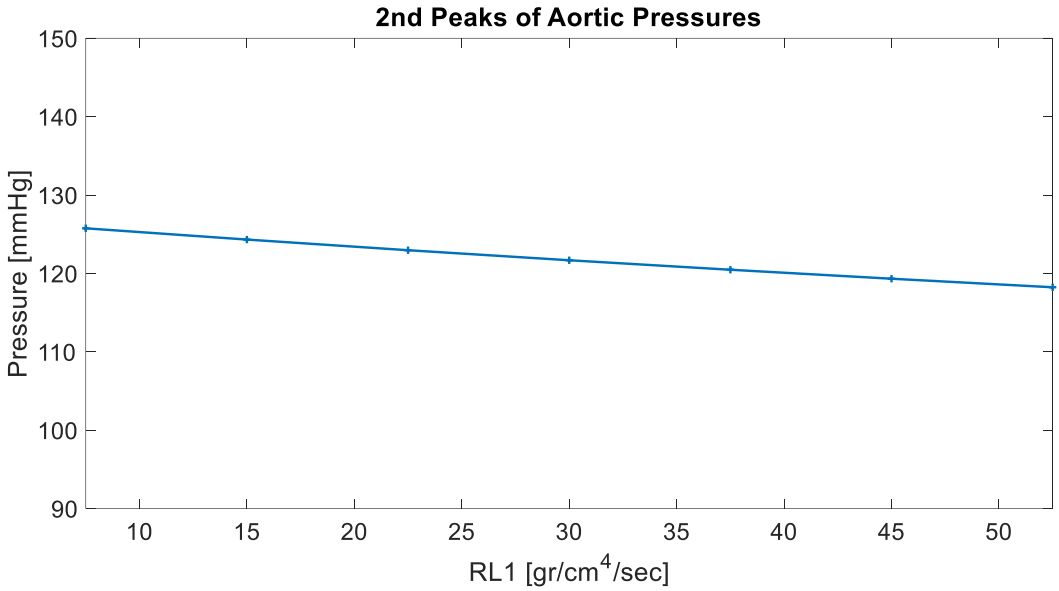

Figure A3.6 Second Peak of PA1 against RL1.

PA1 decreasing when RL1 increases can be seen in Figure A3.5 and Figure A3.6. Change in Rl1 has no effect on the changes in the shape of PA1 signal. RL1 is the resistance at the first part of the pulmonary vein where blood flows from the pulmonary vein into the heart. RL1 has less effect on PA1 because it is located further before the aortic vessel.

4. Pulmonary Vein 2 Resistance (RL2)

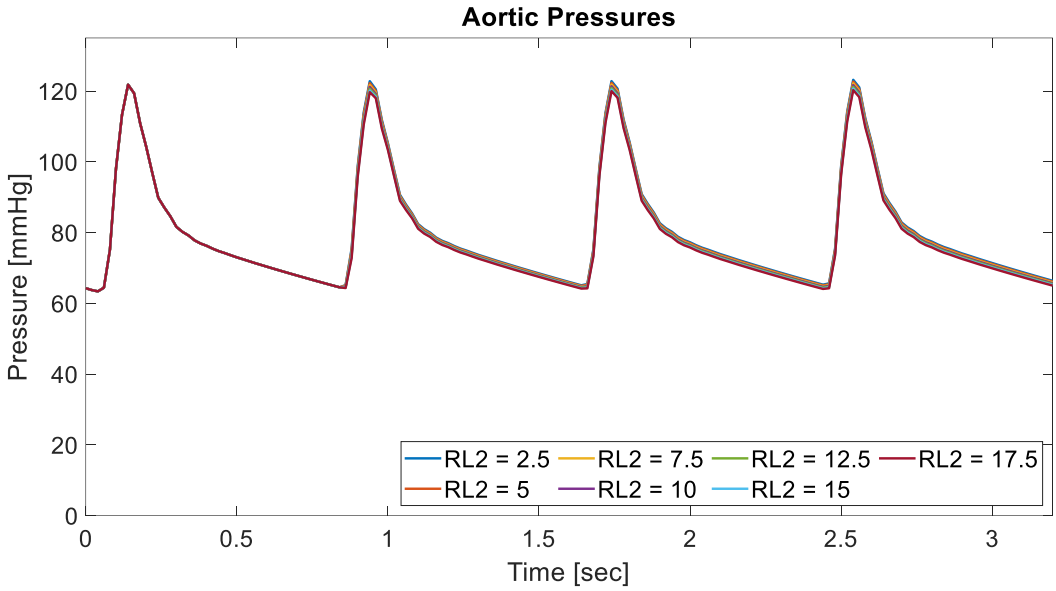

Figure A3.7 Effect of RL2 on PA1.

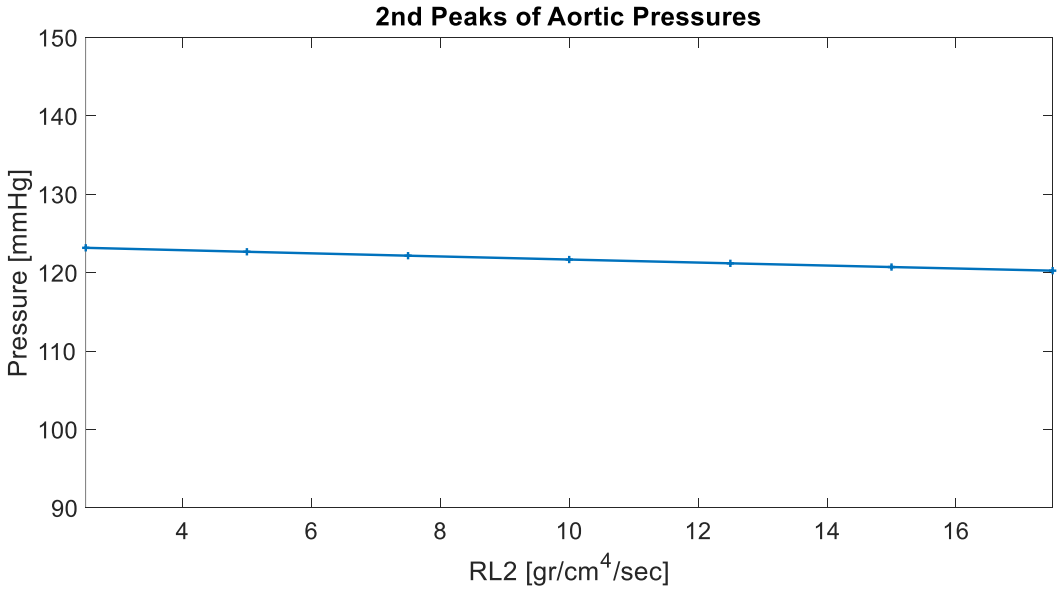

Figure A3.8 Second Peak of PA1 against RL2.

PA1 decreasing as RL2 increases, as shown in Figures A3.7 and A3.8. However, there are no changes to the shape of the PA1 signal. RL2 is the resistance at the second part of the pulmonary vein where blood flows from the pulmonary vein into the heart. RL2 has only a mild effect on the peaks of the signal in PA1.

5. Left Atrium Resistance (RLA)

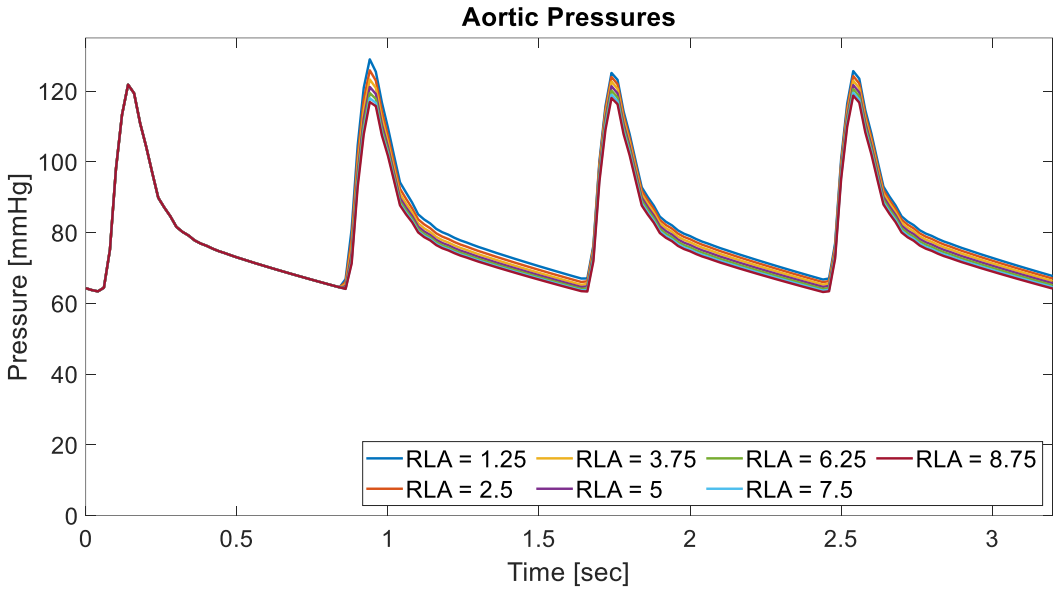

Figure A3.9 Effect of RLA on PA1.

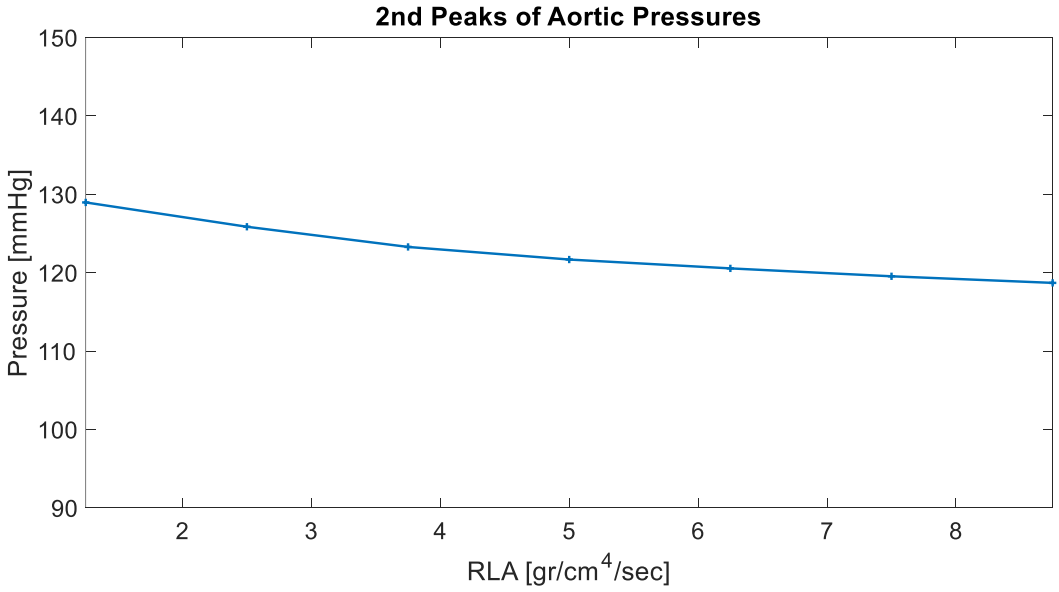

Figure A3.10 Second Peak of PA1 against RLA.

RLA increases resulting in PA1 decreases significantly can be seen in Figures A3.9 and A3.10. PA1 signal shape is not affected by the RLA. RLA is the resistance at the left atrium which as effect to the PA1 because blood flows from the left atrium into the left ventricle then into the aorta. Therefore, an increase in friction in the left atrium will increase the pressure drop the aorta. Since this a 0D model which is related to the electrical circuit, as RLA increases, PA1 decreases which is the voltage drop across at a point after RLA.

6. Aortic 1 Resistance (RA1)

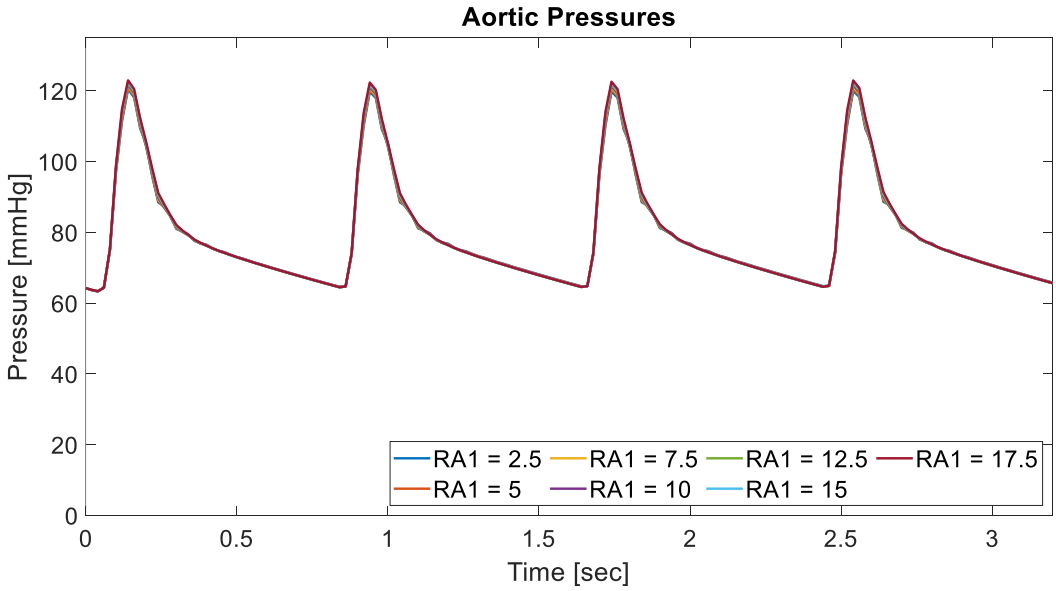

Figure A3.11 Effect of RA1 on PA1.

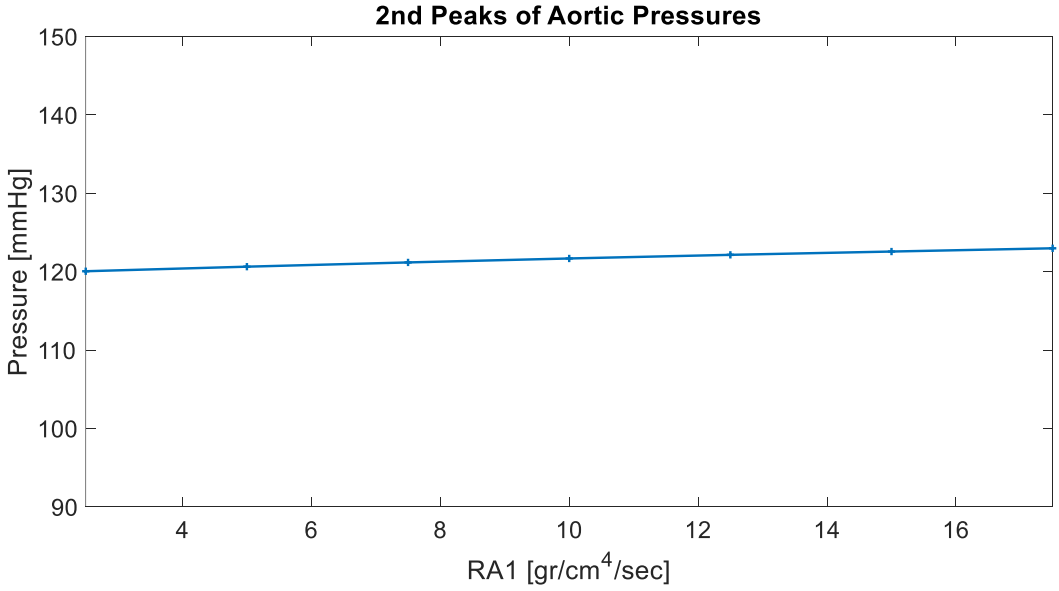

Figure A3.12 Second Peak of PA1 against RA1.

When RA1 increases, PA1 increases as can be seen from Figures A3.11 and A3.12. RA1 has some changes to the shape of the PA1 when RA1 is very small. RA1 is the resistance at the first part of the aorta where the blood from the heart flows into the rest of the body. However, RA1 shows less effect on the PA1 compared to the other parameters even though RA1 is located near to PA1 because the RA1 is a big artery with lesser resistance compared to a smaller artery in the loop whereby a small change in resistance effects a small change in PA1.

7. Aortic 2 Resistance (RA2)

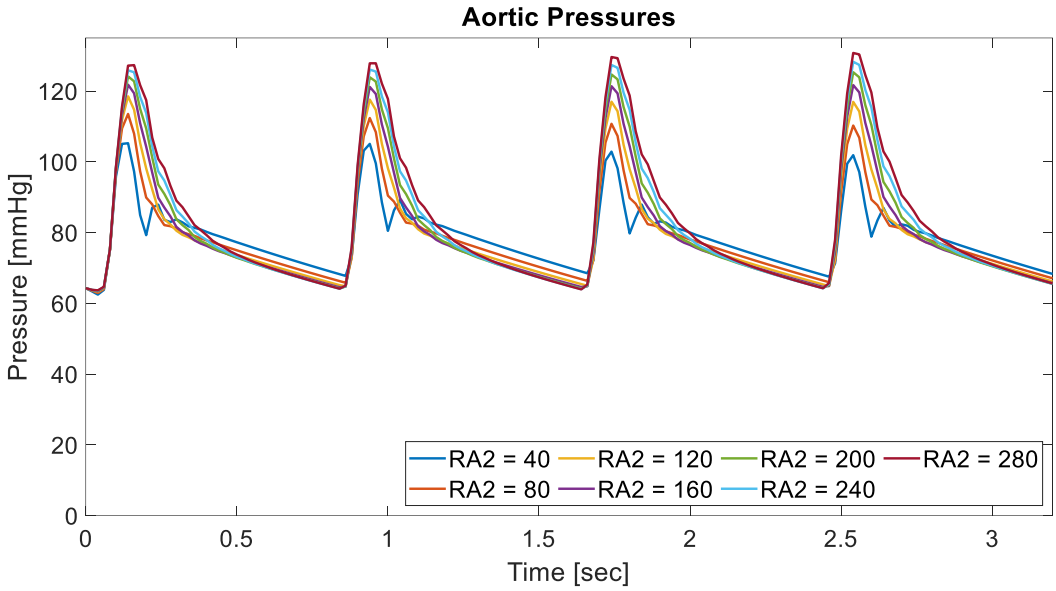

Figure A3.13 Effect of RA2 on PA1.

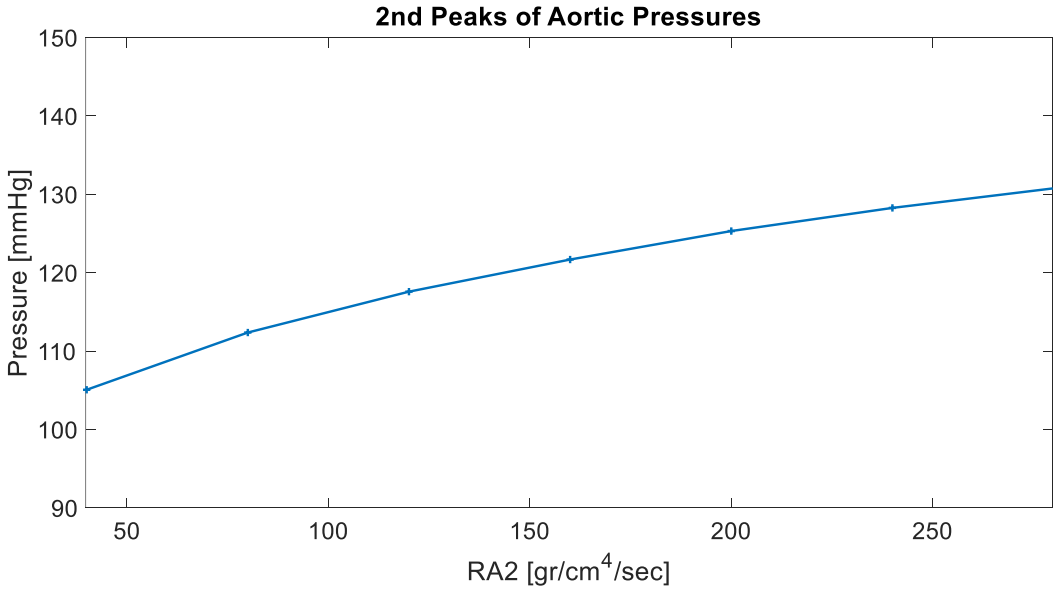

Figure A3.14 Second Peak of PA1 against RA2

PA1 increasing significantly as RA2 increases can be seen in the above Figures A3.13 and A3.14. The shape of the response changes drastically when RA2 is very small. RA2 has a big impact on PA1 because RA2 is the resistance at the second part of the aorta which flows blood out to the rest of the part of the body. When RA2 increases, PA1 increases because of the blood from PA1 flows into RA2. Since this a 0D model which related to the electrical circuit, when RA2 increases, the voltage drops across it also increases resulting to increase in PA1.

8. Systemic Artery Resistance (RA3)

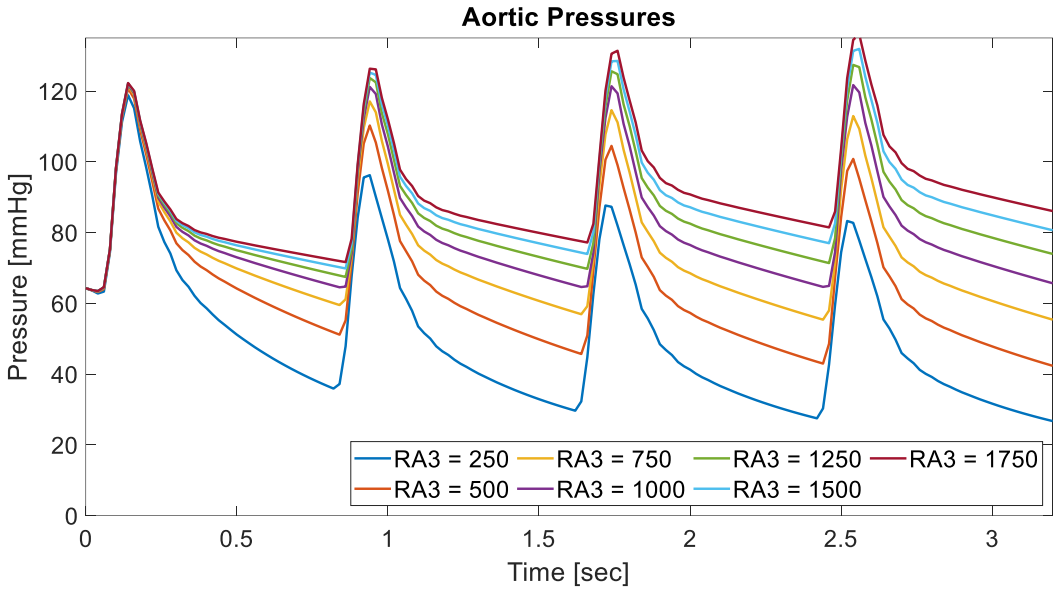

Figure A3 .15 Effect of RA3 on PA1.

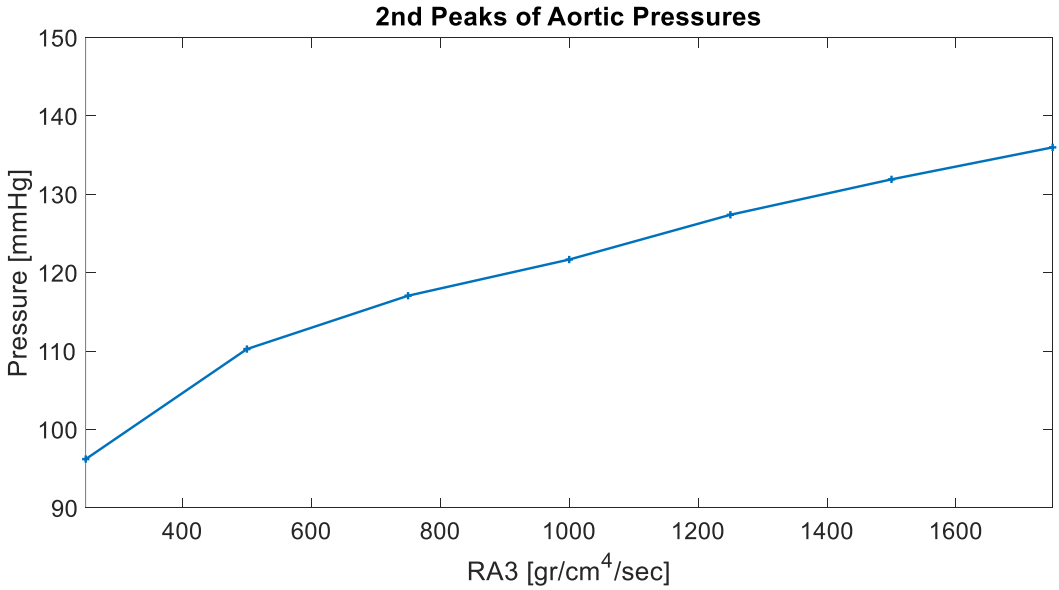

Figure A3.16 Second Peak of PA1 against RA3.

PA1 increases significantly as RA3 increases and vice versa as shown in Figure A3.15 and Figure A3.16 above. The change in RA3 is very responsive to the change in the PA1and also in the shape of the signal of PA1.RA3 is a systemic resistance which is the resistance to the blood flow from the aorta to the rest of the part of the body. Therefore, RA3 gives a very big impact to the blood flow to the body which resolved in the big change in the PA1 because of the higher the resistance at the systemic partway flow, the higher the pressure at PA1.Since this a 0D model which related to the electrical circuit, the voltage drop across it also increases when RA3 increases using Kirchhoff's

circuit laws. As the voltage drop across RA3 increases, it results in PA1 also increases because PA1 is represented by the voltage at a point before RA3.

9. Left Atrium Inertance (LLA)

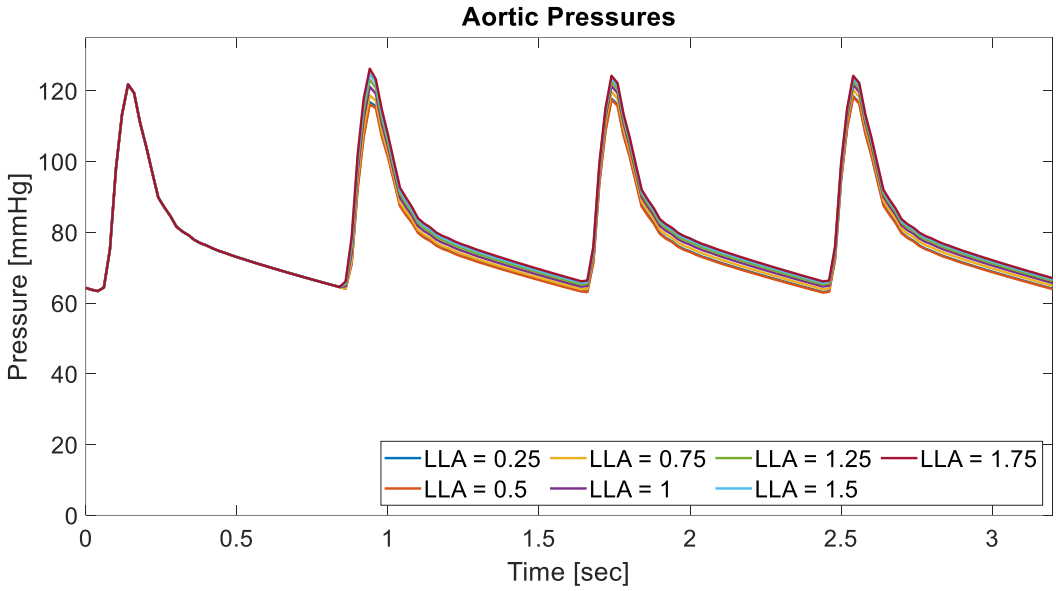

Figure A2.17 Effect of LLA on PA1.

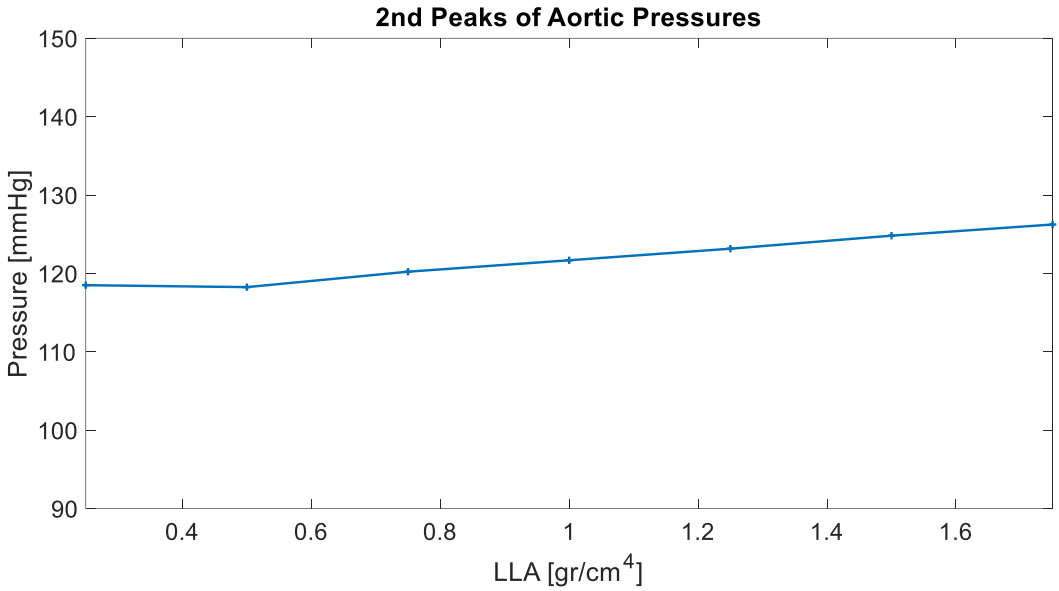

Figure A2.18 Second Peak of PA1 against LLA

PA1 increases significantly as LLA increases, as shown in Figures A3.17 and A3.18. PA1 signal has no changes to the shape of the signal when LLA changes. LLA has an impact on the PA1 signal because LLA is the inertance at the left atrium where blood flows from the left atrium into the left ventricle then into the aorta which means LLA is a measurement of the required pressure gradient to cause a unit change in blood flow rate at the left atrium. Since this a 0D model which related to the electrical circuit, LLA is represented by the inductance and PA1 is represented by the voltage at a point after

LLA. Therefore, when LLA increases, the back EMF across it also increases resulting in an increase in PA1.

10. Left Ventricle Inertance (LLV)

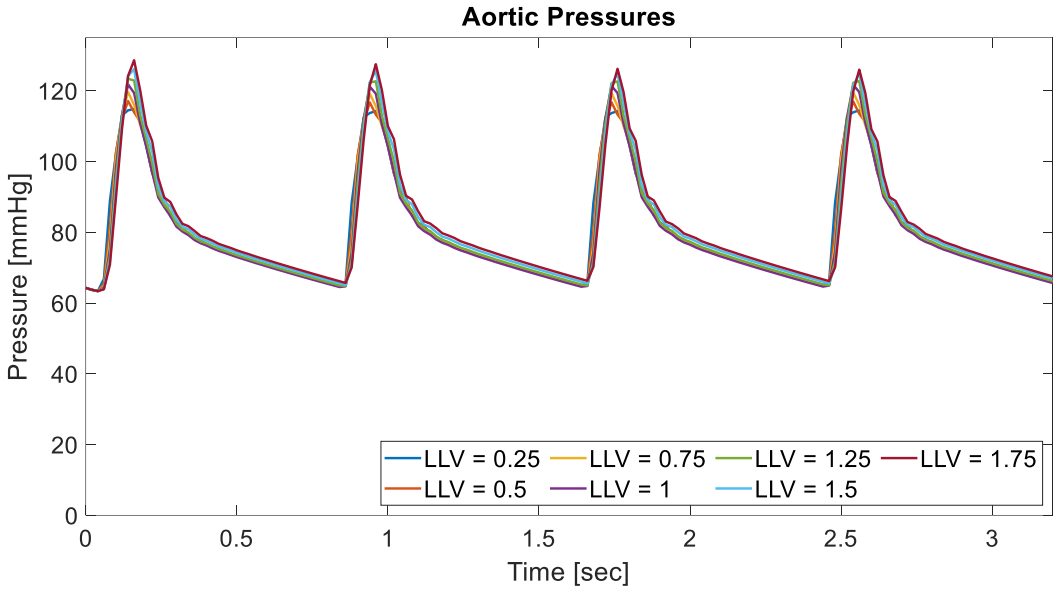

Figure A3.19 Effect of LLV on PA1.

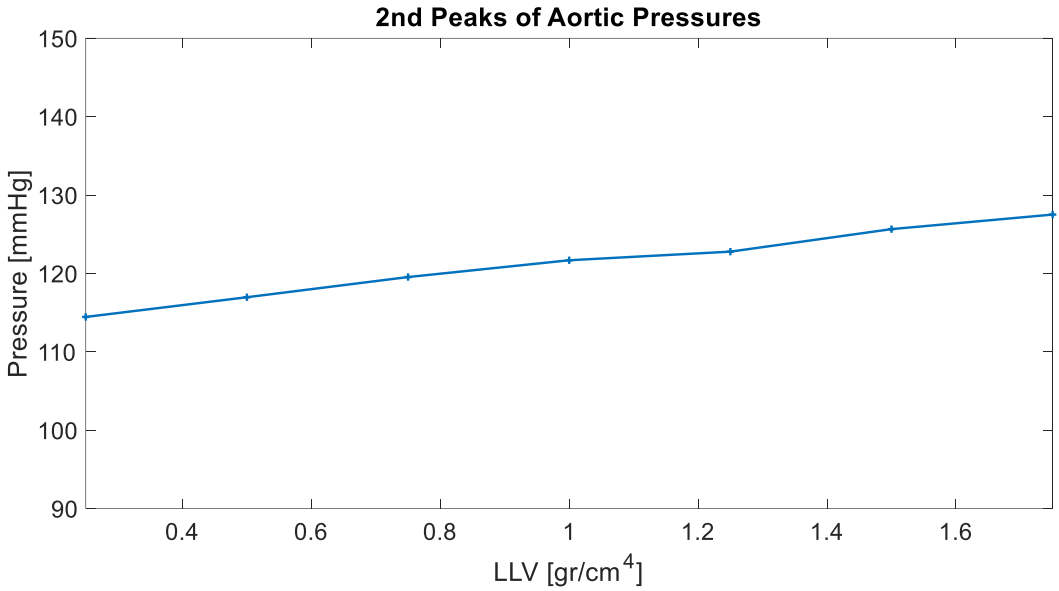

Figure A3.20 Second Peak of PA1 against LLV.

PA1 increasing significantly as LLV increases and vice versa can be seen in Figures A3.19 and A3.20. Change in LLV shows a significant change in the shape of the signal of PA1. LLV is the inertance at the left ventricle where blood from the left ventricle flows to the aorta which results in a change in PA1. Moreover, LLV is a measurement of the required pressure gradient to cause a unit change in blood flow rate at the left ventricle. Since this a 0D model which related to the electrical circuit, LLV is represented by the inductance and PA1 is represented by the voltage at a point after LLV

shows that, when LLV increases, the back Electromotive force (EMF) across it also increases resulting PA1 to increase as well.

11. Aortic 1 Inertance (LA1)

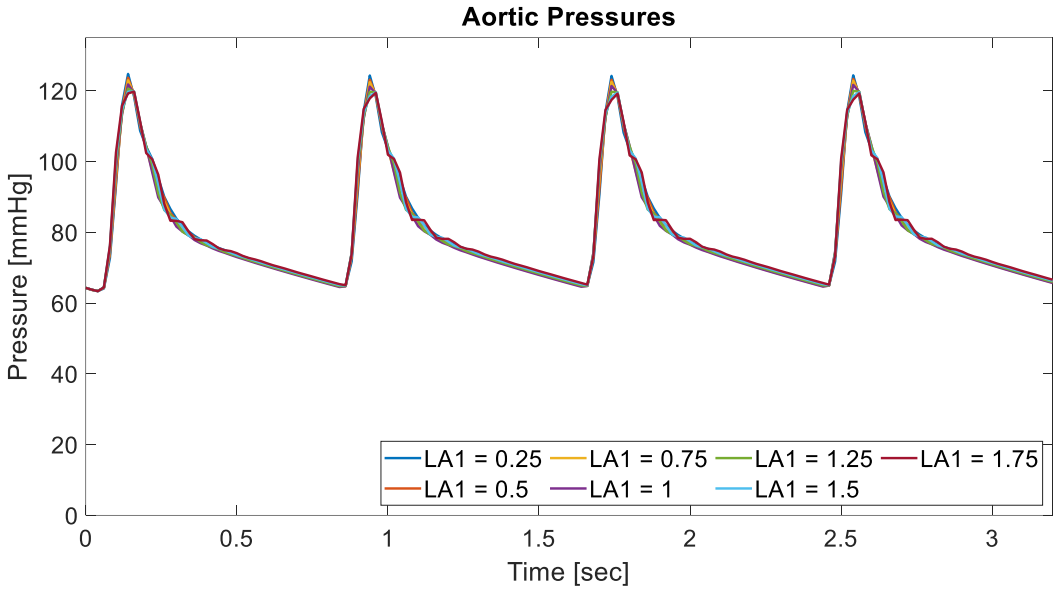

Figure A3.21 Effect of LA1 on PA1.

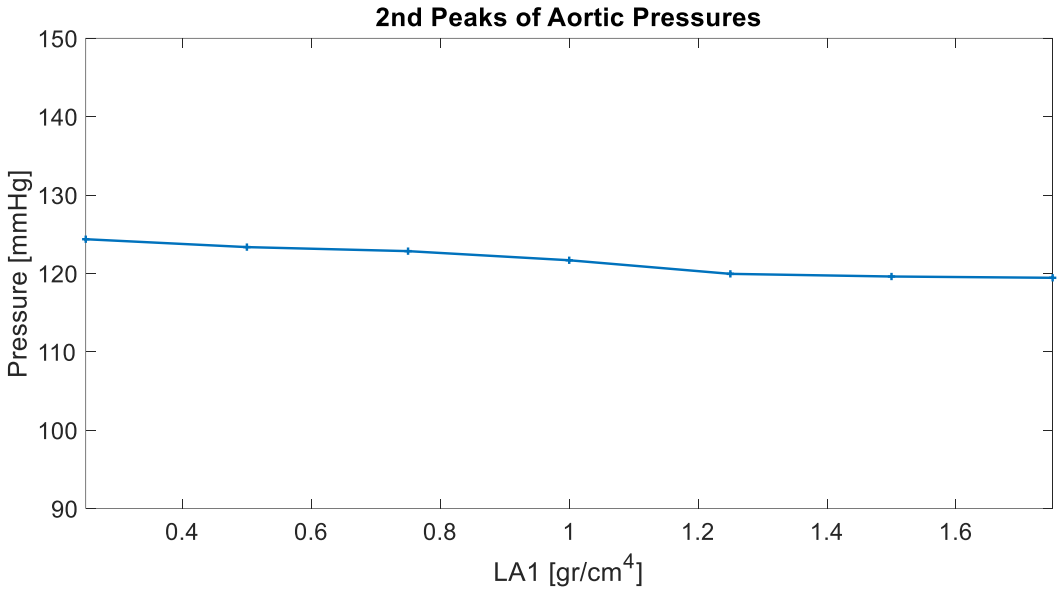

Figure A3.22 Second Peak of PA1 against LA1.

Both Figure A3.21 and Figure A3.22 show that as LA1 increases, PA1 decreases. There are some changes to the shape of PA1 signal when LA1 value is very big or very small. LA1 is the inertance in the first part of the aorta where the blood from the heart flows to the rest of the body. LA1 does not have a huge effect on the aortic signal because LA1 is after the PA1 which small impact since the model is a close loop system. Therefore, more blood circulation must be done to see a drastic change due to the effect of LA1.

12. Pulmonary Artery 3 Compliance (CP3)

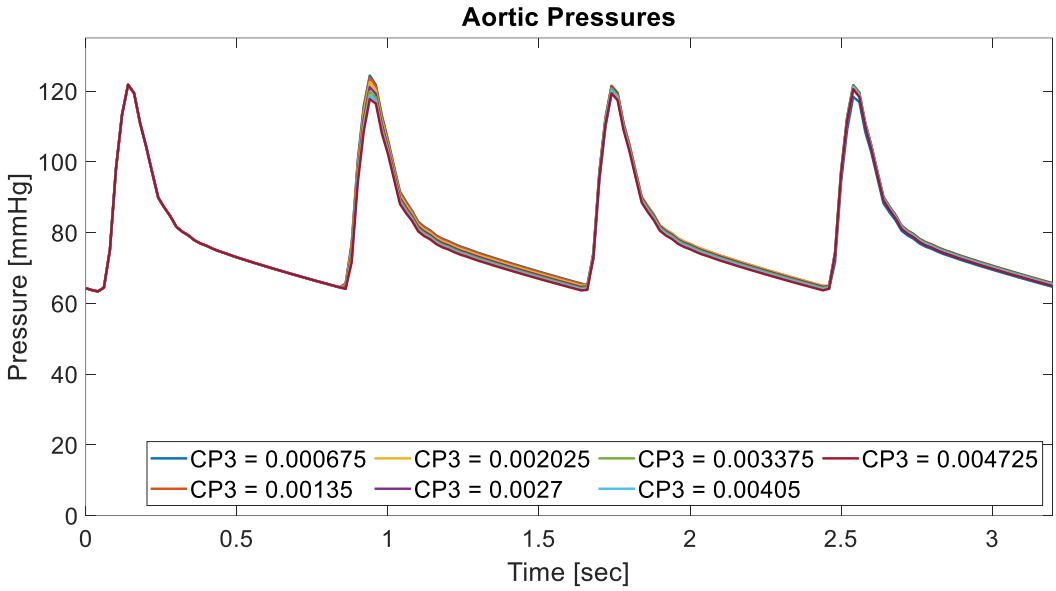

Figure A3.23 Effect of CP3 on PA1.

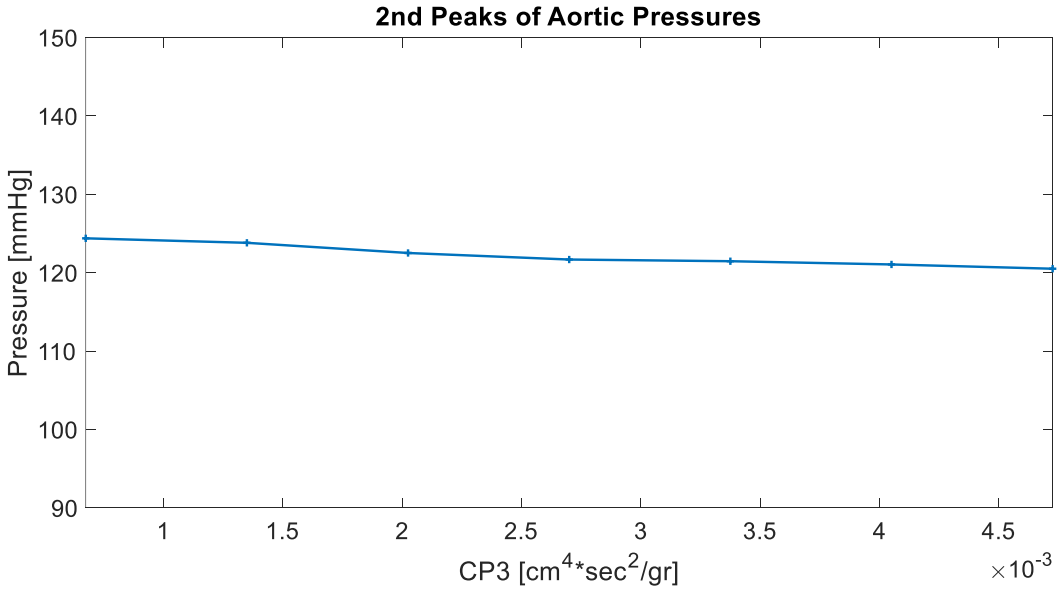

Figure A3.24 Second Peak of PA1 against CP3.

PA1 decreases as CP3 increases can be seen in Figure A3.23 and Figure A3.24. CP3 does not affect the shape of the response of the signal of PA1. CP3 is the compliance at the third part of the pulmonary artery where the blood flows from the pulmonary artery into the heart through the pulmonary vein. CP3 is a component located before the lungs which too far to give a big impact in aortic pressure response.

13. Left Atrium Compliance (CLA)

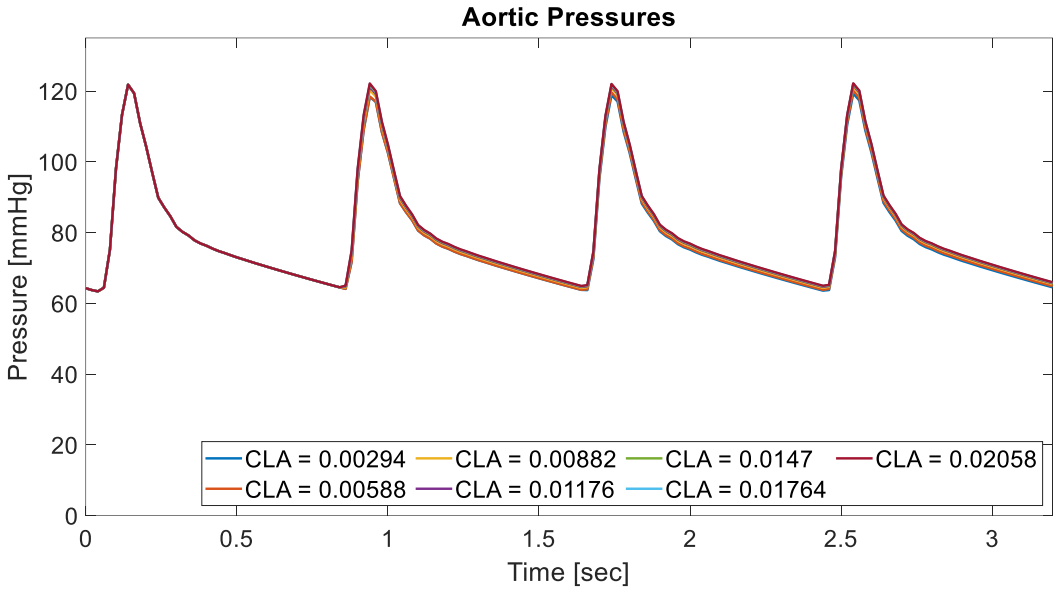

Figure A3.25 Effect of CLA on PA1.

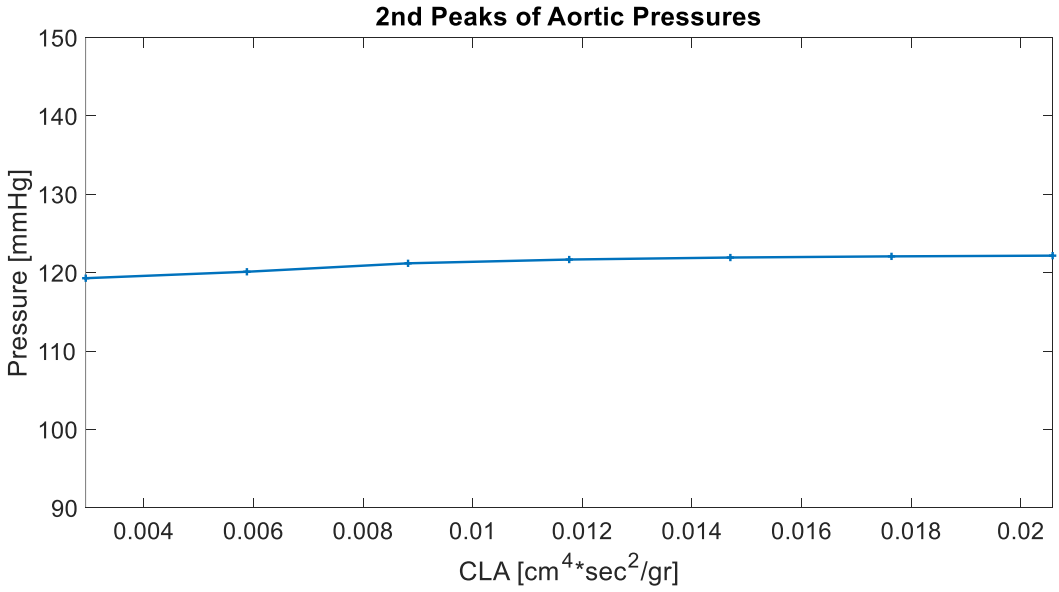

Figure A3.26 Second Peak of PA1 against CLA.

The above Figure A3.25 and Figure A3.26 shows that PA1 increases as CLA increases. CLA has no effect on the shape of the PA1 signal. CLA is the compliance at the left atrium where blood flows from the left atrium into the left ventricle then into the aorta. CLA has less effect on the aortic pressure signal.

14. Aortic 1 Compliance (CA1)

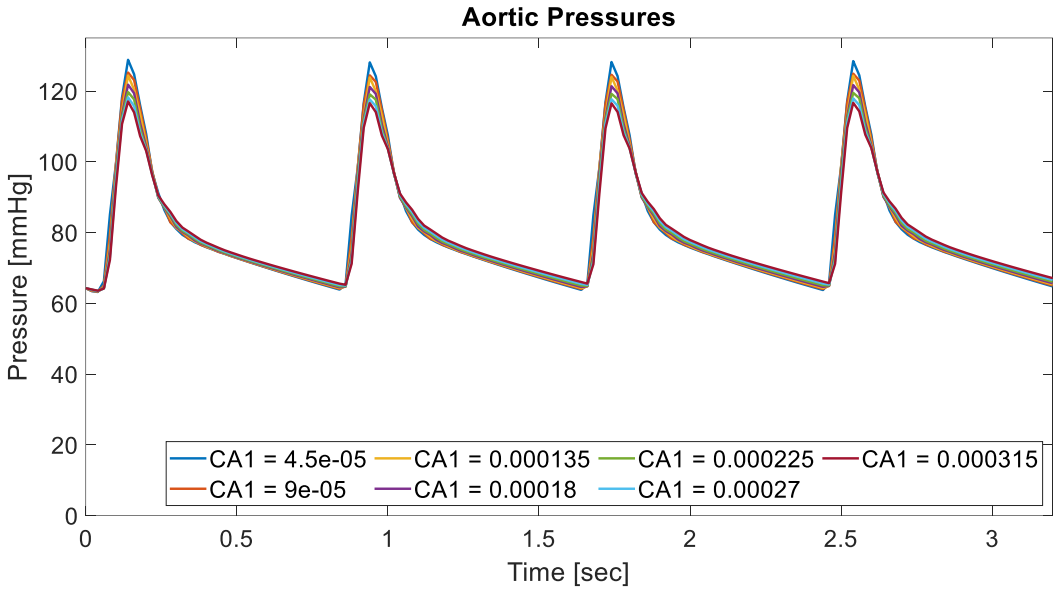

Figure A3.27 Effect of CA1 on PA1.

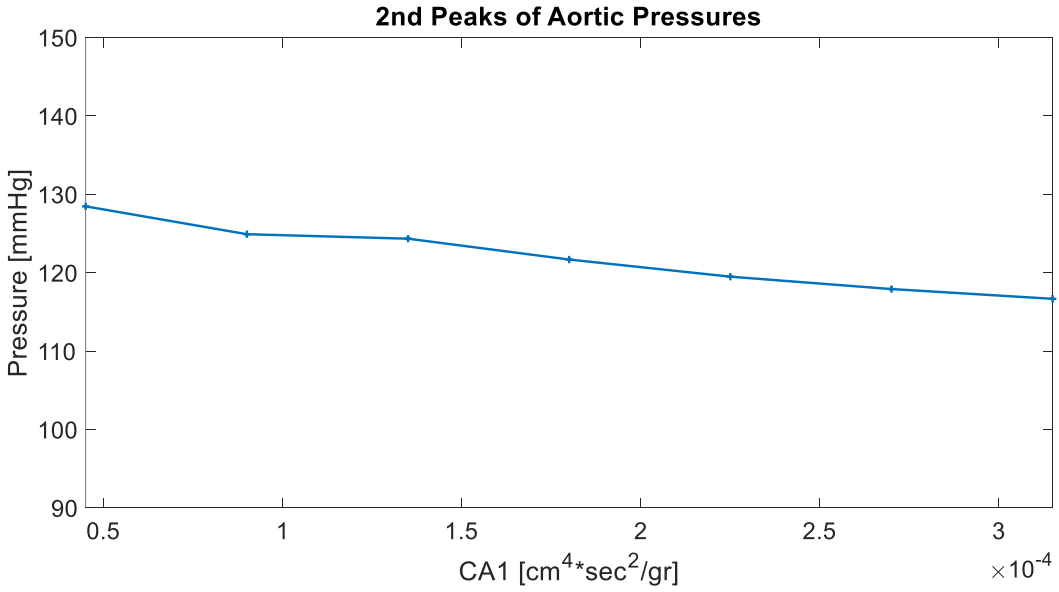

Figure A3.28 Second Peak of PA1 against CA1.

Figures A3.27 and A3.28 show the effect of CA1 on PA1 which shows that the systolic part of the response decreases significantly as CA1 increases while the diastolic part increases significantly. Change in CA1 has a significant effect on PA1 signal shape. CA1 is the compliance which is the elasticity of the wall in the first part of the aorta which has an impact on PA1. Therefore, when CA1 decreases the blood vessels becomes narrower resulting in the pressure to increases at PA1. Since this a 0D model which related to the electrical circuit, CA1 is represented by capacitance while PA1 is represented by the voltage at a point before CA1 resulting at the systolic part of the

response decreases due to capacitance charging while the diastolic part increases due to capacitance discharging.

15. Aortic 2 Compliance (CA2)

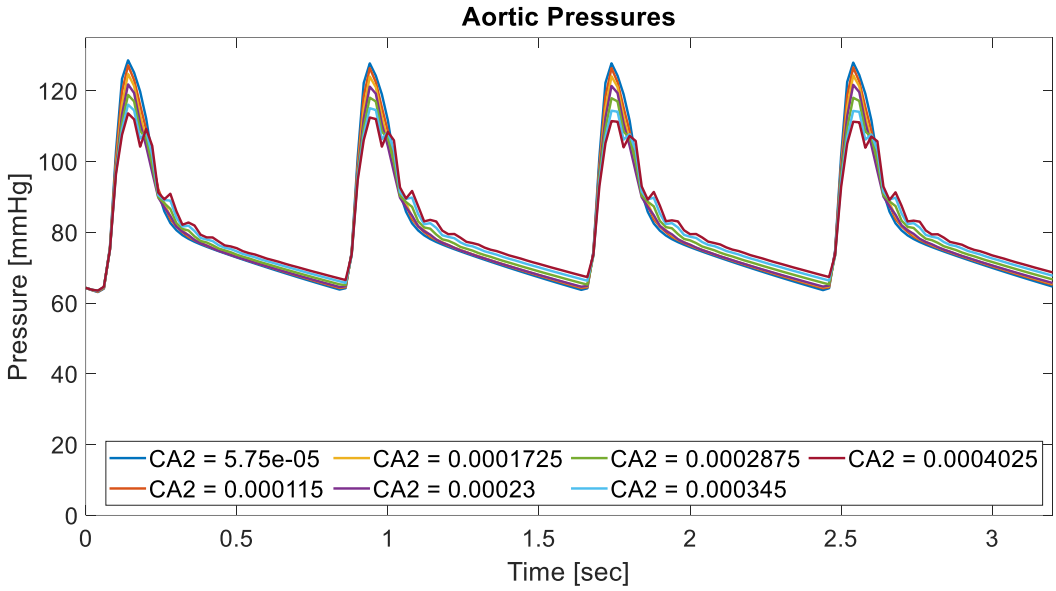

Figure A3.29 Effect of CA2 on PA1.

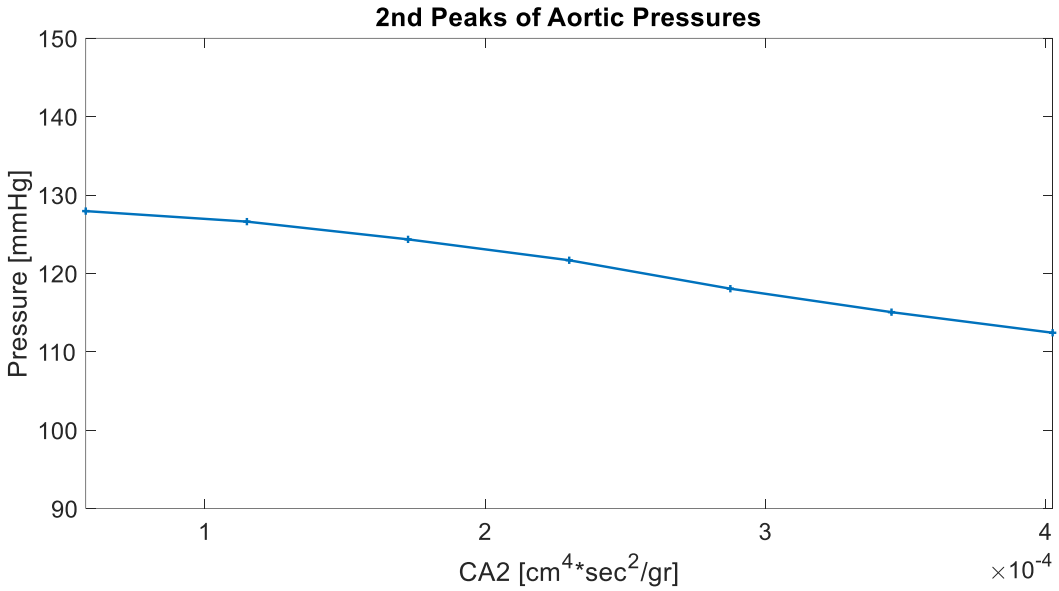

Figure A3.30 Second Peak of PA1 against CA2.

Both Figures A3.29 and A3.30 show how PA1 is affected by CA2. When CA2 increases, the systolic part of the response decreases while the diastolic part increases significantly. The shape of the response changes drastically when CA2 changes. Pa1 is effect by CA2 because CA2 is the compliance which is the elasticity of the wall in the second part of the aorta where the blood from the heart flows to the rest of the body. Therefore, CA2 increases, the pressure of the blood flow experience decreases due to the widening of the vessel. Since this a 0D model which related to the electrical circuit, CA2 is represented by capacitance while PA1 is represented by the voltage at a point

before CA2. Therefore, as CA2 increases, the systolic part of the response decreases due to the charging of capacitance while the diastolic part increases due to discharging of capacitance.

16. Aortic 3 Compliance (CA3)

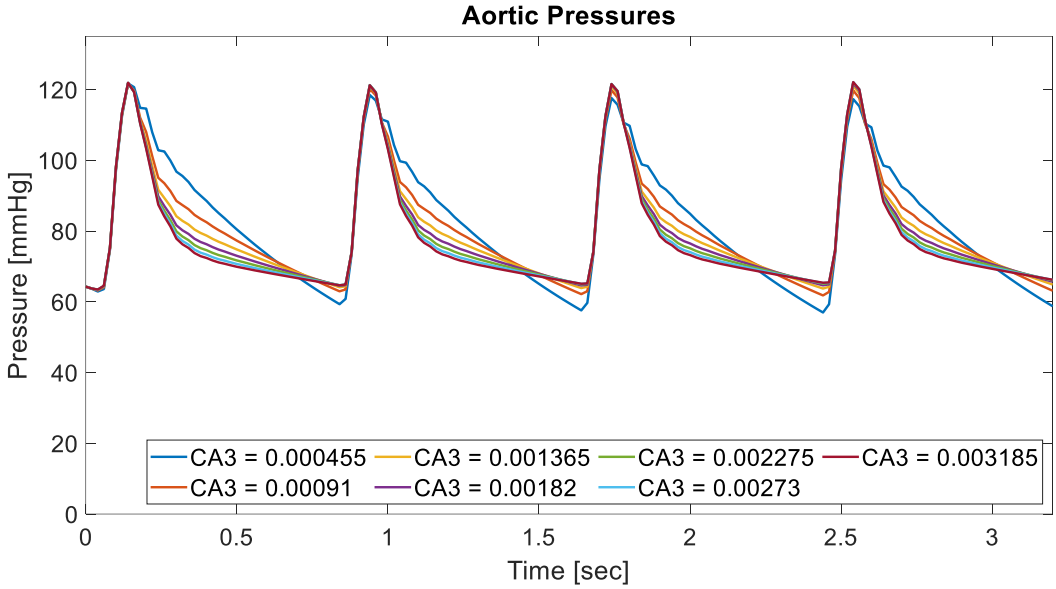

Figure A3.31 Effect of CA3 on PA1.

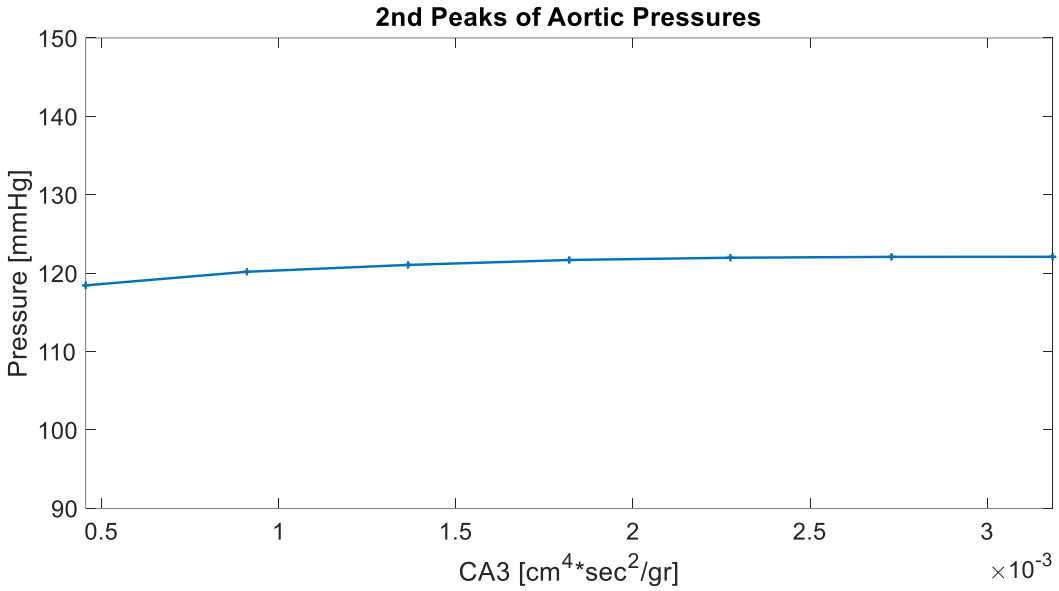

Figure A3.32 Second Peak of PA1 against CA3.

The effects of CA3 on PA1 both can be viewed on the above Figure A3.31 and Figure A3.32. The systolic part of the response increases as CA3 increases. The change in the PA1 signal due to the effect of CA3 is greater than the change of the peak. Moreover, an increment in CA3 causes the change of PA1 signal to be less at the systolic which is the peak of PA1signal but there is an increase at the diastolic part which is the valley of the PA1 signal.CA3 is the compliance at the third part of the aorta where the blood

from the heart flows to the rest of the body. CA3 does not have a huge impact on the Aortic signal.

The other 20 parameters do not have any significant effect on PA1. Some of these parameters have an effect on blood flow in other parts of the blood flow but not the aortic part. Therefore, even though these parameters do not affect PA1 which it the aortic pressure signal, but the parameter would affect other parts of the cardiovascular circulation system such as the pulmonary artery pressure (PP1).

Appendix 4

Table A4.1 The parameters values of the non-cardiovascular disease' signal (no clinical class and bleed) for the data obtained from the online database, PhysioNet [328].(Using EIF as the transfer function)

Parameters	**No Clinical class-subject 037**	**No Clinical class-subject 430**	**No Clinical class-subject 474**	**No Clinical class-subject 484**	**No Clinical class-subject 485**	**Bleed- Subject039**
RP2	39.23801	39.877243	39.574337	39.786343	39.542168	39.618458
RP3	80.074959	84.566902	80.300171	82.190086	82.343307	81.849365
RL1	28.938517	28.536709	29.759373	29.428387	28.893711	29.250366
RL2	10.98221	10.364404	10.419588	10.303884	10.472708	10.436772
RLA	5.2627368	5.34199	5.1317215	5.1972051	5.2490606	5.2122388
RA1	9.6456795	9.3374348	9.8979464	9.7775906	9.5212793	9.7677408
RA2	161.39848	164.26396	159.73138	161.28148	161.93599	161.18443
RA3	998.10468	983.66211	999.82172	992.10449	990.08618	992.06769
LLA	0.97762614	0.9961468	1.0099547	1.0092995	1.0052911	1.0057852
LLV	0.95166695	0.94926155	0.98413348	0.97552592	0.96106601	0.9693464
LA1	1.0309312	1.013317	0.99762625	0.99834746	1.0106878	1.0054561
CP3	0.002556005	0.00257289	0.00269266	0.002668403	0.002634889	0.002653254
CLA	0.01107895	0.011455808	0.011548613	0.01159981	0.011453104	0.011499938
CA1	0.000181434	0.000182436	0.000179722	0.000180513	0.000181671	0.000180926
CA2	0.000221951	0.000221192	0.000228239	0.000226575	0.00022315	0.000225127
CA3	0.001973349	0.001928198	0.001841168	0.001854143	0.001909321	0.00188379

Table A4.2 The parameters values of the non-cardiovascular disease' signal (respiratory failure) for the data obtained from the online database, PhysioNet [328].(Using EIF as the transfer function)

Parameters	**Respiratory failure-Subject055**	**Respiratory failure-Subject211**	**Respiratory failure-Subject226**	**Respiratory failure-Subject 252**	**Respiratory failure-Subject 411**	**Respiratory failure-Subject 437**	**Respiratory failure-Subject 439**	**Respiratory failure-Subject 443**
RP2	39.517422	39.93232	39.391911	39.76881	40.10714	39.598797	39.826	39.775715
RP3	79.926659	85.126015	81.184982	82.788895	84.910583	82.673134	82.164146	82.439407
RL1	29.728354	28.480762	29.010981	29.096697	28.725775	28.882122	29.42907	29.303665
RL2	10.442408	10.445491	10.558474	10.585011	10.685589	10.438455	10.290394	10.286405
RLA	5.1205125	5.3951035	5.2269154	5.2899885	5.4409852	5.2659864	5.2031355	5.2125897
RA1	9.8907404	9.3036785	9.5606956	9.6338949	9.4455423	9.4874802	9.751406	9.6590147
RA2	159.62439	164.39464	160.77388	162.51581	164.74991	161.89949	161.49274	161.38727
RA3	1001.031	980.50067	994.41626	988.09186	980.46362	988.98212	993.95392	991.31628
LLA	1.0112896	0.98666453	1.0057306	0.98567295	0.96037871	1.0051284	1.0078899	1.0108261
LLV	0.98382866	0.94391632	0.96334386	0.95866191	0.93809539	0.96022439	0.97527027	0.97332418
LA1	0.99837852	1.019208	1.0127746	1.015558	1.0295196	1.010524	0.99819678	0.99936163
CP3	0.00269475	0.002542545	0.002642749	0.002580919	0.002463145	0.002631717	0.002657501	0.002666679
CLA	0.01152809	0.01138217	0.011377756	0.011372162	0.011184433	0.011454619	0.011581975	0.011593985
CA1	0.00017978	0.000182588	0.00018144	0.000181203	0.000182008	0.000181735	0.000180431	0.000180779
CA2	0.00022816	0.000220074	0.000223283	0.00022358	0.000220549	0.000222797	0.000226663	0.000225795
CA3	0.00184678	0.001950905	0.001921367	0.001916062	0.001976528	0.001914376	0.001854239	0.001863527

Table A4.3 The parameters values of the non-cardiovascular disease' signal (brain injury and sepsis) for the data obtained from the online database PhysioNet [328].(Using EIF as the transfer function)

Parameters	**Brain injury-Subject220**	**Brain injury-Subject449**	**Sepsis-Subject222**	**Sepsis-Subject224**	**Sepsis-Subject438**
RP2	39.805714	39.949261	39.62365	39.689896	40.007732
RP3	83.461334	82.93	82.714546	82.163231	83.22155
RL1	28.972458	29.327848	28.919117	29.119371	29.303034
RL2	10.296579	10.225227	10.378671	10.666796	10.407898
RLA	5.2711945	5.2059598	5.2525506	5.2730412	5.2632961
RA1	9.5002909	9.7514456	9.499012	9.6278868	9.767061
RA2	162.23996	162.36986	161.88405	162.2583	163.10709
RA3	986.62372	989.80725	989.00177	993.37231	988.79169
LLA	1.0077012	1.0091474	1.0094477	0.98885149	0.98952574
LLV	0.96364099	0.97404778	0.96263808	0.96064675	0.96573919
LA1	1.0047547	0.99653339	1.0073178	1.0140712	1.0061437
CP3	0.002639245	0.002657074	0.002645341	0.002584516	0.002592569
CLA	0.011553092	0.011652189	0.011503946	0.011351477	0.011500692
CA1	0.000181552	0.00018065	0.000181651	0.000181065	0.000180655
CA2	0.000223628	0.000226793	0.000223366	0.000223814	0.00022569
CA3	0.001893274	0.00184561	0.00190219	0.001912523	0.001874694

Appendix 5

Table A5.1 The parameters values of the healthy signal (Subject 1- 8) for the data obtained from the online database, HaeMod [329] (Using EIF as the transfer function)

Parameters	Subject 1	Subject 2	Subject 3	Subject 4	Subject 5	Subject 6	Subject 7	Subject 8
RP2	39.3634	39.45466	38.82823	39.15096	38.96346	39.29315	38.54703	39.61002
RP3	79.68325	80.74871	76.25531	78.76041	77.66467	80.18013	74.80547	81.27654
RL1	29.41972	29.53754	28.88779	29.30357	29.03619	29.46703	28.70813	29.60924
RL2	10.58623	10.69536	10.7728	10.7802	10.88211	10.86863	10.97402	10.52111
RLA	5.135997	5.204149	5.038442	5.138916	5.125074	5.21669	5.020054	5.189476
RA1	9.85941	9.861643	9.782794	9.855654	9.795561	9.858142	9.775116	9.866318
RA2	160.2174	159.6792	160.8645	159.9473	160.3926	159.3242	160.7011	160.0154
RA3	1037.815	1012.574	1104.227	1047.605	1070.363	1015.869	1124.946	1009.464
LLA	0.96337	0.967909	0.922633	0.948609	0.932143	0.957423	0.902588	0.978737
LLV	1.016646	0.996717	1.055176	1.019516	1.028232	0.995395	1.065438	0.998162
LA1	1.007509	1.012231	1.019206	1.016116	1.023308	1.01998	1.028421	1.004393
CP3	0.002597	0.002609	0.002485	0.002562	0.002507	0.002584	0.002437	0.002634
CLA	0.011349	0.011326	0.011041	0.011189	0.011043	0.011195	0.010853	0.011457
CA1	0.000179	0.00018	0.000178	0.000179	0.000179	0.00018	0.000178	0.00018
CA2	0.000222	0.000223	0.000215	0.00022	0.000217	0.000222	0.000213	0.000225
CA3	0.001812	0.001856	0.001781	0.00183	0.001833	0.001878	0.001789	0.001833

Table A5.2 The parameters values of the healthy signal (Subject 9- 16) for the data obtained from the online database, HaeMod [329] (Using EIF as the transfer function)

Parameters	**Subject 9**	**Subject 10**	**Subject 11**	**Subject 12**	**Subject 13**	**Subject 14**	**Subject 15**	**Subject 16**
RP2	39.5615	39.10828	39.10661	39.69418	39.42353	39.2716	38.72961	39.45816
RP3	81.31915	78.54604	77.66157	81.72363	80.87667	79.50324	75.94761	80.26513
RL1	29.5813	29.10068	29.0699	29.64329	29.52089	29.36436	28.80427	29.46777
RL2	10.62658	10.79023	10.57131	10.46582	10.78625	10.70709	10.87062	10.52721
RLA	5.211567	5.143284	5.054874	5.194953	5.226018	5.154395	5.047381	5.148018
RA1	9.857966	9.789357	9.792316	9.863374	9.853756	9.853432	9.76925	9.857489
RA2	159.7813	160.5163	161.0228	160.0956	159.4483	160.0243	160.795	160.2775
RA3	1007.405	1060.076	1083.892	1005.432	1009.504	1038.572	1109.143	1030.763
LLA	0.972144	0.939773	0.942725	0.982155	0.962489	0.955014	0.913754	0.968519
LLV	0.995167	1.023362	1.045201	0.996982	0.993437	1.015352	1.056634	1.013402
LA1	1.009556	1.019541	1.009897	1.002245	1.016784	1.012963	1.024012	1.004977
CP3	0.00262	0.002525	0.002533	0.002643	0.002598	0.002578	0.002464	0.00261
CLA	0.011388	0.01113	0.011228	0.011506	0.01127	0.011262	0.010959	0.011407
CA1	0.00018	0.000179	0.000179	0.00018	0.00018	0.00018	0.000179	0.000179
CA2	0.000224	0.000219	0.000218	0.000225	0.000223	0.000221	0.000214	0.000223
CA3	0.001851	0.00183	0.001772	0.001829	0.001872	0.001828	0.001791	0.00181

Table A5.3 The parameters values of the healthy signal (Subject 17- 24) for the data obtained from the online database, HaeMod [329] (Using EIF as the transfer function)

Parameters	**Subject 17**	**Subject 18**	**Subject 19**	**Subject 20**	**Subject 21**	**Subject 22**	**Subject 23**	**Subject 24**
RP2	39.22804	39.55336	39.2251	38.97998	39.66813	39.55244	39.39134	39.13189
RP3	78.41201	81.5733	79.5961	77.19939	81.88821	80.84541	80.24587	78.14745
RL1	29.13207	29.57586	29.33695	28.96669	29.6257	29.51641	29.42599	29.045
RL2	10.50111	10.70512	10.79926	10.68595	10.55872	10.46883	10.63496	10.59914
RLA	5.072667	5.235426	5.178124	5.06092	5.2188	5.16008	5.169992	5.083656
RA1	9.787481	9.850073	9.848184	9.777402	9.854924	9.855939	9.851732	9.771596
RA2	161.0941	159.5639	159.8447	160.947	159.8761	160.332	160.093	161.0293
RA3	1073.542	1003.143	1035.739	1091.194	1002.245	1023.726	1029.53	1078.14
LLA	0.950202	0.967451	0.949356	0.931939	0.976299	0.973618	0.961356	0.941224
LLV	1.039378	0.991547	1.012437	1.04789	0.993682	1.010191	1.011218	1.040568
LA1	1.006932	1.013618	1.017117	1.015521	1.006912	1.002472	1.00984	1.011858
CP3	0.002551	0.002612	0.002567	0.002507	0.002632	0.002623	0.002595	0.002529
CLA	0.011298	0.011344	0.011203	0.011129	0.01145	0.011465	0.011334	0.011216
CA1	0.000179	0.00018	0.00018	0.000179	0.00018	0.00018	0.00018	0.000179
CA2	0.000219	0.000223	0.000221	0.000217	0.000224	0.000224	0.000222	0.000218
CA3	0.001773	0.001867	0.001844	0.001782	0.001846	0.001808	0.001826	0.001783

Table A5.4 The parameters values of the healthy signal (Subject 25- 32) for the data obtained from the online database, HaeMod [329] (Using EIF as the transfer function)

Parameters	**Subject 25**	**Subject 26**	**Subject 27**	**Subject 28**	**Subject 29**	**Subject 30**	**Subject 31**	**Subject 32**
RP2	39.3498	38.91232	39.45691	39.5949	39.72555	39.05441	39.24838	39.43858
RP3	79.16554	77.09496	81.6878	82.01167	82.28635	78.97825	79.72244	80.42806
RL1	29.1936	28.89993	29.55291	29.602	29.6542	29.04164	29.16634	29.29392
RL2	10.43081	10.76729	10.94787	10.76099	10.57326	10.96506	10.76969	10.57252
RLA	5.090658	5.075052	5.284634	5.261414	5.235075	5.199034	5.187316	5.173844
RA1	9.782234	9.762976	9.838061	9.843357	9.850899	9.775809	9.786634	9.798039
RA2	161.167	160.8871	158.9397	159.3991	159.8249	160.2594	160.4829	160.7013
RA3	1063.18	1093.315	995.0317	995.6318	996.3172	1053.592	1045.02	1036.54
LLA	0.957666	0.924881	0.954875	0.965352	0.97632	0.927654	0.943063	0.958883
LLV	1.033522	1.047804	0.982069	0.985866	0.989764	1.017436	1.015417	1.013353
LA1	1.003979	1.019631	1.02537	1.016741	1.008023	1.027674	1.01883	1.00981
CP3	0.002568	0.00249	0.002586	0.002609	0.002633	0.002501	0.002538	0.002575
CLA	0.011367	0.011065	0.011188	0.011319	0.011451	0.011027	0.011185	0.011342
CA1	0.000179	0.000179	0.000181	0.00018	0.00018	0.00018	0.00018	0.00018
CA2	0.00022	0.000216	0.000222	0.000223	0.000224	0.000217	0.000219	0.000221
CA3	0.001774	0.001792	0.001912	0.001884	0.001855	0.00186	0.001839	0.001818

Table A5.5 The parameters values of the healthy signal (Subject 33-40) for the data obtained from the online database, HaeMod [329] (Using EIF as the transfer function)

Parameters	**Subject 33**	**Subject 34**	**Subject 35**	**Subject 36**	**Subject 37**	**Subject 38**	**Subject 39**	**Subject 40**
RP2	38.63203	38.89622	39.59066	39.15894	39.70489	39.8109	39.36528	39.19706
RP3	76.13477	77.38908	82.40346	78.59615	82.59269	82.73679	80.4429	79.85748
RL1	28.72286	28.89561	29.61086	29.06998	29.64824	29.69006	29.22264	29.11112
RL2	11.05255	10.83981	10.86837	10.62447	10.69436	10.51983	10.69678	10.87865
RLA	5.093838	5.101328	5.294824	5.106488	5.268708	5.240518	5.202097	5.217327
RA1	9.754626	9.763469	9.835151	9.773136	9.841186	9.849159	9.783763	9.77312
RA2	160.5396	160.7243	159.0598	160.9134	159.498	159.9019	160.5582	160.3445
RA3	1105.995	1088.268	988.3912	1070.965	990.2877	992.2103	1036.548	1043.246
LLA	0.900544	0.920809	0.959701	0.941294	0.969378	0.97958	0.949194	0.934916
LLV	1.052592	1.044276	0.980061	1.036218	0.984344	0.988623	1.011532	1.012797
LA1	1.032587	1.022852	1.02225	1.012936	1.014136	1.005924	1.015801	1.024067
CP3	0.002436	0.002484	0.0026	0.002532	0.00262	0.002642	0.002553	0.00252
CLA	0.010843	0.011032	0.011262	0.01122	0.011381	0.0115	0.011256	0.011113
CA1	0.000179	0.000179	0.000181	0.000179	0.00018	0.00018	0.00018	0.00018
CA2	0.000213	0.000215	0.000222	0.000218	0.000224	0.000225	0.00022	0.000218
CA3	0.001818	0.001805	0.001907	0.001792	0.001879	0.001851	0.001836	0.001857

Appendix 6

Table A6.1 The parameters values of the cardiovascular disease' signal (Subject 1- 8) for the data obtained from the hospital. (Using EIF as the transfer function)

Parameters	**Subject 1**	**Subject 2**	**Subject 3**	**Subject 4**	**Subject 5**	**Subject 6**	**Subject 7**	**Subject 8**
RP2	39.78507	40.30789	40.88503	39.21776	39.7222	40.28477	39.13254	39.64227
RP3	83.86764	84.29356	83.204	79.83035	84.99749	82.67987	84.92927	82.25959
RL1	28.31026	28.8603	28.16808	29.0582	28.1491	29.0618	27.94537	28.66923
RL2	10.56688	10.64069	9.909514	10.3	10.54658	10.70567	10.42001	10.61057
RLA	5.326618	5.317311	5.492189	5.103679	5.310422	5.277943	5.307738	5.269579
RA1	9.393786	9.766793	9.23714	9.550888	9.307847	9.897266	9.073786	9.525552
RA2	165.1514	167.1254	174.1016	159.775	166.9591	166.1713	163.2065	164.3492
RA3	1002.1	998.4396	1038.48	1018.067	989.8737	1014.259	979.0867	1004.518
LLA	0.970028	0.945039	0.947885	1.012827	0.970503	0.938475	1.011862	0.975358
LLV	0.961852	0.965004	0.92405	0.99447	0.950684	0.977872	0.951308	0.961934
LA1	1.022592	1.020726	1.019698	0.999867	1.022458	1.021082	1.017333	1.01955
CP3	0.002515	0.002453	0.002124	0.002686	0.002504	0.002449	0.002651	0.00253
CLA	0.011345	0.01135	0.0108	0.011504	0.011369	0.011293	0.011539	0.011283
CA1	0.000182	0.000181	0.000181	0.000181	0.000183	0.00018	0.000184	0.000182
CA2	0.000219	0.000223	0.000227	0.000223	0.000218	0.000224	0.000216	0.000221
CA3	0.001918	0.001876	0.001877	0.001854	0.001926	0.001862	0.001939	0.001915

Table A6.2 The parameters values of the cardiovascular disease' signal (Subject 9-16) for the data obtained from the hospital. (Using EIF as the transfer function)

Parameters	**Subject 9**	**Subject 10**	**Subject 11**	**Subject 12**	**Subject 13**	**Subject 14**	**Subject 15**	**Subject 16**
RP2	40.54387	39.83043	39.59547	40.62866	39.42387	39.3453	39.89477	39.54234
RP3	81.83505	82.39291	81.43162	81.2783	85.11646	85.85989	84.00452	82.76717
RL1	29.32577	29.16047	28.78874	29.64231	27.94984	27.34894	28.86354	28.96233
RL2	10.5466	10.14465	10.2885	10.30415	10.17203	10.13845	10.16344	10.15528
RLA	5.333625	5.200994	5.141122	5.249208	5.378904	5.36537	5.228127	5.200161
RA1	9.81105	9.612562	9.510343	9.823032	9.017818	8.783681	9.515554	9.47038
RA2	166.9731	162.4019	162.687	165.9248	163.0648	163.8258	163.793	161.7707
RA3	1025.926	1012.259	1019.552	1020.928	994.895	990.5536	994.2947	1004.232
LLA	0.923156	1.000082	0.995354	0.947447	1.013042	1.021234	1.005024	1.0109
LLV	0.967051	0.98941	0.99184	0.970147	0.958887	0.956608	0.975147	0.983533
LA1	1.019816	0.996013	1.002669	1.004207	1.011423	1.015187	0.998447	0.996751
CP3	0.002303	0.002628	0.00262	0.002365	0.002628	0.002643	0.002633	0.002668
CLA	0.010969	0.011599	0.011524	0.011129	0.011554	0.011601	0.011677	0.011635
CA1	0.000179	0.00018	0.000181	0.000179	0.000183	0.000185	0.000181	0.000181
CA2	0.000226	0.000224	0.000222	0.000229	0.000216	0.000213	0.000224	0.000222
CA3	0.001867	0.001825	0.001846	0.001836	0.001919	0.001943	0.001842	0.001843

Table A6.3 The parameters values of the cardiovascular disease' signal (Subject 17-24) for the data obtained from the hospital. (Using EIF as the transfer function)

Parameters	**Subject 17**	**Subject 18**	**Subject 19**	**Subject 20**	**Subject 21**	**Subject 22**	**Subject 23**	**Subject 24**
RP2	39.39385	39.29086	39.70902	39.2767	39.28117	39.55988	39.74094	40.04008
RP3	78.83205	81.59177	81.7802	79.57944	83.05164	80.21077	81.84816	83.66762
RL1	29.39375	28.8961	29.18708	28.9141	28.27311	29.6099	30.16972	28.88827
RL2	10.27394	10.31232	10.29064	10.39899	10.49385	10.61272	10.61423	10.46158
RLA	5.044195	5.201638	5.187767	5.120599	5.245221	5.277572	5.136154	5.298171
RA1	9.776069	9.465458	9.651126	9.577251	9.268559	9.748384	10.1629	9.668142
RA2	160.4531	159.7257	161.897	161.2044	164.0056	159.8327	157.9113	165.5795
RA3	1040.676	1005.591	1009.426	1035.342	994.9805	1020.362	980.4936	1003.523
LLA	0.996036	1.014249	0.999234	0.991952	0.998714	0.964383	0.991526	0.966342
LLV	1.015396	0.984984	0.985367	1.000161	0.956473	0.983099	1.000064	0.969848
LA1	0.994428	1.003306	1.000074	1.00584	1.016476	1.014608	1.000617	1.01372
CP3	0.002652	0.002695	0.002634	0.002619	0.002597	0.002514	0.002744	0.002512
CLA	0.01151	0.011551	0.011541	0.011395	0.011405	0.011097	0.011693	0.011419
CA1	0.000179	0.000181	0.00018	0.00018	0.000183	0.000179	0.00018	0.000181
CA2	0.000224	0.000221	0.000224	0.000221	0.000219	0.000225	0.000228	0.000223
CA3	0.001794	0.001872	0.001844	0.001848	0.001924	0.001866	0.001809	0.001865

Table A6.4 The parameters values of the cardiovascular disease' signal (Subject 25-32) for the data obtained from the hospital. (Using EIF as the transfer function)

Parameters	**Subject 25**	**Subject 26**	**Subject 27**	**Subject 28**	**Subject 29**	**Subject 30**	**Subject 31**	**Subject 32**
RP2	39.5972	39.76974	39.66606	39.95445	40.51241	40.35958	40.04538	39.35351
RP3	84.88481	82.39924	79.97308	83.28428	86.03311	80.70664	83.89916	79.51886
RL1	28.39052	28.93549	29.71853	29.01123	28.82498	29.52481	28.68183	29.18839
RL2	10.56845	10.49408	10.22441	10.60476	10.7668	10.26776	10.50201	10.4595
RLA	5.2762	5.275491	5.068581	5.315076	5.352051	5.283338	5.309228	5.121681
RA1	9.488317	9.598325	9.914555	9.74966	10.00933	9.77284	9.608981	9.735082
RA2	166.0678	162.9983	160.5467	165.4936	169.9439	165.6393	167.0605	160.7611
RA3	985.1636	1014.361	1023.81	1013.24	983.1848	1032.466	1008.491	1033.788
LLA	0.979904	0.968277	1.00176	0.944958	0.934605	0.959635	0.954665	0.98734
LLV	0.957801	0.982314	1.009456	0.976561	0.957342	0.970556	0.967173	1.003714
LA1	1.017615	1.01344	0.989354	1.019168	1.023267	1.005387	1.017635	1.004607
CP3	0.002567	0.002539	0.002678	0.002464	0.002434	0.002385	0.002463	0.002624
CLA	0.011524	0.011342	0.011634	0.011291	0.011493	0.011091	0.011343	0.011419
CA1	0.000182	0.000181	0.000179	0.00018	0.00018	0.000179	0.000181	0.00018
CA2	0.00022	0.000221	0.000227	0.000222	0.000226	0.000229	0.000222	0.000223
CA3	0.001881	0.001875	0.001778	0.00186	0.001827	0.001831	0.001871	0.001828

Table A6.5 The parameters values of the cardiovascular disease' signal (Subject 33-40) for the data obtained from the hospital. (Using EIF as the transfer function)

Parameters	**Subject 33**	**Subject 34**	**Subject 35**	**Subject 36**	**Subject 37**	**Subject 38**	**Subject 39**	**Subject 40**
RP2	40.28597	39.72188	39.25089	39.41731	40.61163	39.49765	40.69701	39.28664
RP3	82.73221	83.20364	83.251	82.76387	83.01474	82.81028	83.28427	83.72625
RL1	29.05312	28.75974	28.38106	28.79524	29.35284	28.84336	28.89037	28.46718
RL2	10.34022	10.46508	10.49065	10.33247	10.18529	10.40445	10.54909	9.801131
RLA	5.304462	5.266884	5.25467	5.245479	5.284536	5.227933	5.302068	5.205571
RA1	9.57909	9.571782	9.35922	9.513878	9.709211	9.593871	9.749054	8.920178
RA2	165.5589	164.4319	163.1355	162.052	166.4116	162.5748	168.7897	158.968
RA3	1012.221	1005.655	998.2877	1002.356	1005.299	1003.181	1011.8	971.9353
LLA	0.967057	0.977012	0.995127	1.003545	0.967801	0.994731	0.93193	1.070081
LLV	0.964486	0.972362	0.968121	0.976432	0.962214	0.980278	0.963681	0.962165
LA1	1.008828	1.012479	1.014889	1.005645	1.003111	1.006584	1.018852	0.990393
CP3	0.002456	0.002554	0.002617	0.002649	0.002435	0.002632	0.002353	0.002806
CLA	0.011262	0.011444	0.011476	0.011571	0.011315	0.011568	0.011197	0.011767
CA1	0.00018	0.000181	0.000183	0.000181	0.00018	0.000181	0.00018	0.000184
CA2	0.000225	0.000222	0.000219	0.000222	0.000228	0.000222	0.000225	0.00022
CA3	0.001881	0.001868	0.001894	0.001856	0.001851	0.001845	0.001885	0.001927

Appendix 7

Table A7.1 The parameters values of the non-cardiovascular disease' signal (no clinical class and bleed) for the data obtained from the online database, PhysioNet [328].(Using GTF as the transfer function)

Parameters	**No Clinical class-subject 037**	**No Clinical class-subject 430**	**No Clinical class-subject 474**	**No Clinical class-subject 484**	**No Clinical class-subject 485**	**Bleed- Subject039**
RP2	39.768658	39.753468	39.576603	39.772488	39.479378	39.574848
RP3	81.376137	82.722649	79.993423	81.518333	80.656593	80.708054
RL1	29.675625	29.168232	29.819574	29.645863	29.324749	29.527449
RL2	10.257393	10.26039	10.42291	10.244063	10.480638	10.416709
RLA	5.1482286	5.2257934	5.1163015	5.148932	5.1834812	5.1569929
RA1	9.8412342	9.5899153	9.939229	9.8213844	9.716485	9.7976999
RA2	160.60188	161.69409	159.72935	160.66144	160.56093	160.35089
RA3	995.69684	987.31006	1002.1807	995.95044	997.3241	998.81708
LLA	1.014523	1.0138181	1.0092772	1.0152485	1.0081882	1.0096961
LLV	0.98363459	0.96775228	0.98687732	0.98374516	0.97237849	0.97917503
LA1	0.99228376	0.99956363	0.99655628	0.99242324	1.0043818	1.0002393
CP3	0.002696325	0.002664338	0.002693882	0.002697173	0.002664788	0.002678379
CLA	0.011653398	0.011600327	0.011549922	0.011659592	0.011461013	0.01152595
CA1	0.000179949	0.000181314	0.000179532	0.000179973	0.00018067	0.000180185
CA2	0.000228428	0.00022524	0.000228738	0.000228202	0.000225783	0.000227023
CA3	0.001827581	0.001875537	0.001833441	0.001827616	0.001881245	0.001857216

Table A7.2 The parameters values of the non-cardiovascular disease' signal (respiratory failure) for the data obtained from the online database, PhysioNet [328].(Using GTF as the transfer function)

Parameters	**Respiratory failure-Subject055**	**Respiratory failure-Subject211**	**Respiratory failure-Subject226**	**Respiratory failure-Subject 252**	**Respiratory failure-Subject 411**	**Respiratory failure-Subject 437**	**Respiratory failure-Subject 439**	**Respiratory failure-Subject 443**
RP2	39.495876	39.699436	39.450138	39.686386	39.823921	39.626617	39.802177	39.743797
RP3	79.441338	82.766586	80.183662	81.645142	83.015152	81.349869	81.591476	81.512054
RL1	29.815395	29.02664	29.476547	29.439188	29.166794	29.414686	29.664755	29.578247
RL2	10.481297	10.360232	10.488004	10.377567	10.389877	10.347476	10.213487	10.250495
RLA	5.1089425	5.2580209	5.1507535	5.1894989	5.2649937	5.1737456	5.1492915	5.154984
RA1	9.9491205	9.5351076	9.7866592	9.7502203	9.6110926	9.7248087	9.8213301	9.7886992
RA2	159.49049	161.83818	159.9827	160.95259	162.09496	160.66196	160.68362	160.6367
RA3	1003.4719	990.32684	1001.7001	992.4165	988.75983	995.82245	996.42041	996.51959
LLA	1.0090551	1.0064955	1.0075123	1.0077864	0.9989209	1.0129194	1.0160317	1.0152379
LLV	0.98568058	0.9649359	0.9800055	0.9740318	0.9657251	0.9769172	0.9849215	0.9832512
LA1	0.9981938	1.0060638	1.0031554	1.0005518	1.0063852	0.9992666	0.9910886	0.9934284
CP3	0.00269310	0.0026391	0.0026752	0.0026657	0.0026231	0.0026806	0.0026989	0.0026951
CLA	0.01150705	0.0115065	0.0114701	0.0115565	0.0115019	0.011564	0.0116744	0.0116453
CA1	0.00017951	0.0001814	0.0001803	0.0001806	0.0001811	0.0001805	0.0001799	0.0001801
CA2	0.00022873	0.0002238	0.0002264	0.0002265	0.0002244	0.0002265	0.0002283	0.0002277
CA3	0.00184172	0.0018953	0.0018665	0.0018641	0.0018881	0.0018599	0.0018228	0.0018329

Table A7.3 The parameters values of the non-cardiovascular disease' signal (brain injury and sepsis) for the data obtained from the online database PhysioNet [328].(Using GTF as the transfer function)

Parameters	**Brain injury-Subject220**	**Brain injury-Subject449**	**Sepsis-Subject222**	**Sepsis-Subject224**	**Sepsis-Subject438**
RP2	39.711735	39.798492	39.708889	39.533443	39.849735
RP3	81.860451	81.754906	81.600784	80.791618	82.155609
RL1	29.375975	29.549376	29.477337	29.401257	29.542809
RL2	10.275523	10.237569	10.255637	10.506886	10.264812
RLA	5.1836247	5.1592989	5.1630878	5.1848025	5.1813192
RA1	9.6935406	9.7911081	9.7409868	9.7498617	9.7787857
RA2	160.97676	161.10236	160.757	160.70084	161.32257
RA3	994.82574	996.12524	995.80432	997.63959	992.16217
LLA	1.0140227	1.0138409	1.016547	1.0034988	1.0097182
LLV	0.97762704	0.98264277	0.98065037	0.97197443	0.97773916
LA1	0.99717951	0.99322808	0.99471974	1.0061612	0.99567628
CP3	0.002680806	0.002687736	0.002693187	0.002649067	0.002670346
CLA	0.011605487	0.011656588	0.011633269	0.011442668	0.011635758
CA1	0.000180568	0.000180114	0.000180338	0.000180527	0.000180305
CA2	0.000226366	0.000227817	0.000227169	0.000225906	0.00022744
CA3	0.001853255	0.001829117	0.00184157	0.001882756	0.001842299

Appendix 8

Table A8.1 The parameters values of the healthy signal (Subject 1- 8) for the data obtained from the online database, HaeMod [329] (Using GTF as the transfer function)

Parameters	Subject 1	Subject 2	Subject 3	Subject 4	Subject 5	Subject 6	Subject 7	Subject 8
RP2	39.5445	39.58885	39.18506	39.37123	39.19151	39.45853	38.97633	39.71614
RP3	80.4643	80.81493	78.54472	79.7028	78.89607	80.26527	77.54218	81.33041
RL1	29.70308	29.64831	29.59438	29.64576	29.53598	29.59827	29.54167	29.7042
RL2	10.55335	10.60015	10.87809	10.74488	10.89888	10.75615	11.1004	10.4443
RLA	5.156299	5.174516	5.158398	5.163935	5.170693	5.183504	5.162485	5.165338
RA1	9.893453	9.869649	9.909936	9.899509	9.878242	9.869545	9.926168	9.872599
RA2	159.7714	160.0009	159.2056	159.4139	159.1981	159.7692	158.744	160.219
RA3	995.2844	991.7814	1004.955	996.8105	1000.781	992.013	1007.512	991.7078
LLA	1.002133	0.997993	0.989529	0.994663	0.989141	0.991937	0.981244	1.004246
LLV	0.977568	0.974179	0.9726	0.972838	0.968727	0.969085	0.967784	0.979208
LA1	1.004657	1.007421	1.01754	1.012794	1.019829	1.014361	1.026692	1.000436
CP3	0.00267	0.002659	0.002632	0.00265	0.002629	0.00264	0.00261	0.002678
CLA	0.011474	0.011445	0.011216	0.01134	0.011213	0.011334	0.011061	0.011556
CA1	0.00018	0.00018	0.00018	0.00018	0.00018	0.00018	0.00018	0.00018
CA2	0.000227	0.000227	0.000226	0.000226	0.000225	0.000226	0.000225	0.000228
CA3	0.001869	0.001881	0.00191	0.001898	0.001925	0.001908	0.001943	0.001854

Table A8.2 The parameters values of the healthy signal (Subject 9- 16) for the data obtained from the online database, HaeMod [329] (Using GTF as the transfer function)

Parameters	**Subject 9**	**Subject 10**	**Subject 11**	**Subject 12**	**Subject 13**	**Subject 14**	**Subject 15**	**Subject 16**
RP2	39.67374	39.31225	39.39604	39.78303	39.56205	39.47203	39.10983	39.62471
RP3	81.29128	79.5831	79.5287	81.70443	80.84918	80.26904	78.30803	80.91361
RL1	29.65393	29.54514	29.65096	29.70945	29.60441	29.65481	29.55058	29.71061
RL2	10.52278	10.78527	10.65595	10.38253	10.66318	10.64997	10.96784	10.47777
RLA	5.177673	5.175704	5.152721	5.168098	5.187659	5.167144	5.167679	5.158804
RA1	9.85769	9.859713	9.895996	9.863571	9.854463	9.884921	9.903633	9.881987
RA2	160.197	159.4834	159.6611	160.3725	160.0113	159.647	159.0752	159.9552
RA3	990.2155	998.3325	1002.367	990.5041	990.0393	994.6905	1005.049	993.6136
LLA	1.000349	0.992862	0.997919	1.006194	0.994724	0.997886	0.985634	1.004704
LLV	0.975633	0.97044	0.977443	0.980342	0.970797	0.97418	0.969839	0.978675
LA1	1.004461	1.015563	1.008345	0.998064	1.010809	1.009247	1.021709	1.001815
CP3	0.002666	0.002639	0.002655	0.002683	0.002649	0.002658	0.002621	0.002677
CLA	0.011502	0.011294	0.011372	0.011601	0.011402	0.011409	0.011154	0.011529
CA1	0.00018	0.00018	0.00018	0.00018	0.00018	0.00018	0.00018	0.00018
CA2	0.000227	0.000226	0.000227	0.000228	0.000226	0.000227	0.000225	0.000228
CA3	0.00187	0.00191	0.001877	0.001845	0.001895	0.001886	0.001925	0.001859

Table A8.3 The parameters values of the healthy signal (Subject 17- 24) for the data obtained from the online database, HaeMod [329] (Using GTF as the transfer function)

Parameters	Subject 17	Subject 18	Subject 19	Subject 20	Subject 21	Subject 22	Subject 23	Subject 24
RP2	39.48743	39.66507	39.44004	39.29813	39.75785	39.70482	39.57325	39.41251
RP3	80.03927	81.43114	80.2872	79.18324	81.76599	81.36444	80.83997	79.82837
RL1	29.65605	29.60987	29.61301	29.60061	29.65909	29.7182	29.66375	29.60589
RL2	10.56633	10.57089	10.70993	10.76658	10.44624	10.40262	10.55541	10.65449
RLA	5.155795	5.191802	5.17904	5.162395	5.181514	5.16137	5.170507	5.166656
RA1	9.880495	9.839521	9.872047	9.890505	9.845931	9.870669	9.870306	9.870442
RA2	159.8895	160.2521	159.6124	159.489	160.3925	160.137	159.8795	159.7771
RA3	1000.705	988.1204	993.3007	1002.89	988.7014	991.9263	992.524	1000.794
LLA	1.000925	0.997444	0.994859	0.993253	1.002704	1.007248	1.001082	0.996989
LLV	0.978764	0.97256	0.971395	0.97426	0.977057	0.979791	0.975516	0.975883
LA1	1.004997	1.007279	1.012408	1.01337	1.001517	0.998985	1.005711	1.009196
CP3	0.002662	0.002657	0.00265	0.002641	0.002673	0.002684	0.002667	0.00265
CLA	0.011434	0.01147	0.01137	0.011294	0.011558	0.011584	0.011478	0.011371
CA1	0.00018	0.00018	0.00018	0.00018	0.00018	0.00018	0.00018	0.00018
CA2	0.000227	0.000226	0.000226	0.000226	0.000227	0.000228	0.000227	0.000227
CA3	0.001866	0.001882	0.001899	0.001896	0.00186	0.00185	0.001875	0.001882

Table A8.4 The parameters values of the healthy signal (Subject 25- 32) for the data obtained from the online database, HaeMod [329] (Using GTF as the transfer function)

Parameters	**Subject 25**	**Subject 26**	**Subject 27**	**Subject 28**	**Subject 29**	**Subject 30**	**Subject 31**	**Subject 32**
RP2	39.57947	39.24485	39.5853	39.69245	39.79748	39.26957	39.43388	39.59672
RP3	80.5537	79.08131	81.33955	81.71782	82.05849	79.84477	80.49457	81.11146
RL1	29.6607	29.55748	29.52234	29.57838	29.64327	29.44714	29.52012	29.59651
RL2	10.47649	10.83398	10.74403	10.58948	10.43544	10.88391	10.70024	10.51714
RLA	5.159038	5.172685	5.223948	5.206867	5.189331	5.203254	5.193657	5.182801
RA1	9.864705	9.879975	9.811967	9.819113	9.830335	9.822307	9.825626	9.830712
RA2	160.1201	159.4131	160.2724	160.4307	160.5593	159.4102	159.7454	160.0761
RA3	999.0258	1002.55	984.1193	985.0693	986.1657	994.5076	993.6832	993.0326
LLA	1.003925	0.990068	0.988978	0.995706	1.002557	0.987572	0.994655	1.001808
LLV	0.98007	0.971842	0.962894	0.968889	0.974943	0.965021	0.970207	0.975483
LA1	1.001652	1.016725	1.016354	1.009129	1.001857	1.021385	1.013235	1.005019
CP3	0.002669	0.002632	0.002627	0.002648	0.002669	0.002625	0.002645	0.002665
CLA	0.011496	0.011247	0.011342	0.011453	0.011564	0.011237	0.011364	0.01149
CA1	0.00018	0.00018	0.000181	0.000181	0.00018	0.000181	0.00018	0.00018
CA2	0.000227	0.000226	0.000225	0.000226	0.000227	0.000224	0.000225	0.000227
CA3	0.001855	0.001908	0.001922	0.001893	0.001864	0.001935	0.001904	0.001873

Table A8.5 The parameters values of the healthy signal (Subject 33-40) for the data obtained from the online database, HaeMod [329] (Using GTF as the transfer function)

Parameters	**Subject 33**	**Subject 34**	**Subject 35**	**Subject 36**	**Subject 37**	**Subject 38**	**Subject 39**	**Subject 40**
RP2	39.05636	39.25047	39.69007	39.44601	39.77812	39.8649	39.53255	39.38912
RP3	78.45943	79.33719	81.94082	80.1771	82.20667	82.43998	81.06274	80.53265
RL1	29.46433	29.52763	29.52633	29.59229	29.58224	29.64743	29.52817	29.45663
RL2	11.07952	10.85991	10.65169	10.64114	10.51281	10.37429	10.60773	10.77313
RLA	5.193861	5.186354	5.22818	5.176637	5.209959	5.191532	5.197901	5.208348
RA1	9.875371	9.865059	9.795512	9.856928	9.806128	9.820714	9.811149	9.805167
RA2	159.0115	159.4401	160.5306	159.8527	160.6345	160.7133	159.9717	159.6818
RA3	1001.626	999.9763	981.9153	998.4294	983.3174	984.8151	991.6944	992.0664
LLA	0.979708	0.988189	0.991739	0.996806	0.998051	1.004471	0.997611	0.991093
LLV	0.964172	0.969477	0.964427	0.97489	0.970224	0.976041	0.971715	0.966836
LA1	1.027978	1.018616	1.012862	1.009252	1.006223	0.999532	1.009745	1.017207
CP3	0.002604	0.002627	0.002635	0.00265	0.002655	0.002675	0.002653	0.002635
CLA	0.011085	0.011236	0.01141	0.011387	0.01151	0.01161	0.011432	0.011319
CA1	0.00018	0.00018	0.000181	0.00018	0.000181	0.00018	0.00018	0.000181
CA2	0.000224	0.000225	0.000225	0.000226	0.000226	0.000227	0.000226	0.000225
CA3	0.001951	0.001917	0.001909	0.001883	0.001883	0.001856	0.001892	0.00192

Appendix 9

Table A9.1 The parameters values of the cardiovascular disease' signal (Subject 1- 8) for the data obtained from the hospital. (Using GTF as the transfer function)

Parameters	**Subject 1**	**Subject 2**	**Subject 3**	**Subject 4**	**Subject 5**	**Subject 6**	**Subject 7**	**Subject 8**
RP2	39.48489	39.83276	40.78819	39.32645	39.41952	39.80734	39.38723	39.33627
RP3	81.87954	82.59654	82.98445	79.38236	81.89964	81.4248	82.07401	80.06594
RL1	28.92918	29.11627	28.46696	29.59531	28.7352	29.2267	28.86228	29.08274
RL2	10.52413	10.45041	9.951665	10.47857	10.53097	10.58008	10.46327	10.68811
RLA	5.259716	5.261061	5.278796	5.10826	5.236255	5.225773	5.203735	5.176829
RA1	9.567681	9.673813	9.290019	9.831304	9.515271	9.78192	9.510389	9.707521
RA2	161.1827	162.8195	171.3965	159.1422	162.3637	162.5307	161.1756	161.3963
RA3	992.6669	997.7219	1013.021	1003.445	998.2712	997.0507	985.5994	1010.958
LLA	1.004189	0.988326	0.982139	1.010844	1.000189	0.98381	1.017013	0.983743
LLV	0.964205	0.970119	0.939469	0.985345	0.964929	0.970534	0.964438	0.979708
LA1	1.012131	1.009303	1.000951	1.001267	1.013147	1.009991	1.008269	1.015096
CP3	0.00264	0.002591	0.002377	0.002695	0.00262	0.00259	0.002688	0.002602
CLA	0.011431	0.011461	0.011241	0.011471	0.011422	0.01141	0.011531	0.011287
CA1	0.000181	0.000181	0.000182	0.00018	0.000182	0.00018	0.000182	0.000181
CA2	0.000223	0.000224	0.000226	0.000227	0.000222	0.000226	0.000223	0.000223
CA3	0.00191	0.001878	0.001909	0.001859	0.0019	0.001881	0.001901	0.001889

Table A9.2 The parameters values of the cardiovascular disease' signal (Subject 9-16) for the data obtained from the hospital. (Using GTF as the transfer function)

Parameters	**Subject 9**	**Subject 10**	**Subject 11**	**Subject 12**	**Subject 13**	**Subject 14**	**Subject 15**	**Subject 16**
RP2	39.92352	39.76912	39.43577	40.09892	39.45123	39.67042	39.85128	39.62494
RP3	82.03384	81.67575	80.7895	82.41819	83.04952	82.80645	82.50504	82.0472
RL1	29.11441	29.48886	29.43381	29.52453	28.96404	28.71149	29.3213	29.48842
RL2	10.47843	10.22183	10.45567	10.36816	10.20002	10.18953	10.16791	10.23972
RLA	5.299032	5.145182	5.140284	5.229685	5.23192	5.209682	5.171741	5.162353
RA1	9.605334	9.763435	9.758049	9.750955	9.411598	9.417604	9.685202	9.691297
RA2	163.3366	161.1021	160.2383	163.1353	161.0701	162.6327	161.824	160.1288
RA3	1003.91	997.1014	993.1077	993.5541	986.0823	986.1953	993.2683	986.8405
LLA	0.977833	1.014111	1.015836	0.990105	1.026726	1.019137	1.017578	1.025317
LLV	0.961506	0.9849	0.974509	0.963163	0.963408	0.966323	0.979828	0.97558
LA1	1.014421	0.99295	1.00104	1.003465	1.000212	1.000147	0.992667	0.993937
CP3	0.002513	0.00269	0.002696	0.002567	0.002693	0.002668	0.002688	0.002722
CLA	0.011232	0.011661	0.011553	0.011442	0.011617	0.011624	0.011704	0.011679
CA1	0.000181	0.00018	0.000181	0.00018	0.000182	0.000182	0.000181	0.000181
CA2	0.000225	0.000227	0.000227	0.000227	0.000223	0.000223	0.000227	0.000227
CA3	0.0019	0.001828	0.001863	0.001879	0.001888	0.001883	0.001832	0.00185

Table A9.3 The parameters values of the cardiovascular disease' signal (Subject 17-24) for the data obtained from the hospital. (Using GTF as the transfer function)

Parameters	**Subject 17**	**Subject 18**	**Subject 19**	**Subject 20**	**Subject 21**	**Subject 22**	**Subject 23**	**Subject 24**
RP2	39.52656	39.46106	39.68716	39.44966	39.32376	39.739	39.5114	39.737
RP3	79.34243	80.87238	81.10783	79.86361	80.75299	81.1183	79.79271	82.02567
RL1	29.80361	29.44894	29.49865	29.55946	28.94326	29.5164	29.88124	29.15939
RL2	10.44271	10.40568	10.33518	10.51108	10.52323	10.5322	10.493	10.36373
RLA	5.069019	5.166297	5.182553	5.125267	5.207943	5.21004	5.064616	5.218765
RA1	9.954361	9.739871	9.778802	9.826389	9.541282	9.764541	10.03839	9.653446
RA2	159.7329	159.6249	160.7334	159.8091	161.5667	161.3465	158.9681	162.4916
RA3	1003.345	994.6257	995.3369	992.4132	999.1645	994.5236	1014.694	1000.302
LLA	1.007059	1.016572	1.010694	1.009013	1.009943	0.993088	0.984938	0.999682
LLV	0.989834	0.978055	0.977503	0.974579	0.962719	0.962457	1.015599	0.97206
LA1	0.996491	1.000832	0.996393	1.003093	1.00825	1.009417	0.99619	1.004099
CP3	0.002688	0.002705	0.002677	0.002678	0.002644	0.002588	0.002685	0.002618
CLA	0.011534	0.011549	0.01157	0.011471	0.01139	0.011354	0.011568	0.011496
CA1	0.00018	0.000181	0.00018	0.000181	0.000181	0.00018	0.000179	0.000181
CA2	0.000229	0.000226	0.000227	0.000227	0.000224	0.000227	0.000227	0.000225
CA3	0.001832	0.001866	0.001851	0.001882	0.001902	0.001896	0.001785	0.001868

Table A9.4 The parameters values of the cardiovascular disease' signal (Subject 25-32) for the data obtained from the hospital. (Using GTF as the transfer function)

Parameters	**Subject 25**	**Subject 26**	**Subject 27**	**Subject 28**	**Subject 29**	**Subject 30**	**Subject 31**	**Subject 32**
RP2	39.48824	39.63016	39.76022	39.55689	39.84219	40.11076	39.80352	39.3517
RP3	82.10339	81.58847	80.49598	82.21823	83.08931	81.54981	82.29425	79.25897
RL1	28.97926	29.27498	29.86958	29.22255	29.05821	29.43023	28.98265	29.62423
RL2	10.39449	10.48375	10.28651	10.45776	10.36289	10.3183	10.39615	10.56296
RLA	5.234726	5.206081	5.113496	5.254781	5.26243	5.216736	5.211336	5.1296
RA1	9.576602	9.700585	9.94878	9.677911	9.717631	9.721399	9.604254	9.884292
RA2	161.723	160.9613	160.3692	162.3522	163.9663	163.6838	163.9226	159.415
RA3	999.5613	992.7621	998.9238	997.3371	1005.221	1001.305	1000.254	1007.984
LLA	1.006826	1.002794	1.01324	0.992151	0.984266	0.991882	0.992382	1.003073
LLV	0.970824	0.971097	0.988064	0.966298	0.977683	0.965018	0.968438	0.984629
LA1	1.006364	1.006794	0.989596	1.009266	1.005556	1.001372	1.006782	1.004645
CP3	0.002646	0.002649	0.002702	0.002593	0.002581	0.002555	0.002586	0.002672
CLA	0.011515	0.011483	0.011645	0.011412	0.01154	0.01138	0.011457	0.011421
CA1	0.000181	0.000181	0.000179	0.000181	0.00018	0.00018	0.000181	0.00018
CA2	0.000224	0.000225	0.00023	0.000225	0.000224	0.000228	0.000224	0.000227
CA3	0.001874	0.001885	0.001814	0.001871	0.001833	0.001871	0.001877	0.00186

Table A9.5 The parameters values of the cardiovascular disease' signal (Subject 33-40) for the data obtained from the hospital. (Using GTF as the transfer function)

Parameters	**Subject 33**	**Subject 34**	**Subject 35**	**Subject 36**	**Subject 37**	**Subject 38**	**Subject 39**	**Subject 40**
RP2	39.8433	39.51954	39.41205	39.53022	40.12373	39.60985	39.6891	39.56434
RP3	82.28047	81.64627	81.11388	81.73153	82.78087	81.47105	81.8131	81.95381
RL1	29.28419	29.20968	29.09204	29.36095	29.34658	29.33991	29.14038	29.19156
RL2	10.36369	10.40757	10.43072	10.32437	10.25505	10.37391	10.52824	10.06718
RLA	5.231378	5.214317	5.204834	5.1829	5.23778	5.17593	5.250284	5.123662
RA1	9.649571	9.653884	9.603117	9.694396	9.685567	9.749589	9.667126	9.52218
RA2	162.3321	161.4434	160.925	161.1268	163.4125	161.0907	161.9616	160.0878
RA3	992.2258	1000.082	1002.767	988.2906	996.3292	998.9056	998.551	987.2289
LLA	1.000968	1.004804	1.0092	1.016589	0.994885	1.008042	0.982098	1.03683
LLV	0.963796	0.972674	0.973013	0.970255	0.97072	0.980221	0.971124	0.981025
LA1	1.004507	1.004608	1.006353	0.996912	0.999595	1.000304	1.014157	0.989515
CP3	0.002609	0.002643	0.002656	0.002688	0.00259	0.002674	0.002573	0.002747
CLA	0.011475	0.011494	0.01146	0.011603	0.011507	0.011581	0.011335	0.011735
CA1	0.000181	0.000181	0.000181	0.000181	0.000181	0.00018	0.000181	0.000181
CA2	0.000226	0.000225	0.000224	0.000226	0.000227	0.000226	0.000224	0.000226
CA3	0.001888	0.00187	0.001884	0.001858	0.00186	0.001846	0.001896	0.001849